Targeting Aberrant Transcription in Invasive Lobular Carcinoma Breast Cancer

AUTHOR(S)

Louise Walsh

CITATION

Walsh, Louise (2018): Targeting Aberrant Transcription in Invasive Lobular Carcinoma Breast Cancer. Royal College of Surgeons in Ireland. Thesis. https://doi.org/10.25419/rcsi.10802195.v1

DOI

10.25419/rcsi.10802195.v1

RCSI

Targeting Aberrant Transcription in Invasive Lobular Carcinoma Breast Cancer

Louise Walsh BSc

Department of Molecular and Cellular Therapeutics

RCSI

A thesis submitted to the School of Postgraduate Studies, Faculty of Medicine and Health Sciences, Royal College of Surgeons in Ireland, in fulfilment of the degree of Doctor of Philosophy

Supervisor(s): **Dr. Darran O'Connor**

Dr. Tríona Ní Chonghaile

December 2017

I declare that this thesis, which I submit to RCSI for examination in consideration of the award of a higher degree of Doctor of Philosophy is my own personal effort. Where any of the content presented is the result of input or data from a related collaborative research programme this is duly acknowledged in the text such that it is possible to ascertain how much of the work is my own. I have not already obtained a degree in RCSI or elsewhere on the basis of this work. Furthermore, I took reasonable care to ensure that the work is original, and, to the best of my knowledge, does not breach copyright law, and has not been taken from other sources except where such work has been cited and acknowledged within the text.

Signed _____

Student Number _____

Date _____

Table of Contents

List of Abbreviations

HRT	Hormone replacement therapy
BRCA1	Breast cancer 1, early onset
BRCA2	Breast cancer 2, early onset
HER2	Human epidermal growth factor receptor 2
TNBC	Triple-negative breast cancer
ER	Estrogen receptor
PgR	Progesterone receptor
DCIS	Ductal carcinoma in situ
LCIS	Lobular carcinoma in situ
IDC	Invasive ductal carcinoma
ILC	Invasive lobular carcinoma
NHG	Nottingham histological grade
NPI	Nottingham ProgMolnostic Index
FDA	Food and Drug Administration
RS	Recurrence score
RT-PCR	Reverse transcriptase polymerase chain reaction
TAILORx	Trial Assigning Individualised Options for Treatment
WSG	West German Study Group
RxPONDER	Positive Node, Endocrine-Responsive Breast Cancer
E2	Estradiol
ERE	Estrogen response elements
HAT	Histone acetyltransferase
RNA Pol II	RNA polymerase II
LOH	Loss of heterozygosity
KO	Knockout
Mrip	Myosin phosphatase Rho-interacting protein
PI3Ks	Phosphatidylinositol 3-kinases
EMT	Epithelial to mesenchymal transition
BCT	Breast conservation therapy
BET	Bromodomain and extra-terminal domain

HDAC	Histone deacetylase
BD	Bromodomain
ET	Extra-terminal
NUT	Nuclear protein in testis
BCL-2	B-cell lymphoma 2
BH	BCL-2 homology
DED	Death effector domain
DISC	Death-inducing signalling complex
tBID	Truncated BID
APAF-1	Apoptotic peptidase activating factor 1
MOMP	Mitochondrial outer membrane permeabilisation
SMAC	Second mitochondria-derived activator of caspase
XIAP	X-linked inhibitor of apoptosis protein
CLL	Chronic lymphocytic leukemia
CST	Cell Signaling Technology
HRP	Horseradish peroxidase
FBS	Fetal bovine serum
MTT	3-(4,5-dimethylthiazol-2-yl)-2,5diphenyltetrazolium bromide
DMSO	Dimethyl sulfoxide
PI	Propidium iodide
PBS	Phosphate buffer saline
RT	Room temperature
EDTA	Ethylenediaminetetraacetic acid
dNTP	Deoxynucleotide
DTT	Dithiothreitol
qPCR	Quantitative polymerase chain reaction
cDNA	Complementary DNA
SDS-PAGE	Sodium Dodecyl Sulfate Polyacrylamide Gel Electrophoresis
siRNA	Small interfering RNA
BCA	Bicinchoninic acid
BSA	Bovine serum albumen
TBST	Tris buffer saline with Tween 20

DE	Differential expression/ differentially expressed
FDR	False discovery rate
FPKM	Fragments-per-kilobase per million reads
3D	3-dimensional
PDX	Patient derived xenograft
NOD-SCID	Nonobese diabetic/severe combined immunodeficiency
IHC	Immunohistochemistry
H & E	Haematoxylin and Eosin
IMS	Industrial methylated spirits
DH_2O	Distilled H_2O
SERM	Selective estrogen receptor modulator
SERD	Selective estrogen receptor downregulator
AI	Aromatase inhibitor
rRNA	Ribosomal RNA
mRNA	Messenger RNA
CI	Confidence interval/ combination index
SEM	Standard error of the mean
IC50	The half maximal inhibitory concentration
ANOVA	Analysis of variance
PROTACs	Proteolysis Targeted Chimeras
AML	Acute myeloid leukemia
shRNA	Short hairpin RNA
HSPC	Haematopoietic stem and progenitor cells
LSC	Leukemic stem cells
c-FLIP	Cellular FADD-like IL-1β-converting enzyme inhibitory protein
GFP	Green fluorescent protein
SCLC	Small-cell lung carcinoma
T-ALL	T-cell acute lymphoblastic leukemia
CDK7	Cyclin-dependent kinase 7

List of Figures

List of Tables

Summary

Invasive lobular carcinoma (ILC) is an understudied breast cancer subtype comprising 8-14% of breast tumours. The majority of ILC (90%) are estrogen receptor (ER)-positive and candidates for endocrine therapy. Unfortunately, de novo resistance to endocrine therapies occurs in 33% of women and a further 40% will relapse on treatment. Therefore, novel therapeutic targets are required for ILC. Deregulated transcription is a recurring theme in cancer, which can be due to epigenetic events. The bromodomain & extra-terminal domain (BET) family of proteins (BRD2, BRD3, BRD4, BRDT) function as chromatin readers that bind acetylated lysine residues on histones and regulate transcription. RNA sequencing analysis was performed on 61 primary ILC samples and it was found that high expression of BRD3 was associated with poor survival in ILC (log rank test, p=0.037). This finding was validated in a second cohort of 99 ILC primary samples from the METABRIC dataset (log rank test, p=0.0157).

Next, it was tested if ILC cell lines were sensitive to BET inhibition using the small molecule inhibitor JQ1, which inhibits all BET family proteins. JQ1 downregulated growth promoting genes in ILC cell lines including ER and MYC. JQ1 inhibited cell growth in all ILC cell lines tested, however apoptosis was only induced in two out of four ILC cell lines. ILC cell lines resistant to JQ1-induced apoptosis had sustained or upregulated expression of the anti-apoptotic BCL-XL following JQ1 treatment by RNA sequencing and qPCR validation. This led us to assess the combination of JQ1 and ABT-263 (BCL-2, BCL-XL and BCL-W inhibitor). The drug combination was synergistic in ILC cell lines and induced apoptosis in ILC cell lines previously apoptotic resistant. The drug combination also inhibited the number and size of 3D spheroids and induced apoptosis in a ILC primary sample grown *ex vivo*. These findings suggest that the combination of JQ1 and ABT-263 is an effective treatment strategy for ILC.

Acknowledgment

Completion of this PhD project would not have been possible without the support and guidance of my dedicated supervisors Dr. Tríona Ní Chonghaile and Dr. Darran O'Connor. They were always happy to discuss the direction of my project, my research findings and took a keen interest in my development as an independent researcher. My supervisors also gave me encouragement and confidence in both myself and my research that will greatly stand to me during my career.

This work was kindly supported by the Irish Cancer Society Collaborative Cancer Research Centre BREAST-PREDICT [grant CCRC13GAL] (www.breastpredict.com). I was extremely lucky to be a part of this collaborative research centre, which comprised PhD students, postdoctoral researchers, principle investigators and clinicians. BREAST-PREDICT provided training, fostered the development of long-term collaborations and provided opportunity to present your research and have it critiqued by experts from all over the world that contributed to the success of this project.

I would like to say a warm thank you to all the laboratory members of the Dr. Darran O'Connor lab (Lisa Dwane, Dr. Sudipto Das, Brian Mooney, Camille Hurley and Kate O'Connor) as well as from the Dr. Tríona Ní Chonghaile laboratory (Alessandra Di Grande and Dr. Catríona Dowling). You are all great life-long friends and colleagues whose advice, support and friendship I have greatly appreciated and relied on throughout my PhD.

Finally, I would like to acknowledge University College Dublin (in which the first year of the project was carried out) and the Royal College of Surgeons in Ireland for providing me with the facilities and supports needed for this project.

Dedication

I would like to dedicate this PhD to my fiancée Ciarán Dooley, whose daily support, encouragement and confidence in me has been a huge part in the completion of this PhD. I would also like to dedicate this PhD to my Mam, Patricia Yeates Walsh, my Dad, Brian Walsh and brother, Jeffery Walsh. Without them none of this would have been possible. When times were tough you were all always there to lift my spirits and provide me with inspiring words of kindness and confidence.

I have an amazing family for which I will always be grateful and I love you all dearly.

Chapter One: Introduction

1.1 Breast Cancer Incidence

Breast cancer is the most common cancer in women with an estimated one in eight women afflicted with breast cancer worldwide (1). Breast cancer remains the principal cause of cancer mortality in women with 508,000 deaths in 2011 (2, 3). The median age of Irish women at diagnosis is 60-64 years old (4). There are 2,919 newly diagnosed cases of invasive breast cancer resulting in 694 deaths annually in Ireland (4). However, breast cancer incidence is declining with effective treatment strategies and early detection (5, 6), and the net survival of breast cancer patients has improved from 74.3% in 1994-1999 to 84.7% in 2006-2012 because of this (4). Many risk factors are known for the development of breast cancer. These include inherited mutations in breast cancer 1, early onset (BRCA1) and breast cancer 2, early onset (BRCA2) genes, hormone replacement therapy (HRT), oral contraceptives, smoking, extended estrogen exposure, obesity and alcohol consumption (7-13). BRCA1 and BRCA2 are tumour suppressors that are involved in transcriptional regulation and DNA repair (14). BRCA1 and BRCA2 mutations increase the risk of breast cancer by 70 years of age by 57% and 49%, respectively (7). Women taking the combined estrogen and progesterone HRT had increased risk of breast cancer, with a hazard ratio of 2.74 at 5.4 years and 3.27 for more than 15 years on HRT (8). Risk in women taking HRT with just oestrogen was much lower, with a hazard ratio of 1 (8). There is a 1-1.5-fold increased risk of breast cancer in women aged 40-49 with the use of oral contraceptives, first childbirth at 30 years of age or older as well as nulliparity (9). Women who have smoked for 35 years or more have an odds ratio of 1.7% for breast cancer risk (10). Extended estrogen exposure in women increases breast cancer risk by a factor of 1.029 (for each year older at menopause) and 1.05 (for each year younger at menarche) (11). Obese women have an increased risk of postmenopausal invasive breast cancer with a hazard ratio of 1.58 (12). There is also an increased relative risk in patients who consume 5-9.9 g of alcohol per day (13). In contrast, breast feeding decreases breast cancer risk (3, 4). Although breast cancer can occur in men it is much rarer, with the estimated incidence of male breast cancer in Ireland of 1 in 1000 men (15).

1.2 Breast Cancer Subtypes

1.2.1 Molecularly defined subtypes and targeted therapies

Breast cancer is a highly complex and heterogeneous disease. There are five main subtypes of breast cancer based on gene expression data (16-18), each subtype differs in survival. The main subtypes include estrogen receptor (ER)-positive, human epidermal growth factor receptor 2 (HER2) overexpressing, normal-like and triple-negative (TNBC) or basal-like breast cancer, with basal-like having the worst prognosis (16, 18). The ER-positive breast cancer subtype can be further divided into Luminal A and Luminal B tumours. Both Luminal A and Luminal B tumours are of low grade but Luminal A tumours grow slower and have better prognosis (18). Approximately 70% of breast tumours are ER positive (19). Estrogen signals through the ER, which drives proliferation and breast tumourigenesis (20). Therefore, therapeutic approaches include antagonism or downregulation of the ER (endocrine therapy), as well as aromatase inhibitors in postmenopausal women to prevent estrogen production (21, 22). ER positivity in breast tumours is a predictive marker of response to endocrine therapy such as tamoxifen (23) and of a more favourable clinical outcome (24). The HER2 oncogene is a member of the epidermal growth factor receptor family. HER2 overexpressing breast cancers are dependent on HER2 signalling and HER2 is amplified in 25% of breast cancers (25). Inhibition of HER2 with either monoclonal antibodies, (e.g. trastuzamab, pertuzamab) (26, 27), or with small molecule kinase inhibitors (e.g. lapatinib, afatinib) is an effective treatment strategy (28-30). TNBC occurs in approximately 15% of breast cancers (31). The TNBC subtype of breast cancer is so-called as it lacks expression of ER, progesterone receptor (PgR) and HER2. As TNBC lacks hormonal receptors and HER2, there is currently no available targeted therapy and treatment mainly relies on cytotoxic chemotherapy (32). Basal-like breast cancer also does not express ER, PgR and HER2 and overlaps in approximately 77% of cases with TNBC (17, 33). However, basal-like breast cancer additionally expresses basal markers (34) and thus represents a distinct breast cancer subtype. Lastly, normal-like breast cancers are ER-positive and PgR-positive and are associated with the expression of genes related to adipose non-epithelial cell types and low expression of genes associated with luminal epithelial cells (17, 18). Normal-like tumours resemble the luminal A

subtype and comprise 7.8% of all breast cancers (35). This being said, as many as 10 distinct subtypes of breast cancer have been reported using nearly 2,000 breast tumours from METABRIC (Molecular Taxonomy of Breast Cancer International Consortium) and both transcriptomic and genomic data platforms (36).

1.2.2 Histologically defined subtypes

Histological subtypes of breast cancer are categorised based on the tumour growth pattern and the tumour architecture. The primary histological types are *in situ* carcinoma and invasive carcinoma (37). *In situ* carcinoma refers to a breast cancer that is confined to its site of origin, whereas invasive carcinoma has evaded the site of origin. *In situ* carcinoma and invasive carcinoma can be further categorised as either ductal or lobular i.e. ductal or lobular carcinoma *in situ* (DCIS or LCIS) or invasive ductal or lobular carcinoma (IDC or ILC) (37). Ductal carcinomas arise in the milk ducts whereas lobular breast cancer arises in the milk producing gland known as the lobules. DCIS is more common than LCIS and has been categorised into further subtypes known as: Solid, Papillary, Cribiform, Micropapillary and Comedo DCIS (37, 38). Likewise, IDC is substantially more common compared to ILC accounting for approximately 75% of invasive breast cancers, while ILC accounts for approximately 8-14% (39, 40).

1.3 Histological staging and grading

1.3.1 Histological staging

Tumour staging refers to the size of the tumour and also whether the tumour has metastasised from the primary tumour. Staging is carried out using the so-called TNM classification system, originally developed by Denoix (41), which refers to the primary tumour size (T), lymph node negativity/positivity (N) and whether the tumour has metastasised (M) (42). T1-4 indicates the increasing size of the tumour (T0=no tumour, T1= <2 cm, T2= 2-5 cm, T3= >5 cm and T4= tumour is present in the skin or chest wall), N0-3 indicates extent of lymph node involvement (N0= no lymph nodes positive for cancer, N1= 1-3 lymph nodes positive, N2= 4-9 lymph node positivity, N3= >10 lymph node positivity) and M0 or M1 indicates the absence or presence of distant metastasis, respectively. Based on the above criteria, tumours can be grouped into stages of prognostic importance (Table 1.1) (42). Stage 0 refers to

breast carcinoma *in situ*, stage I-III indicates spread of the tumour to local regions with potential lymph node involvement and stage IV denotes metastatic spread (42).

Table 1.1 TNM Tumour Staging in Breast Cancer. Adapted from (42). T1 includes T1 microinvasion less than or equal to 0.1 cm. N1mi= Micrometastasis less than 2 mm. Tis= carcinoma *in situ*.

Stage	Tumour	Node	Metastasis
0	Tis	N0	M0
1A	T1	N0	M0
1B	T0, T1	N1mi	M0
2A	T0. T1	N1	M0
	T2	N0	M0
2B	T2	N1	M0
	T3	N0	M0
3A	T0, T1, T2	N2	M0
	T3	N1, N2	M0
3B	T4	N0, N1, N2	M0
3C	Any T	N3	M0
4	Any T	Any N	M1

1.3.2 Histological grading

Tumours are graded using histology and gives an indication of how aggressive a tumour is based on cell characteristics. Breast tumours are histologically graded using the Nottingham grading system or the Nottingham histological grade (NHG), that provides prognostic information to the clinician (43). Three features including mitotic count, tubule formation and nuclear polymorphism are semi-quantified and applied to a numerical scoring system that assigns the tumour grade. Grade II and III tumours display significantly worse survival compared to patients with grade I

tumours (43). The Nottingham histological grading system/NHG is used in the Nottingham Prognostic Index (NPI) that is used to stratify patients for therapy. The NPI uses tumour grade, tumour stage and tumour size to assign 3 groups of good, moderate or poor prognosis based on the formula: Tumour diameter in centimetres + NHG (1-3) + N (1-3) X 0.2, where N= lymph node stage (0 positive lymph nodes=0, 1-3 positive lymph nodes=2, more than 3 positive lymph nodes=3) and 15-year survival rates (43, 44). Recently, NPI Plus (NPI+) was developed that utilises 10 biomarkers (ER, PgR, p53, epidermal growth factor receptor (EGFR), HER2, HER3, HER4, cytokeratin 5/6, cytokeratin 7/8 and Mucin 1) that first identifies the molecular subtype of the tumour and then uses conventional prognostic markers (including tumour size, grade, positive lymph nodes, lymphovascular invasion and hormone status), that provides improved patient stratification (45, 46).

1.4 Prognostic assays

Prognostic assays that help predict response in breast cancer include Oncotype DX and Mammaprint. Mammaprint uses a 70 gene signature assessed by DNA microarray analysis to predict risk of metastases that is not based on hormonal or HER2 status (47). This gene expression signature was subsequently shown to be an independent predictive factor in a follow-up study of a larger cohort of 295 patients (48). Mammaprint was approved by the Food and Drug Administration (FDA) in 2007 to predict risk of recurrence in breast cancer. Oncotype DX is a 21 gene recurrence score (RS) assay using reverse transcriptase polymerase chain reaction (RT-PCR) that can predict risk of recurrence. Oncotype DX can predict risk of recurrence in ER-positive, lymph node negative patients treated with tamoxifen and/or chemotherapy (49, 50). Risk groups are defined as patients with a RS of less than 18 as low risk, RS of 18-30 as intermediate risk and RS of >31 as high risk (49). The prognostic potential of the Oncotype DX assay was validated in two phase 3 trials. These were TAILORx (Trial Assigning Individualised Options for Treatment) trial and West German Study Group (WSG) PlanB (51, 52). Patients enrolled on the TAILORx trial have hormone receptor positive, HER2 negative, lymph node negative breast cancer. Patients with a RS <11 were treated with endocrine therapy whereas patients with a RS >25 were treated with chemotherapy and endocrine therapy. Findings from the TAILORx trial to date is an overall survival at 5 years of 98% and rate of freedom from distant recurrence at 5 years of 99.3% in 1,626 patients with a

RS of <11 receiving endocrine treatment alone (51). In the WSG PlanB trial, patients enrolled had hormone positive, lymph node positive/high risk lymph-node negative and HER2 negative breast cancer. Omission of chemotherapy was advised in patients with a RS of less than or equal to 11 and the disease free survival at 3 years was 98% in 348 patients (52). Final results from the TAILORx trial and a trial, which incorporates lymph node positive patients, RxPonder (Positive Node, Endocrine-Responsive Breast Cancer) are not yet published but aim to provide further validation of Onoctype DX.

1.5 ER signalling pathway

The ER is a steroid hormone receptor that drives breast tumorigenesis (53). There are two ERs, namely ERα and ERβ. In normal breast tissue estradiol (E2) is known to signal via both ERα and ERβ. However, in breast cancer tissue ERα is thought to be the main receptor that E2 signals through and the ERβ receptor is not detected in breast cancer patient samples (54). Unoccupied or ligand free ER forms a complex with the heatshock protein Hsp90 and chaperones and cannot bind DNA (55).

In order for ER to be activated an agonist needs to bind the receptor (Figure 1.1) or the ER receptor needs to be phosphorylated (54). Phosphorylation of ER can occur on a number of different serine target residues (56). These include phosphorylation on S118, which has been shown to (i) promote recruitment of coactivators to the receptor such as SRC1 and CBP/p300 (57, 58), (ii) facilitate dimerization of the ER (59), (iii) ligand-dependent and -independent activation (60, 61) and (iv) facilitate binding to ER target genes (62). Other serine phosphorylation sites include S167 that is involved in the transcriptional activation of the ER; S104/106 that promotes ER activity (63); S305 that partakes in ER transcriptional activity (64, 65) and S236 that provides protection against proteasomal degradation and promotes ER dimerisation (66, 67). Other post-translational modifications on the ER include ubiquitination, sumoylation, acetylation and lysine methylation (56). When E2 agonist binds the ER a conformational change occurs causing the ER to dimerise and Hsp90 to disassociate (Figure 1.1). The ER is now capable of binding estrogen response elements (ERE) on DNA and recruit cofactors to the ERE bound E2/ER receptor complex (Figure 1.1) (54). Cofactors recruited to the ER include the p300/CBP protein that acts a transcriptional coactivator (68, 69), remodels the chromatin via its

histone acetyltransferase (HAT) activity (70) and also interacts with other HATs including PCAF (71). P300/CBP and PCAF use their HAT activity to acetylate the basal transcription machinery (70, 72) and are required for ER dependent gene transcription (54). Other ER coactivators are involved in recruitment of the DRIP/TRAP pre-initiation complex, namely SRC1, SRC2, SRC3 (Figure 1.1). The CARM1 and PRMT1 methyltransferases also function as ER coactivators (54). Once the E2/ER complex along with ER transcriptional coactivators assemble at the 13 base pair sequence CGGGTCAnnnTGACCTG known as the ERE on target genes, the transcription of genes involved in cell proliferation and survival ensue (Figure 1.1) (54).

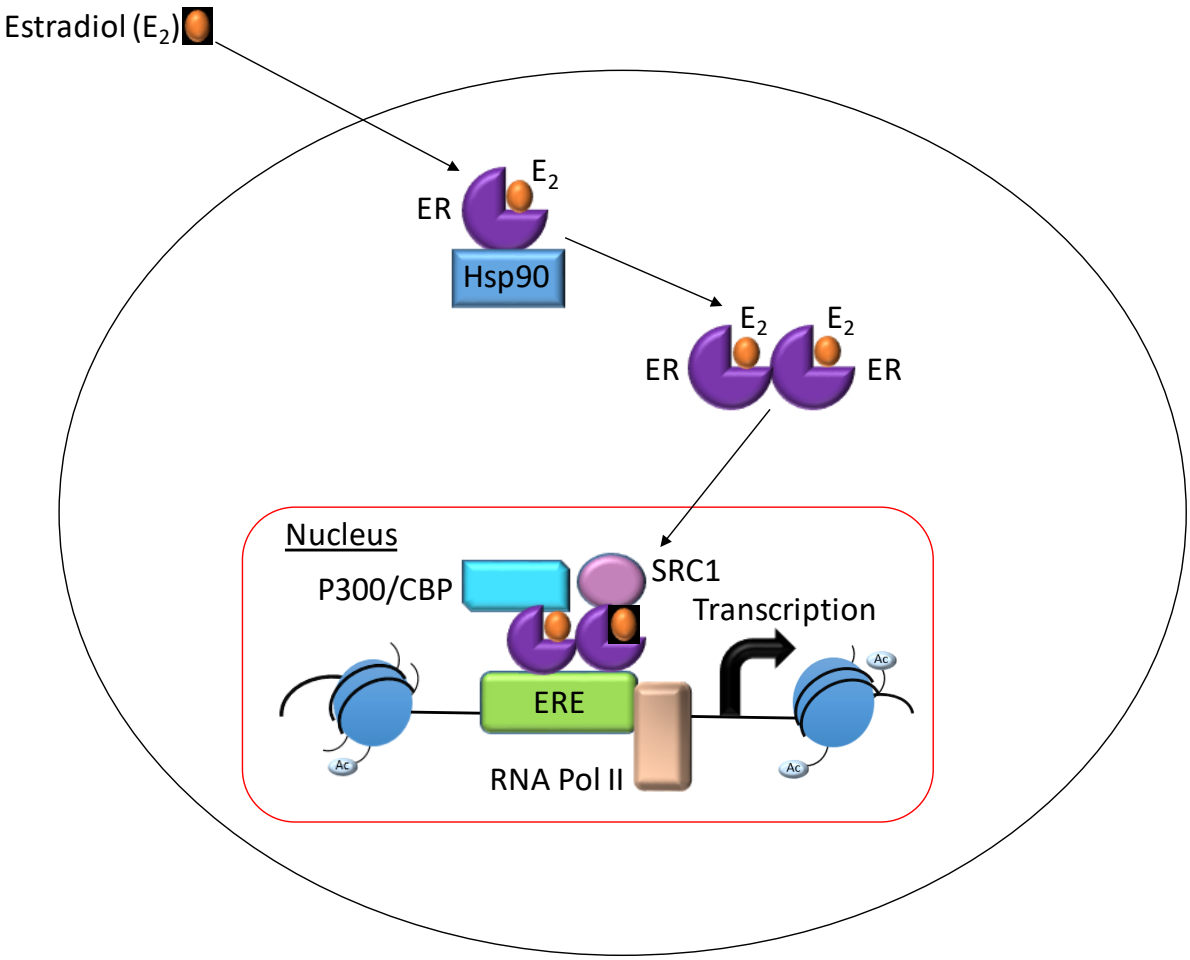

Figure 1.1: The ER signalling pathway. Estrasiol binds the ER, which induces a conformational change in the receptor. The ER dimerises and Hsp90 dissociates from the receptor. Dimerised ER translocates to the nucleus where it binds ERE elements on ER-target genes and recruits transcriptional coactivators such as p300/CBP and SRC1 in order to promote gene transcription (54). RNA Pol II= RNA polymerase II.

1.6 Invasive Lobular Carcinoma

As mentioned, Invasive Lobular Carcinoma (ILC) accounts for approximately 8-14% of all breast tumours (39, 40). ILC represents an understudied type of breast cancer in which resources including cell lines and murine models are lacking (73). ILC are also commonly grouped with IDC in clinical trials and not appreciated as a separate breast cancer subtype (74). ILC are usually diagnosed later than IDC, with lymph node invasion, larger tumours and metastasise to the ovary and gastrointestinal tract

(40, 75). ILC typically have low grade tumours, usually grade 1-2 tumours (76, 77), although some reports suggest they are usually diagnosed with stage III/IV tumours (75).

1.6.1 ILC subtypes

ILC comprises many histological subtypes including classical, trabecular, pleomorphic, solid, alveolar and solid mixed lobular carcinoma (Figure 1.2) (78, 79), with the trabecular and classical form of ILC associated with a more favourable prognosis (79). In classical ILC cells lack consistency, are small and look similar to each other. These cells are in a concentric pattern and display the classic single-file pattern of invasion infiltrating the surrounding stroma. Pleomorphic ILC also displays the unique single-file pattern of invasion, nuclear pleomorphism, cellular atypia and may also comprise signet ring cells and increased mitotic rate (80). HER2 overexpression is rare in ILC except for in pleomorphic subtypes (80, 81). TP53 mutations occur in pleomorphic ILC (82, 83) but are uncommon in other ILC subtypes (84). Solid ILC resembles classical ILC but the cells are arranged in sheets. Likewise, alveolar ILC resembles classical ILC but the cells are arranged in groups or 20 or more cells. The solid mixed subtype comprises classical ILC mixed with solid ILC and classical ILC can also occur mixed with other subtypes. Finally, the trabecular subtype refers to tumours cells in a tubular-like structure growing two cells or more in width creating prominent bands of cells (79).

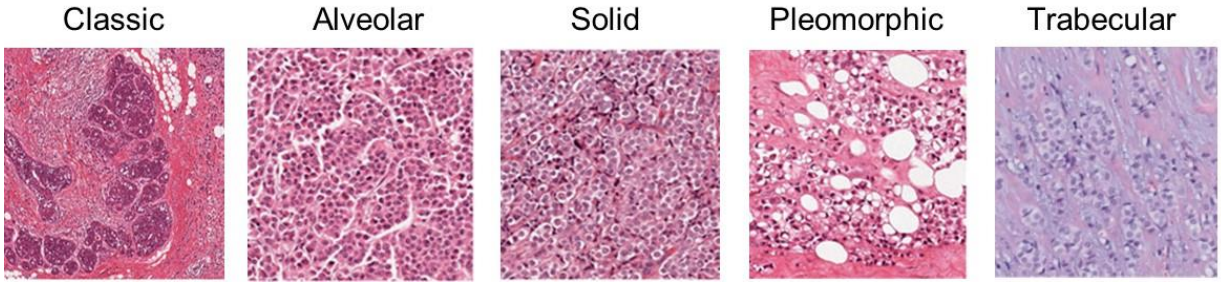

Figure 1.2: Subtypes of ILC breast cancer. Immunohistochemistry images depicting classic, alveolar, solid, pleomorphic and trabecular subtypes of ILC. Adapted from (80, 85).

1.6.2 ILC detection

Due to the distinct growth pattern of ILC, it is more difficult to detect compared to IDC. ILC may not present as a palpable mass (80), detection by clinical examination is difficult and mammography can produce false negative results due to lack of calcification in ILC (39, 86). Ultrasonography (although may incorrectly assess the size of the tumour) and magnetic resonance imaging display enhanced sensitivity for the detection of ILC (87-89).

1.6.3 ILC characteristics

A characteristic of ILC is loss of E-cadherin and 90-95% of ILC primary samples are ER-positive (Figure 1.3) and as such are treated with endocrine therapy (75, 80, 90).

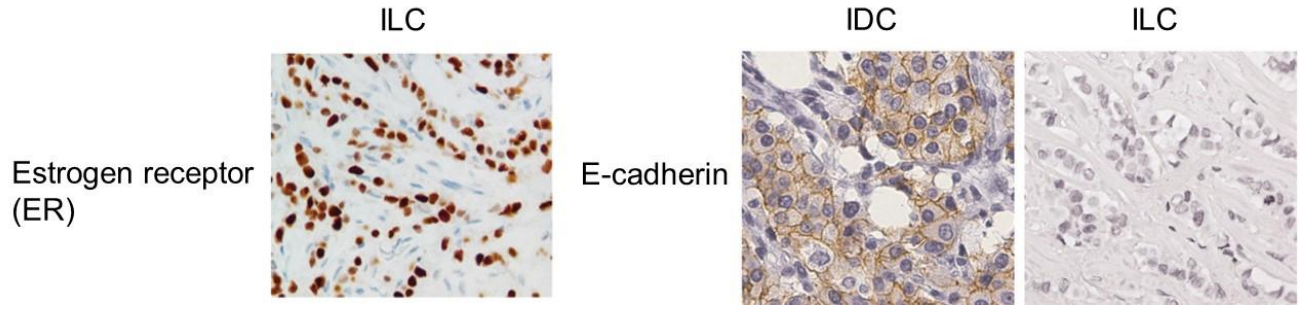

Figure 1.3: Characteristics of Invasive lobular carcinoma. Positive immunohistochemistry staining in ILC primary samples for ER (91) and negative immunohistochemistry staining for E-cadherin (92). Invasive ductal carcinoma (IDC) acts as a positive control for E-cadherin staining.

E-cadherin is a transmembrane glycoprotein that is a critical cell-cell adhesion molecule and regulates cell polarity (80, 93). On the apical side of the cell, adherens junctions are formed by the association of E-cadherin with catenin proteins thereby forming bonds between microtubules and actin to the plasma membrane (93). E-cadherin also acts as a tumour suppressor due to its anti-metastatic and anti-invasive roles and maintains epithelial cell structure and function (94). E-cadherin dysregulation is a common feature in many epithelial cancers (95). This can come in the form of loss of heterozygosity (LOH) of chromosome 16q where the CDH1 gene

encoding E-cadherin is located (94, 96, 97), promoter hypermethylation (98), missense mutations (99), inactivating CDH1 mutations (100, 101), and mutational hotspots (97). In ILC E-cadherin is commonly lost via CDH1 promoter methylation, LOH, CDH1 frameshift mutations and also germline CDH1 mutations have been reported (102-104). The majority (approximately 90%) of ILC display loss of E-cadherin that is responsible for the discohesive pattern of growth (Figure 1.2, 1.3) (80). Loss of E-cadherin is thought to be an early event in tumorigenesis, as it is also present in LCIS (105, 106). Germline knockout (KO) of E-cadherin in murine models is lethal (107) and conditional KO of E-cadherin induces widespread apoptosis (108). Some have suggested it is likely that loss of E-cadherin in ILC occurs after other tumorigenic events or oncogenic hits have occurred (93), as has been shown with loss of p53 and E-cadherin (109, 110).

Cytosolic localisation of p120 is another characteristic of ILC and is used in addition with E-cadherin loss and ER expression to identify ILC (111). p120 is re-located from the cell membrane to the cytoplasm (or nucleus) as a result of E-cadherin dysfunction in ILC (112, 113). Cytosolic p120 is oncogenic and inhibits myosin phosphatase Rho-interacting protein (Mrip). Thereby, causing activation of Rho/Rock signalling and anoikis resistance that was also confirmed in ILC primary samples (113).

Phosphatidylinositol 3-kinases (PI3Ks) are a family of proteins that lead to the activation of the protein kinase AKT and are involved in the regulation of cell survival, proliferation and motility (114). PIK3CA is the p110α catalytic subunit of PI3Ks and is frequently mutated in cancer with one study reporting mutations in 32% of colon, 27% brain, 25% gastric, 6% of breast and 4% of lung cancers (115). PIK3CA mutations are common (approximately 36%) in ILC and are believed to be selected for during ILC tumour progression to local recurrence (116). Interestingly PIK3CA are not selected for distant metastasis (116).

Recent evidence shows that ILC is both clinically (see section 1.6.4 ILC treatment) and molecularly distinct from IDC (117). Furthermore, ILC does not fit well with breast cancer molecular subtype classifications that were primarily founded using IDC breast tumours (17, 18), with most ILC tumours classified as either the luminal A or B molecular subtypes (36). Recent efforts have identified novel subtypes of ILC,

as well as distinct mutations that occur in ILC (117, 118). Ciriello et al. identified three novel transcriptional subtypes of ILC including reactive-like, immune-related and proliferative ILC subtypes. The reactive-like subtype had the best outcome and was characterised by cancer fibroblast signalling and/or active microenvironment (117). Michaut et al. identified an immune related subtype and a hormone related ILC subtype that was characterised by epithelial to mesenchymal transition (EMT) (118). The authors found that eIF4B protein expression and the rate of somatic mutation was associated with ILC survival (118). Furthermore, loss of PTEN, E-cadherin and mutations in PIK3CA, FOXA1 and TBX3 are hallmarks of ILC (117, 118). ILC breast cancer is treated with a combination of surgery, chemotherapy and endocrine therapy and are discussed below.

1.6.4 ILC treatment

1.6.4.1 Surgery

Characteristically, ILC typically displays a single-file pattern of invasion with low proliferative potential, atypical cell nuclei, non-polarised cells and an inconsistent growth pattern (93). ILC are usually treated with surgery that is often more extensive compared to IDC. This is because there is a higher rate of tumour margin involvement and it is difficult to obtain clear margins (119, 120). There is a higher rate of mastectomy (an aggressive treatment option) in ILC compared to IDC (119), with ILC shown to have a greater occurrence of bilateral breast cancer, multicentricity and multifocal involvement (40, 121-123). Some studies have shown that there are high rates of local recurrence in ILC patients receiving breast conservation therapy (BCT) versus those that receive mastectomy (124, 125). This is on contrast to other studies that show minimal effect, varying from 2-8% (126-129). The use of sentinel lymph node biopsy with BCT has also been reported to have added value (129).

1.6.4.2 Endocrine treatment

On E2 stimulation, the ER translocates to the nucleus where the E2/ER complex binds ERE elements on DNA in order to promote ER-target gene transcription (see section 1.5 ER signalling pathway). Common ER target genes that are interrogated in the literature to elucidate ER signalling include the PgR and TFF1 genes (130,

131). PgR is a transcriptional regulator that promotes proliferation (132) and TFF1 has been shown to promote invasion, migration and proliferation of breast cancer cells (133-135). Most ILCs are ER positive and therefore treated with endocrine therapy (136). Selective estrogen receptor modulators (SERMs), selective estrogen receptor downregulators (SERDs) and aromatase inhibitors (AIs) are all forms of endocrine therapies and treatment depends on both the menopausal state of the patient and the treating physician. SERMs act as ER antagonists in breast tissue (137). SERMs compete with E2 for ER binding and on ER binding induce a conformational change in the ER preventing recruitment of coactivators, thereby disrupting ER dependent gene transcription (137-139). Examples of SERMs include tamoxifen and raloxifene and both have been shown to recruit transcriptional corepressors to ER target genes on binding ER (140). Both drugs function as ER antagonists in breast tissue but have agonist effects in the bone and tamoxifen additionally has agonist effects in the uterus by recruiting transcriptional coactivators (137, 140). Tamoxifen was discovered in the 1960s (141) and approved by the FDA in 1998 for pre- and post-menopausal women (142). The structure of tamoxifen is shown (Figure 1.4a). The Study of Tamoxifen and Raloxifene (STAR) trial found that both drugs were effective in decreasing invasive breast cancer risk, there were lower rates of uterine cancer in patients treated with raloxifene, as well as thromboembolism, but higher risk of non-invasive breast cancer after 5 years on therapy (143). SERDs (e.g. fulvestrant) are selective estrogen downregulators that function as high affinity ER antagonists that compete with E2 for ER binding (144, 145). SERDs inhibit ER dimerization and translocation to the nucleus; cause inactivation of AF1 and AF2 transactivation domains of the ER; and also target the ER for degradation by the proteasome (144, 145). Fulvestrant has a higher affinity for the ER than E2 does, namely 89% that of E2 (145). The ER is still functional in endocrine resistant disease and SERDs are used for the treatment of ER positive breast cancer that have relapsed on SERM or AI therapy (144). Fulvestrant was discovered in the 1990s (146) and approved by the FDA in 2002 for postmenopausal metastatic breast cancer that had relapsed on previous endocrine therapy (147). Recently, fulvestrant was approved by the FDA for the treatment of postmenopausal women with no prior endocrine treatment with hormone receptor positive and HER2 negative advanced breast cancer (148). The structure of fulvestrant is shown (Figure 1.4b). Finally, AI therapy is used for the treatment of breast cancer in

postmenopausal women (149). AI therapy functions by inactivating or inhibiting the aromatase enzyme that synthesises estrogens, resulting in decreased estrogen levels in circulation (149). Type I AI therapies, for example formestane, bind irreversibly to the aromatase enzyme and are analogues of androstenedione. Type II AI therapies, for example letrozole, bind reversibly to the aromatase enzyme (149).

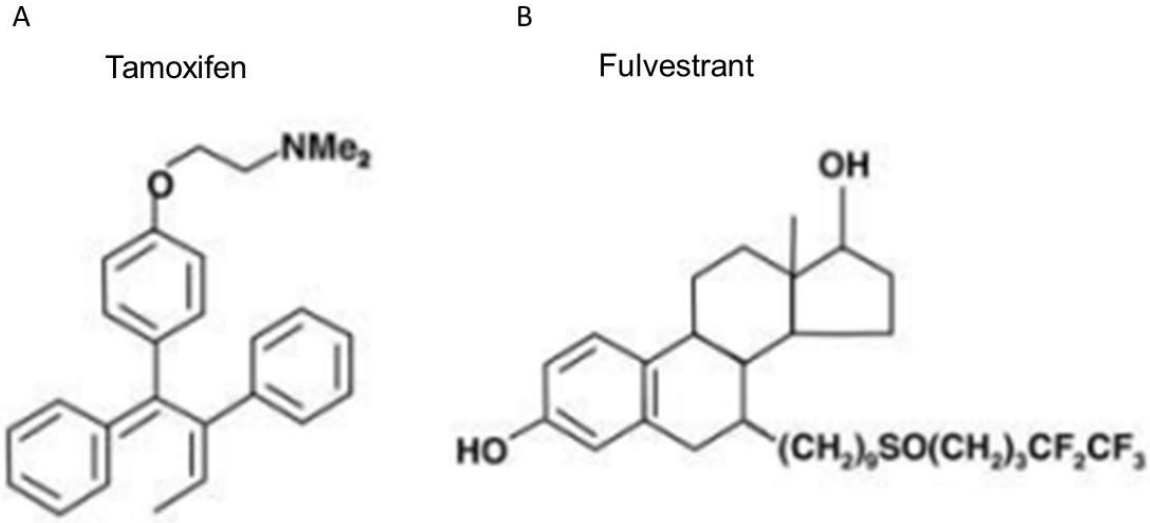

Figure 1.4: Structure of the SERM, tamoxifen and SERD, fulvestrant. The chemical structure of (A) tamoxifen and (B) fulvestrant used in the treatment of hormone receptor positive breast cancer. Adapted from (150).

Unfortunately, endocrine treatment fails in one third of women whom are de novo resistant to endocrine therapy and as many as 40% will relapse on treatment (151, 152). Mechanisms attributing to this resistance include loss of ER expression, ER mutations, ER hypermethylation, altered expression of co-regulatory proteins, crosstalk with other growth factor signalling pathways, among others (151, 152).

Controversy exists in the field regarding response to endocrine therapy in ILC. Some studies found that there is a similar recurrence-free survival for ILC and IDC patients treated with endocrine therapy (153). This is in contrast to Pestalozzi et al. who identified in ER positive cohorts that ILC patients displayed worse disease-free survival after 10 years and worse overall survival after 10 years compared to IDC patients (154). Adachi et al. also reported that ILC have worse overall survival and worse disease-free survival after 50 months, with the majority of ILC and IDC

patients treated with endocrine therapy in this cohort (155). Additionally, data from the BIG 1-98 trial showed that ILC patients display poorer disease-free survival and poorer overall survival on tamoxifen treatment compared to IDC patients (156). Conflicting to these studies, improved survival in ILC patients treated with endocrine therapy compared to IDC patients after 5 years has also been reported (40, 77). Therefore, it remains to be seen whether there is a difference in endocrine therapy response in ILC versus IDC.

1.6.4.3 Chemotherapy

ILC are also known to have a poor response to neoadjuvant chemotherapy (157). Low mitotic count in ILC has been suggested to contribute to this poor response (80). Compared to IDC, ILC do not respond as well to neoadjuvant chemotherapy and Tubiana-Hulin et al. suggest that neoadjuvant endocrine therapy may be a preferred option (158).

Thus, ILC represents a subtype of breast cancer, which has a poor patient outcome and novel therapeutic agents are required for the improved treatment of ILC.

1.7 Epigenetics

Alterations in the epigenetics has been shown to be involved in both the initiation and progression of cancer (159). Epigenetics can be defined as heritable changes in gene expression without alterations in DNA sequence (160). The regulation of the epigenome is crucial for normal growth and development, while alterations to the epigenome are associated with aberrant gene expression and diseases including cancer (161). Chromatin is comprised of the repeating basic units known as nucleosomes, which consist of DNA coiled around core histone proteins H2A, H2B, H3 and H4 along with non-histone proteins (162). Dynamic changes in the chromatin are brought about through a series of posttranslational modifications. To date, more than sixteen various histone modifications have been identified including acetylation and methylation and they usually occur at the unstructured amino terminal tail of the histone (163). Epigenetic modifiers can be assembled into three main groups: (i) epigenetic writers are enzymes that catalyse the addition of specific chemical covalent modifications to a histone tail, (ii) epigenetic readers recognize and bind specific histone modifications and subsequently recruit other proteins to the

chromatin, and finally, (iii) epigenetic erasers remove specific covalent histone modifications from the histone tails (Figure 1.5) (164). In simplistic terms, chromatin structure is altered by either enabling access of transcriptional machinery to the underlying DNA through an 'open' chromatin state known as euchromatin, or, by preventing access to the underlying DNA through a 'closed' heterochromatin (165). In addition to genetic mutations, epigenetic alterations also contribute to tumorigenesis with many examples in breast cancer (166, 167).

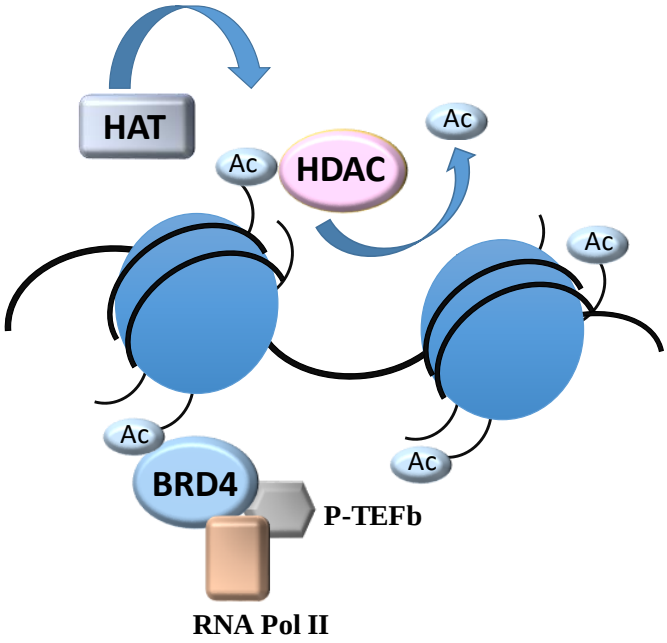

Figure 1.5: Epigenetic regulation of histone acetylation. HATs catalyse the addition of acetyl groups on histones (168). The bromodomain and extra-terminal domain (BET) protein BRD4 reads the acetylation mark on nucleosomal histones and recruits co-factors in order to regulate gene transcription (169-171). Histone deacetylases (HDACs) catalyse the removal of the acetylation mark from the histones (168).

1.7.1 Histone acetylation readers: Bromodomain and extra-terminal domain family of proteins

Deregulated transcription mediated by epigenetic events is a recurring theme in cancer (172-174). The bromodomain and extra-terminal domain (BET) family of

proteins are a family of chromatin readers and comprise BRD2, BRD3, BRD4 and BRDT (175). BRDT is the only member that its expression is restricted to the testis (176). Each member contains two tandem bromodomains in the amino terminal region and an extra-terminal domain in the carboxy-terminal region (Figure 1.6) (177, 178). Acetylated lysine residues are a mark of active transcription (179). BET proteins bind acetylated lysine residues on nucleosomal histones, via their bromodomains, and recruit transcription factors and chromatin modifying enzymes to gene promoter and enhancers (Figure 1.6, 1.7) (180-182). In this manner BET proteins regulate gene transcription. BRD4 interacts with Mediator (183) and regulates transcriptional elongation by RNA polymerase II (RNA Pol II) by recruiting the positive transcription elongation factor P-TEFb to gene promoters and enhancers, thus facilitating RNA Pol II (Figure 1.7) (170, 171, 184). It has also been reported that BRD4 can phosphorylate RNA Pol II directly. BRD4 acts first to phosphorylate Ser2 of RNA Pol II at transcription initiation-elongation and it is at this stage that further phosphorylation of Ser2 occurs by P-TEFb (185). BRD4 has also been implicated in mitotic memory, remaining bound during mitosis to M/G1 genes (186). BRD3 has been shown to act as a cofactor to the acetylated form of the transcription factor GATA1 (187). BRD2 is associated with E2F-dependent cell cycle gene promoters and progression of the cell cycle (188, 189). BRD2 and BRD3 have also been shown to facilitate RNA Pol II gene transcription (190). It is thought that the BET protein functions are redundant due to sequence homology but the exact distinct and overlapping roles of these proteins has not yet been elucidated (191).

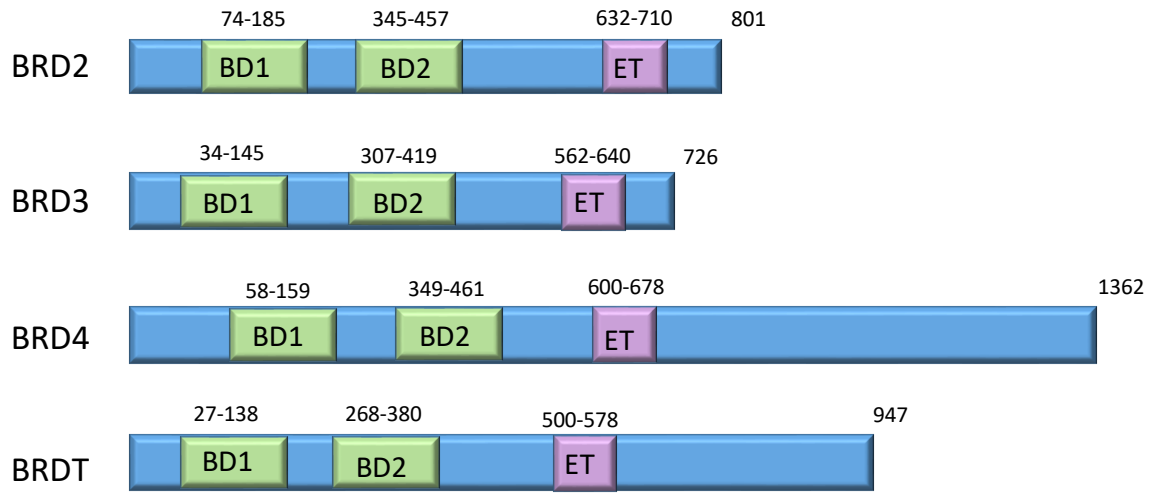

Figure 1.6: Schematic representing the structure of BET proteins. Each BET protein contains two tandem bromodomains (BD1 and BD2) and an extra-terminal domain (ET) in the carboxy region. Adapted from (192).

Expression of the BRD proteins has been associated with cancer. In NUT midline carcinoma, a translocation occurs to fuse BRD3 or BRD4 with nuclear protein in testis (NUT) that causes a block in differentiation and increased proliferation (193). Constitutive expression of BRD2 in the B lymphocytes of mice caused an aggressive B cell lymphoma and transcriptional analysis showed a similar transcriptional profile to that observed of diffuse large B-cell lymphomas from patients (194).

1.8 Transcriptional Inhibitors

1.8.1 BET inhibition

Through the development of BET inhibitor(s) the diverse function of the BET family proteins in cancer has been revealed. One of the first BET inhibitors to be developed was JQ1, a small molecule inhibitor that competitively binds to BET protein bromodomains preventing interaction with acetylated histones (Figure 1.7) (195). Since then, other BET inhibitors such as OTX-015 (196), IBET-151 and IBET-762 have been developed (197, 198). BET inhibitors have shown efficacy in a wide variety of cancers including multiple myeloma (199, 200), NUT-midline carcinoma (195), neuroblastoma (201, 202), prostate cancer (203) and breast cancer (204-207).

A recurring theme in these publications is a selective inhibition of oncogenic transcriptional networks by BET inhibitors. BET proteins are ubiquitously expressed (175), except for BRDT that is expressed in the testis (176), therefore it may be postulated that targeting BET proteins may lead to wide spread toxicity. In contrast, JQ1 is well tolerated *in vivo* in numerous studies (195, 207, 208) and does not affect the viability of normal cells (199, 209). Young et al. have shown that high levels of BET proteins and cofactors are located at large enhancer regions described as 'super-enhancer' regions (210). Super-enhancers define a collection of enhancer regions that drive gene expression, which determines cell identity and ultimately, cell fate (211). In cancer cells, super-enhancers are found preferentially at proto-oncogenes or lineage-specific survival genes (211). Preferential inhibition of BET proteins at these super-enhancer regions such as at Myc, with resulting transcription elongation defects, may explain the selective inhibition of target genes and the broad efficacy of BET inhibitors in a wide variety of transcriptionally driven cancers (195, 197, 200, 208, 210, 212), including breast cancer (204-207) and the observed tolerance *in vivo* and in normal cells.

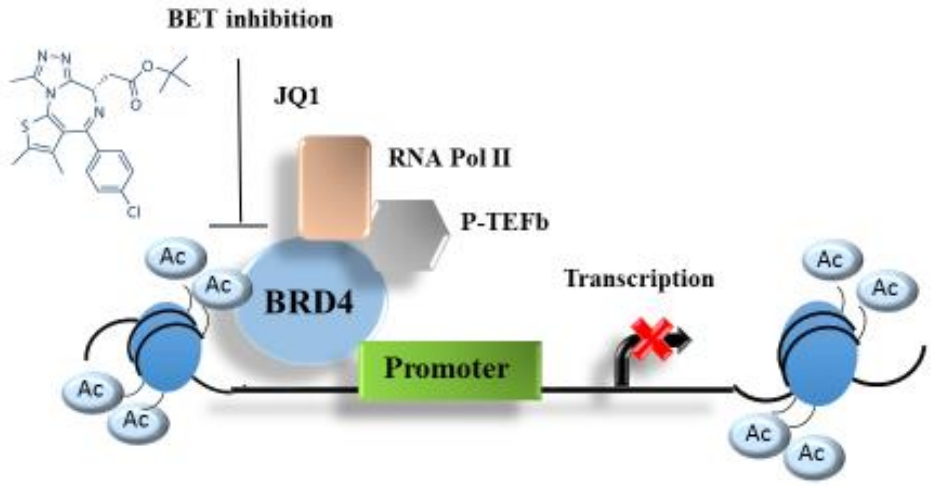

Figure 1.7: Mechanism of action of the BET inhibitor JQ1. BRD4 proteins bind acetylated lysine residues on nucleosomal histones, recruiting P-TEFb and RNA Pol II to promote transcription at gene promoters. JQ1 is an inhibitor of the BET family of proteins that inhibits BET protein binding to acetylated histones, thereby inhibiting transcription.

JQ1 is used as a research tool due to its short half-life. Intravenous injection of JQ1 (5mg/kg) *in vivo* displayed a half-life of 0.897 hours and oral administration of JQ1 (10mg/kg) *in vivo* had a half-life of 1.39 hours (195). There are many BET inhibitors that are being explored in clinical trials and further clinical trials are planned for both solid and haematological tumours including combination regimens (213). Responses have been shown in NUT midline carcinoma trials (214), leukemia (215) and lymphoma (216). Stathis et al. reported patient responses in a phase I clinical trial in four patients with NUT-midline carcinoma, treated with the BET inhibitor OTX015 (214). Two patients responded to therapy and another patient displayed stable disease (214). In an on-going phase I trial of the BET inhibitor OTX015 in 36 AML patients, three patients attained complete response, while two other patients displayed partial clearance of blasts (215). Finally, in another on-going phase I trial, 45 patients with lymphoma or multiple myeloma were recruited to the study (216). Two lymphoma patients achieved a complete response, one lymphoma patient achieved a partial response and clinical activity was observed in another six lymphoma patients (216).

Despite, JQ1 being well tolerated *in vivo* in numerous studies (195, 207, 208) and anticipated non-toxicity on normal cells (199, 209), toxicity has been observed in the clinic with other BET inhibitors. In NUT-midline carcinoma observed toxicities with the BET inhibitor OTX015 included thrombocytopenia, gastrointestinal toxicity and fatigue (214), in lymphoma and multiple myeloma toxicities included thrombocytopenia, fatigue, anaemia, nausea, diarrhoea, neutropenia (216) and in leukemia observed toxicities included elevated bilirubin and fatigue (215).

1.8.2 CDK7 inhibition

Like JQ1, cyclin-dependent kinase 7 (CDK7) inhibitors are transcriptional inhibitors that have been shown to target super-enhancers (217, 218). CDK7 is a member of the cyclin dependent kinase family and exhibits dual function in both transcriptional regulation as well as regulation of the cell cycle. CDK7 is known to bind MAT1 and cyclin H resulting in the formation of a cyclin activating kinase (CAK) (219, 220). CAK is part of the basal transcription factor complex TFIIH and directly phosphorylates RNA Pol II (219, 220). Additionally, CAK phosphorylates other CDK components of

the cell cycle and is required for activation of CDK2/cyclin-E as well as CDK1/cyclin-B in the G1-S transition and G2-M transition of the cell cycle, respectively (220-222).

CDK7 inhibitors include BS-181 and THZ1 (217, 223). BS-181 is a selective CDK7 inhibitor that has been shown to inhibit growth, promote apoptosis and inhibit tumour growth in an IDC ER-positive breast xenograft (223). THZ1 is a novel selective CDK7 inhibitor that covalently and irreversibly binds to CDK7 (217). THZ1 has shown to induce apoptosis and inhibit proliferation in T-cell acute lymphoblastic leukemia (T-ALL) cell lines (217), inhibit tumour growth and promote tumour regression in neuroblastoma (224) and also inhibit tumour growth and improve survival in *in vivo* models of small cell lung cancer (SCLC) (218). These studies also report that CDK7 inhibition causes disruption at super-enhancer regions and downregulate highly transcribed genes such as the Myc oncogene (217, 218).

1.9 Apoptotic pathways

Inhibition of BET proteins has been shown to induce cell death through apoptosis (195, 203, 208). There are two types of apoptotic pathways, the extrinsic pathway and the intrinsic or mitochondrial pathway. The mitochondrial pathway utilises internal stress signals in order to regulate apoptosis. In contrast, the extrinsic pathway relies on extrinsic signals in the form of ligands in order to regulate apoptosis.

1.9.1 Extrinsic pathway of apoptosis

The extrinsic pathway of apoptosis involves transmembrane death receptors located on the cell surface and their ligands that are expressed by effector immune cells (225, 226). The transmembrane death receptors are members of the TNF superfamily, such as TNFR1 and FasR (225), and harbour a characteristic death domain of 80 amino acids (227). Death receptor ligands include TNF-α and FasL, which bind to their respective TNFR1 and FasR receptors that results in receptor trimerization and clustering of the three death domains (228). The clustered death domains recruit adaptor proteins to the receptor complex via death domains located on both the receptor and adaptor proteins (225). The adaptor protein TRADD is recruited in the case of the TNF-α /TNFR1 receptor complex. TRADD also recruits another adaptor protein known as FADD. The FasL/FasR complex recruits the

adapter protein FADD directly (225). FADD contains a death effector domain (DED) and via the DED, FADD can recruit the initiator procaspase 8 to form the death-inducing signalling complex (DISC) (229-231). Pro-caspase 8 recruits Cellular FADD-like IL-1β-converting enzyme inhibitory protein (c-FLIP) to the DISC complex, which regulates DISC activation based on the ratio of c-FLIP isoforms, c-FLIPL (long isoform) or c-FLIPS (short isoform) (232). A high ratio of c-FLIPS: pro-caspase 8 inhibits pro-caspase 8 activation whereas a high ratio of c-FLIPL: pro-caspase 8 promotes oligomer assembly of pro-caspase 8 (232). Procaspase 8 undergoes autoproteolytic cleavage into its activate caspase 8 form (231). Activated caspase 8 is released from the DISC complex where it cleaves and activates executioner caspase 3 to initiate apoptosis (231, 233). Crosstalk to the mitochondrial apoptotic pathway also occurs via caspase 8 or caspase 3 cleavage of BID into truncated BID (tBID) that initiates MOMP at mitochondrial membranes (234).

RIP1 contains a DD and can also be recruited to the DISC complex following TNFR1 signalling (235). RIP1 recruits and interacts with RIP3 via a RIP homology domain (235). Caspase 8 cleaves RIP1 and RIP3 resulting in their inactivation, which promotes apoptosis (236). However, when caspase 8 is inhibited, RIP1 and RIP3 are phosphorylated and necroptosis cell death occurs (236).

1.9.2 Mitochondrial pathway of apoptosis

Most cancer targeting drugs exert their anti-cancer effect through the mitochondrial pathway, which is regulated by the family of BCL-2 proteins (237). BCL-2 proteins contain regions of homology known as BCL-2 homology (BH) domains (BH1-4) and each BCL-2 family member contains at least one BH domain (238). BH domains are critical for function (238). BCL-2 family members can be classified into three group that consist of (i) multi-domain anti-apoptotic proteins that have 4 BH domains (BH1-4), (ii) multi-domain pro-apoptotic proteins that have 3 BH domains (BH1-3) and (iii) BH3-only pro-apoptotic proteins that only have a BH3 domain (239). Mitochondrial apoptosis is initiated when the reserve of pro-apoptotic BCL-2 members is greater than that of anti-apoptotic family members. Likewise, if the reserve of anti-apoptotic proteins is greater than that of pro-apoptotic BCL-2 family proteins, apoptosis is inhibited (240).

Multi-domain anti-apoptotic proteins inhibit apoptosis by binding to pro-death proteins and are located on the outer mitochondrial membrane, but can also be located in the endoplasmic reticulum membrane or cytosol (241). Anti-apoptotic BCL-2 members comprise BCL-2, BCL-XL, BCL-W, MCL-1, and BFL-1 (Figure 1.8) (240). BCL-2 was the first BCL-2 protein to be identified due to its involvement in t(14;18) chromosomal translocation in follicular lymphoma (242). Anti-apoptotic proteins contain a hydrophobic binding groove on the protein surface composed of 3 BH domains, BH1, BH2 and BH3 (238). Two hydrophobic α-helices define the bottom of the hydrophobic groove (238). The BH4 domain stabilises the BH1-3 domains that make up the binding groove (241). This binding groove binds and inhibits the BH3 domain of BH3-only activator proteins or of BAX and BAK (Figure 1.8) (240, 241).

Multi-domain pro-apoptotic proteins consist of BAX and BAK. BAX and BAK also have a binding groove composed of BH1-3 domains (241). BAK is located in the mitochondrial membrane, whereas BAX is usually located in the cytosol (241). In the cytosol, the C-terminal transmembrane tail of BAX is inserted into its binding groove. Following apoptotic stimuli, BAX translocates from the cytosol to the mitochondria, where it's C-terminal transmembrane tail inserts into the mitochondrial outer membrane (241). BAX and BAK undergo a conformational change upon activation and homoligomerise forming pores in the mitochondrial membrane to initiate mitochondria outer membrane permeabilisation (MOMP) (Figure 1.8) (239). MOMP is usually a point of no return for the cell, as mitochondria that have undergone MOMP have diminished ATP generation capacity (243).

Finally, BH3-only pro-apoptotic proteins can be further divided into BH3 sensitiser proteins and BH3 activator proteins (Figure 1.8) (240). The BH3-only proteins only have a BH3 domain composed of 9-16 amino acids and a 7 amino acid sequence motif LXXXGDE (239). Following stress signalling, BH3 only proteins are induced and activated post-translationally or transcriptionally (244, 245). BH3-only proteins are present in a range of different locations in the cell including microtubules, cytosol and the endoplasmic reticulum (reviewed in (245)), but translocate to the mitochondria and/or endoplasmic reticulum following activation (245). The activator BH3 proteins (BIM, BID) can activate BAX and BAK directly at the mitochondrial membrane via their binding groove in order to initiate MOMP (Figure 1.8) (244),

whereas the BH3 sensitiser proteins (PUMA, BIK, BAD, NOXA, HRK, BMF) cannot activate BAX and BAK directly but do so indirectly by inhibiting the binding groove of anti-apoptotic proteins (Figure 1.8) (240, 244, 246). It was shown that BIM has a binding preference for BAX, whereas BID has binding preference for BAK (247). Full length PUMA has also been shown to activate BAX and BAK and may also function as an activator BH3 protein (Figure 1.8) (248). In the absence of BAX and BAK, BOK can initiate mitochondrial apoptosis (249). Furthermore, BOK protein stability is regulated by the endoplasmic reticulum-associated degradation pathway and not by anti-apoptotic BCL-2 proteins (249).

Once MOMP is induced, cytochrome *c* is released from the mitochondrial intermembrane/intercristae spaces (250) and interacts with the adaptor molecule apoptotic peptidase activating factor 1 (Apaf-1) in the cytosol (Figure 1.8) (243). Cytochrome *c* causes a conformational change and activation of Apaf-1 (251). The Apaf-1/cytochrome *c* complex oligomerises in the presence of dATP resulting in the formation of the apoptosome (251). Pro-caspase 9 is recruited to the apoptosome where it dimerises, producing active caspase 9 (Figure 1.8) (251, 252). It has been recently reported that the apoptosome functions to activate caspase 9 by sequestration of its caspase recruitment domain (CARD) (253). Caspase 9 proteolytic activity is inhibited by the CARD domain (253). Caspases comprise a family of cysteine-dependent aspartate-directed proteases (254). Active caspase 9 in turn cleaves pro-caspase 3 and 7 into the active effector caspases 3 and 7, which cleave numerous proteins causing apoptosis (Figure 1.8) (237, 255). When the effector caspases, caspase 3 and 7, are activated they proceed in the proteolytic cleavage of numerous proteins including regulatory protein targets, structural protein targets, the phospholipid flippase enzymes ATP11A and ATP11C and scramblase Xkr8 (256-258). Effector caspase cleavage of ATP11A and ATP11C results in their inactivation, whereas cleavage of Xkr8 results in its activation. Via these flippase and scramblase cleavage events, phosphatidylserine (a lipid membrane) is no longer located on the inner plasma membrane and is exposed on the outer plasma membrane and functions as a “eat me” signal to macrophages (257, 258). Xkr4 and Xkr9 are other scramblases which can be cleaved by effector caspases and promote phosphatidylserine exposure (258). The effector caspases also have been shown to cleave inhibitor of caspase-activated DNase (ICAD) that in turn results in the

activation of DNases, known as caspase-activated DNase (CAD), which cleave DNA resulting in DNA fragmentation (259). Other molecules, in addition to cytochrome *c*, such as OMI, second mitochondria-derived activator of caspase (SMAC) and apoptosis-inducing factor (AIF) are released from the mitochondria following MOMP. OMI and SMAC function to inhibit the inhibitor of caspase activity, X-linked inhibitor of apoptosis protein (XIAP) (260). Whereas, AIF causes DNA fragmentation, chromatin condensation and mitochondrial membrane permeabilisation (261).

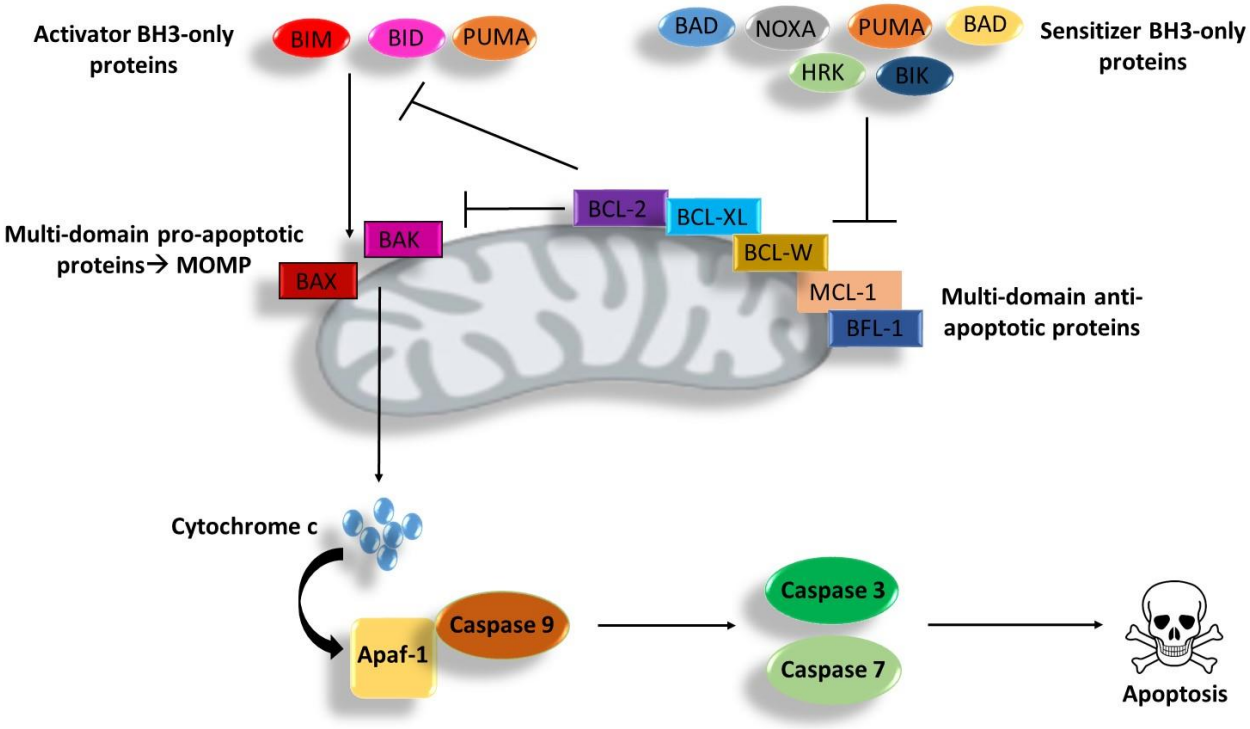

Figure 1.8: Mitochondrial apoptotic pathway. Multi-domain anti-apoptotic proteins inhibit apoptosis by inhibiting activator BH3-only proteins and multi-domain pro-apoptotic proteins. Sensitiser BH3-only proteins inhibit multi-domain anti-apoptotic proteins. Activator BH3-only proteins (BIM, BID, possibly PUMA) bind and activate the multi-domain pro-apoptotic proteins BAX and BAK that homoligomerise at the mitochondrial membrane causing pores and MOMP. Cytochrome *c* is released by MOMP, leading to the formation of the apoptosome and activation of caspase 9. Caspase 9 cleaves and activates caspase 3/7 that results in the initiation of apoptosis.

1.9.3 BH3 profiling to assess mitochondrial apoptosis

BH3 profiling is a functional assay that can determine dependencies on BCL-2 anti-apoptotic proteins and also determine how primed mitochondria are for apoptosis (262). The BCL-2 family is composed of numerous members that have selective binding for one another, therefore it can be difficult to assess sensitivity to apoptosis based on protein expression alone. It is possible to immunoprecipitate each of the proteins and measure bound BCL-2 family members but that is very labour intensive. BH3 profiling is a high throughput standardised test that functionally assesses the interactions of the BCL-2 family, which enables comparison between cells and primary human samples (262, 263). BH3 profiling was developed by the laboratory of Dr. Anthony Letai in Dana-Farber. BH3 sensitiser and activator peptides that are derived from the BH3 helix of these proteins are used in BH3 profiling that contain the conserved LXXXXD motif and are 20-25mer in length (Table 1.2) (262).

Table 1.2: Sequence of BH3 peptides. Table illustrating the sequence of the BID, BIM, BAD, NOXA, HRK, PUMA and BMF BH3 peptides used in BH3 profiling. Adapted from (264).

Peptide	Sequence
BID	EDIIRNIARHLAQVGDSMDR
BIM	MRPEIWIAQELRRIGDEFNA
BAD	LWAAQRYGRELRRMSDEFEGSFKGL
NOXA	AELPPEFAAQLRKIGDKVYC
HRK	SSAAQLTAARLKALGDELHQ
PUMA	EQWAREIGAQLRRMADDLNA
BMF	HQAEVQIARKLQLIADQFHR

BH3 profiling uses a readout of MOMP in the form of loss of mitochondrial membrane potential that can be measured following treatment with known concentrations of BH3 peptides and using a potential sensitive dye, JC-1 (262). Cells that undergo MOMP following treatment with both sensitiser and activator BH3

peptides are “primed” for death and the reserve of anti-apoptotic proteins in the cell is already occupied by BH3-only proteins. By treatment with sensitiser BH3 peptides, anti-apoptotic proteins are inhibited resulting in release of activator BH3 protein which can initiate MOMP. Cells that undergo MOMP following treatment with activator peptides have anti-apoptotic proteins unoccupied by BH3-only proteins and are “unprimed”. Therefore, activator BH3 proteins are not released from anti-apoptotic proteins following treatment with sensitiser BH3 peptides. Furthermore, BH3-only proteins have specific binding interactions with anti-apoptotic proteins that BH3 profiling utilises to identify anti-apoptotic dependencies (Figure 1.9) (263). The BH3 profiling functional assay proves a read out of cell priming as well as anti-apoptotic protein dependencies by taking into account both BCL-2 protein expression and binding interactions (262).

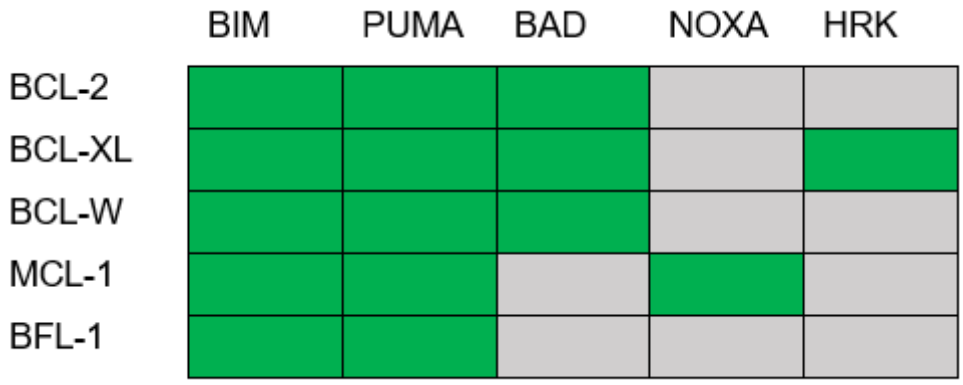

Figure 1.9: BH3 peptide specific binding interactions. Anti-apoptotic proteins are indicated left to right and pro-apoptotic peptides are shown going from top to bottom in the matrix. Pro-apoptotic BH3 peptides have specific binding interactions for the anti-apoptotic proteins. Green box denotes interaction between the indicated anti-apoptotic protein and the indicated pro-apoptotic peptide. Activator BH3 peptide: BIM. Sensitiser BH3 peptides: PUMA, BAD, NOXA, HRK. Anti-apoptotic proteins: BCL-2, BCL-XL, BCL-W, MCL-1. Adapted from (263).

Intracellular BH3 profiling (iBH3) is the latest method of BH3 profiling (265) that fixes and stains cells for cytochrome *c* and percentage loss of cytochrome c is measured. In cells that have undergone MOMP, cytochrome c will have been released from the permeablised cell and will stain negative for cytochrome c. In contrast, cells that

have not undergone MOMP will stain positive for cytochrome c, which is analysed by flow cytometry (265).

1.9.4 BH3 mimetics

BH3 mimetics are small molecule inhibitors that bind and competitively inhibit the BH3 binding groove of anti-apoptotic proteins by mimicking BH3-only proteins, which have been developed by AbbVie, Inc (266). The development of therapeutics targeting protein-protein interactions is notoriously difficult (267). The first BH3 mimetic to be developed was the pre-clinical inhibitor ABT-737 that inhibits the BCL-2, BCL-XL and BCL-W anti-apoptotic proteins (268) that showed efficacy in a range of cancers. ABT-737 showed efficacy in lymphoma, small-cell lung cancer (SCLC), multiple myeloma, chronic lymphocytic leukemia (CLL) and acute myeloid leukemia (AML) (268-272). Sensitivity to ABT-737 has been attributed to the requirement of BCL-2 to sequester BIM, as shown in CLL (270). Resistance to ABT-737 has been credited to high expression of the anti-apoptotic protein MCL-1 that is not targeted by ABT-737 (272, 273). Due to the role of MCL-1 in drug resistance and MCL-1 amplifications in many cancers, numerous MCL-1 inhibitors have been developed (274).

ABT-263 is a second-in-class BH3 mimetic that was developed from ABT-737 and is orally bioavailable (275). ABT-263, or tradename Navitoclax, is also a selective inhibitor for the anti-apoptotic proteins BCL-2, BCL-XL and BCL-W (Figure 1.11) (266). Tumour regression was achieved in ALL and SCLC xenografts with ABT-263 (275). ABT-263 monotherapy was not effective in xenograft models of multiple myeloma or B-cell lymphoma, however, the combination of ABT-263 and chemotherapy was significantly better than chemotherapy or ABT-263 treatment alone (275). In a phase I clinical trial in resistant CLL, 90.5% of patients displayed a reduction in lymphocytosis by more than 50% (276). Response to ABT-263 was associated with high BIM: BCL-2 or BIM: MCL-1 ratios and low MCL-1 expression in CLL cells (276). ABT-263 achieved stable disease in clinical trials of resistant high grade serious ovarian cancer (32.6%) (277) and relapsed SCLC (23%) (278). ABT-263 also produced partial response in a clinical trial in lymphoid cancer (21.7%) (279). Unfortunately, platelets rely on BCL-XL for cell survival therefore, the limitation with ABT-263 is that it causes dose-dependent thrombocytopenia (276-280).

ABT-199, tradename Venetoclax (266), is a selective BCL-2 inhibitor (Figure 1.10, 1.11) and therefore thrombocytopenia is usually not a side effect of this drug (281). However, tumour lysis was a side effect of ABT-199 in a study of 3 CLL patients and in order to prevent this in future trials the starting dose of ABT-199 was reduced and increased weekly (281). Like ABT-737 and ABT-263, sensitivity to ABT-199 has been attributed to the disruption of BCL-2 in complex with pro-apoptotic BIM (281). In a clinical trial with resistant CLL or small lymphocytic lymphoma, 79% of patients responded to ABT-199 and 20% had complete remission (282). Another trial reported overall response of 79.4% of patients in resistant CLL following ABT-199 (283). ABT-199 was approved by the FDA in 2016 for the treatment of CLL patients with chromosome 17p deletion (284, 285).

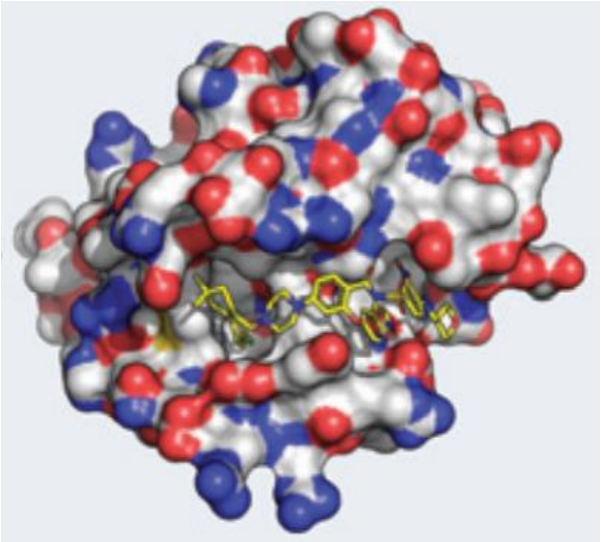

Figure 1.10: Structure of BCL-2 complexed with a ABT-199 analogue in 3D. BCL-2 in complex with ABT-199 analogue, 4-(4-{[4-(4-chlorophenyl)-5,6-dihydro-2H-pyran-3-yl]methyl}piperazin-1-yl)-N-{[3-nitro- 4-(tetrahydro-2H-pyran-4-ylamino)phenyl]sulfonyl}benzamide. ABT-199 analogue is in yellow bound to the BCL-2 binding groove. Sulphur is coloured yellow, oxygen is coloured blue and carbon is coloured white. Taken from (286).

BCL-XL is another anti-apoptotic that is frequently altered in cancer (287). BCL-XL overexpression occurs in solid tumours more often than BCL-2 overexpression (288). Sensitivity to chemotherapeutic agents was negatively correlated with BCL-XL

mRNA expression, using over 60 cancer cell lines (289). A BH3 mimetic, WEHI-539, has been developed that is a BCL-XL selective inhibitor (Figure 1.11) (290).

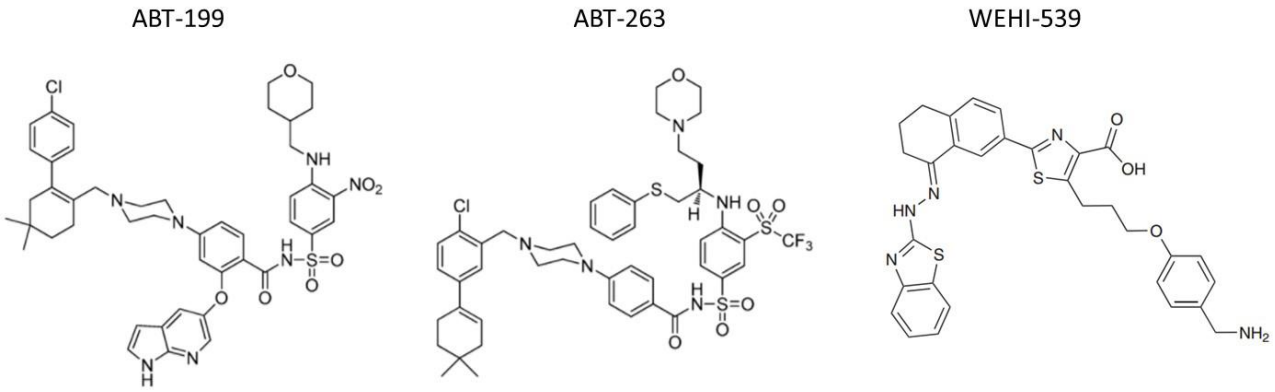

Figure 1.11: The structure of BH3 mimetics. The structure of ABT-199 (BCL-2 selective inhibitor), ABT-263 (BCL-2, BCL-XL, BCL-W inhibitor) and WEHI-539 (BCL-XL selective inhibitor). Taken from (290, 291).

1.10 Hypothesis

For this study, it was first hypothesised that targeting deregulated transcription as a whole may be more effective than targeting specific pathways for the treatment of ILC. In line with this, it was additionally hypothesised that, epigenetic modifiers which regulate gene transcription, may be a novel therapeutic option for the treatment of ILC breast cancer patients who do not respond to current modes of treatment.

1.11 Aims

The aim of this project was to first identify a novel therapeutic target in ILC. This was done using *in silico* gene expression data from two primary patient cohorts, namely the discovery cohort (RATHER dataset) and the validation cohort (METABRIC).

The second aim of this project was to investigate the therapeutic efficiency of inhibiting that target *in vitro* using a variety of functional assays in ILC cell line models.

The final aim of the project was to identify mechanisms of resistance to the therapeutic target using RNA sequencing followed by validation assays and identify combination treatment options.

Chapter Two: Materials and Methods

2.1 ILC patient cohorts

Paired-end RNA sequencing as has been previously described (292) was performed on 61 ILC patient samples as part of the EU FP7 project RATHER (www.RATHER.com) that formed the discovery cohort. For the RATHER samples, tumours were sourced from two biobanks using the Illumina HiSeq platform. RNA sequencing data from 99 ILC samples from the METABRIC dataset formed the validation cohort (36). Read pairs were aligned to the GRCh37 genome using TopHat (version 2.0.10), and quantified against the Ensembl 75 annotation using featureCounts (version 1.4.6). DESeq2 (version 1.6.3) was used to apply a regularised log transformation, and Limma (version 3.22.7) was used to remove batch effects associated with biobank. Survival analysis was carried out using the R survival package (version 2.38-3). Cox regression analysis on continuous expression was stratified by biobank. The expression of BRD2, BRD3 and BRD4 in the tumours was grouped into low- and high-expression categories (split by median expression value) for the purposes of category-based analysis. BRD2/3/4 association with recurrence-free survival (RATHER) or disease-specific survival (METABRIC) due to the number of events was carried out. Benjamini-Hochberg correction was applied independently to correct for the three genes under investigation.

2.2 Reagents and antibodies

JQ1 was a kind gift from the laboratory of Dr. James Bradner, while THZ1 was a kind gift from Dr. Nathanael Gray both at the Dana-Farber Cancer Institute, Harvard Medical School, USA. ABT-199, ABT-263 and BS-181 were purchased from Selleck Chemicals Houston, TX, USA. Tamoxifen and fulvestrant were purchased from Sigma-Aldrich St Louis, MO, USA.

For Western blotting, the antibodies that were used were: ER alpha 1:250 (Leica Biosystems, NCL-ER-6F11), E-cadherin 1:500 (Cell Signaling Technology (CST), 5296), PgR 1:250 (CST, 3157), BCL-2 1:500 (Santa Cruz, sc-7382), BCL-XL 1:1000 (CST, 2764), MYC 1:500 (Abcam, ab32072), PARP 1:1000 (CST, 9542), MCL1 1:500 (Santa Cruz, sc-819), BRD2 1:1000 (Atlas Antibodies, HPA042816), BRD3 1:1000 (Bethyl Laboratories, A302368A), BRD4 1:1000 (Bethyl Laboratories, A301-985A50), Wnt4 1:500 (Santa Cruz, sc-376279), Wnt11 1:1000 (Abcam, ab31962), Bim 1:1000 (CST, 2933), BCL-W 1:500 (CST, 2724), BAX 1:1000 (CST, 5023), BAK

1:1000 (CST, 12105), α/β tubulin 1:1000 (CST, 2148), β-actin 1:10,000 (Sigma-Aldrich, A5316, Santa Cruz, sc-81178). Secondary antibodies used were: anti-mouse immunoglobulins conjugated to horseradish peroxidase (HRP) (Dako, P026002-2) and anti-rabbit immunoglobulins conjugated to HRP (Dako, P039901-2).

For immunohistochemistry, the antibodies used were BCL-XL 1:300 (CST, 2764) and cleaved caspase 3 1:200 (CST, 9661).

For analysis of primary patient samples by flow cytometery all antibodies were used at a concentration of 1:100. These included EpCAM-APC (BD Bioscience, 347200), IgG-APC (BD Bioscience, 345818), CD45-PE (BD Bioscience, 555483) and IgG-PE (BD Bioscience, 555749).

2.3 Cell culture

The SUM44-PE, MDA-MB-134VI, OCUB-M and CAMA-1 cell lines were obtained from the RATHER consortium and were validated at the start of the project by short tandem repeat profiling, carried out by American Culture Collection. Cell lines were grown in RPMI supplemented with 10% FBS (Gibco, Thermo Fisher Scientific, Dublin, Ireland), 1% v/v L-glutamine (2 mM) (Gibco, Thermo Fisher Scientific, Dublin, Ireland) and 1% v/v penicillin/streptomycin (50 units/ml) (Gibco, Thermo Fisher Scientific, Dublin, Ireland) in a humidified atmosphere at 37°C and 5% CO_2. Prior to treatment with endocrine therapy, ILC cell lines were cultured in phenol red-free RPMI supplemented with 5% v/v charcoal/dextran treated FBS (Thermo Fisher Scientific, Dublin, Ireland), in addition to 1% v/v L-glutamine and penicillin/streptomycin as above for >48 hr. Mycoplasma testing was carried out routinely every 6-8 weeks using MycoAlert Mycoplasma Detection Kit (Lonza, Basal, Switzerland).

For the TNBC study, the BT549, MDA-MB-231, HCC1937, HS578T cell lines were originally purchased from the American Type Culture Collection and subsequently re-authenticated by short tandem repeat profiling with the European Collection of Authenticated Cell Cultures. The BT-20 & HCC1143 cell lines were a kind gift from Prof. Joe Duffy at Vincent's University Hospital, Dublin, Ireland. BT549, HCC1937, BT-20 and HCC1143 cells were maintained in RPMI cell culture medium. The MDA-MB-231 and HS578T cells were maintained in DMEM cell culture medium. Both cell

culture media were supplemented with 10% FBS, 1% L-glutamine and 1% penicillin/streptomycin.

2.4 MTT assay

Cell viability was assessed using 3-(4,5-dimethylthiazol-2-yl)-2,5diphenyltetrazolium bromide or MTT (Sigma-Aldrich Ltd., Arklow, Ireland). SUM44-PE, MDA-MB-134VI and MCF7 cells lines were seeded at a density of 5,000 cells/well in a 96-well plate in 200 µl media overnight at 37°C. The OCUB-M & CAMA-1 cell lines were seeded at a density of 6,000 cells/well. Cell lines were treated with 0.003 µM, 0.03 µM, 0.1 µM, 0.3 µM, 1 µM, 3 µM (fulvestrant only), or 0.03 µM, 0.1 µM, 0.3 µM, 1 µM, 3 µM and 10 µM of drug for tamoxifen, JQ1, ABT-199 and ABT-263 treatments. Cells were treated for either 72 hr (ABT-199 and ABT-263), 96 hr (JQ1) or 120 hr (tamoxifen or fulvestrant) prior to MTT analysis. For combination treatments of JQ1 and ABT-199 or ABT-263, cells were co-treated at the same time with both drugs for 72 hr. Following the specified time-point, 50 µl of sterile 5 mg/ml MTT solution was added to 200 µl of media to give a final concentration of 1.25 mg/ml in each well of a 96-well plate. The plate was placed in the incubator for 3 hours after which the media/MTT was aspirated off and 200 µl of dimethyl sulfoxide (DMSO) (Sigma-Aldrich Ltd., Arklow, Ireland) added to each well to dissolve formazan crystals. Absorbance was measured at 570 nm on a SpectraMax M2 plate reader.

For the TNBC study, the BT549 and MDA-MB-231 cell lines were seeded at a density of 2,000 cells/well in a 96 well plate overnight. The cells were treated with BS-181 (0.1 µM, 1 µM, 5 µM, 10 µM, 20 µM, 35 µM, 50 µM) or THZ1 (0.001 µM, 0.005 µM, 0.02 µM, 0.05 µM, 0.1 µM, 0.2 µM, 0.5 µM, 1 µM) for 72 hr prior to MTT analysis. For combination treatments in the HCC1143 (5,000 cells/well), HCC1937 (5,000 cells/well), BT-20 (3000 cells/well) and HS578T (5,000 cells/well) cell lines, cells were treated for 48 hr with the combination of THZ1 (0.001 µM, 0.002 µM, 0.05 µM, 0.1 µM) and ABT-263 (0.03 µM, 1 µM, 3 µM, 10 µM) at specified doses, prior to MTT analysis.

2.5 Apoptosis assay

Apoptosis was assessed using Annexin V-FITC/propidium iodide (PI) staining. SUM44-PE and MDA-MB-134VI cell lines were seeded at a density of 75,000

cells/well in 1 ml of media in a 24-well plate overnight at 37°C. The OCUB-M and CAMA-1 cell lines were seeded at 50,000 cells/well. Cell lines were treated with 0.03 µM, 0.1 µM, 0.3 µM, 1 µM, 3 µM and 10 µM JQ1 (96 hr) or ABT-199 (72 hr) or ABT-263 (72 hr). For combination treatments of JQ1 and ABT-199 or ABT-263, cells were co-treated at the same time with both drugs for 72 hr. Cells were trypsinised and centrifuged at 1300 rpm for 3 minutes. Each sample was re-suspended in: 250 µl of annexin binding buffer (10 mM Hepes pH 7.4, 140 mM NaCl, 2.5 mM CaCl2), 1 µl annexin V-FITC (0.25 mg/ml, Medical Supply Company Limited, Dublin, Ireland) and 0.5 µl PI (1 mg/ml, Sigma-Aldrich Ltd., Arklow, Ireland). Apoptosis was determined using flow cytometry on the BD FACSCanto II or the BD Accuri C6 (BD Bioscience, San Jose, California, USA) and analysed using the BD FACSDIVA or FCS Express software.

For the TNBC study, the BT549 cells (30,000 cells/well) and the MDA-MB-231 (40,000 cells/well) were seeded in 24-well plates overnight. Cells were treated with various doses of THZ1 (0.001 µM, 0.005 µM, 0.02 µM, 0.05 µM, 0.1 µM, 0.2 µM, 0.5 µM, 1 µM) or BS-181 (0.1 µM, 1 µM, 5 µM, 10 µM, 20 µM, 35 µM, 50 µM) for 48 hr prior to annexin V/PI staining and flow cytometry.

2.6 Cell cycle analysis

SUM44-PE and MDA-MB-134VI cell lines were seeded at a density of 75,000 cells/well in 1 ml of media in a 24-well plate overnight at 37°C. The OCUB-M and CAMA-1 cell lines were seeded at 50,000 cells/well. Cell lines were treated with 0.03 µM, 0.1 µM, 0.3 µM, 1 µM, 3 µM and 10 µM JQ1 for 96 hr. Cells were trypsinised and re-suspended in 1 ml phosphate buffer saline (PBS) (Sigma Aldrich Ltd., Arklow, Ireland). The cell suspension was supplemented with ethanol to a final concentration of 70% with agitation and incubated on ice for 15 minute to fix the cells. The fixed cells were then pelleted and re-suspended in 500 µl of PI-solution in PBS: 50 µg/ml propidium iodide (Sigma-Aldrich Ltd., Arklow, Ireland) from 50X stock solution (2.5 mg/ml), 0.1 mg/ml RNase A (SigmaAldrich Ltd., Dublin, Ireland), 0.05% Triton X-100, and incubated for 40 min at 37°C. 3 ml of PBS was then added to the sample and centrifuged at 1500 rpm for 5 minutes. The supernatant was removed and the cells were re-suspended in 500 µl PBS for flow analysis using the BD Accuri C6 and FCS Express software.

2.7 BH3 profiling

The cell membrane of cells was permeabilised using 0.005% digitonin followed by the addition of JC-1 mitochondrial fluorescent dye. BH3 peptides were plated in a black 384-well plate at 70 uM/L followed by cells at a concentration of 30,000 cells/peptide for the OCUB-M and CAMA-1 cell lines and at a concentration of 40,000 cells/peptide for the MDA-MB-134VI cell line. Mitochondrial potential was measured using the CLARIOstar (BMG LABTECH, Ortenberg, Germany) kinetic plate reader at excitation 545 nm and emission 590 nm over 2 hours. Kinetic measurements were taken every 5 minutes. Mitochondrial depolarisation was normalised to DMSO control. FCCP acts as a positive control. PUMA2A is a PUMA mutant and a negative control for the experiment.

2.7.1 iBH3 profiling

MDA-MB-134VI cells were treated with DMSO or 0.05 µM THZ1 for 16 hr followed by dynamic BH3 profiling. MDA-MB-231 cells were mixed with 0.005% of digitonin to permeabilise the cells and also with BH3 peptides at a concentration of 70 uM/L for 1 hour. The MDA-MB-231 cells were then fixed with 8% formaldehyde for 15 minutes prior to neutralization for 15 minutes. The cells were spun down at 1500 rcf for 5 minutes at RT and the cell pellet was resuspended in 50 µl of 1% BSA/PBS/0.05% saponin with 1:100 cytochrome *c* antibody conjugated to FITC and incubated at 4°C overnight. The loss of cytochrome *c* was measured by flow cytometry on a CyAn ADP Analyzer (Beckman Coulter). Mitochondrial depolarisation induced by the peptides was normalised to the DMSO control.

2.8 RNA extraction and quantification polymerase chain reaction

2.8.1 RNA extraction

The SUM44-PE cell line was seeded 750,000 cells per T25 flask, MDA-MB-134VI 900,000 cells per T25 flask, and the OCUB-M and CAMA-1 cell lines 500,000 cells per T25 flask overnight. The cell lines were then treated with 1 µM JQ1 for either 48 hr or 72 hr. Cells were harvested using TRI Reagent (Sigma-Aldrich Ltd, Arklow, Ireland) and RNA extracted using an in-house protocol. 300 µl of chloroform (Sigma-

Aldrich Ltd, Arklow, Ireland) was added to each sample and incubated at room temperature (RT) for 3 minutes. Samples were centrifuged at 14,000 rpm at 4°C for 20 minutes and the clear aqueous upper phase was transferred into a fresh Eppendorf tube. 500 µl of isopropanol (Sigma-Aldrich Ltd, Arklow, Ireland) was added to each sample. The sample was incubated at RT for 15 minutes followed by centrifugation at 14,000 rpm at 4°C for 15 minutes. Supernatant was removed and the RNA pellet was washed in 70% v/v ethanol and centrifuged at 9,500 rpm at 4°C for 5 minutes. The supernatant was removed, the pellet was air dried for 15-20 minutes and then re-suspended in nuclease free water (Thermo Fisher Scientific, Dublin, Ireland). RNA was quantified using the NanoDrop 2000 (Thermo Fisher Scientific, Waltham, MA, USA) and stored at -80°C.

2.8.2 cDNA synthesis

1 µg of RNA was diluted in nuclease-free water up to 7 µl. 1 µl of DNase 1 (1 U/µL) (Thermo Fisher Scientific, Dublin, Ireland) and 1 µl DNase 1 10X reaction buffer (Thermo Fisher Scientific, Dublin, Ireland) was added to each sample. The sample was mixed well and incubated at RT for 15 minutes. 1 µl of 25 mM Ethylenediaminetetraacetic acid (EDTA; Thermo Fisher Scientific, Dublin, Ireland) was added to each sample and incubated at 65°C for 10 minutes to inactivate DNase 1. 1 µl of random primers (50 ng/µL; Thermo Fisher Scientific, Dublin, Ireland) and 1 µl deoxynucleotide (dNTPs) (10 mM; Thermo Fisher Scientific, Dublin, Ireland) was added to each sample and incubated on ice for 5 minutes. 4 µl of Superscript II 5X reverse transcriptase reaction buffer (Thermo Fisher Scientific, Dublin, Ireland), 2 µl of Dithiothreitol (DTT; 100 mM) and 1 µl of RNase OUT (40 U/µL; Thermo Fisher Scientific, Dublin, Ireland) was added to each sample and pipetted up and down to mix well with the sample. Samples were incubated for 3 minutes at RT. 1 µl of Superscript II reverse transcriptase (200 U/µL; Thermo Fisher Scientific, Dublin, Ireland) was added to each sample and complementary DNA (cDNA) was synthesised by incubating the RNA at 42°C for 90 minutes and 70°C for 15 minutes in an Eppendorf Mastercycler Gradient Thermal Cycler (Eppendorf, Hamburg, Germany). cDNA was stored at -20°C.

2.8.3 Quantitative polymerase chain reaction

Quantitative polymerase chain reaction (qPCR) was performed using SYBR green reaction mixture real-time PCR master mix in duplicate. The qPCR reaction mixture consisted of 1 µl cDNA, 1.2 µl reverse primer (5 µM; Eurofins MWG, Kraainem, Belgium), 1.2 µl forward primer (5 µM; Eurofins MWG, Kraainem, Belgium), 10 µl 2X SYBR green PCR master mix (Applied Biosystems, Foster City, CA, USA) and 6.6 µl water. A master mix was generated for each cDNA sample and 20 µl pipetted in duplicate into a 96-well real time PCR plate and sealed with Microseal B adhesive seals. The plate was centrifuged at 4,000 rpm for 3 minutes at 4°C and samples were run on 7500 Real Time PCR System (Applied Biosystems, California, USA) using the following conditions: 95°C for 10 minutes followed by 40 cycles of 95°C for 15 seconds, 60°C for 1 minute and fluorescence was captured. Relative expression of target genes was determined by the 2-ΔΔCt method (58) and normalised to a GAPDH endogenous control. See table 2.2 for primer sequences.

Table 2.1: qPCR primer sequences

Gene Symbol	Forward (F)/ Reverse (R)	Sequence 5'-3'
ER	F	ATCCACCTGATGGCCAAG
	R	GCTCCATGCCTTTGTTACTCA
PgR	F	CGCGCTCTACCCTGCACTC
	R	TGAATCCGGCCTCAGGTAGTT
TFF1	F	CCCTCCCAGTGTGCAAATAAG
	R	GAACGGTGTCGTCGAAACAG
MYC	F	GGCTCCTGGCAAAAGGTCA
	R	CTGCGTAGTTGTGCTGATGT
BCL-XL	F	GAGCTGGTGGTTGACTTTCTC
	R	TCCATCTCCGATTCAGTCCCT
BCL-2	F	GGTGGGGTCATGTGTGTGG
	R	CGGTTCAGGTACTCAGTCATCC
BCL-W	F	GCGGAGTTCACAGCTCTATAC

	R	AAAAGGCCCCTACAGTTACCA
Wnt4	F	AGGAGGAGACGTGCGAGAAA
	R	CGAGTCCATGACTTCCAGGT
Wnt11	F	GGAGTCGGCCTTCGTGTATG
	R	GCCCGTAGCTGAGGTTGTC
β-catenin	F	AAAGCGGCTGTTAGTCACTGG
	R	CGAGTCATTGCATACTGTCCAT
TCF7L1	F	TCGTCCCTGGTCAACGAGT
	R	ACTTCGGCGAAATAGTCCCG
TCF7L2	F	AGAAACGAATCAAAACAGCTCCT
	R	CGGGATTTGTCTCGGAAACTT
PPARδ	F	CAGGGCTGACTGCAAACGA
	R	CTGCCACAATGTCTCGATGTC
LEF1	F	AGAACACCCCGATGACGGA
	R	GGCATCATTATGTACCCGGAAT
TCF7	F	CTGGCTTCTACTCCCTGACCT
	R	ACCAGAACCTAGCATCAAGGA
Wnt9a	F	AGCAGCAAGTTCGTCAAGGAA
	R	CCTTCACACCCACGAGGTTG
Cyclin D	F	GCTGCGAAGTGGAAACCATC
	R	CCTCCTTCTGCACACATTTGAA
GAPDH	F	ATGGGGGAAGGTGAAGGTCG
	R	GGGGTCATTGATGGCAACAAT

2.9 Sodium Dodecyl Sulfate Polyacrylamide Gel Electrophoresis and Western blotting

For the 48 hr and 72 hr 1 μM JQ1 treatments, the SUM44-PE cell line was seeded 750,000 cells per T25 flask, MDA-MB-134VI 900,000 cells per T25 flask, and the OCUB-M and CAMA-1 cell lines 500,000 cells per T25 flask. For siRNA knockdown experiments the MDA-MB-134VI cell line was seeded 300,000 cells/well, and the OCUB-M and CAMA-1 cell lines were seeded 500,000 cells/well in a 6-well plate.

2.9.1 Protein extraction

Cells were trypsinised and centrifuged at 1300 rpm for 3 minutes to pellet the cells. The supernatant was removed and cells were re-suspended in 1 ml of cold PBS. The cell suspension was centrifuged at 11,000 rpm for 1 minute. PBS was removed and cells were re-suspended in 50 µl of RIPA lysis buffer (50 mM Tris pH 7.4, 150 mM NaCl, 1% Triton X-101, 1 mM EDTA, Triton X-100) supplemented with 1X protease inhibitors (Sigma-Aldrich Ltd., Dublin, Ireland). The cells were vortexed in the lysis buffer and incubated on ice for 30-40 minutes.

2.9.2 Protein quantification

Protein quantification was done using a bicinchoninic acid (BCA) protein assay (Pierce, Illinois, USA). 25 µl of bovine serum albumen (BSA) protein standards were pipetted into a 96-well plate in triplicate. 24 µl of dH_2O was pipetted into separate wells in triplicate followed by 1 µl of protein to be quantified. 200 µl of BCA working reagent (1:50 ratio of reagent B: reagent A) was pipetted on top of the 25 µl in each well followed by incubation at 37°C for 30 minutes. Absorbance was measured at 570 nm on a SpectraMax M2 plate reader.

2.9.3 Sodium dodecyl sulfate polyacrylamide gel electrophoresis

Protein samples were prepared in a total volume of 15 µl with 15-25 µg of protein, 5 µl of NuPAGE LDS sample buffer (Thermo Fisher Scientific, Dublin, Ireland), 2 µl of β-mercaptoethanol (Sigma-Aldrich Ltd, Arklow, Ireland) and dH_2O. Samples were boiled at 100°C for 5 minutes and then cooled on ice. 8-10% sodium dodecyl sulfate (SDS)-polyacrylamide gels were prepared in a Bio-Rad Mini Trans-Blot Cell (Bio-Rad Laboratories, Hercules, CA, USA) and filled with 1X running buffer (1 litre solution: 3.03 g Tris base, 14.4 g glycine, 1 g SDS, dH_2O). 4 µl of PageRuler Prestained Protein Ladder Plus (Thermo Fisher Scientific, Dublin, Ireland) was loaded in the first well of the gel followed by 15 µl of the prepared protein sample in subsequent wells. Sodium dodecyl sulfate polyacrylamide gel electrophoresis (SDS-PAGE) was run at 90 V for 15 minutes followed by 120 V for approximately 1 hour.

2.9.4 Western blotting

Following SDS-PAGE, the gel was transferred to a PVDF membrane (Bio-Rad, Munich, Germany) using a transfer sandwich comprising sponge, 2 x whatman filter papers, PVDF membrane, gel, 2 x whatman filter paper and sponge in a transfer cassette. Everything was kept wet with 1X transfer buffer (1 litre solution: 3.03 g Tris base, 14.26 g glycine, 200 ml methanol, dH_2O) and the transfer cassette was put in a Bio-Rad Trans-Blot Cell (Bio-Rad Laboratories, Hercules, CA, USA). The Bio-Rad Trans-Blot Cell was also filled with 1X transfer buffer. Western blotting was carried out using 300 mA for 3 hours in the cold room and in a bucket filled with ice to keep the transfer cold. The membrane was washed with 1X TBST (For 1 litre solution: 6.05 g Tris base, 8.76 g NaCl, dH_2O, pH 7.5) and blocked with 5% milk in 1X TBST for 1 hour at RT before antibody probing. Membranes were incubated in primary antibody overnight at 4°C. Membranes were then washed 3 x 5 minutes in 1X TBST followed by incubation in HRP-linked secondary antibody (Dako, Glostrup, Denmark) for 2 hours at RT. Membranes were then washed again for 3 x 5 minutes. Membranes were developed using Enhanced Chemiluminescence Western Blotting Substrate Kit (Thermo Fisher Scientific, Dublin, Ireland) and signal was captured using the Amersham Imager 600 (GE Healthcare Life Sciences, Buckinghamshire, UK) or films (Fuji SuperRX film, Fuji, Tokyo, Japan) and fixer/developer.

2.10 Small interfering RNA knockdown

Cells were transfected with i) non-targeting negative control, BRD2, BRD3 or BRD4 ON-TARGETplus small interfering RNA (siRNA) SMARTpool or ii) non-targeting siRNA control #1, Wnt11 siRNA #1, Wnt11 siRNA #2, Wnt11 siRNA #3, Wnt4 siRNA #1, Wnt4 siRNA #2, Wnt4 siRNA #3 ON-TARGETplus siRNA (Dharmacon, GE Healthcare Life Sciences, Buckinghamshire, UK) using Lipofectamine 2000 (Thermo Fisher Scientific, Dublin, Ireland) according to the manufacturer's guidelines. siRNA was transfected at a concentration of 100 pmol for western blotting and at 5 pmol for MTT assay for SMARTpool siRNAs (BRD2, BRD3, BRD4 proteins). siRNA was transfected at a concentration of 200 pmol for western blotting and at 40 pmol for annexin V/PI analysis for ON-TARGETplus siRNA (Wnt11, Wnt4 protein). The MDA-MB-134VI cell line was seeded 300,000 cells/well, and the OCUB-M and CAMA-1 cell lines were seeded 500,000 cells/well in a 6-well plate followed by SDS-PAGE

and western blotting 48 hr (BET proteins) or 72hr (Wnt11, Wnt4) post siRNA knockdown. For MTT assay, the MDA-MB-134VI cell line was seeded at 20,000 cells/well in a 96-well plate and the OCUB-M and CAMA-1 cell lines seeded at a density of 3,500 cells/well. siRNA knockdown was carried out for 48 hr, 50 µl of RPMI (supplemented with 1% FBS, 1% L-glutamine, 1% penicillin/streptomycin) was added to each well, followed by another 48 hr or 96 hr and MTT assay performed. For annexin V/PI assay, the CAMA-1 cell line was seeded at 60,000 cells/well in a 24-well plate and siRNA knockdown was carried out for 72 hr followed by 1 µM JQ1 treatment for a further 72 hr.

2.11 RNA Sequencing of ILC cell lines

The SUM44-PE cell line was seeded at a density of 4 million cells and the MDA-MB-134VI seeded at a density of 5 million cells in T75 flasks and treated for 48 hr with 1 µM JQ1. RNA was extracted as previously described and cleaned using RNeasy Mini Kit (Qiagen, Manchester, UK). RNA was quantified using NANODROP 1000 (Mason Technology, Dublin, Ireland) and quality was validated using bioanalyser (Agilent Technologies, Cork, Dublin). 100 ng RNA was used for library preparation. Libraries were prepared as per manufacturing instructions using TruSeq Stranded mRNA Library Prep Kit for NeoPrep (Illumina, Cambridge, UK). Paired-end RNA sequencing was carried out using the NEXTseq 500 Sequencing System (Illumina, Cambridge, UK).

2.11.1 Data preparation

Paired-end data was downloaded using the BaseSpaceFastqDownload tool from Illumina BaseSpace, as fastq files. The fastq files were quality assessed following FastQC. In the event that a single sample had multiple fastq files, these were concatenated using the ‘cat’ command in Unix shell. Data was trimmed using the BBDuk tool in the BBMap package in order to remove any sequencing adapters and poor quality base calls (Phred score < 20) before alignment.

2.11.2 Alignment and processing

The sequencing data was aligned using STAR version 2.5.2a to the human hg19/GRCh37 reference (293), which produced a BAM file (sorted by coordinate). Duplicate reads were marked in the BAM file using Picard-Tools ‘MarkDuplicates’

call. The featureCounts tool from the SubRead package produced read counts (294). The read counts were combined for the samples and used as input for differential gene expression analysis.

2.11.3 Differential expression

Differential expression analysis was carried out using the DESeq2 package (295) in the R statistical environment (296). The data.frame of counts had all genes with a sum of zero across all samples removed. A ‘conditions’ data.frame was created based on treatment condition, biological replicate and the cell line. The counts and conditions data.frames were loaded into a DESeq2DataSet class object using the DESeqDataSetFromMatrix() call, with the design variable set as ‘~ group’. The DESeq() call produced two sets of results, based on SUM44-PE or MDA-MB-134VI cell lines, comparing the 1 µM JQ1 treatment to the control DMSO treatment for the cell line. Four text files resulted, containing each gene expressed, the log2FoldChange value and the false discovery rate (FDR) adjusted p-value. Fragments-per-kilobase per million reads (FPKMs) were produced using the edgeR package (297) rpkm() call. Heatmaps of the top 200 DE genes were produced using Perseus software (298) and gene ontology analysis was carried out using the DAVID functional annotation tool (299, 300). A principal component analysis plot was generated to determine the data quality and consistency.

2.12 3-Dimensional cell culture

In a 12-well plate, 200 µl of matrigel (VWR, Dublin, Ireland) was pipetted per well, spread using the bottom of a sterile p200 tip and incubated at 37°C for 15 minutes to allow the matrigel to set. 30,000 cells/well in 2% matrigel/RPMI of either the SUM44-PE or MDA-MB-134VI cell lines was added on top of the matrigel, followed by a further incubation at 37°C for 20 minutes. 500 µl of 2% matrigel/RPMI was then added on top of the cells in each well. Cells were incubated overnight at 37°C followed by drug treatment for 72 hr. Media was changed twice weekly and each condition was imaged on Day 1, Day 8 and Day 15. On Day 15, 4 µM Calcein AM (Thermo Fisher Scientific, Dublin, Ireland) in serum-free RPMI media was added to a 15 ml falcon tube, mixed well, and incubated at 37°C for 15 minutes. Media was then removed from the 3-dimensional (3D) cultures and 1 ml of Calcein AM/RPMI mix was added/well for 30 minutes at 37°C prior to imaging.

2.13 *Ex vivo* culture and analysis of ILC primary samples and patient derived xenografts

The ILC primary patient samples T509 and T638 (from, which the patient-derived xenograft (PDX) was formed) were obtained in collaboration with Prof. Leonie Young at RCSI and sourced from Beaumont Hospital, Dublin, Ireland. Informed consent from all eligible patients was received and the study was approved by Institutional Review Boards from Royal College of Surgeons IRB #13/09; ICORG 09/07. The T509 primary tumour was resected during surgery and was treatment naïve. The T638 PDX was established by the Prof. Leonie Young laboratory at RCSI. The ILC T638 primary tumour was treated with chemotherapy, radiation therapy and tamoxifen and had relapsed and metastasised to the bone and brain. The ILC PDX was established from brain metastasise that were successfully engrafted as a PDX and then grown and expanded in nonobese diabetic/severe combined immunodeficiency (NOD-SCID) mice. Primary tumours from the PDX established from the ILC metastatic tumour was resected after 1-month growth to 150 mm^3 and were at passage 2.

2.13.1 *Ex vivo* culture of primary ILC samples

A piece of dental sponge (Spongostan, Johnson & Johnson) was placed in each well of a 24-well plate. 1 ml of HBEC media (Hyclone DMEM/F12 with HEPES, 10 mM HEPES, 5% FBS, 1 mg/ml BSA, 1 µg/ml insulin, 0.5 µg/ml hydrocortisone, 50 µg/ml gentamycin, 2.5 µg/ml fungizone) containing desired drug concentration was added on top of the sponge. The sponges were then allowed to soak at 37°C for 1 hr in incubator. Following soaking, a viably frozen ILC PDX (T638) or a ILC primary patient sample (T509) was thawed, washed several times with HBEC media to remove any residual DMSO from freezing media and cut into small pieces. The small tumour pieces were placed on top of the dental sponge soaked with HBEC media and desired drug concentration. After 48 hr or 72 hr, the primary patient tumour sample or the ILC PDX was analysed by flow cytometry or immunohistochemistry.

2.13.2 Antibodies used for flow cytometry analysis of ILC primary patient sample and PDX

Antibodies used to analyse the T638 ILC PDX and T509 primary sample following *ex vivo* culture were the control antibodies IgG-PE and IgG-APC, as well as CD45-PE and EpCAM-APC. All antibodies were used at a concentration of 1:100. CD45-PE antibody was used for the ILC primary patient sample (T509) in order to detect any white blood cells (301), which were omitted from the flow cytometry analysis. EpCAM-APC was used as a positive marker for selection of epithelial tumour cells (302) in the ILC PDX tumour (T638) as the PDX tumour was CD45 negative. EpCAM positivity was validated in ILC cell lines prior to staining the T638 ILC PDX sample. Likewise, CD45 positivity was validated in the Jurkat leukemic cell line and CD45 negativity was validated in ILC cell lines prior to performing flow analysis on the T509 primary ILC sample.

2.13.3 Tumour pieces into single cell suspension

After *ex vivo* culture for 48 hr or 72 hr in drug, tumour was removed from sponge and placed in 1 ml of RPMI media (supplemented with 10% FBS, 1% L-glutamine and 1% penicillin/streptomycin) in a 10 cm dish. The tumour was minced into small pieces using a scalpel (Fisher Scientific, Dublin, Ireland) in the media. The tumour was also pipetted up and down vigorously using a p1000 pipette. The tumour was centrifuges at 1300 rpm for 3 minutes and the media aspirated off. The tumour was digested using 1 ml of 1 mg/ml of collagenase/dispase (Sigma-Aldrich Ltd., Dublin, Ireland) for 1 hour at 37°C. The tumour cells were spun down at 1300 rpm for 3 minutes and re-suspended in fresh RPMI media. A 40 µm cell strainer (Sigma-Aldrich Ltd., Dublin, Ireland) was placed on top of a 6-well plate for each tumour sample and tumour cells were pushed gently through the filter using the top of a 1 ml syringe plunger. The strainer was then washed with a further 500 µl of RPMI to collect any remaining tumour cells in the cell strainer. The cells were collected using a p1000 and placed in an Eppendorf tube. Tumour cells were centrifuged at 0.5 rcf for 5 minutes.

2.13.4 Flow cytometry analysis of single cell suspension

Tumour cells were washed in 1 ml PBS (Sigma-Aldrich Ltd., Dublin, Ireland) and centrifuged at 1300 rpm for 3 minutes. PBS was aspirated off the cells and re-suspended in 100 µl FACS buffer (100 ml solution: 1 ml FBS, 400 µl EDTA (0.5 M), 100 ml PBS, pH 7.4). 1 µl of FCR block (BD Biosciences, Oxford, England) was added to each sample and the cells were incubated on ice for 10 minutes. 1 µl of antibody (1:100 dilution) was then added and the samples were incubated on ice for 30 minutes in dark. Tumour cells were centrifuged for 5 minutes at 0.5 rcf and re-suspended in 250 µl of annexin binding buffer. 1.39 µl of annexin V-FITC ((0.25 mg/ml, Medical Supply Company Limited, Dublin, Ireland) was added to each sample and mixed well. Flow cytometry was carried out using the BD FACSCanto II and BD FACSDIVA software.

2.13.5 Immunohistochemistry analysis of ILC T638 PDX

The T638 ILC PDX tumour was also analysed by immunohistochemistry (IHC) after 72 hr drug treatment *ex vivo*. The ILC PDX tumour pieces were fixed using 10% formalin overnight. After tumour fixation for >12 hours, the tumour pieces were placed in individual embedding cassettes and submerged in 70% ethanol for at least 24 hr. Tumour tissue was processed in the tissue processor and embedded in paraffin. 5-micron thick tissue sections were cut from the paraffin embedded blocks and mounted on slides. Tissue was baked for 8 hr at 65°C prior to haematoxylin and eosin (H & E) or immunohistochemistry (IHC) staining. These methods were adapted from previous publications (303-305).

2.13.6 Haematoxylin and Eosin staining

Slides were deparaffinised using xylene (Sigma-Aldrich Ltd., Arklow, Dublin) for 2 x 3 minutes; then rehydrated with 100% industrial methylated spirits (IMS) (2 x 3 minutes) and 70% IMS (3 minutes); followed by washing with PBS (Sigma-Aldrich Ltd., Arklow, Dublin) for 5 minutes. Slides were stained with haematoxylin (Sigma-Aldrich Ltd., Arklow, Dublin) for 3 minutes and washed with tap water for 5 minutes. Slides were then stained with eosin (Sigma-Aldrich Ltd., Arklow, Dublin) for 5 minutes, and washed in tap water by dipping the slide in and out of the water multiple times. Slides were then washed in 70% IMS, followed by dehydration with

70% IMS (3 minutes) and 100% IMS (2 x 3 minutes) and clearing with xylene for 2 x 3 minutes. Slides were allowed to dry and then mounted with DPX mountant (Sigma-Aldrich Ireland Ltd., Arklow, Ireland) and coverslip.

2.13.7 Immunohistochemistry

Slides were deparaffinised using xylene (Sigma-Aldrich Ltd., Arklow, Dublin) for 2 x 3 minutes; then rehydrated with 100% IMS (2 x 3 minutes) and 70% IMS (3 minutes); followed by washing with PBS (Sigma-Aldrich Ltd., Arklow, Dublin) for 5 minutes. Antigen retrieval was carried out by placing the slides in sodium citrate (Sigma-Aldrich Ltd., Arklow, Dublin) and microwaving for 8 minutes on high power, followed by cooling on bench for 20 minutes. Slides were washed in TBST (2 x 5 minutes). Peroxidase blocking solution was added to the tissue for 5 minutes followed by washing in dH_2O for 5 minutes (Dako Envision+ System HRP (DAB) Kit, Agilent Technologies UK Limited, Cheshire, UK). Primary antibody in antibody diluent (0.05 mol/l Tris-HCl (pH 7.2-7.6) containing 1% BSA) was applied for 1 hr 30 min at RT followed by 3 x 5 minute washes with TBST. Secondary antibody was applied for 30 minutes at RT (Dako Envision+ System HRP (DAB) Kit, Agilent Technologies UK Limited, Cheshire, UK) followed by 3 x 5 minute washes with TBST. DAB+ substrate (Dako Envision+ System HRP (DAB) Kit, Agilent Technologies UK Limited, Cheshire, UK) was added for 5-10 minutes on the tissue followed by washing with dH_2O for 5 minutes to stop the reaction. Slides were counter-stained for 3 minutes using haematoxylin (Sigma-Aldrich Ltd., Arklow, Dublin) at RT. Slides were then washed with tap water for 5 minutes followed by tissue dehydration (70% IMS (3 minutes) and 100% IMS (2 x 3 minutes)) and clearing (xylene for 2 x 3 minutes). Slides were allowed to dry and then mounted with DPX mountant (Sigma-Aldrich Ltd., Arklow, Dublin) and coverslip.

2.14 Statistical analysis

Kaplan-Meier and univariate continuous cox regression analysis was used to determine the effect BRD2/3/4 expression had on recurrence-free survival or disease-specific survival, with a log-rank test determining significance. Differential expression from the RNA sequencing data following 1 µM JQ1 was determined using DESeq2 that uses the Wald test to determine statistical significance. Non-linear regression analysis was used to plot dose-response curves. One-Way Analysis of

Variance (ANOVA) was used to compare the mean of three or more independent groups to determine statistical significance. Two-Way ANOVA was used to test statistical significance between two groups that have been divided on two independent variables. A student's t-test was used to test for statistical significance by comparing the mean of two independent groups. All data, unless stated otherwise, shows +/- standard error of the mean (SEM) from three independent experiments (N=3). GraphPad prism was used to calculate statistics. * denotes p is ≤0.05, ** denotes p is ≤0.01, *** denotes p is ≤0.001 and **** denotes p is ≤0.0001.

Chapter Three: Identification of a Novel Therapeutic Target in ILC

3.1 Introduction

3.1.2 Epigenetic regulation of ILC

ILC represents an understudied subtype of breast cancer and has limited available resources. The majority of ILC breast cancer are ER positive and treated with endocrine therapy (75, 80). Resistance to endocrine therapy is a major problem in the treatment of ILC. One in three women are de novo resistant to endocrine therapies, 40% of patients will relapse on endocrine treatment (151, 152) and furthermore some studies have suggested that ILC may do worse on endocrine therapy (155, 156). ILC tumours also have been reported to have poor response to chemotherapy (157). In order to identify novel therapeutic targets for the treatment of ILC, RNA sequencing data from two independent cohorts was analysed by Dr. Finbarr Tarrant (University College Dublin, Ireland). The cohorts comprised the RATHER discovery dataset that harbours 61 primary ILC patient samples and the METABRIC validation dataset composed of 99 primary ILC patient samples. From this analysis, the epigenetic protein BRD3 was identified as being associated with poor survival in ILC. BRD3 is a member of the BET family of chromatin readers that regulate gene transcription. Other members of the BET family are BRD2, BRD4 and BRDT (175), with BRDT expression restricted to the testis (176). BET proteins bind acetylated lysine residues on nucleosomal histones through their tandem bromodomains and recruit transcription factors and chromatin modifying enzymes to gene promoters and enhancers (180-182). BET protein functions are thought to be redundant due to sequence homology (191) but very little research has been done on the precise roles of these proteins, particularly BRD3. BRD3 has been reported (along with BRD2) to facilitate RNA polymerase II gene transcription (190). BRD3 is also recruited to chromatin by acetylated GATA1 and binds acetylated GATA1 via its BD1 domain, in order to promote erythroid maturation (306).

3.2 Aims of chapter 3

The aims of this chapter was to first test the sensitivity of a panel of ILC cell lines to the endocrine therapies tamoxifen and fulvestrant *in vitro*. Once this was established the sensitivity of the ILC cell lines to BET inhibition using JQ1 was measured, in order to compare endocrine treatment to BET inhibition. The effects of JQ1 on

common growth promoting genes was also assessed in the ILC cell lines. Finally, the BET proteins responsible for sensitivity to JQ1 were identified.

3.3 Results

3.3.1 BRD3 is associated with poor survival in ILC using a discovery cohort of 61 primary ILC samples

As part of the EU FP7 project RATHER (www.ratherproject.com), paired-end RNA sequencing was carried out on 61 primary ILC patient samples using the Illumina HiSeq platform to determine if altered expression of genes was associated with survival in ILC. This cohort of ILC patient tumours had accompanying clinical data with 6.8 years' median clinical follow-up. Gene expression was grouped into low and high expression based on the median value and continuous cox regression analysis was performed to determine recurrence-free survival in ILC (Figure 3.1). From this analysis the BET protein BRD3, but none of the other BET family of proteins, was significantly associated with poor recurrence-free survival in ILC (p-value: 0.0306, Hazard ratio: 8.6261, CI 95%: 1.2228 - 60.85) (Figure 3.1). This result suggests that BRD3 may have a role in ILC tumorigenesis.

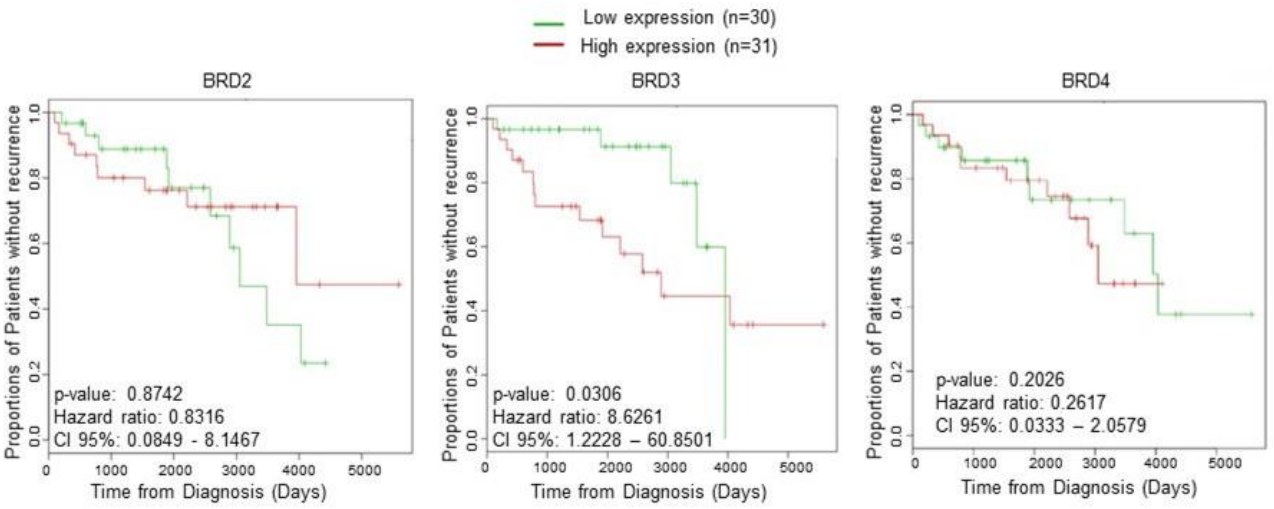

Figure 3.1: BRD3 is associated with poor recurrence-free survival in a ILC patient discovery cohort. Kaplan Meier curves showing the association of BRD2, BRD3 and BRD4 mRNA expression with recurrence-free survival in ILC primary patient samples (n=61) from the RATHER discovery cohort using continuous cox regression analysis. BRD3 was the only BET family member to be associated with poor survival in ILC. This analysis was carried out by a bioinformatician Dr. Tarrant (University College Dublin, Ireland). CI 95%= 95% confidence interval.

3.3.2 BRD3 is associated with poor survival in ILC in the METABRIC validation cohort of 99 primary ILC samples

To validate these findings, the association of BRD3 with survival in RNA sequencing data from 99 ILC patient samples was assessed from the total 2,000 patient samples analysed, as part of the METABRIC dataset (36). There were not sufficient events to calculate recurrence-free survival, therefore disease-specific survival was used. The expression of the BET family of proteins was again grouped into low and high expression based on the median value and continuous cox regression analysis was performed to determine disease-specific survival in ILC (Figure 3.2). In line with the RATHER discovery cohort, BRD3, but none of the other BET family proteins was associated with poor disease-specific survival in ILC (p-value: 0.0159, Hazard ratio: 3.1562, CI 95%: 1.2402 - 8.0324) (Figure 3.2).

This data from both the discovery and validation cohort (Figure 3.1, 3.2) suggest that BRD3 may play a significant role in tumour progression in ILC and that BRD3 may be a novel therapeutic target for ILC.

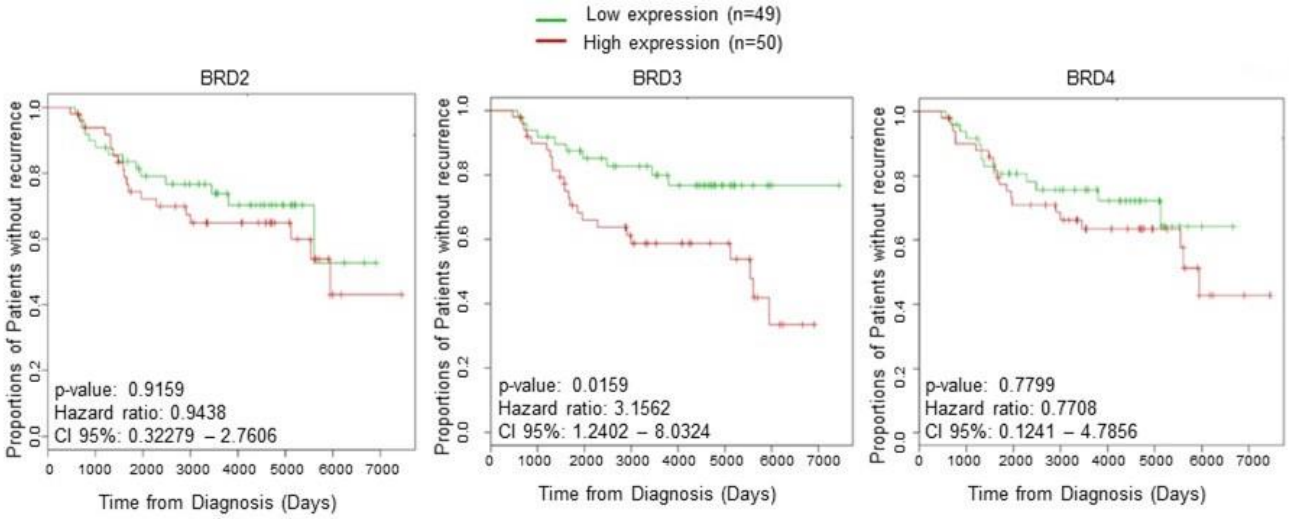

Figure 3.2: BRD3 is associated with poor disease-specific survival in a ILC patient validation cohort. Kaplan Meier curves showing the association of BRD2, BRD3 and BRD4 mRNA expression with disease-specific survival in ILC primary patient samples (n=99) from the METABRIC validation cohort using continuous cox regression analysis. BRD3 was the only BET family member to be associated with poor survival in ILC. This analysis was carried out by Dr. Finbarr Tarrant (University College Dublin, Ireland). CI 95%= 95% confidence interval.

3.3.3 BRD3 is not associated with poor survival in breast cancer as assessed by BreastMark

It was identified that high expression of BRD3 was associated with poor survival in ILC in both the RATHER and METABRIC cohorts (Figure 3.1, 3.2). Next it was sought to ensure that high expression of BRD3 was not associated with poor survival in breast cancer as a whole. For this purpose, the BreastMark online algorithm tool was used that has gene expression data and survival data for 4, 738 breast cancer samples (http://glados.ucd.ie/BreastMark/) (307). High expression of BRD3 was not associated with poor disease-free survival (DFS) in breast cancer (p: 0.6183, Hazard ratio: 1.032, CI 95%: 0.9107 – 1.17) (Figure 3.3). Likewise, high expression of BRD2

was not associated with poor DFS in breast cancer (p: 0.2649, Hazard ratio: 1.07, CI 95%: 0.9501 – 1.205) and neither was BRD4 (p: 0.5722, Hazard ratio: 0.9664, CI 95%: 0.8583 – 1.088) (Figure 3.3). These results suggest that the previous findings, that high expression of BRD3 is associated with poor survival in ILC, was specific to ILC as this finding is not seen in breast cancer as a whole (Figure 3.3)

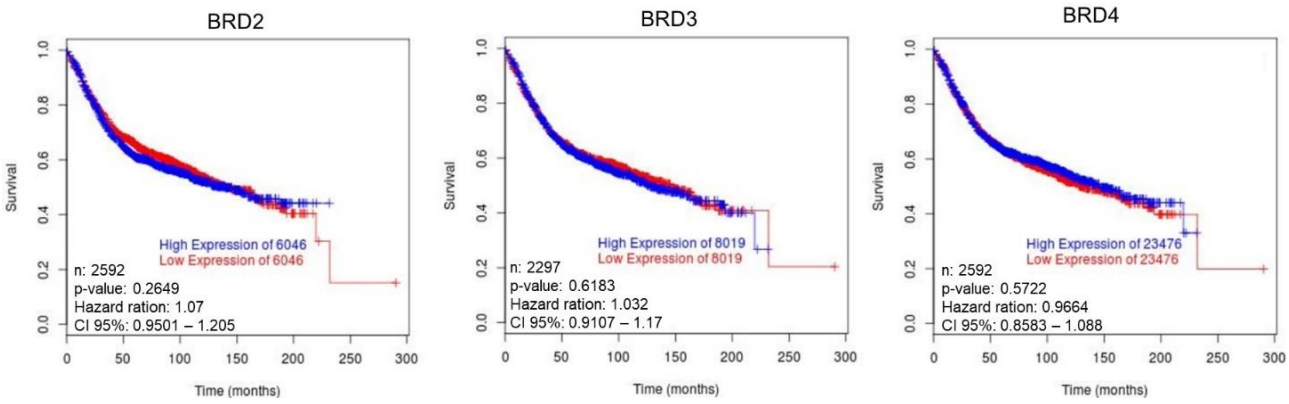

Figure 3.3: BRD3 is not associated with poor disease-free survival in breast cancer as a whole. Kaplan Meier curves showing the association of BRD2 (n=2592), BRD3 (n=2297) and BRD4 (n=2592) mRNA expression with disease-free survival in breast cancer patients using the BreastMark online algorithm tool (307). Neither BRD2, BRD3 or BRD4 were associated with poor survival in breast cancer patients with luminal A, luminal B, HER2 and basal-like breast cancer subtypes. CI 95%= 95% confidence interval.

3.3.4 Characterisation of ILC cell lines

There is an insufficiency of ER-positive ILC cell lines for use in pre-clinical studies (73). Therefore, for this study, the only two widely available true ER-positive ILC cell lines SUM44-PE and MDA-MB-134VI and two 'ILC-like' cell lines OCUB-M and CAMA-1 were chosen (Figure 3.4; Table 3.1). All of the ILC cell lines are negative for E-cadherin, which is characteristic of ILC and three out of four ILC cell lines are positive for the expression of the ER (Figure 3.4; Table 3.1).

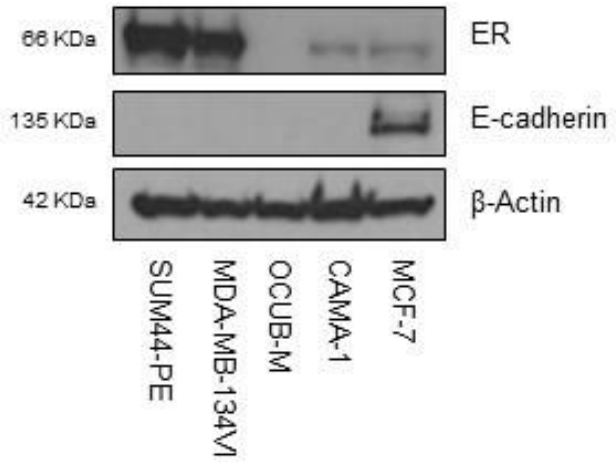

Figure 3.4: Characterisation of ILC cell line models. Representative western blots showing the expression of ER and E-cadherin in the panel of ILC cell lines used in this study. The experiment was done in biological duplicate and β-Actin is shown as a loading control.

Additionally, the SUM44-PE and CAMA-1 cell lines are positive for PgR expression (Table 3.1) (93, 308). Furthermore, all ILC and 'ILC-like' cell lines used in this study display a round cellular phenotype, lack HER2 and have E-cadherin mutations (Table 3.1) (93, 308-314).

Table 3.1: Characteristics of ILC and 'ILC-like' cell lines used in this study. The table shows the tissue of origin, tumour, phenotype, ER/PgR/HER2/E-cadherin status, as well as E-cadherin mutation status. The table was populated based on observations from this study and the literature (93, 308-314). It has been reported that the CAMA-1 cell line expresses E-cadherin protein, but the E-cadherin protein is truncated and non-functional due to a in frame mutation (313). E-cadherin protein expression was not detected in this study. Table was adapted from (93, 308-314).

Cell line	Tissue	Tumour	Phenotype	ER	PgR	HER2	E-cadherin	E-cadherin mutation
SUM44-PE	Breast	ILC	Round	+	+	-	-	Protein truncating
MDA-MB-134VI	Breast	ILC	Round	+	-	-	-	Protein truncating
OCUB-M	Breast	Carcinoma	Round	-	-	-	-	Protein truncating
CAMA-1	Breast	Carcinoma	Round	+	+	-	-	In frame

JQ1 is an inhibitor that targets BRD3, as well as the other BET family proteins in the breast tissue (BRD2 and BRD4) (195). As JQ1 targets all BET family members, the expression of BRD2, BRD3 and BRD4 was measured in the panel of ILC cell lines. BRD2, BRD3 and BRD4 were expressed in all ILC cell lines used in this study (Figure 3.5a). BRD2 is significantly expressed to a greater extent in the MDA-MB-134VI cell line ($p \leq 0.01$) compared the SUM44-PE, OCUB-M and CAMA-1 cell lines (Figure 3.5b). BRD3 appears to have higher expression in the MDA-MB-134VI and OCUB-M cell lines compared to the SUM44-PE and CAMA-1 cell lines, although this is not statistically significant (Figure 3.5b). Likewise, BRD4 appears to have higher expression in the MDA-MB-134VI and CAMA-1 cell lines compared to the SUM44-PE and CAMA-1 cell lines, however this is not statistically significant (Figure 3.5b).

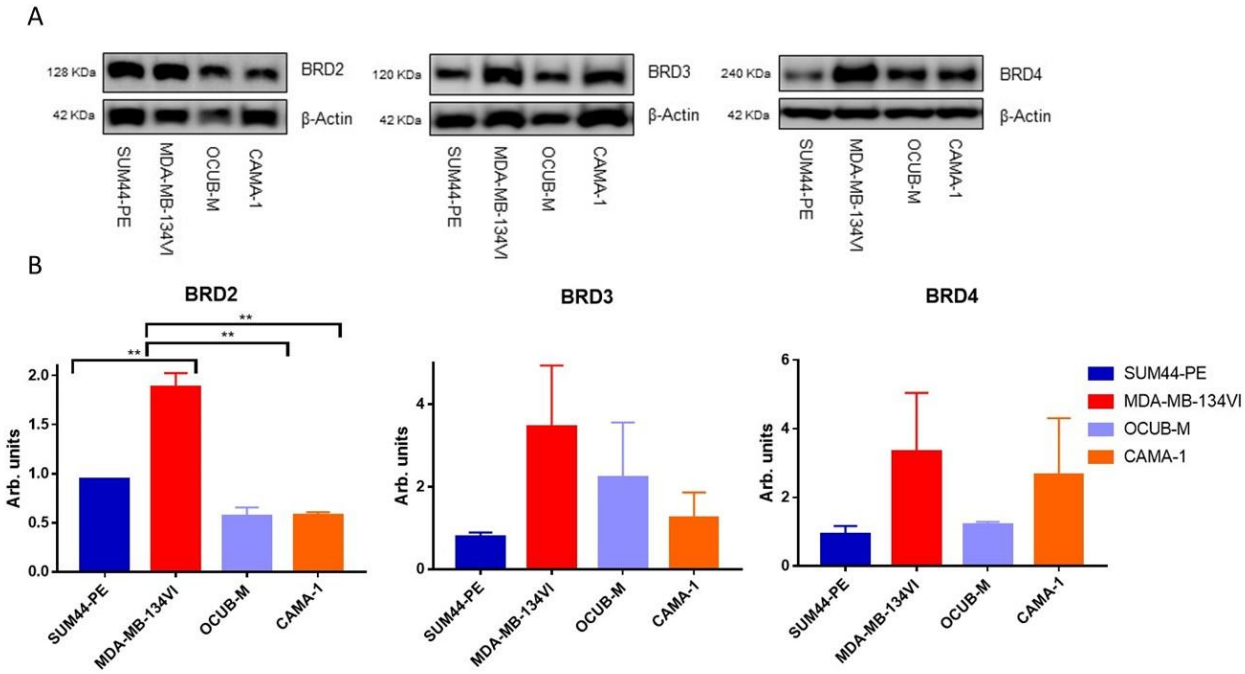

Figure 3.5: The panel of ILC cell lines express BRD2, BRD3 and BRD4. (A) The western blots show the expression of BRD2, BRD3 and BRD4 in the panel of ILC cell lines. The experiment was repeated two times and representative blots are shown. β-Actin is shown as a loading control. (B) Densitometry for the expression of BRD2, BRD3 and BRD4 in the cell lines is shown. Error bars show +/- standard error of the mean (SEM). Asterisks indicates significance using One-Way Analysis of variance (ANOVA) $p \leq 0.05$.

3.3.5 ILC cell lines are relatively insensitive to endocrine therapy *in vitro*

The majority of ILC are ER positive and are therefore treated with endocrine therapy (75, 80). Hence, the sensitivity of the ER-positive cell lines from the ILC panel (SUM44-PE, MDA-MB-134VI and CAMA-1) to endocrine therapies was assessed. The cell lines were treated with either tamoxifen or fulvestrant (Figure 3.6) for 5 days followed by a MTT cell viability assay. Tamoxifen is an endocrine therapy used in the treatment of both pre- and postmenopausal women, whereas fulvestrant is an endocrine therapy used mostly for the treatment of postmenopausal women (315). Most ILC cell lines were not very sensitive to growth inhibition by tamoxifen (Figure 3.6a) or fulvestrant (Figure 3.6b) *in vitro* as compared to the IDC endocrine therapy sensitive cell line MCF-7. The IC50 values for fulvestrant were unable to be calculated as the drug is having a growth plateau effect on the ILC cell lines (Figure 3.6b). The MDA-MB-134VI cell line displayed similar growth inhibitory effects as the MCF-7 cell line following endocrine therapy treatment, but the SUM44-PE and OCUB-M cell lines were relatively more resistant (Figure 3.6a, b).

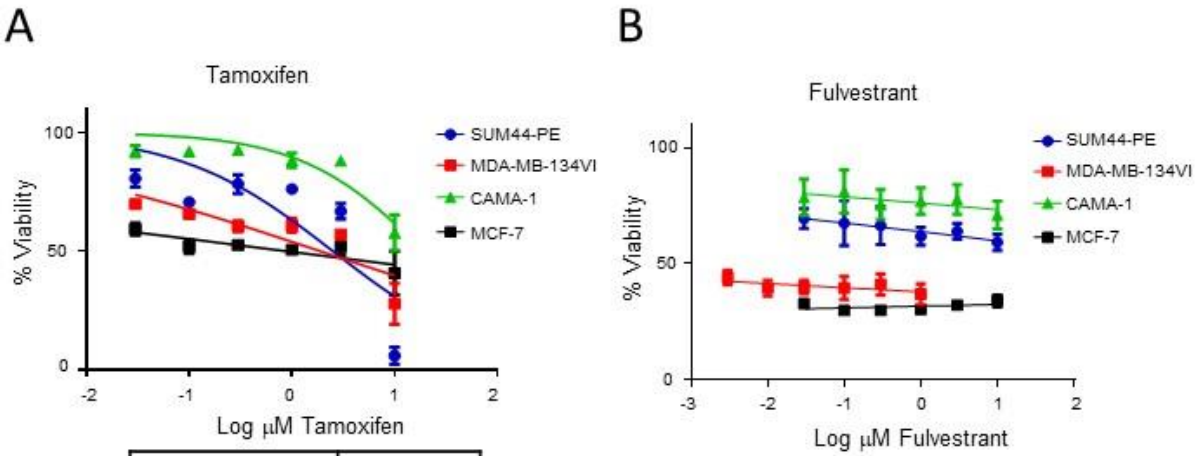

Cell line	IC50
SUM44-PE	2.515 μM
MDA-MB-134VI	1.897 μM
CAMA-1	19.35 μM
MCF-7	0.896 μM

Figure 3.6: Most ILC cell lines are not very sensitive to endocrine therapy *in vitro*. Cell viability curves of ER-positive ILC cell lines and of an ER-positive IDC cell line (MCF-7) as a reference for sensitivity to (A) tamoxifen treatment or (B) fulvestrant treatment after 120 hr using MTT assay. Mean of N=3 experiments plotted using nonlinear regression. Error bars show +/- SEM. IC50 values are listed beside each cell line.

3.3.6 ILC cell lines are sensitive to JQ1-mediated growth inhibition

As mentioned, JQ1 is an inhibitor of the BET family of proteins. It was shown that BRD3 is associated with poor survival in ILC (Figure 3.1, 3.2), therefore the sensitivity of ILC cell lines to JQ1 was examined. JQ1 inhibited the growth of all ILC cell lines tested (Figure 3.7), as assessed using MTT assay and displayed much lower IC50 values compared to tamoxifen (Figure 3.6a). The IC50 values for Fulvestrant were unable to be calculated, as the drug is having a growth plateau effect, but JQ1 is also more effective at inhibiting the growth of ILC cell lines compared to fulvestrant based on the shape of the dose response curves (Figure 3.6b, 3.7). These results suggest that ILC cell lines are more sensitive to JQ1

compared to endocrine therapy *in vitro*. Importantly, ILC cell line sensitivity to JQ1 growth inhibition is not dependent on the level of BRD3 protein expression (Figure 3.5a, b).

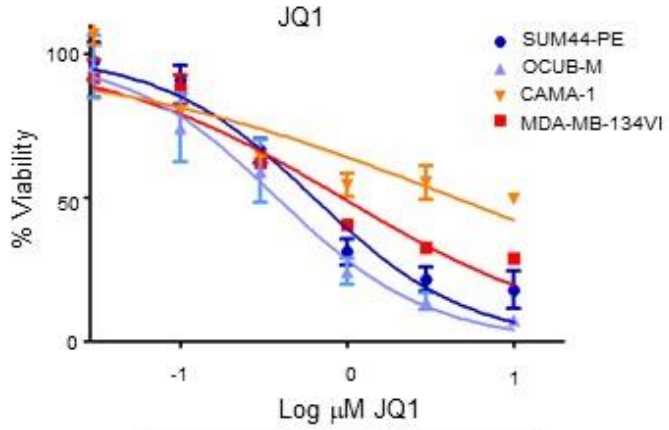

Cell line	IC50
SUM44-PE	0.631μM
OCUB-M	0.379μM
CAMA-1	4.483μM
MDA-MB-134VI	0.934μM

Figure 3.7: JQ1 inhibits growth in ILC cell lines. Dose response curve following 96 hr of treatment with JQ1 assessed by MTT assay. Mean of N=3 experiments plotted using nonlinear regression. Error bars show +/- SEM. IC50 values are listed beside each cell line.

3.3.7 The regulation of growth promoting genes by JQ1 in ILC

Since JQ1 inhibited cell growth of the ILC cell lines it was investigated if JQ1 altered the protein expression of the growth promoting genes MYC, ER and ER-target gene progesterone receptor (PgR) in a time-dependent manner. The results show that JQ1 downregulates the MYC oncogene in all ILC cell lines, as has been previously reported in other cancer cell types (197, 200, 208, 210, 212). Interestingly, JQ1 treatment caused a variable downregulation of ER and PgR in select ILC cell lines (Figure 3.8a). The ER protein was downregulated in the MDA-MB-134VI and CAMA-1 cell line but not in the SUM44-PE cell line. ER was not detected in the OCUB-M cell line (Figure 3.8a). PgR expression was only detected in the SUM44-PE and

CAMA-1 cell lines. In the SUM44-PE cell line PgR was initially downregulated at the protein level at 48 hr JQ1 treatment, but expression recovered at 72 hr (Figure 3.8a). Whereas PgR in the CAMA-1 cell line is downregulated at the protein level at all time-points following JQ1 treatment (Figure 3.8a). There appears to be a variable response in the protein expression of the ER and PgR following JQ1 treatment, therefore ER signalling was assessed using ER and ER-target genes via qPCR (Figure 3.8b).

Next, the mRNA levels of ER and the ER-target genes PgR and TFF1 were assessed by qPCR following JQ1 treatment over time (Figure 3.8b). ER mRNA appeared to be downregulated in all 4 ILC cell lines, with only very slight effects evident in the SUM44-PE and MDA-MB-134VI cell lines (Figure 3.8b). The expression of ER was not altered following JQ1 treatment at the protein level in the SUM44-PE cell line (Figure 3.8a), but the downregulation of ER at the mRNA level is in accordance with the protein data for the MDA-MB-134VI and CAMA-1 cell lines (Figure 3.8a, b). Downregulation of the ER mRNA was only statistically significant in the CAMA-1 cell line at both the 48 hr ($p \leq 0.0001$) and 72 hr (≤ 0.01) time-points (Figure 3.8b). In addition, ER-target gene transcription is downregulated in 3 ILC cell lines, namely in the MDA-MB-134VI, OCUB-M and the CAMA-1 cell lines (Figure 3.8b). Surprisingly, in the SUM44-PE cell line, ER-target gene transcription (PgR and TFF1) seems to be upregulated following JQ1 treatment. TFF1 seems to be upregulated in the SUM44-PE cell line following 48 hr JQ1 treatment and is significantly upregulated following 72 hr JQ1 treatment ($p \leq 0.05$) (Figure 3.8b). Additionally, in the SUM44-PE cell line, although not statistically significant, PgR transcription is initially inhibited at 48 hr but recovers at 72 hr (Figure 3.8b) that is in accordance with the PgR protein data (Figure 3.8a). Also in accordance with the protein data, PgR transcription in the CAMA-1 cell line was significantly downregulated after both 48 hr ($p \leq 0.01$) and 72 hr ($p \leq 0.05$) JQ1 treatment (Figure 3.8a, b). TFF1 is also significantly downregulated in the CAMA-1 cell line following 48 hr ($p \leq 0.0001$) and 72 hr ($p \leq 0.0001$) JQ1 treatment (Figure 3.8b). In the OCUB-M cell line although non-significant, PgR appears to be downregulated and TFF1 is significantly downregulated at both the 48 hr ($p \leq 0.0001$) and 72 hr ($p \leq 0.0001$) following JQ1 treatment (Figure 3.8b).

These results indicate that JQ1 displays context specific regulation of ER and ER-target genes in ILC cell lines. ER and ER-target genes are downregulated both at the mRNA and protein level in ILC cell lines following JQ1 except for the SUM44-PE cell line. As JQ1 inhibits highly transcribed genes in cancer, the SUM44-PE cell line may not be dependent on ER for cell survival or there may be transcriptional rewiring to enable upregulation of the ER in this cell line, which has been suggested previously (207).

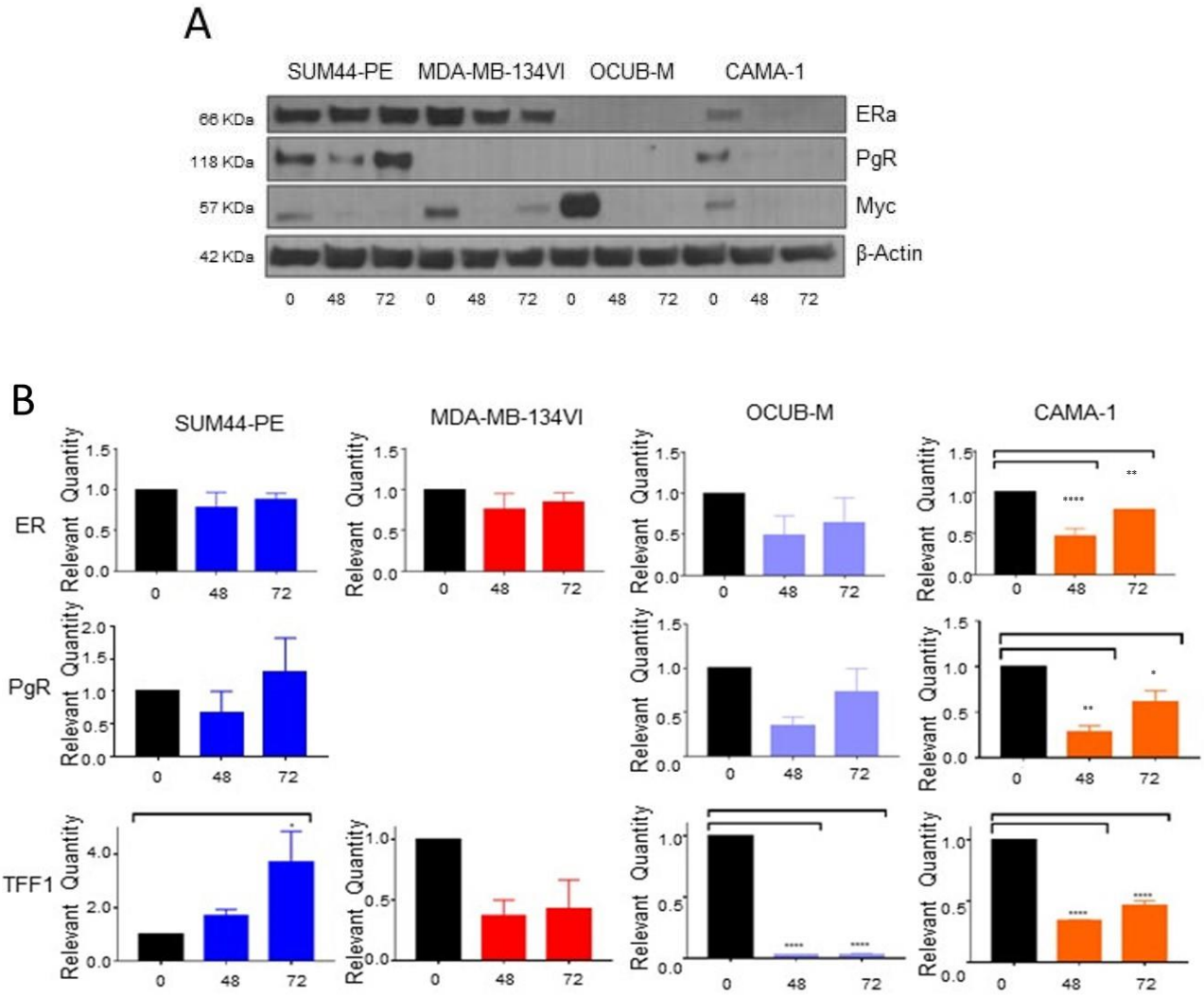

Figure 3.8: JQ1 downregulates growth-promoting genes in ILC cell lines. (A) Representative images of western blotting for growth promoting proteins after 0 hr, 48 hr and 72 hr of 1 µM JQ1 treatment. Western blots were carried out in biological triplicate and β-Actin acts as loading control. (B) qPCR for ER and ER-target genes following 1 µM JQ1 treatment after 0 hr, 48 hr, and 72 hr. Mean of N=3 experiments plotted. Error bars show +/- SEM. Asterisk indicates significance using One-Way ANOVA $p \leq 0.05$.

3.3.8 The combination of JQ1 and endocrine therapy is synergistic in ER-positive ILC cell lines *in vitro*

As JQ1 can regulate the ER and ER-target genes, it was investigated if the combination of JQ1 and tamoxifen or the combination of JQ1 and fulvestrant was

synergistic in the ILC cell lines (Figure 3.9a, b). This was performed using an MTT cell viability assay. Five distinct doses of JQ1 were compared to five distinct doses of tamoxifen or Fulvestrant in a 6 X 6 matrix. Synergy was assessed using the combination index (CI) <0.7 using CompuSyn software. Synergy is marked with an asterisk. Interestingly, synergy with a CI <0.7 was detected with the JQ1 and tamoxifen combination treatment in both the SUM44-PE and MDA-MB-134VI cell lines (Figure 3.9a); and synergy with a CI <0.7 was also detected with the combination of JQ1 and fulvestrant in the MDA-MB-134VI and CAMA-1 cell lines (Figure 3.9b). In line with these findings the combination of JQ1 and fulvestrant has been previously reported to be synergistic in an IDC ER-positive breast cancer xenograft *in vivo* (207). The results suggest that the combination of JQ1 and tamoxifen or the combination of JQ1 and fulvestrant may be a therapeutic option for ILC.

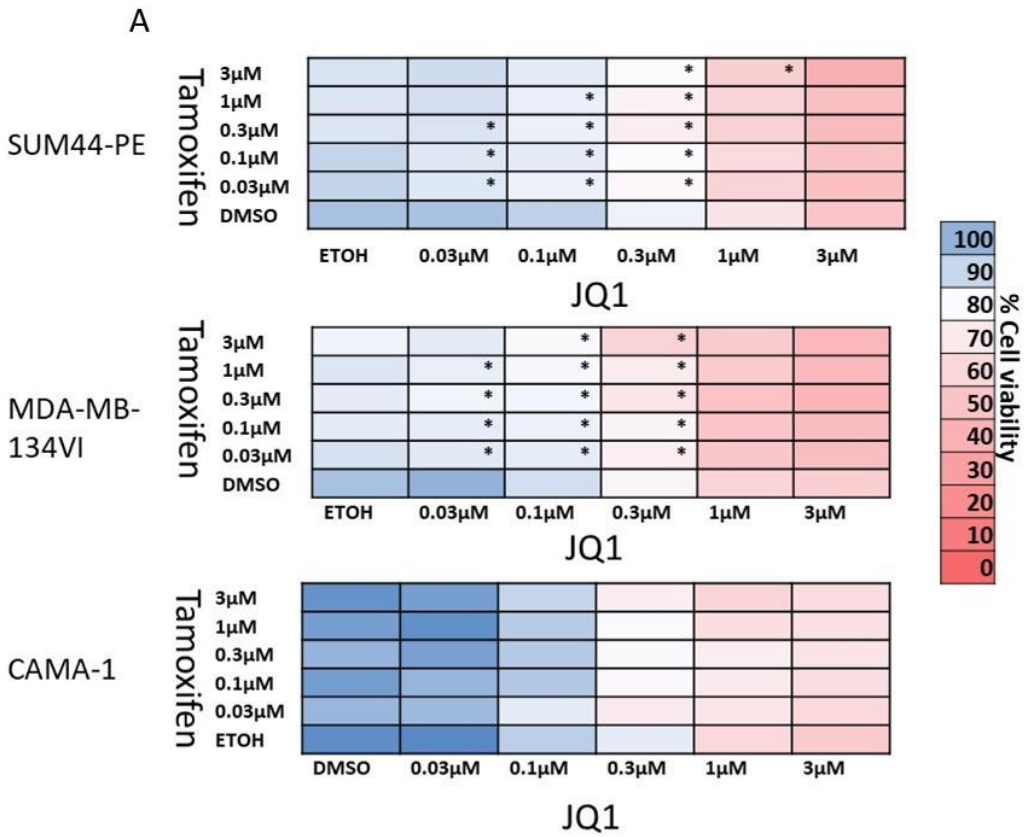

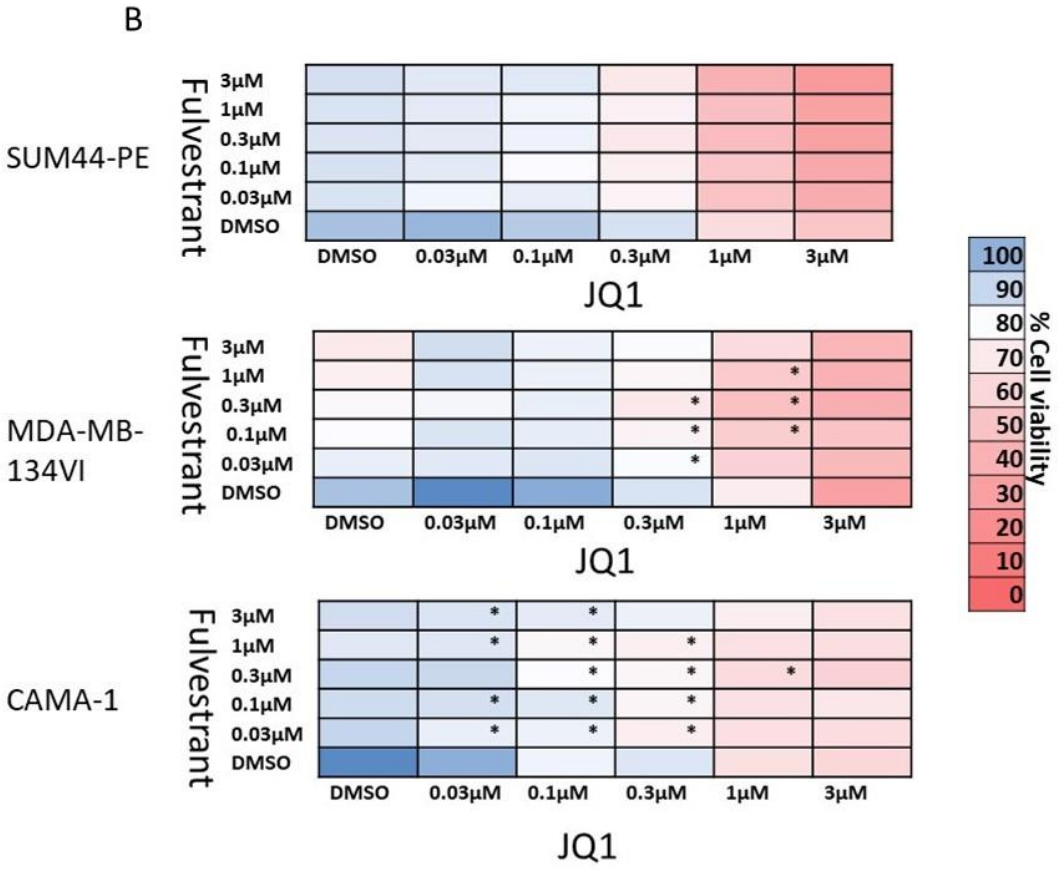

Figure 3.9: JQ1 in combination with tamoxifen or fulvestrant is synergistic in ILC cell lines. Cell viability heatmap matrix using MTT assay 96 hr after JQ1 and tamoxifen combination (A) or JQ1 and fulvestrant combination (B) treatment. The mean of N=3 experiments was analysed using CompuSyn software to detect synergy. Synergy with a combination index (CI) <0.7 is marked with an asterisk.

3.3.9 Multiple BET proteins, including BRD3, are responsible for sensitivity to JQ1

All ILC cell lines tested are sensitive to JQ1 mediated growth inhibition. As JQ1 targets all BET proteins in the breast tissue, BRD2, BRD3 and BRD4, it was next determined what BET protein was responsible for JQ1 sensitivity in the panel of ILC cell lines. siRNA knockdown of BRD2, BRD3 and BRD4 was performed in the OCUB-M, MDA-MB-134VI and CAMA-1 cell lines after 48 hr. Specific siRNA knockdown of each individual BET family protein was achieved in the cell lines, as

assessed by Western blot (Figure 3.10a). Cell growth was then assessed using an MTT assay 48 hr and 96 hr post initial 48 hr siRNA knockdown. The results show that knockdown of BRD2 and BRD3, appeared to reduce cell growth in the OCUB-M cell line at the 48 hr and 96 hr post knockdown time point (Figure 3.10b). BRD3 knockdown at the 96 hr post knockdown time point in the OCUB-M cell line significantly inhibited cell growth ($p \leq 0.05$) (Figure 3.10b). In the CAMA-1 cell line BRD3 ($p \leq 0.01$) and BRD4 ($p \leq 0.05$) significantly inhibited cell growth at the 48 hr post knockdown time point (Figure 3.10c). Likewise, at the 96 hr post knockdown time point BRD3 ($p \leq 0.01$) and BRD4 ($p \leq 0.01$) also significantly inhibited cell growth in the CAMA-1 cell line (Figure 3.10c) Knockdown of BRD4 seemed to slightly reduced cell growth in the MDA-MB-134VI cell line at both the 48 hr and 96 hr post knockdown time points, although this was not statistically significant (Figure 3.10d).

Interestingly, BRD3 knockdown had a slightly greater growth inhibitory effect than the other BET proteins in both the OCUB-M and CAMA-1 cell lines (Figure 3.10b, c) and BRD3 may slightly effect cell growth in the 48 hr post knockdown time point in the MDA-MB-134VI cell line (Figure 3.10d). These results suggest that there are multiple BET proteins contributing to cell viability in the panel of ILC cell lines, and that BRD3 may play a role in maintaining cell viability in all ILC cell lines tested.

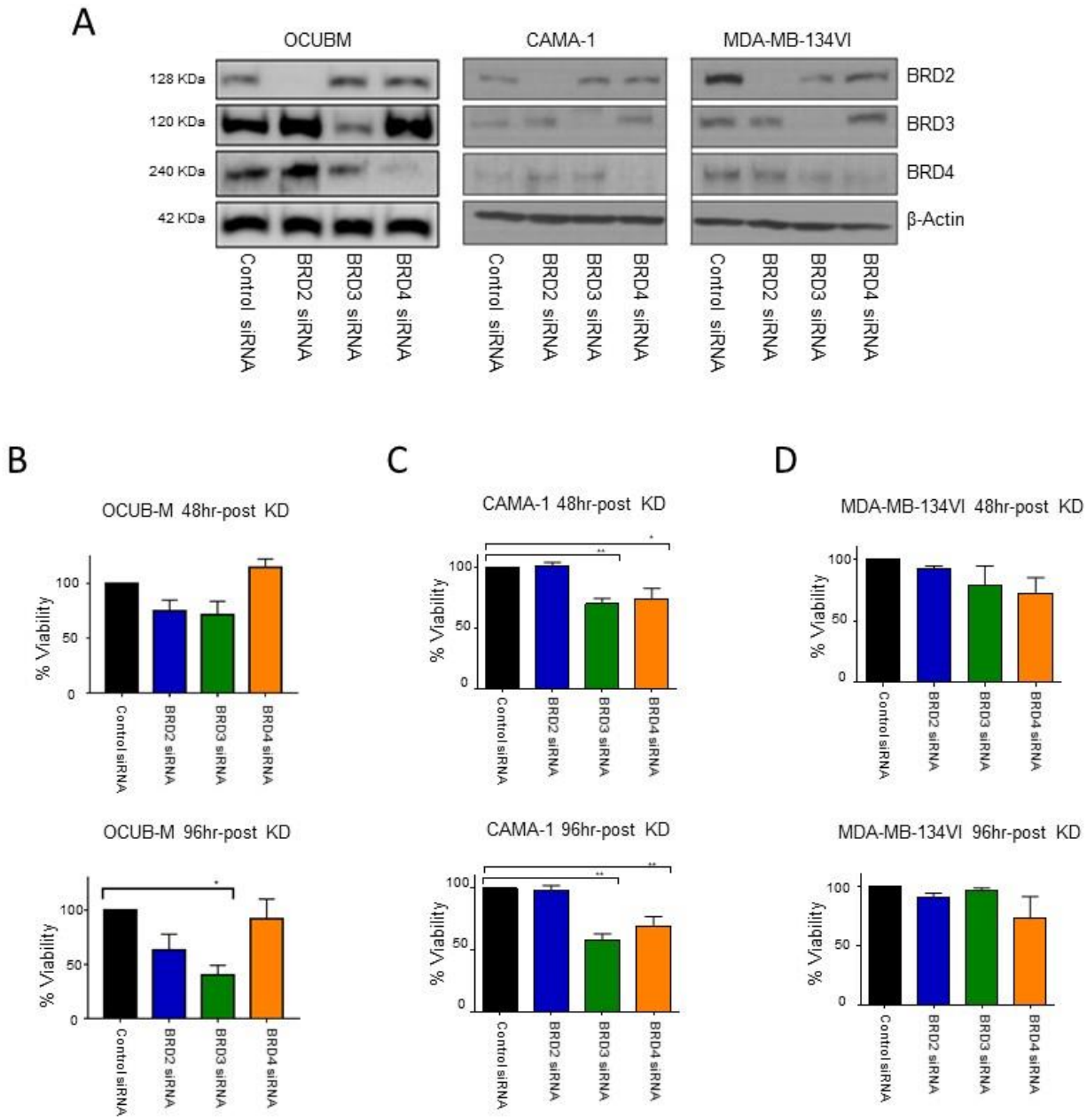

Figure 3.10: Multiple BET proteins are responsible for cell viability in ILC cell lines *in vitro*. (A) Representative western blots from two biological replicates showing representative siRNA knockdown of BRD2, BRD3 and BRD4 in the OCUB-M, CAMA-1 and MDA-MB-134VI cell lines after 48 hr. Cell viability plots from MTT assay data following initial 48 hr BET protein siRNA knockdown followed by either a further 48 hr or 96 hrs in the (B) OCUB-M cell line, (C) CAMA-1 cell line and (D) MDA-MB-134VI cell line. Mean of N=3 experiments plotted. Error bars show +/- SEM. Asterisks indicates significance using One-Way ANOVA p≤ 0.05.

3.4 Discussion

This study emerged from RNA sequencing analysis of 160 primary ILC samples in two separate cohorts from, which high expression of BRD3 was associated with poor survival in ILC. This is a large cohort of patients for ILC, as this subtype of breast cancer only comprises 8-14% of all breast tumours (39, 40). Additionally, ILC breast cancers have in the past been grouped with IDC breast cancers in experimental studies, as well as clinical trials (74) as both are ER positive breast cancers and therefore treated with endocrine therapy. Only recently, it is becoming more and more appreciated that there is a difference between ER positive ILC and IDC, both molecularly, as well as with response to endocrine therapy (117, 154-156). More research is needed on the regulation of ER in ILC, which may differ to IDC in order to understand why there may be a differential response to endocrine therapy. It has been reported that ILC cell lines can regulate distinct E2-regulated genes in comparison with other breast cancer cell lines (316). Another study suggested that IDC may rely on GATA3, as an ER transcriptional coactivator, whereas ILC may rely on FOXA1 as its ER transcriptional activator, due to enrichment mutations in ILC versus IDC (117, 317). However, this suggestion has not yet been confirmed. Recently, novel subtypes of ILC have been identified that are distinct from IDC breast cancer (117, 118). Ciriello et al. identified three novel transcriptional subtypes of ILC including reactive-like, immune-related and proliferative ILC subtypes. The reactive-like subtype had the best outcome and was characterised by cancer fibroblast signalling and/or active microenvironment (117). Michaut et al. identified an immune related subtype and a hormone related ILC subtype that was characterised by epithelial to mesenchymal transition (EMT) (118). The associations of these novel subtypes of ILC with endocrine therapy response has yet to be established but will be important to understand for the appropriate treatment of ILC.

In this study, it was identified that high expression of the epigenetic reader BRD3 was associated with poor survival in ILC in both a discovery cohort of 61 primary patient samples (Figure 3.1, RATHER dataset), as well as a validation cohort of 99 primary patient samples (Figure 3.2, METABRIC dataset (36)). BRD3 is a member of the BET family of proteins and other members include BRD2, BRD4 and BRDT (175), with BRDT expression restricted to the testis (176). Therefore, the association of BRD2 and BRD4 with poor survival in ILC was assessed. Only the BET family

member BRD3 was associated with poor survival in ILC (Figure 3.1, 3.2). The BET family of proteins bind acetylated nucleosomal histones and recruit cofactors and epigenetic machinery to gene promoter and enhancer regions (180-182). Importantly, JQ1 does not affect the viability of normal cells (199, 209) and is tolerated *in vivo* (195, 207, 208), but some toxicities have been observed with other BET inhibitors in the clinic (214-216). JQ1 was shown to effectively and selectively inhibit the bromodomains of BET proteins but no other bromodomain containing proteins outside of the BET family, such as p300 (195). This first publication also showed that JQ1 displaced the oncogenic BRD4-NUT fusion protein from chromatin, inhibited growth and promoted differentiation in NUT midline carcinoma (195). The findings suggest that high expression of the BET protein BRD3 is associated with poor survival in ILC, therefore the therapeutic potential of the BET inhibitor JQ1 in ILC breast cancer was assessed, which has not been done previously.

For this study two ‘true’ ER positive ILC cell lines and two ‘ILC-like’ cell lines were chosen, as there is a lack of available resources in order to study ILC (73). The ILC cell lines, SUM44-PE and MDA-MB-134VI, are ER positive and also E-cadherin negative, while the OCUB-M and CAMA-1 cell lines, are ‘ILC-like’ IDC cell lines and are negative for E-cadherin that is characteristic of ILC (80) (Figure 3.4). The CAMA-1 cell line is also positive for the ER (Figure 3.4). The BET family of proteins BRD2, BRD3 and BRD4 were expressed in all ILC cell lines investigated (Figure 3.5a, b). Next, the inherent sensitivity of the ER positive ILC cell lines to the endocrine therapies tamoxifen and fulvestrant was tested using a cell viability assay. The ER positive ILC cell lines tested were relatively insensitive to both tamoxifen (Figure 3.6a) and fulvestrant (Figure 3.6b) when compared to the endocrine sensitive cell line MCF-7. The MDA-MB-134VI cell line was the closest in sensitivity to the endocrine sensitive cell line following treatment with both tamoxifen and fulvestrant (Figure 3.6a, b), but this cell line has been reported to be resistant to tamoxifen in a previous publication (316). Next, the sensitivity of the panel of ILC cell lines to the BET inhibitor JQ1 was measured (195). All ILC cell lines tested were sensitive to JQ1-mediated growth inhibition (Figure 3.7), with the IC50 values following JQ1 treatment much lower for each cell line compared to the IC50 values following tamoxifen treatment (Figure 3.6a). The IC50 values for the ILC cell lines following fulvestrant treatment was unable to be calculated due to a growth plateau effect of

the drug, but the shape of the dose response curves indicated that JQ1 was more effective at mediating growth inhibition compared to fulvestrant (Figure 3.6b, 3.7).

The effect of JQ1 over time on growth promoting genes in ILC was then assessed (Figure 3.8a, b). JQ1 downregulated the expression of the Myc oncogene (Figure 3.8a), which has been widely published in many cancer types and BET proteins have also been shown to associate with the Myc super-enhancers (197, 200, 208, 210, 212). Myc is involved in the regulation of cell proliferation, growth, apoptosis and metabolism (318). Myc gene amplification occurs in approximately 15% of all breast cancers, but this percentage varies greatly from study to study in the literature (318). Likewise, Myc has been reported to be amplified in 21% of ILC (319), however other reports suggest that Myc amplification is associated with breast tumours of non-lobular origin (320) and ILC tumours have low Myc expression (321). Therefore, the importance of Myc in ILC breast cancer is not yet clear.

JQ1 has also previously been reported to downregulate the expression of ER in IDC breast cancer (207, 322). In ER-positive breast cancer cells that were made resistant to tamoxifen, resistant cells showed enhanced sensitivity to BET inhibition over the parental cells (207). Upon treatment with JQ1, the tamoxifen-resistant cells showed persistent ER suppression, while the parental cells showed reduced expression of the ER initially that recovered with time. The authors postulated that recovery of ER alpha expression in the parental cells could be because of a rewiring of the transcriptional program by the increased expression of the transcription factor GATA3 (207). BRD3 and BRD4 both have important roles in the regulation of ER gene transcription (207, 322). BRD3 and BRD4 recruit the H3K36 methyltransferase and positive regulator of ER signalling, WHSC1, to the ER in order to facilitate ER gene transcription (207). BRD4 binding is also required for recruitment and elongation of RNA polymerase II on estrogen response elements (EREs), for H2B monoubiquitination on ER target genes and for the production of ER enhancer RNA; with JQ1 abrogating these effects (322). JQ1 has also been shown to be effective in other models of breast cancer, including TNBC, basal-like breast cancer and HER2 lapatinib resistant models. The BET inhibitor JQ1 inhibited cell proliferation and promoted cell cycle arrest, apoptosis or senescence in TNBC cell lines (204). It was also identified in basal-like breast cancer that Twist, a transcription factor with a role in EMT, induces widespread changes in gene expression by binding to BRD4 and

recruiting P-TEFb and RNA polymerase II to gene promoters and enhancers (205). Interruption of the BRD4-Twist interaction with JQ1 suppressed cell invasion and tumourigenicity, thus identifying an actionable target to prevent EMT in basal-like breast cancer (205). Additionally, resistance to lapatinib in HER2-positive breast cancer caused transcriptional reprogramming leading to an adaptive response from alternative receptor tyrosine kinases to drive proliferation (206). Combining lapatinib with either JQ1 or IBET-762 BET inhibitors could reverse the epigenetic reprogramming and resensitise the cells to lapatinib treatment (206).

In this study, it was identified that JQ1 over time can downregulate the expression of ER and ER-target genes at both the mRNA and protein level in both the MDA-MB-134VI and CAMA-1 cell lines (Figure 3.8a, b). Similarly, ER and ER-target genes are downregulated in the OCUB-M cell line at the mRNA level following JQ1 treatment (Figure 3.8b), but expression of ER or an ER-target gene were not detected at the protein level (Figure 3.8a). Surprisingly, in the SUM44-PE cell line, while ER was slightly downregulated following JQ1 treatment at the mRNA level (Figure 3.8b), the ER at the protein level showed no change in expression (Figure 3.8a). In addition, the ER-target gene, PgR, at both the protein and mRNA, showed initial downregulation following JQ1 treatment at 48 hr that was recovered at 72 hr to a greater extent than control (Figure 3.8a, b). The ER-target gene TFF1 also showed upregulated expression following JQ1 treatment in the SUM44-PE cell line (Figure 3.8b). These results indicate that JQ1 displays context specific regulation of ER and ER-target genes in ILC cell lines. ER and ER-target genes are downregulated in the panel of ILC cell lines following JQ1 except for the SUM44-PE cell line in which ER-mediated gene transcription is upregulated (Figure 3.8b). The BET family may not regulate ER transcription in the SUM44-PE cell line or there may be transcriptional rewiring following initial inhibition by an alternative transcription factor, such as GATA3, which was previously reported in IDC breast cancer (207).

Since it was shown that JQ1 can display context specific regulation of the ER in ILC cell lines, it was next sought to investigate whether the combination treatment of JQ1 with the endocrine therapies tamoxifen or fulvestrant was synergistic using a cell viability assay. Synergy was detected in the SUM44-PE and MDA-MB-134VI cell lines with the combination of JQ1 and tamoxifen (Figure 3.9a). Synergy was also detected in the CAMA-1 cell line and minor synergy in the MDA-MB-134VI cell line

with the combination of JQ1 and fulvestrant (Figure 3.9b). The combination of JQ1 and fulvestrant has been reported to have a synergistic anti-tumour effect in a tamoxifen resistant IDC breast cancer model *in vivo* previously (207), but there have been no reports with the combination of JQ1 and endocrine therapies in ILC to date. More research is required to understand the effects of the combination of JQ1 and endocrine therapies on ER signalling in ILC both *in vitro* and *in vivo*, but this was beyond the scope of this project.

Finally, as the panel of ILC cell lines used in this study were sensitive to JQ1-mediated growth inhibition, it was determined what BET protein was responsible for sensitivity to JQ1. In order to address this, specific siRNA knockdown of each BET family member expressed in the breast tissue was performed (BRD2, BRD3 and BRD4) after 48 hr (Figure 3.10a). Additionally, cell viability assays 48 hr- and 96 hr-post the original 48 hr siRNA knockdown of individual BET proteins was carried out (Figure 3.10b, c, d). The findings show that knockdown of BRD2 and BRD3 reduced cell growth in the OCUB-M cell line (Figure 3.10b); knockdown of BRD3 and BRD4 reduced cell growth in the CAMA-1 cell line (Figure 3.10c); and knockdown of BRD4 reduced cell growth in the MDA-MB-134VI cell line (Figure 3.10d). Furthermore, BRD3 knockdown had a slightly greater growth inhibitory effect than the other BET proteins in both the OCUB-M and CAMA-1 cell lines and BRD3 also inhibits cell growth in the 48 hr post knockdown time-point in the MDA-MB-134VI cell line (Figure 3.10b, c, d). These results suggest that there are multiple BET proteins contributing to cell viability in the panel of ILC cell lines, and that BRD3 may play a role in maintaining cell viability in all ILC cell lines tested. The development of more selective or specific BET protein inhibitors would be useful in order to probe the role of each specific BET protein in ILC.

In conclusion, this study has shown that the panel of ILC cell lines are more sensitive to JQ1 compared to the endocrine therapies tamoxifen and fulvestrant tested *in vitro*. Additionally, JQ1 downregulates the Myc oncogene but displays context specific regulation of the ER and ER-target genes in the ILC cell lines. Thus, the downregulation of Myc may be responsible for causing growth inhibition in the ILC cell lines, rather than the ER. However, despite context specific regulation of the ER and ER-target genes, ILC cell lines can be synergistically combined with endocrine therapy in order to enhance the growth inhibiting effect of JQ1 treatment alone

illustrating that the ER still has an important role in ILC. Finally, multiple BET proteins, including combinations of BET proteins involving BRD3, are responsible for sensitivity to JQ1 in ILC cell lines.

Chapter Four: JQ1 altered gene signalling in ILC

4.1 Introduction

4.1.1 Epigenetic regulation of apoptosis

JQ1 has been shown to induce apoptosis in a wide variety of cancer types. G1 arrest and subsequent apoptosis has been reported in a tamoxifen resistant IDC ER positive cell line, TNBC cell lines and leukaemia and lymphoma cell lines (204, 207, 208). Apoptosis is also induced by JQ1 in NUT-midline carcinoma cell lines and in a xenograft model of NUT-midline carcinoma (195). In contrast, JQ1 caused G1 cell cycle arrest in multiple myeloma cells sensitive to JQ1 (199). JQ1 mediates apoptosis in castration resistant prostate cancer cell lines that are positive for androgen signalling and sensitive to JQ1, but only causes G1 cell cycle arrest in cell lines that are negative for androgen signalling and relatively insensitive to JQ1 (203). Some authors suggest that sensitivity to JQ1 is attributed to the ability of JQ1 to induce apoptosis in a study using melanoma and acute myeloid leukaemia cells (323).

4.1.3 Evidence of altered BCL-2 anti-apoptotic proteins in breast cancer

Anti-apoptotic proteins are commonly dysregulated in breast cancer. The anti-apoptotic B-cell lymphoma 2 (BCL-2) protein is an estrogen receptor (ER) target gene (324, 325) that is frequently overexpressed in of 86% of ER positive breast cancers (326). BCL-2 expression is marker of good prognosis in ER positive breast cancer (327), but of poor prognosis in TNBC (328). Importantly, anti-apoptotic proteins have been associated with resistance to therapy. Increased expression of the anti-apoptotic protein BCL-2 has been associated with resistance to chemotherapy in breast cancer samples (329). MCL-1 has been reported to be amplified in 54% of residual TNBC after chemotherapy (330). Furthermore, resistance to doxorubicin in an ER positive cell line was attributed to the regulation of BCL-2 by the ER (325). Resistance to targeted therapy has also been attributed to anti-apoptotic proteins. HER2 positive cells resistant to trastuzumab had an increased ratio of BCL-2 bound to BAX (331) and in a ER positive cell line expressing a HER2 oncogenic isoform, tamoxifen resistance was due to increased

expression of BCL-2 (332). Due to the role of anti-apoptotic proteins in cancer, BH3 mimetics were developed.

4.1.4 Resistance mechanism to BET inhibition

Wnt signalling is implicated in resistance to JQ1 (333, 334). In both acquired and de novo BET inhibitor resistance, Wnt signalling was shown to be responsible for transcriptional rewiring in leukemia (334). 17 out of 38 genes upregulated in BET inhibitor resistant leukemic cell lines were members of the Wnt signalling pathway (334). Suppression of two of these targets, IGF2BP1 and TCF4, inhibited the transcriptional rewiring that promoted Myc expression and also increased sensitivity to JQ1 (334). The Wnt pathway TCFL2 transcription factor was identified to be highly associated with a Myc focal enhancer in resistant leukemic cell lines (334). In a de novo model of BET inhibitor resistance, cells from a AML mouse model sensitive to JQ1 was transduced with an activating mutant of CTNNB1 (β-catenin) or shRNA targeting APC, which both promote Wnt signalling. Following JQ1 treatment, these constructs promoted the rapid proliferation of the AML mouse cells and altered the response to JQ1 *in vivo* (334). In another study, haematopoietic stem and progenitor cells (HSPCs) were immortalised with MLL-AF9 to produce AML resistant clones that were selected after treatment with the BET inhibitor, I-BET. AML resistant cells were enriched for leukemic stem cells (LSC) both *in vitro* and *in vivo* (333). BET target genes such as Myc remained expressed in AML resistant cells despite BET protein displacement from chromatin following I-BET treatment. Transcriptional rewiring in BET inhibitor resistant cells was attributed to the canonical Wnt pathway where β-catenin replaced sites on chromatin previously occupied by BET proteins resulting in maintained expression of BET target genes such as Myc (333). Inhibition of the Wnt pathway using dickkopf Wnt signalling pathway inhibitor 1 (DKK1) reduced the expression of Myc and inhibited β-catenin association with the BET target gene Myc (333).

4.1.5 Wnt ligands implicated in cancer

Wnt11 and Wnt4 are non-canonical Wnt ligands (335), that have been implicated in cancer. Wnt11 promotes cell migration, invasion and cell survival in prostate cancer (336), in colorectal cancer (337), in intestinal epithelial cells (338) and in high grade serious ovarian cancer (339). These studies suggest that Wnt11 may be a key factor

in promoting EMT as well as cell proliferation in cancer. Furthermore, Wnt4 is another non-canonical Wnt ligand that has been associated with endocrine resistance in ILC (340). Wnt4 is involved in E2-induced ILC cell proliferation and was shown to be regulated by the ER (340). ILC cell lines resistant to endocrine therapy relied on Wnt4 for proliferation, suggesting that Wnt4 may have a role in endocrine resistance in ILC (340).

4.2 Aims of chapter four

The aims of this chapter were to first measure if JQ1 induced apoptosis in the ILC cell lines. As the transcriptomic landscape following JQ1 treatment in ILC is not known, pathways altered in ILC cell lines by JQ1 were identified using RNA sequencing. Then, the transcriptome following JQ1 treatment of an apoptosis sensitive cell line was compared to that of an apoptosis resistant cell line in order to identify factors that may promote resistance to JQ1-induced apoptosis in ILC. Next, a rational JQ1 combination treatment was validated in order improve sensitivity to JQ1. Finally, this JQ1 drug combination was tested *ex vivo* in a primary ILC sample.

4.3 Results

4.3.1 JQ1 induced apoptosis in select ILC cell lines

To investigate whether JQ1 induced apoptosis in ILC cell lines, apoptosis was assessed by measuring annexin V/propidium iodide (PI) staining following JQ1 treatment. An example of the flow cytometry dot plots for the SUM44-PE cell line treated with DMSO and 10 µM JQ1 for 96 hr is shown (Figure 4.1a). JQ1 induced apoptosis in the SUM44-PE and OCUB-M cell lines (Figure 4.1b). However, the MDA-MB-134VI and CAMA-1 cell lines were relatively more resistant to JQ1 (Figure 4.1b). In confirmation of this finding, PARP cleavage that can be used as a read out of apoptosis (341) was detected in the SUM44-PE and OCUB-M cell lines by western blotting (Figure 4.1c). This data was further supported by cell cycle analysis using PI staining following JQ1 treatment (Figure 4.1d). JQ1 caused the CAMA-1 cell lines to arrest in G1 (Figure 4.1d). This finding is in accordance with the annexin V/PI data that showed that the CAMA-1 cell line was most resistant to JQ1-induced apoptosis (Figure 4.1b). The MDA-MB-134VI cell line arrested in G1 at low doses of JQ1 treatment, but when the JQ1 doses were increased to higher concentrations

there was increased number of cells in the sub G1 phase (Figure 4.1d). This is also in accordance with the annexin V/PI data where some apoptosis is seen in the MDA-MB-134VI cell line at higher doses of JQ1 treatment (Figure 4.1b). The SUM44-PE and OCUB-M cell lines, which are both sensitive to JQ1-induced apoptosis (Figure 4.1b), both showed an increase in the sub G1 phase even at lower JQ1 treatment concentrations (Figure 4.1d). The SUM44-PE and OCUB-M cell lines are sensitive to JQ1-induced apoptosis, whereas the MDA-MB-134VI and CAMA-1 cell lines are relatively more resistant to JQ1-induced apoptosis.

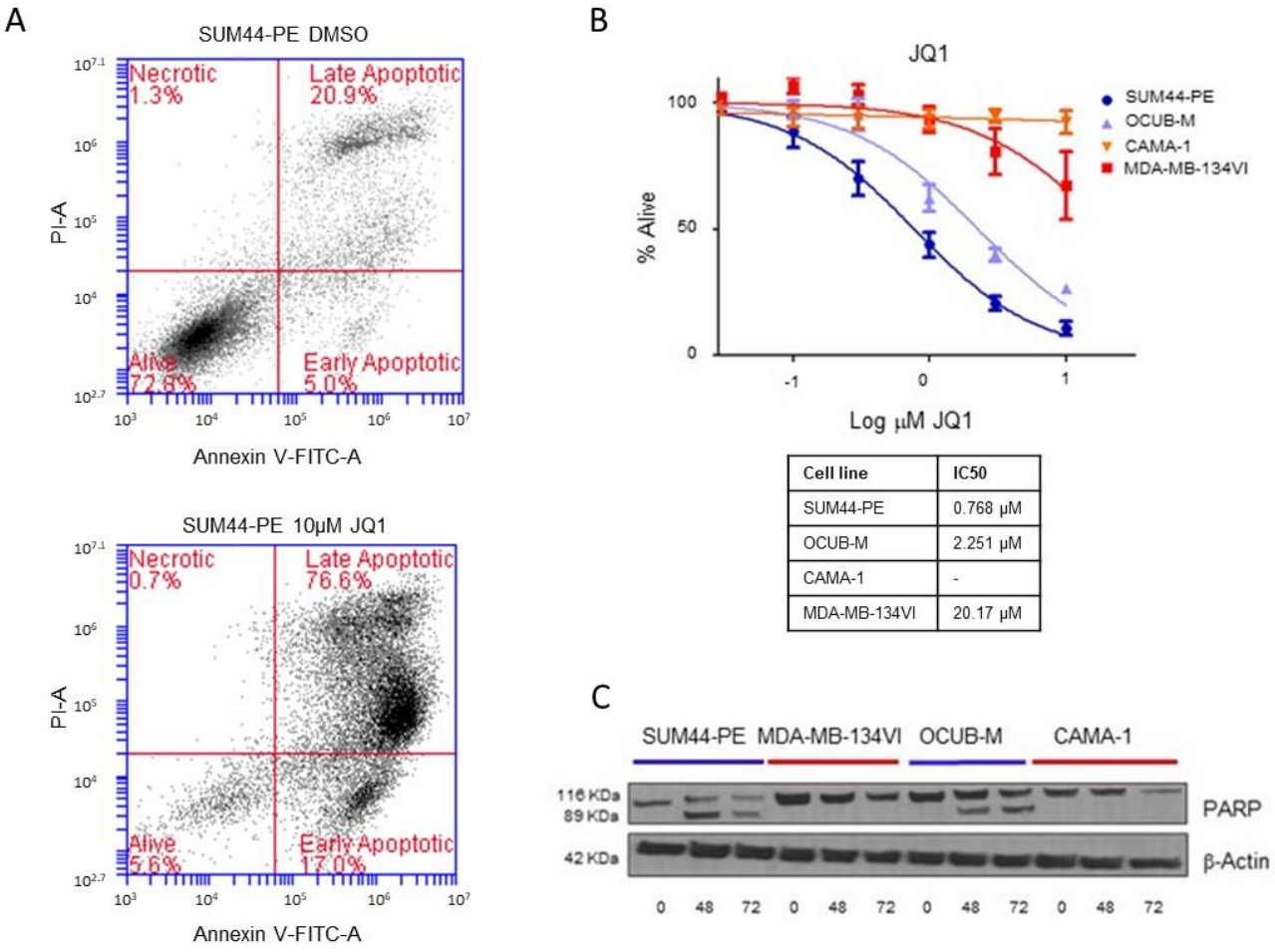

Cell line	IC50
SUM44-PE	0.768 μM
OCUB-M	2.251 μM
CAMA-1	-
MDA-MB-134VI	20.17 μM

D

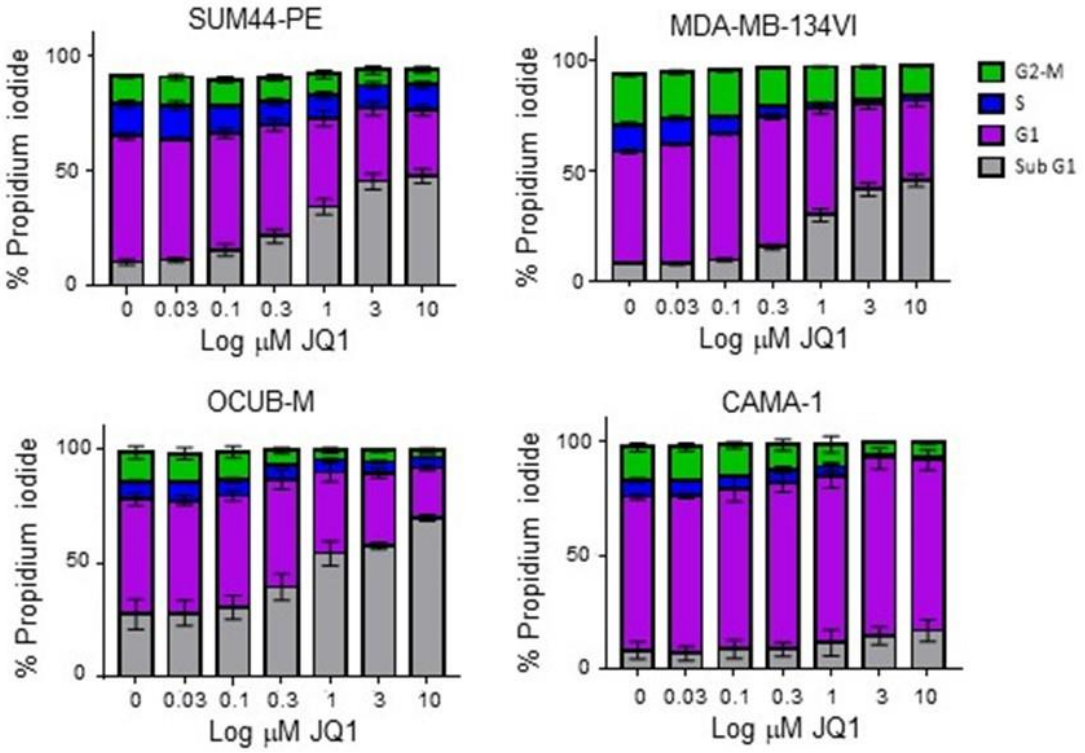

Figure 4.1: JQ1 induces apoptosis in select ILC cell lines. (A) Representative dot plots of the SUM44-PE cell line treated with DMSO and 10 μM JQ1, analysed by flow cytometry. (B) Apoptosis analysis using annexin V-FITC/PI staining and flow cytometry 96 hr following 1 μM JQ1 treatment. Mean of N=3 experiments plotted using nonlinear regression. Error bars show +/- SEM. IC50 values are listed beside each cell line. (C) Representative images of western blotting for cleaved PARP after 0 hr, 48 hr and 72 hr of 1 μM JQ1 treatment. Western blots were carried out in biological triplicate (N=3) and β-Actin acts as loading control. (D) PI staining measured by flow cytometry to quantify percentage of cells in sub G1, G1, S, and G2-M phases following 1 μM JQ1 after 96 hr. Mean of N=3 experiments plotted. Error bars show +/- SEM.

4.3.2 BH3 profiling may predict apoptotic response to JQ1

BH3 profiling is a functional assay that can be used to predict anti-apoptotic protein dependencies as well as measure how primed or how close to the apoptotic threshold cells or patient samples are (262). Basal ILC cell lines were treated with

BH3 peptides that have specific binding interactions for anti-apoptotic proteins (Figure 1.9) and the percentage of mitochondrial depolarisation is measured using a mitochondrial membrane sensitive dye known as JC-1. FCCP is a positive control for the experiment and PUMA2A (a PUMA mutant), acts as a negative control respectively (262). At high doses of 100 µM BIM and BID, which can bind/inhibit all anti-apoptotic proteins, 100% mitochondrial depolarisation is expected (that is used to indicate apoptosis) as at this concentration both BIM and BID saturate the reserve of anti-apoptotic proteins in the cell and activate BAX and BAK directly to initiate apoptosis. However, when the concentration of BIM or BID is reduced, in this study the concentration of BIM was lowered to 3 µM, 1 µM and 0.3 µM, a differential response of the cell lines to percentage mitochondrial depolarisation was observed. The differential response from the 100 µM PUMA peptide, the 3 µM BIM peptide and the 1 µM BIM peptide (Figure 4.2a) was plotted against the IC50 value from the JQ1 annexin V/PI apoptosis assay (Figure 4.1b) and the results show that BH3 profiling may be a potential biomarker to predict cell death in response to JQ1 treatment (Figure 4.2b). Unfortunately, the SUM44-PE cell line was unable to be optimised for BH3 profiling and with only 3 cell lines tested no statistical analyses could be performed.

From the basal BH3 profiling analysis insights into anti-apoptotic dependencies in ILC cell lines can be gained. The BAD peptide binds BCL-2, BCL-XL and BCL-W; the NOXA peptide binds MCL-1 and the HRK peptide binds BCL-XL (Figure 1.9). The response from the NOXA and HRK peptides are similar to the PUMA2A negative control and were discarded from the analysis (Figure 4.2a). However, after BAD peptide treatment a response in percentage mitochondrial depolarisation was seen, which indicates dependency on BCL-2 and/or BCL-XL and/or BCL-W anti-apoptotic proteins in ILC cell lines (Figure 4.2a).

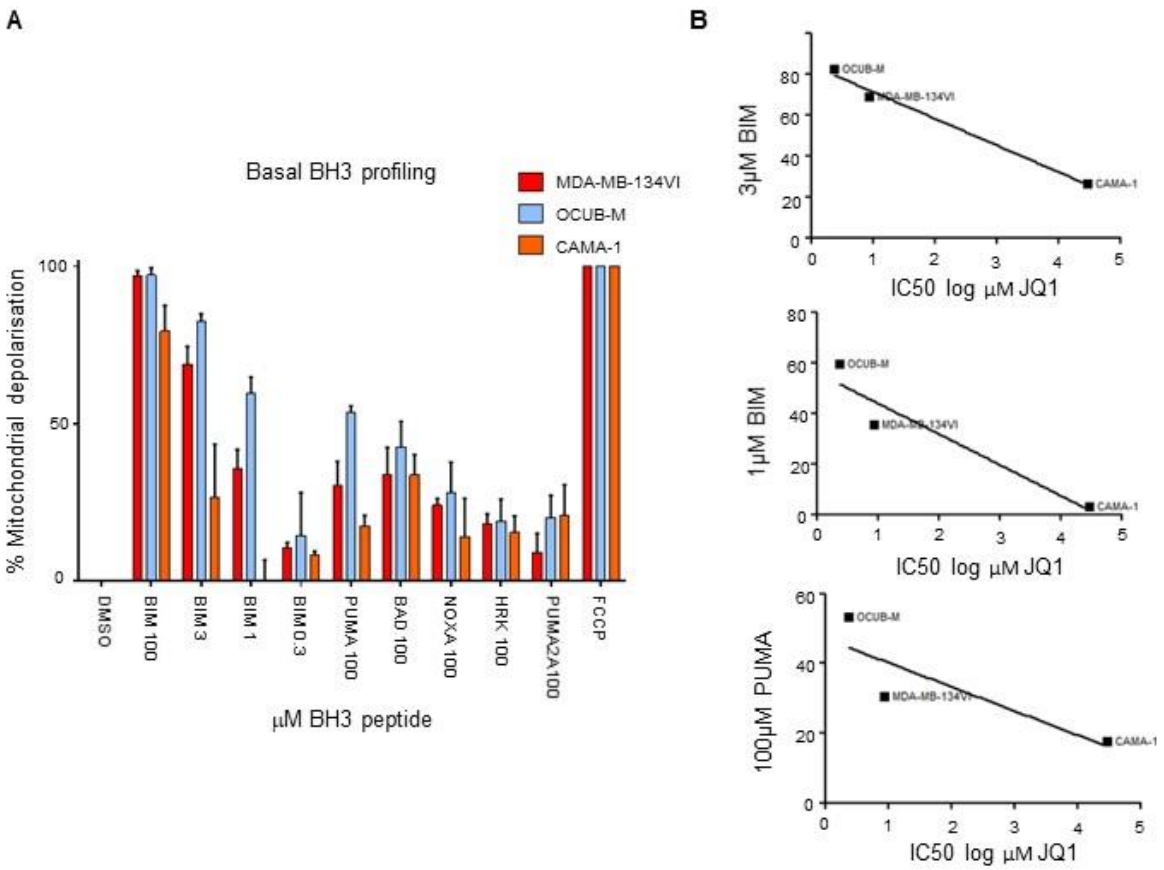

Figure 4.2: Basal BH3 profiling shows dependence on BCL-2 and/or BCL-XL and/or BCL-W. (A) BH3 profiling of basal ILC cell lines plotted in a bar chart using JC-1 fluorescence and kinetic measurement every 5 minutes for 110 minutes in order to quantify percentage (%) mitochondrial depolarisation. Mean of N=3 experiments. Error bars show +/- SEM. (B) IC50 value from JQ1 annexin V/PI apoptosis assay (Figure 4.1b) versus BH3 profiling response for the 3 µM BIM peptide, the 1 µM BIM peptide or the 100 µM PUMA peptide.

4.3.3 RNA sequencing identifies altered gene transcription in ILC cell lines following JQ1

JQ1 induced apoptosis in only some ILC cell lines (Figure 4.1b-d). In order to identify potential factors contributing to JQ1-induced apoptotic resistance, paired-end RNA sequencing analysis was performed following 48 hr JQ1 treatment using the NEXTseq 500 Sequencing System and in conjunction with Dr. Sudipto Das (Royal College of Surgeons in Ireland, Ireland). For this purpose, a ILC cell line sensitive to

JQ1-induced apoptosis (SUM44-PE) and a ILC cell line relatively more resistant to JQ1-induced apoptosis (MDA-MB-134VI) was used. The RNA sequencing data was analysed by Dr. Bruce Moran (University College Dublin, Ireland). Dr. Moran generated a principle component analysis (PCA) plot for the data that showed that minimal variance exists between treatment replicates and cell lines (Figure 4.3).

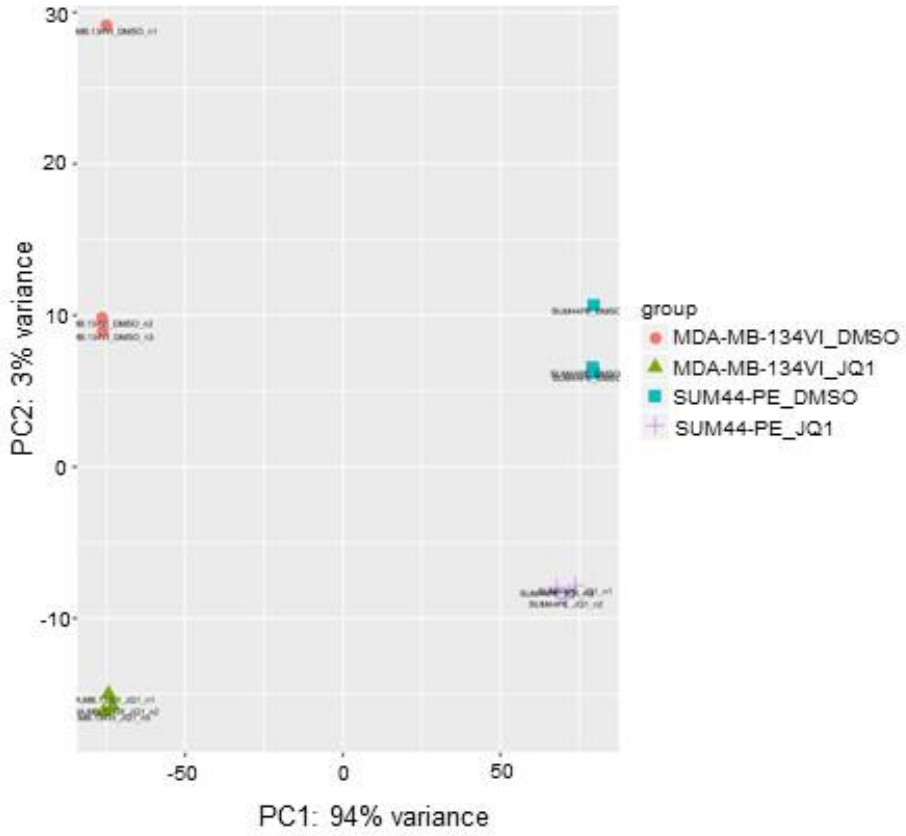

Figure 4.3: Good quality data was obtained from RNA sequencing in ILC cell lines. Principle component analysis of RNA sequencing data following 48 hr of 1 µM JQ1 treatment shows minimal variance between replicates of the same treatment sample.

4.3.3.1 Transcriptomic analysis of the SUM44 PE cell line following JQ1

A heatmap of the top 200 differentially expressed (DE) genes in the SUM44 JQ1-induced apoptosis sensitive cell line was generated using the Perseus software (298), which illustrated that treatment conditions as well as treatment replicates cluster together (Figure 4.4a). JQ1 downregulated the expression of a huge amount of genes (green) but also upregulated the expression of other genes (red) in the

SUM44-PE cell line (Figure 4.4a). Next, gene ontology analysis was performed using the DAVID functional annotation tool (299, 300) that would give insight into the pathways altered in the SUM44-PE cell line following JQ1 treatment. The top 10 downregulated pathways following JQ1 treatment in the SUM44-PE cell line were chronic myeloid leukemia, PgR-mediated oocyte maturation, pyrimidine metabolism, aldosterone synthesis and secretion, fanconi anemia pathway, circadian rhythm, DNA replication, metabolic pathways, cell cycle and purine metabolism (Figure 4.4b). Some of the pathways downregulated by JQ1 were in line with previous findings including inhibition of the cell cycle and inhibition of DNA replication. The top 10 upregulated pathways following JQ1 treatment in the SUM44-PE cell line were pathogenic Escherichia coli infection, protein processing at the endoplasmic reticulum, phosphatidylinositol signalling system, vibrio cholera infection, metabolic pathways, synaptic vesicle cycle, endocytosis, sphingolipid metabolism, other glycan degradation and lysosome (Figure 4.4c).

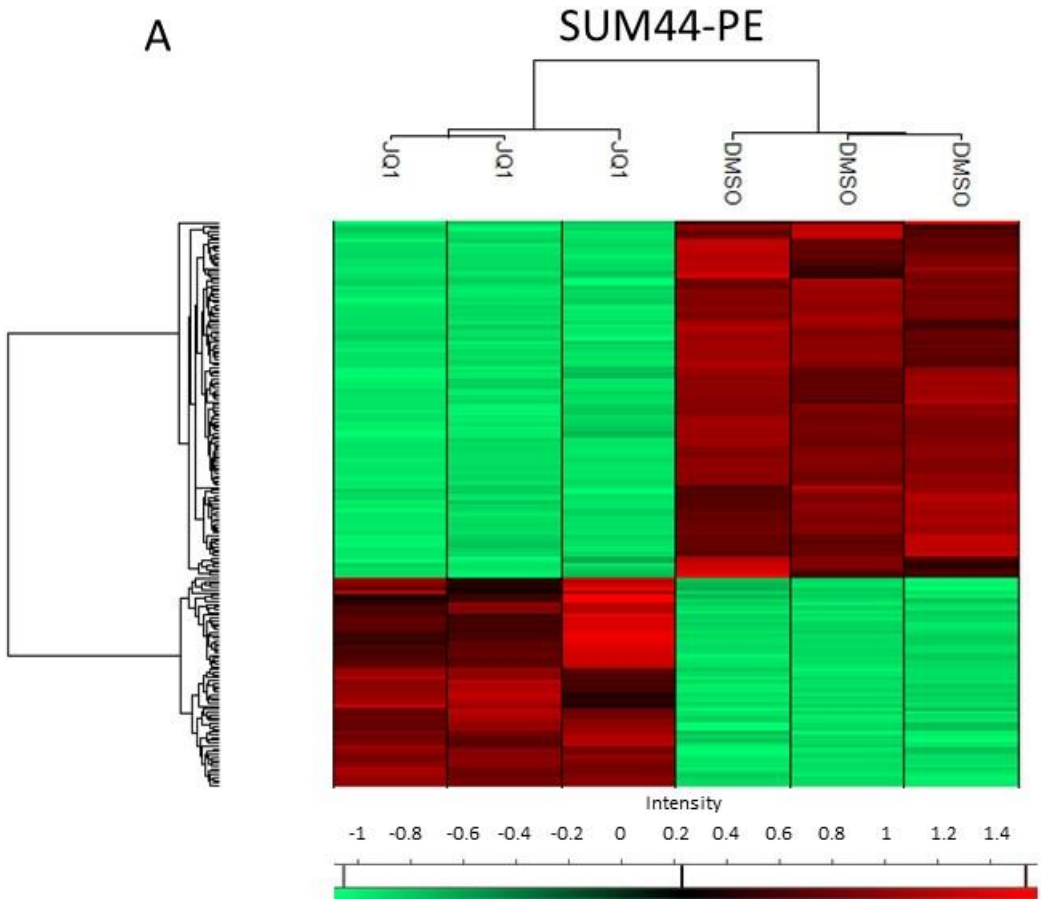

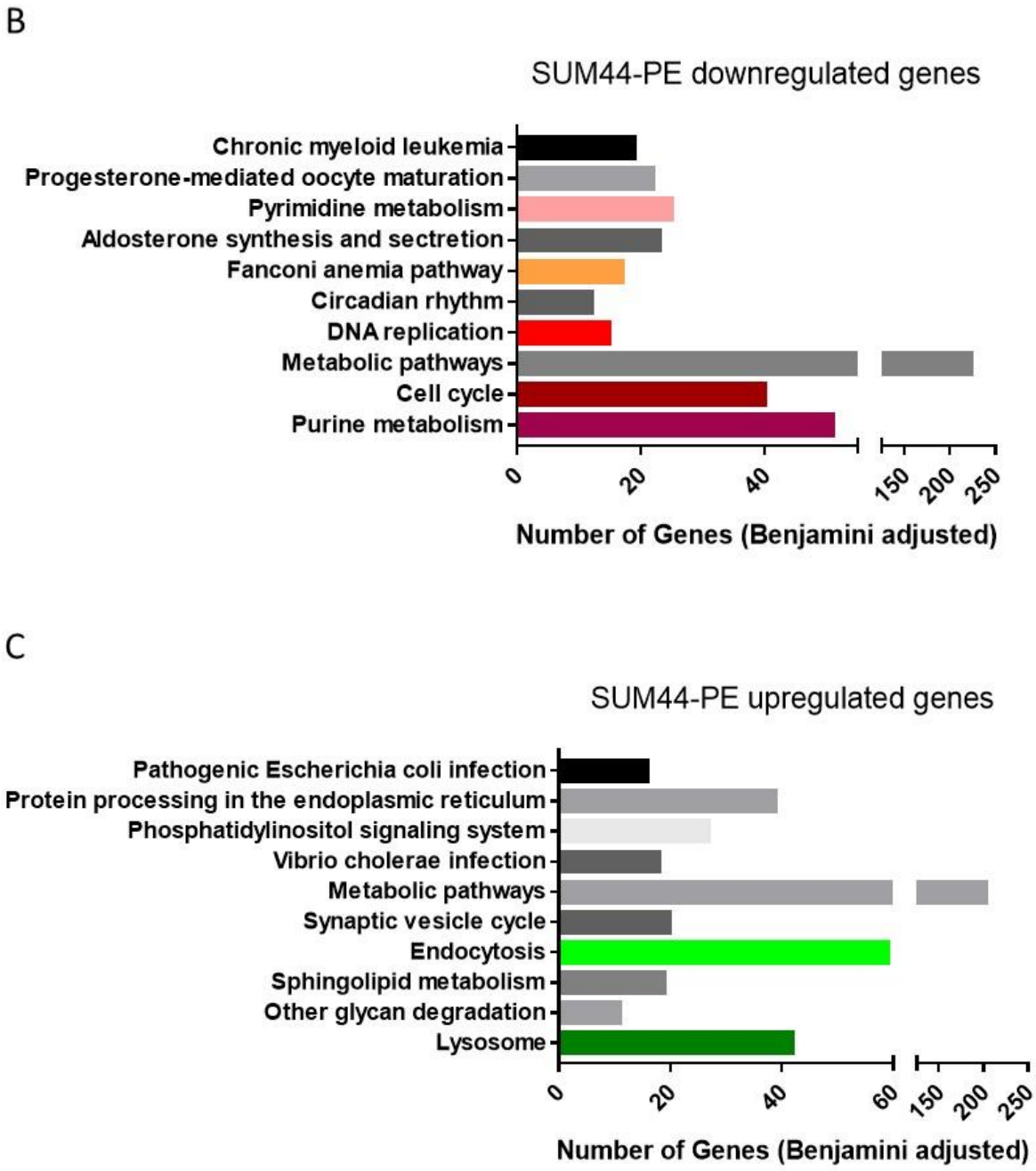

Figure 4.4: JQ1 altered gene transcription in the SUM44-PE cell line. (A) Heatmap of the top 200 DE genes following 48 hr 1 µM JQ1 from RNA sequencing analysis for the SUM44-PE cell line. Z-scores are plotted using Persues software (298). Treatment conditions and replicates cluster together. Top 10 (B) downregulated or (C) upregulated pathways and the number of genes DE in each pathway in the SUM44-PE cell line following 48 hr 1 µM JQ1 treatment as assessed by RNA sequencing and the DAVID functional annotation tool ($p < 0.05$). Genes commonly altered in the SUM44-PE and MDA-MB-134VI cell lines are colour-coded.

4.3.3.2 Transcriptomic analysis of the MDA-MB-134VI cell line following JQ1

A heatmap was also generated for the top 200 DE genes in the MDA-MB-134VI cell line, which was relatively resistant to JQ1-induced apoptosis, following JQ1 treatment and RNA sequencing (Figure 4.5a). Treatment conditions as well as treatment replicates cluster together (Figure 4.5a). Gene ontology analysis using DAVID revealed the top 10 downregulated (Figure 4.5b) and upregulated (Figure 4.5c) pathways in the MDA-MB-134VI cell line following JQ1 treatment. The top 10 downregulated pathways in the MDA-MB-134VI cell line were the fanconi anemia pathway, pyrimidine metabolism, purine metabolism, DNA replication, cell cycle, nucleotide excision repair, p53 signalling, base excision repair, homologous recombination and mismatch repair pathways (Figure 4.5b). The top 10 upregulated pathways included endocytosis, lysosome, proteoglycans in cancer, SNARE interactions in vesicular transport, MAPK signalling pathway, circadian rhythm, Wnt signalling, long-term potentiation, insulin signalling pathway, and insulin resistance (Figure 4.5c).

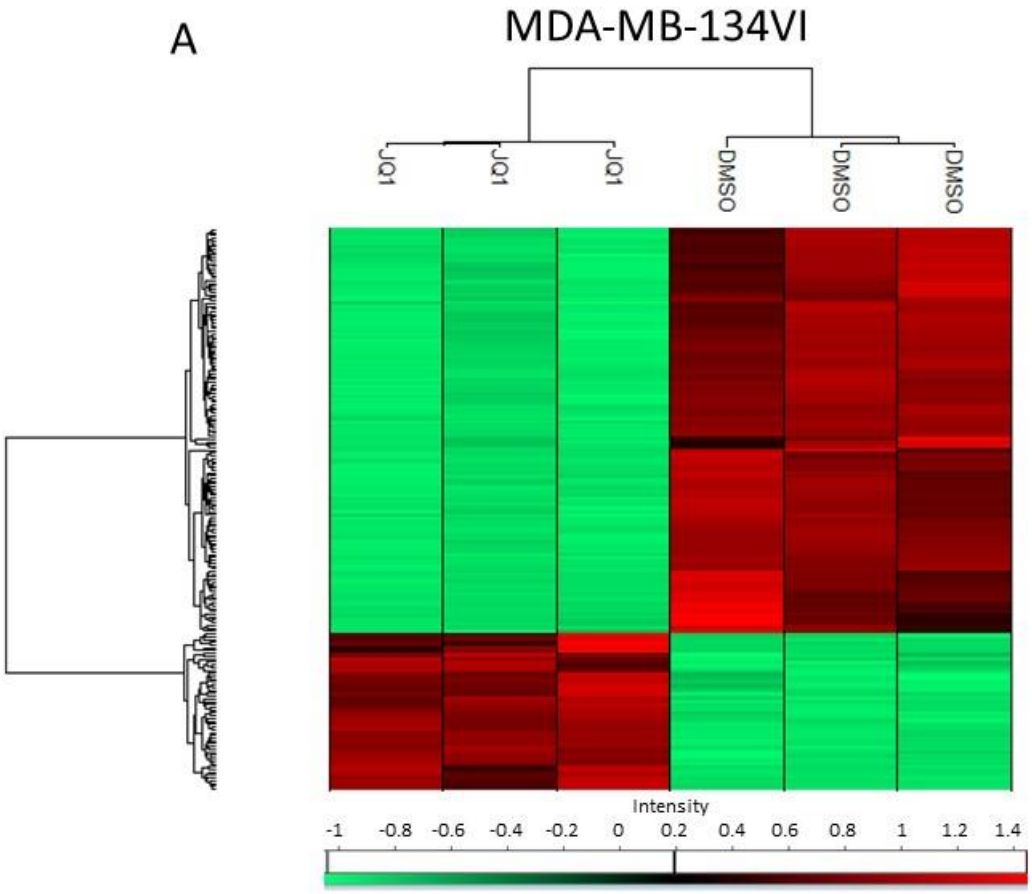
A
MDA-MB-134VI
JQ1
JQ1
JQ1
DMSO
DMSO
DMSO
Intensity
-1
-0.8
-0.6
-0.4
-0.2
0
0.2
0.4
0.6
0.8
1
1.2
1.4

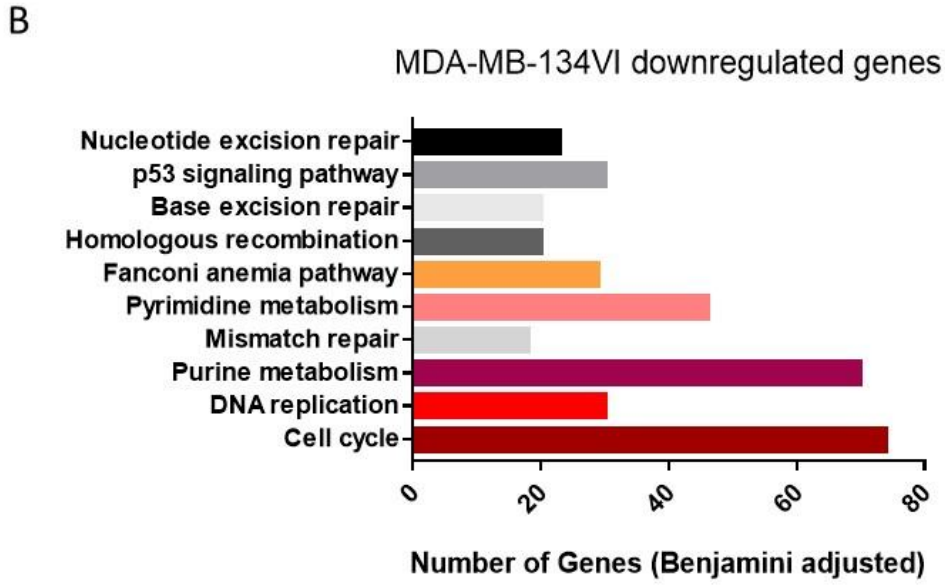
B
MDA-MB-134VI downregulated genes
Nucleotide excision repair
p53 signaling pathway
Base excision repair
Homologous recombination
Fanconi anemia pathway
Pyrimidine metabolism
Mismatch repair
Purine metabolism
DNA replication
Cell cycle
0
20
40
60
80
Number of Genes (Benjamini adjusted)

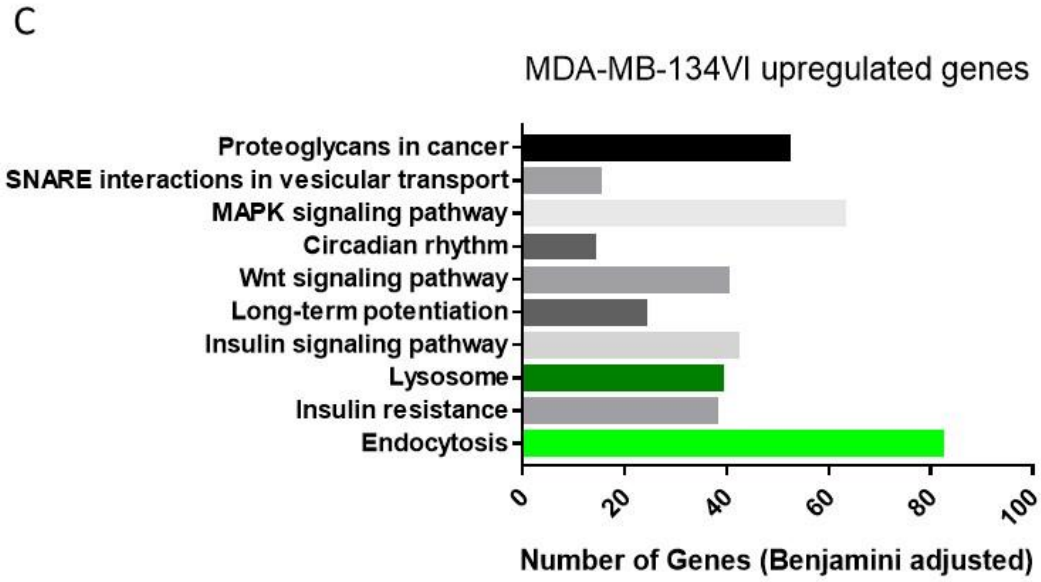

Figure 4.5: JQ1 altered gene transcription in the MDA-MB-134VI cell line. (A) Heatmap of the top 200 genes DE following 48 hr 1 µM JQ1 from RNA sequencing analysis for the MDA-MB-134VI cell line. Z-scores are plotted using Persues software (298). Treatment conditions and replicates cluster together. Top 10 (B) downregulated or (C) upregulated pathways and number of genes DE in each pathway in the MDA-MB-134VI cell line following 48 hr 1 µM JQ1 treatment as assessed by RNA sequencing and the DAVID functional annotation tool ($p < 0.05$). Genes commonly altered in the SUM44-PE and MDA-MB-134VI cell lines are colour-coded.

4.3.3.3 Wnt signalling is upregulated in the JQ1 apoptotic resistant MDA-MB-134VI cell line but not in the JQ1 apoptotic sensitive SUM44-PE cell line

Following on from this, the exact number of differentially expressed (DE) genes in both the cell lines and the number of overlapping genes commonly regulated was determined. DE genes with a p value of less than 0.05 were included in this analysis. 3792 downregulated genes were identified in the SUM44-PE cell line, 4618 downregulated genes were identified in the MDA-MB-134VI cell line, as well as 2150 commonly downregulated genes in both cell lines (Figure 4.6a). 3061 upregulated

genes were also identified in the SUM44-PE cell line, 4302 upregulated genes were identified in the MDA-MB-134VI cell line, as well as 2048 commonly upregulated genes in both cell lines (Figure 4.6a). From the previous DAVID analysis, the fanconi anemia pathway, pyrimidine metabolism, purine metabolism, DNA replication and cell cycle pathways were commonly downregulated in both the SUM44-PE and MDA-MB-134VI cell lines (Figure 4.4b, 4.5b, coloured). The endocytosis and lysosome pathways were also commonly upregulated in the SUM44-PE and MDA-MB-134VI cell lines (Figure 4.4c, 4.5c, coloured).

The SUM44-PE cell line is sensitive to JQ1-induced apoptosis whereas the MDA-MB-134VI cell line is relatively more resistant to JQ1-induced apoptosis (Figure 4.1b). In order to identify factors contributing to JQ1-induced apoptotic resistance, gene ontology pathways were focused on, which were upregulated in the MDA-MB-134VI cell line (relatively resistant to JQ1-induced apoptosis) but not upregulated in the SUM44-PE cell line (apoptotic sensitive cell line) (Figure 4.6b). The pathways upregulated in the MDA-MB-134VI cell line following JQ1 treatment, but not in the sensitive SUM44-PE cell line, include the circadian rhythm pathway ($p= 0.0190$), the MAPK signalling pathway ($p= 0.0203$), SNARE interactions in vesicular transport ($p= 0.0212$), Wnt signalling pathway ($p= 0.0142$), long-term potentiation ($p= 0.0115$) as well as insulin resistance ($p= 0.0006$) (Figure 4.6b).

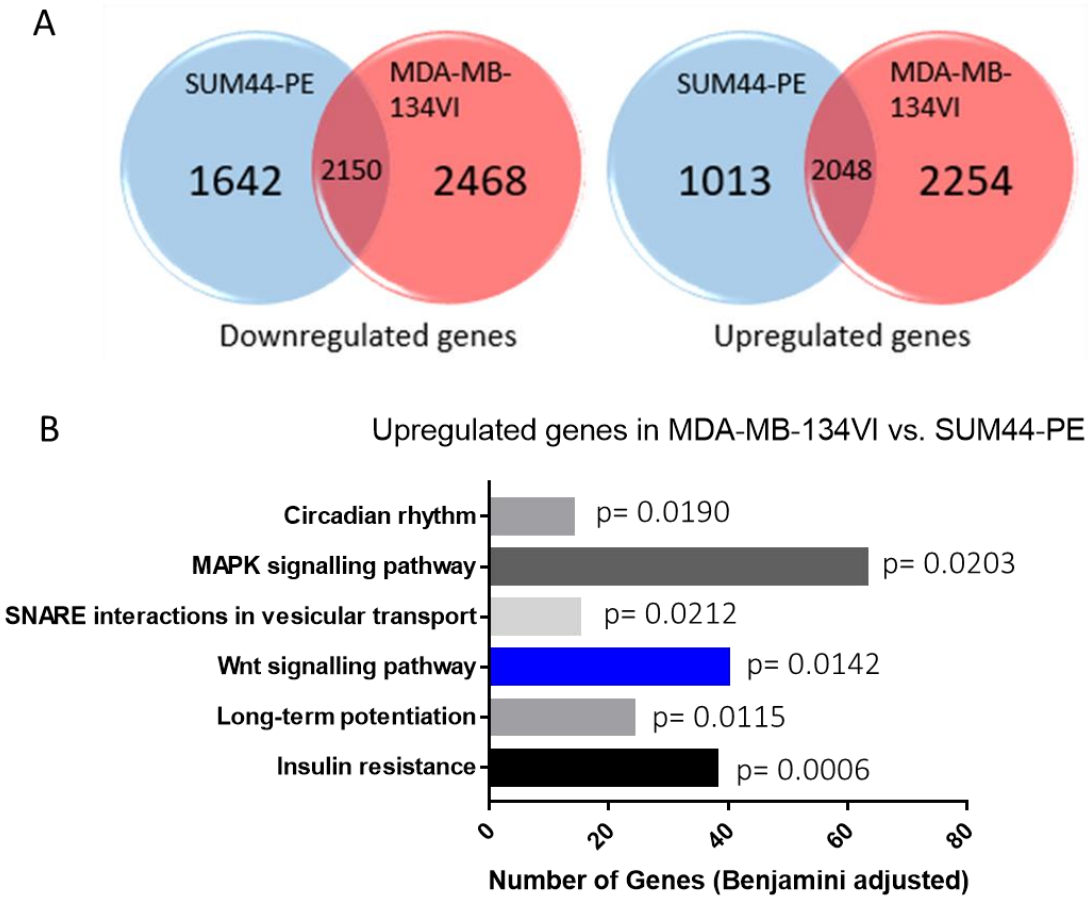

Figure 4.6: Pathways upregulated in the MDA-MB-134VI cell line but not the SUM44-PE cell line. (A) Pie chart illustrating the number of DE genes in the SUM44-PE and MDA-MB-134VI cell lines using p< 0.05 as cut-off. (B) Pathways upregulated in top 10 in the MDA-MB-134VI cell line but not in the SUM44-PE cell line following 1 μM JQ1 treatment for 48 hr as measured by RNA sequencing and the DAVID functional annotation tool (p<0.05).

4.3.4 Wnt11 may contribute to JQ1-induced apoptosis resistance

From this list of pathways potentially contributing to JQ1-induced apoptotic resistance (Figure 4.6b), the Wnt signalling pathway was of interest as associations with JQ1 resistance and the Wnt signalling pathway have been previously reported (333, 334). There were 40 genes from the Wnt signalling pathway, which were upregulated in the MDA-MB-134VI cell line following JQ1 (Figure 4.6b). A panel of 7

genes from this list of 40 genes were chosen and additionally other widely published members of the Wnt signalling pathway were also included in the analysis in order to try and gain an understanding of overall Wnt pathway activation, whether canonical or non-canonical. From the gene list obtained from DAVID, the following genes were chosen: CCND1 (Cyclin D), CTNNB1 (β-catenin), Wnt4, Wnt11, Wnt9a, PPARδ and TCFL2 for further qPCR validation in the panel of ILC cell lines. The other widely published Wnt pathway genes were: TCFL1, LEF1, TCF7 and Myc that were included in the qPCR analysis. TCF7L1, LEF1, TCF7 (and TCFL2) are members of the T-cell factor/lymphoid enhancer factor (TCF/LEF) transcription factor family that function in canonical Wnt signalling (342) and Myc is a canonical Wnt pathway target gene (343). In the SUM44-PE JQ1 apoptosis sensitive cell line JQ1 significantly downregulated cyclin D ($p \leq 0.001$), Wnt11 ($p \leq 0.05$), LEF1 ($p \leq 0.0001$), and Myc ($p \leq 0.0001$) (Figure 4.7a). In the other JQ1 apoptotic sensitive cell line, OCUB-M, JQ1 significantly downregulated Wnt11 ($p \leq 0.05$), LEF1 ($p \leq 0.01$), Myc ($p \leq 0.0001$) and significantly upregulated Wnt9a ($p \leq 0.05$) (Figure 4.7a). In the MDA-MB-134VI apoptotic resistant cell line JQ1 significantly downregulated LEF1 ($p \leq 0.0001$), TCF7 ($p \leq 0.001$), Myc ($p \leq 0.01$) and significantly upregulated β-catenin ($p \leq 0.01$), TCF7L1 ($p \leq 0.05$), TCF7L2 ($p \leq 0.01$), cyclin D ($p \leq 0.05$), Wnt11 ($p \leq 0.05$), Wnt4 ($p \leq 0.01$) and Wnt9a ($p \leq 0.01$) (Figure 4.7a). In the CAMA-1 apoptotic resistant cell line JQ1 significantly downregulated cyclin D ($p \leq 0.001$), TCF7 ($p \leq 0.01$), Myc ($p \leq 0.01$) and significantly upregulated β-catenin ($p \leq 0.01$), TCF7L1 ($p \leq 0.001$), TCF7L2 ($p \leq 0.01$), Wnt11 ($p \leq 0.05$), Wnt4 ($p \leq 0.01$), Wnt9a ($p \leq 0.0001$) and PPARPδ ($p \leq 0.01$) (Figure 4.7a).

From this qPCR analysis it was noted that Wnt11 transcription following JQ1 treatment is significantly upregulated in the apoptotic resistant MDA-MB-134VI ($p \leq 0.05$) and CAMA-1 ($p \leq 0.05$) cell lines but downregulated in the JQ1 apoptotic sensitive SUM44-PE ($p \leq 0.05$) and OCUB-M ($p \leq 0.05$) cell lines (Figure 4.7a). This validates the findings from the RNA sequencing data, in that Wnt11 is significantly upregulated in the JQ1 apoptotic resistant MDA-MB-134VI cell line but not in the apoptotic sensitive SUM44-PE cell line (Figure 4.7b, c). These results suggest that increased expression of the Wnt11 ligand may contribute to JQ1-induced apoptotic resistance in the MDA-MB-134VI and CAMA-1 cell lines.

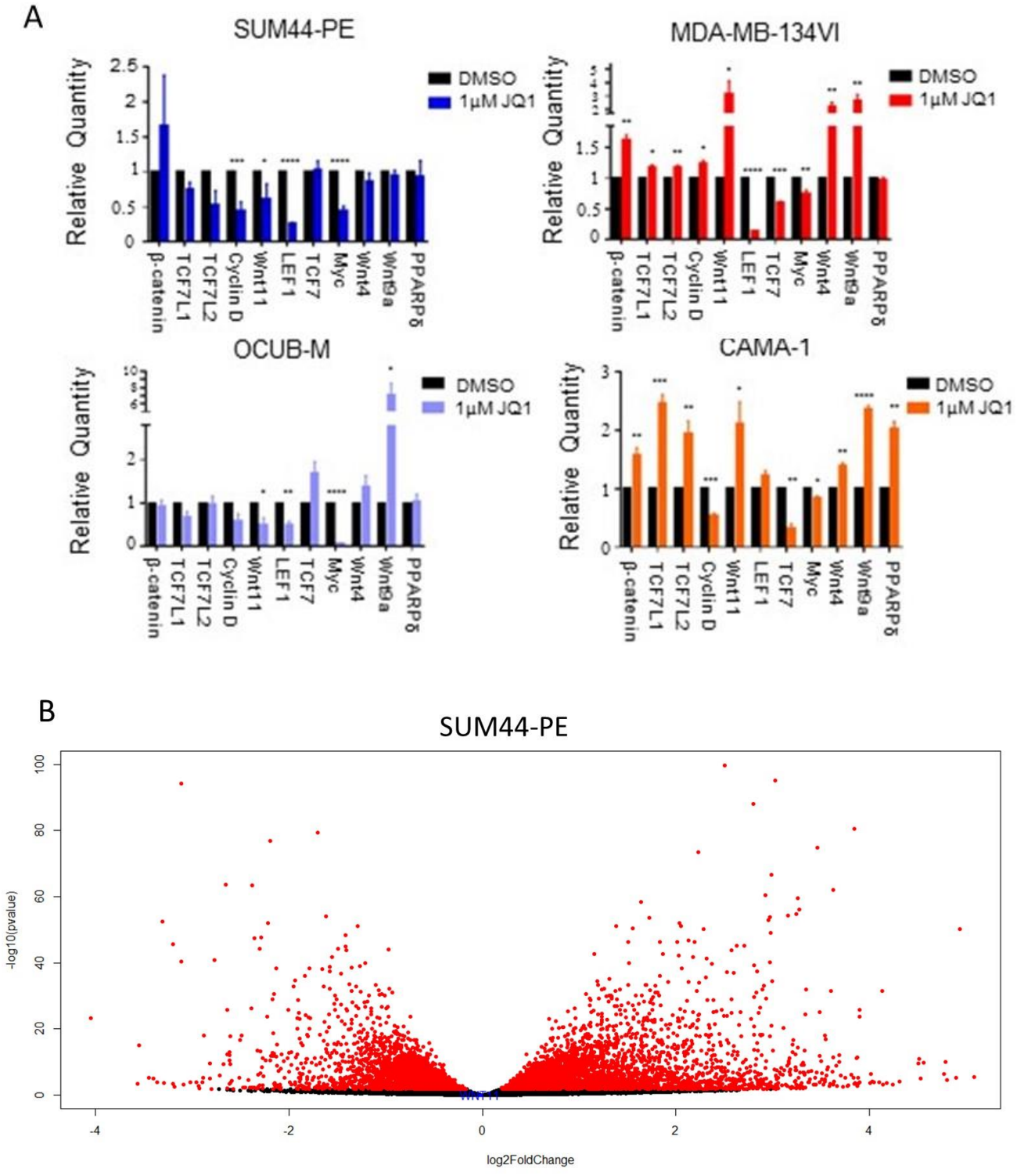
A
SUM44-PE
MDA-MB-134VI
OCUB-M
CAMA-1
Relative Quantity
DMSO
1μM JQ1
β-catenin
TCF7L1
TCF7L2
Cyclin D
Wnt11
LEF1
TCF7
Myc
Wnt4
Wnt5a
PPARPδ
B
SUM44-PE
-log10(pvalue)
log2FoldChange

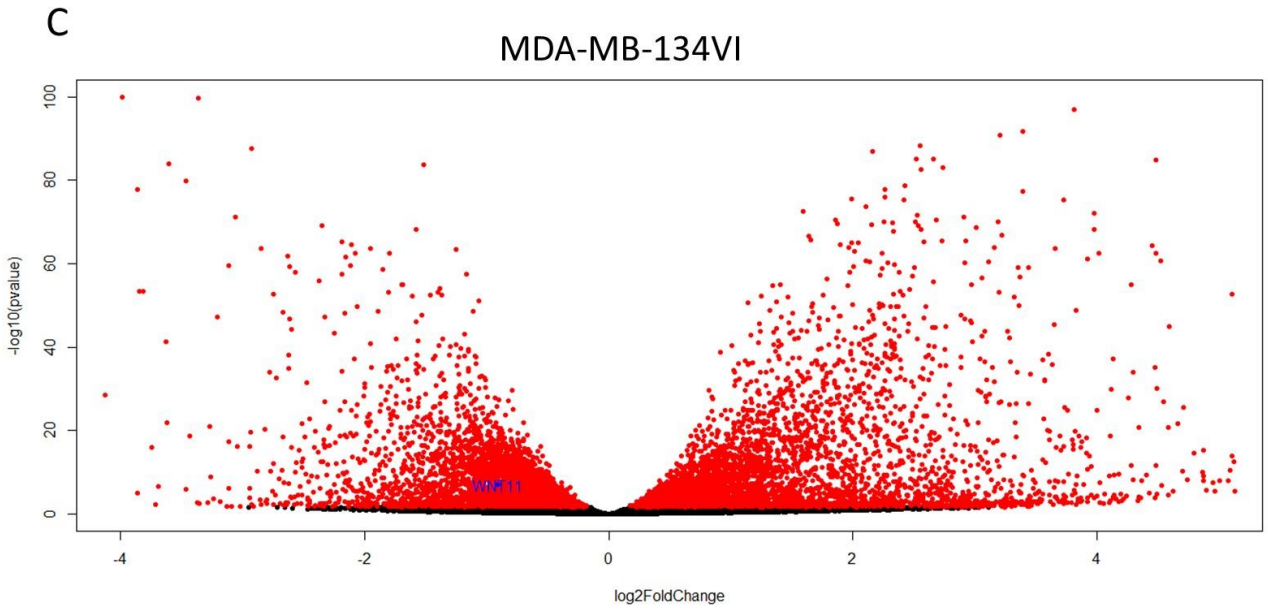

Figure 4.7: Wnt11 may promote resistance to JQ1-induced apoptosis. (A) qPCR validation of genes from DAVID gene ontology analysis (Cyclin D, β-catenin, Wnt4, Wnt11, Wnt9a, PPARδ and TCFL2) as well as other Wnt pathway genes (TCFL1, LEF1, TCF7 and Myc) following 48 hr of 1 µM JQ1 treatment. Mean of N=3 experiments plotted. Error bars show +/- SEM. Asterisks indicates significance using unpaired t-test p≤ 0.05. Volcano plots generated from the RNA sequencing data using R software in the (B) SUM44-PE and (C) MDA-MB-134VI cell lines. Red indicates p≤ 0.05. Wnt11 is marked in blue.

Next, siRNA knockdown optimisation was carried out in the CAMA-1 cell line that is relatively resistant to JQ1-induced apoptosis using siGlo control siRNA, which fluoresces green when transfected into the cells. Transfection efficiency can be approximated based on the number of green fluorescent protein (GFP)-positive cells. 2 µl, 5 µl and 10 µl of siGlo was transfected into cells in a 1:1 ratio with lipofectamine. Only 2-3 cells were GFP positive with 2 µl of siGlo, approximately 50% of cells were weakly GFP positive with 5 µl of siGlo, whereas approximately 100% of cells were strongly GFP positive with the 10 µl of siGlo which had the greatest transfection efficiency (Figure 4.8a) and this concentration of siRNA was used in further Wnt11 siRNA experiments (Figure 4.8b, c).

To assess the role of Wnt11 in resistance to JQ1-induced apoptosis, siRNA knockdown of Wnt11 was performed using 3 independent siRNA's and measured knockdown by qPCR. Wnt11 #1 siRNA was found to inhibit Wnt11 transcription by 80% after 72 hr (Figure 4.8b). Similarly, Wnt11 #3 siRNA inhibited Wnt11 transcription by 70% but Wnt11 #2 siRNA did not inhibit Wnt11 transcription after 72 hr, in fact Wnt11 transcription was enhanced (Figure 4.8b). After optimisation of siRNA concentration and Wnt11 knockdown at the RNA level, an apoptosis assay was carried out using annexin V/PI. In this apoptosis assay the CAMA-1 cells were pre-treated for 72 hr with Wnt11 siRNA to allow Wnt11 knockdown, followed by 1 μM JQ1 treatment for a further 72 hr to test if knocking down Wnt11 could increase sensitivity to JQ1 in this resistant cell line (Figure 4.8c). No difference in sensitivity to JQ1-induced apoptosis was detected following Wnt11 knockdown (Figure 4.8c).

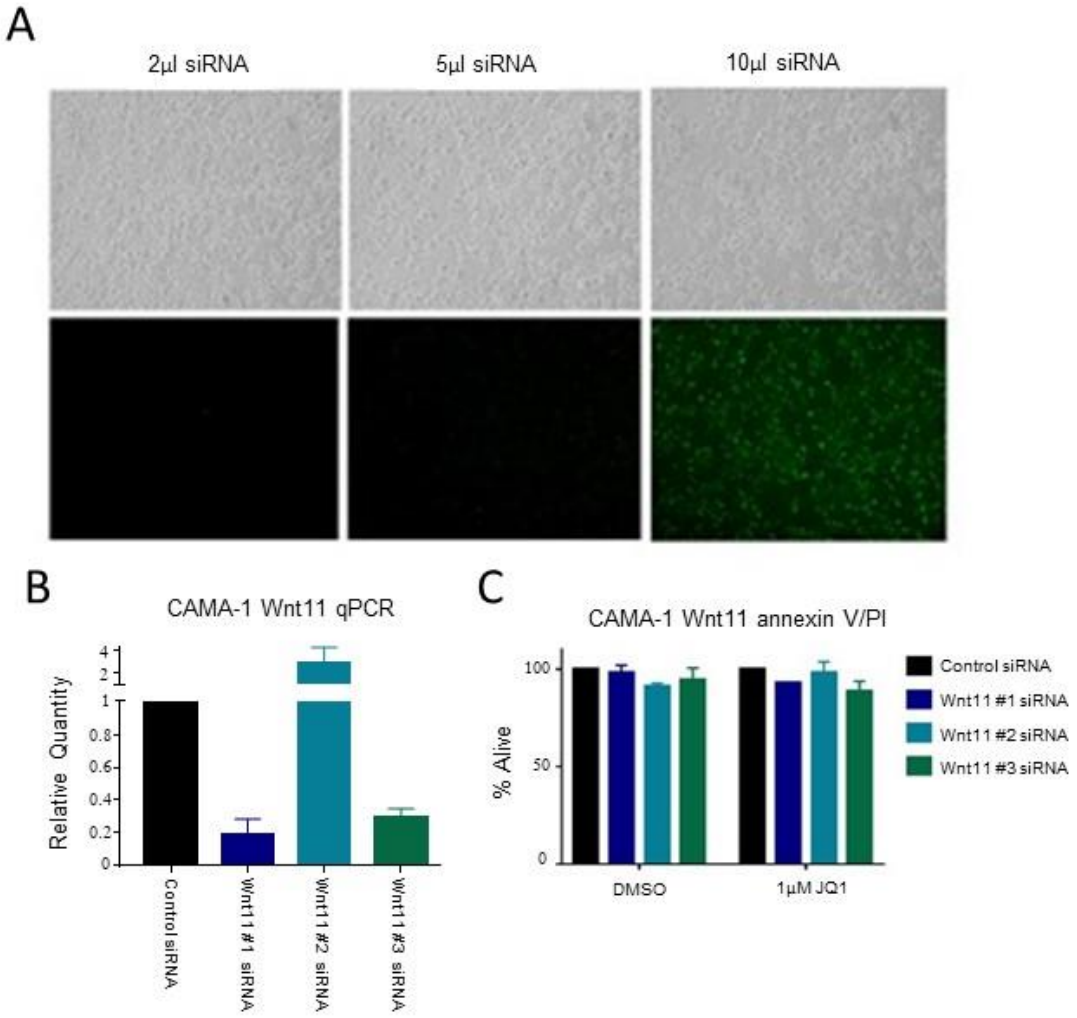

Figure 4.8: Wnt11 knockdown in the CAMA-1 cell line. (A) Optimisation of siRNA concentration after 72 hr using siGlo control siRNA. GFP positive cells indicates transfection efficiency (N=1). (B) Wnt11 knockdown by 3 individual siRNA's measured by qPCR after 72 hr. Mean of N=2 experiments plotted. Error bars show +/- SEM. (C) Annexin V/PI staining following initial Wnt11 knockdown for 72 hr, followed by 1 µM JQ1 treatment for a further 72 hr. Mean of N=2 experiments plotted. Error bars show +/- SEM.

The findings that there was no difference in sensitivity to JQ1-induced apoptosis following Wnt11 knockdown (Figure 4.8c) was surprising, given that Wnt11 is upregulated following JQ1 treatment in cell lines relatively resistant to JQ1-induced apoptosis and downregulated in cell lines sensitive to JQ1-induced apoptosis (Figure 4.7a). In order to confirm knockdown of Wnt11 at the protein level, western blotting

following 72 hr Wnt11 knockdown was performed. No knockdown of Wnt11 in either the CAMA-1 cell line or the MDA-MB-134VI cell line using the high dose of 10 µl siRNA after 72 hr was detected (Figure 4.9a). Although there is efficient knockdown of Wnt11 by two individual Wnt11 siRNA's (#1 and #3) at the mRNA level (Figure 4.8b), this is not translated to the protein level (Figure 4.9a) which suggests that Wnt11 is a highly stable protein. The protein levels of Wnt11 following JQ1 treatment were also measured over time and it was observed that Wnt11 protein expression remains relatively unchanged (Figure 4.9b) in both the cell lines that are sensitive to JQ1-induced apoptosis (SUM44-PE and OCUB-M) and also in those that are relatively more resistant (MDA-MB-134VI and CAMA-1). In order to investigate whether Wnt11 in fact contributes to JQ1-induced apoptotic resistance in ILC cell lines, Wnt11 will need to be stably knocked down/out using either shRNA or CRISPR-cas technology. Unfortunately, time constraints with this project did not allow for the generation of ILC cell lines with Wnt11 stably knocked down/out and will be one of the focuses of our laboratory's research in the future.

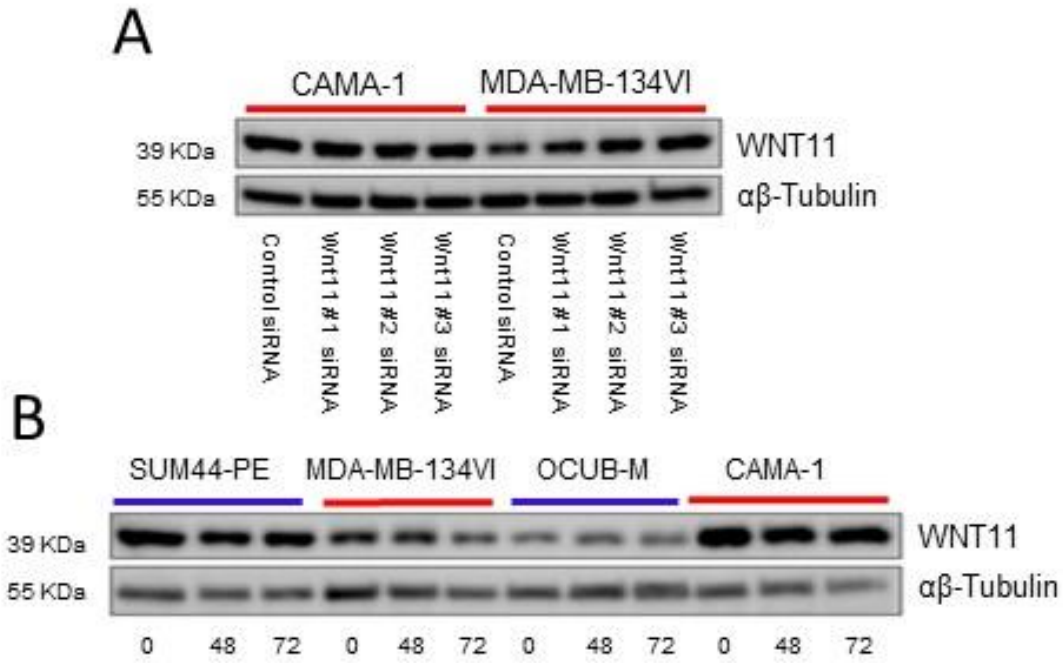

Figure 4.9: Wnt11 protein expression following siRNA knockdown or 1 μM JQ1 treatment. (A) Wnt11 protein expression following individual siRNA knockdown for 72 hr measured by western blotting (N=1). (B) Representative western blots done in biological triplicate (N=3) showing Wnt11 protein expression following 1 μM JQ1 treatment at 0 hr, 48 hr and 72 hr. αβ-Tubulin acts as a loading control.

Similar results were obtained with Wnt4 protein knockdown by siRNA in both the MDA-MB-134VI and CAMA-1 cell lines (Figure 10a). Wnt4 protein levels also remain relatively stable following JQ1 treatment over time (Figure 10b). Wnt4 has previously been associated with endocrine resistance in ILC (340).

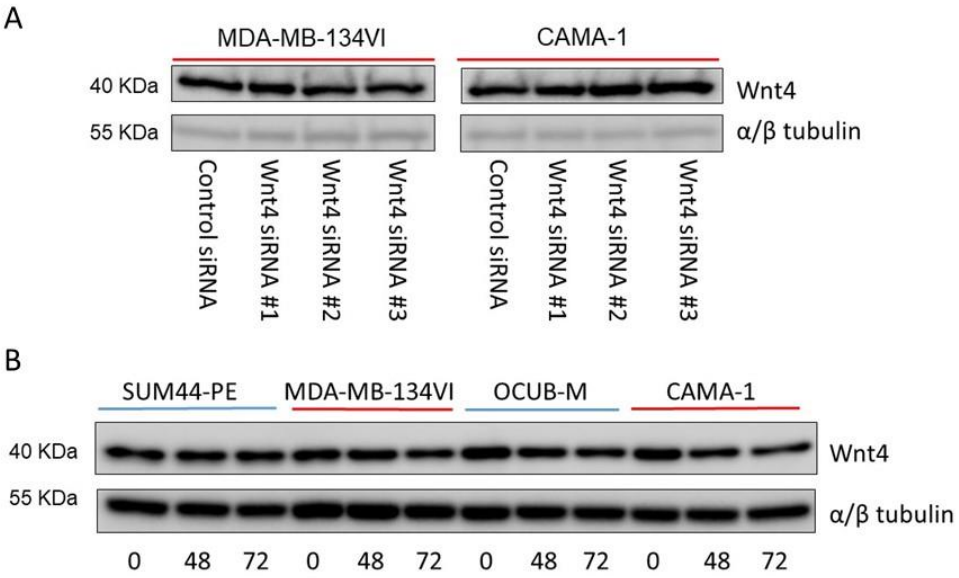

Figure 4.10: Wnt4 protein expression following siRNA knockdown or 1 μM JQ1 treatment. (A) Wnt4 protein expression following individual siRNA knockdown for 72 hr measured by western blotting (N=1) in the MDA-MB-134VI and CAMA-1 cell lines. (B) Representative western blots done in biological triplicate (N=3) showing Wnt4 protein expression following 1 μM JQ1 treatment at 0 hr, 48 hr and 72 hr. αβ-Tubulin acts as a loading control.

4.3.5 RNA sequencing identifies that the anti-apoptotic BCL-XL may contribute to JQ1-induced apoptosis resistance

As anti-apoptotic proteins have been previously implicated in resistance to JQ1 (204, 323), and the availability of BH3 mimetics such as ABT-199 and ABT-263 (275, 281, 285), this group of proteins became of interest. Although the apoptosis pathway did not come up as part of the DAVID gene ontology analysis, JQ1 induced apoptosis in some ILC cell lines (Figure 4.1b, d). Therefore, the raw FPKM values from the RNA sequencing data was interrogated for anti-apoptotic proteins (BCL-2, BCL-XL, BCL-W and MCL-1) as well as the pro-apoptotic protein BIM, to see if changes in gene expression following JQ1 treatment were observed (Figure 4.11a). BIM expression has been reported to be upregulated following JQ1 in the literature (344). In the SUM44-PE cell line that is sensitive to JQ1-induced apoptosis, JQ1 downregulated BCL-2 ($p= 0.00098$) and BCL-XL, but MCL-1 was upregulated ($p= 7.06 \times 10^{-8}$) along

with the pro-apoptotic protein BIM (p= 0.00039) (Figure 4.11a, left). The expression of BCL-W was relatively unchanged and BCL-W FPKM values were very low in the SUM44-PE cell line (Figure 4.11a, left). In the MDA-MB-134VI cell line that is relatively resistant to JQ1-induced apoptosis, BCL-2 was downregulated (p= 7.8199 X 10^{-7}) but both BCL-XL (p= 0.02) and MCL-1 (p=1.74 x 10^{-8}) were upregulated (Figure 4.11a, right). Although BCL-W expression is significantly upregulated in the MDA-MB-134VI cell line following JQ1, the actual BCL-W FPKM values are very low (Figure 4.11a, right; DMSO BCL-W FPKM= 0.185; JQ1 BCL-W FPKM= 0.354). In the MDA-MB-134VI JQ1 apoptotic resistant cell line, BIM expression following JQ1 treatment remained relatively unchanged (Figure 4.11a, right).

Next, the results from the RNA sequencing were validated by qPCR in the two cell lines sensitive to JQ1-induced apoptosis (SUM44-PE and OCUB-M) and in the two cell lines relatively more resistant to JQ1-induced apoptosis (MDA-MB-134VI and CAMA-1), following JQ1 treatment (Figure 4.10b). Importantly, both the SUM44-PE and OCUB-M apoptotic sensitive cell lines showed significant downregulation of BCL-2 (SUM44-PE and OCUB-M p≤ 0.0001) and BCL-XL (SUM44-PE p≤ 0.0001; OCUB-M p≤ 0.05) by qPCR (Figure 4.11b). While the ILC cell lines that are relatively more resistant to JQ1-induced apoptosis, only showed downregulation of BCL-2 and not of BCL-XL by qPCR (Figure 4.11b).

These findings suggest that cell lines relatively resistance to JQ1-induced apoptosis may be dependent on sustained or high expression of the anti-apoptotic BCL-XL after JQ1 treatment, which was confirmed by RNA sequencing and qPCR validation in resistant cell lines. Sustained or high expression of the anti-apoptotic BCL-XL following JQ1 treatment is absent in ILC cell lines sensitive to JQ1-induced apoptosis by both RNA sequencing and qPCR analysis.

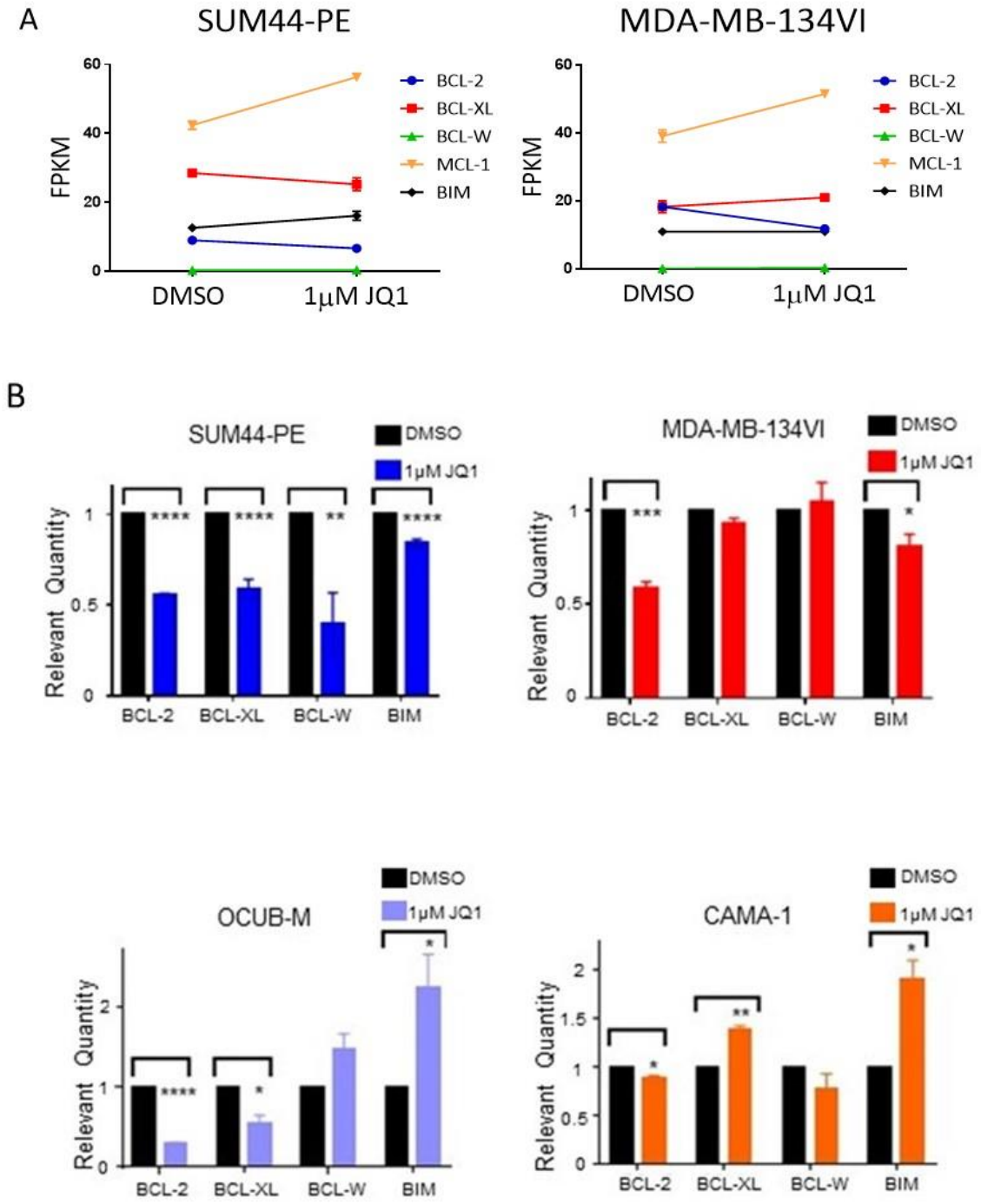

Figure 4.11: BCL-XL is highly expressed in ILC cell lines relatively resistant to JQ1-induced apoptosis. (A) FPKM values from RNA sequencing plotted for the anti-apoptotic proteins BCL-2, BCL-XL, BCL-W and the pro-apoptotic BIM following 1 μM JQ1 treatment for 48 hr. Mean of N=3 experiments plotted. Error bars show +/- SEM. (B) qPCR analysis showing mRNA expression following 1 μM JQ1 treatment after 48 hr for BCL-2, BCL-XL, BCL-W and BIM. Mean of N=3 experiments plotted. Error bars show +/- SEM. Asterisks indicates p≤ 0.05 as measured by t-test.

4.3.6 The regulation of pro- and anti-apoptotic proteins following JQ1 treatment in ILC

The results have shown that JQ1 can induce apoptosis in some ILC cell lines and that ILC cell lines relatively resistant to JQ1-induced apoptosis may be reliant on sustained or upregulated expression of BCL-XL (Figure 4.1b; 4.11a, b). It was desired to further understand the importance of BCL-XL in resistance to JQ1-induced apoptosis and whether there were any other BCL-2 family members involved. Western blotting following JQ1 treatment over time was performed in order to identify protein expression changes in both pro- and anti-apoptotic BCL-2 family members (Figure 4.12a, b).

BCL-2 protein expression remained unchanged in the ILC cell lines following JQ1 treatment, with high expression of BCL-2 in cell lines relatively resistant to JQ1-induced apoptosis compared to sensitive cell lines (Figure 4.12a). BCL-XL was downregulated in the JQ1 apoptosis sensitive cell line OCUB-M as well as in JQ1 apoptosis resistant cell lines, however basal expression of BCL-XL was much higher in JQ1-induced apoptotic resistant cell lines (Figure 4.12a). BCL-W expression was downregulated in JQ1 apoptotic resistant cell lines and upregulated in JQ1 apoptotic sensitive cell lines (Figure 4.12a). PARP cleavage, which can be used as a read-out of apoptosis, is detected as expected in the JQ1 apoptosis sensitive cell lines (SUM44-PE and OCUB-M) but not in the cell lines relatively more resistant to JQ1-induced apoptosis (MDA-MB-134VI and CAMA-1) (Figure 4.12a).

Similarly, pro-apoptotic proteins were interrogated following JQ1 treatment. Increased expression of BAX in cell lines sensitive to JQ1-induced apoptosis was observed following JQ1 (Figure 4.12b). BAK was additionally upregulated in the OCUB-M JQ1 apoptotic sensitive cell line (Figure 4.12b). In cell lines relatively resistant to JQ1-induced apoptosis BAX was downregulated following JQ1 treatment (Figure 4.12b). The BIM protein was upregulated in all ILC cell lines, but only modestly for the CAMA-1 cell line (Figure 4.12b). The upregulation of BIM by JQ1 has been previously reported in melanoma cell lines but apoptosis was not necessarily dependent on BIM, which is in accordance with results from this study (344).

These findings from interrogation of the anti-apoptotic proteins suggest that the anti-apoptotic BCL-2 may be implicated in JQ1 apoptotic resistance as BCL-2 protein expression remains high and unchanged following JQ1 treatment in the MDA-MB-134VI and CAMA-1 resistant cell lines. Furthermore, JQ1 displays context specific regulation of BCL-XL in ILC cell lines. This being said, because sustained or increased transcription of BCL-XL following JQ1 treatment was detected in the ILC cell lines relatively resistant to JQ1-induced apoptosis by RNA sequencing and qPCR analysis in chapter four (Figure 4.11a, b), but not in the sensitive ILC cell lines, transcriptional rewiring may be occurring in resistant ILC cell lines that is enabling expression of BCL-XL to recover.

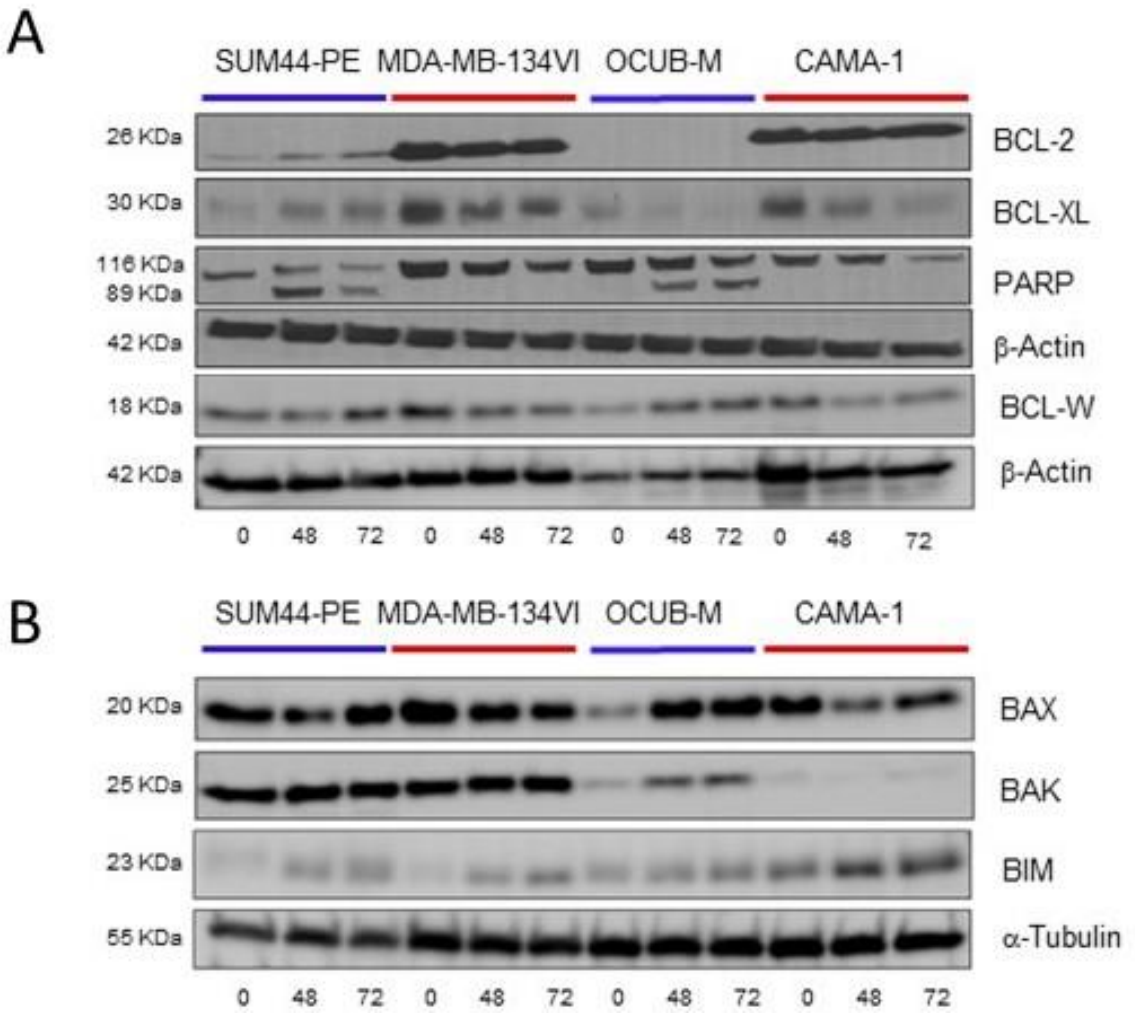

Figure 4.12: The expression of anti-apoptotic and pro-apoptotic proteins following JQ1 treatment. Representative images of western blotting carried out in biological triplicate (N=3) for anti- (A) and pro-apoptotic proteins (B) after 0 hr, 48 hr and 72 hr of 1 μM JQ1 treatment. β-actin or α-Tubulin acts as loading control. PARP cleavage is also shown in (A).

4.3.7 Some ILC cell lines are sensitive to ABT-263, but not to ABT-199

Since high expression of BCL-2 protein was detected in the MDA-MB-134VI and CAMA-1 cell lines that are relatively resistant to JQ1-induced apoptosis (Figure 4.12a), the sensitivity of ILC cell lines to BH3 mimetics was assessed. The BH3 mimetic ABT-199 is a selective BCL-2 inhibitor (281) and the BH3 mimetic ABT-263

is an inhibitor of BCL-2, BCL-XL and BCL-W anti-apoptotic proteins (266). The sensitivity of the panel of ILC cell lines to ABT-199 treatment was first measured by both cell viability and apoptosis assay (Figure 4.13a, b). ABT-199 only mediated slight growth inhibition at the highest does of 10 µM (Figure 4.13a) and did not mediate apoptosis (Figure 4.13b). Representative dot plots for annexin V/PI stained SUM44-PE cells treated with DMSO and 10 µM ABT-199 are shown (Figure 4.13c). These findings suggest that ILC cell lines are not solely dependent on BCL-2 for cell survival as the panel of ILC cell lines are insensitive to ABT-199 treatment both in terms of mediating growth inhibition and apoptosis (Figure 4.13a, b).

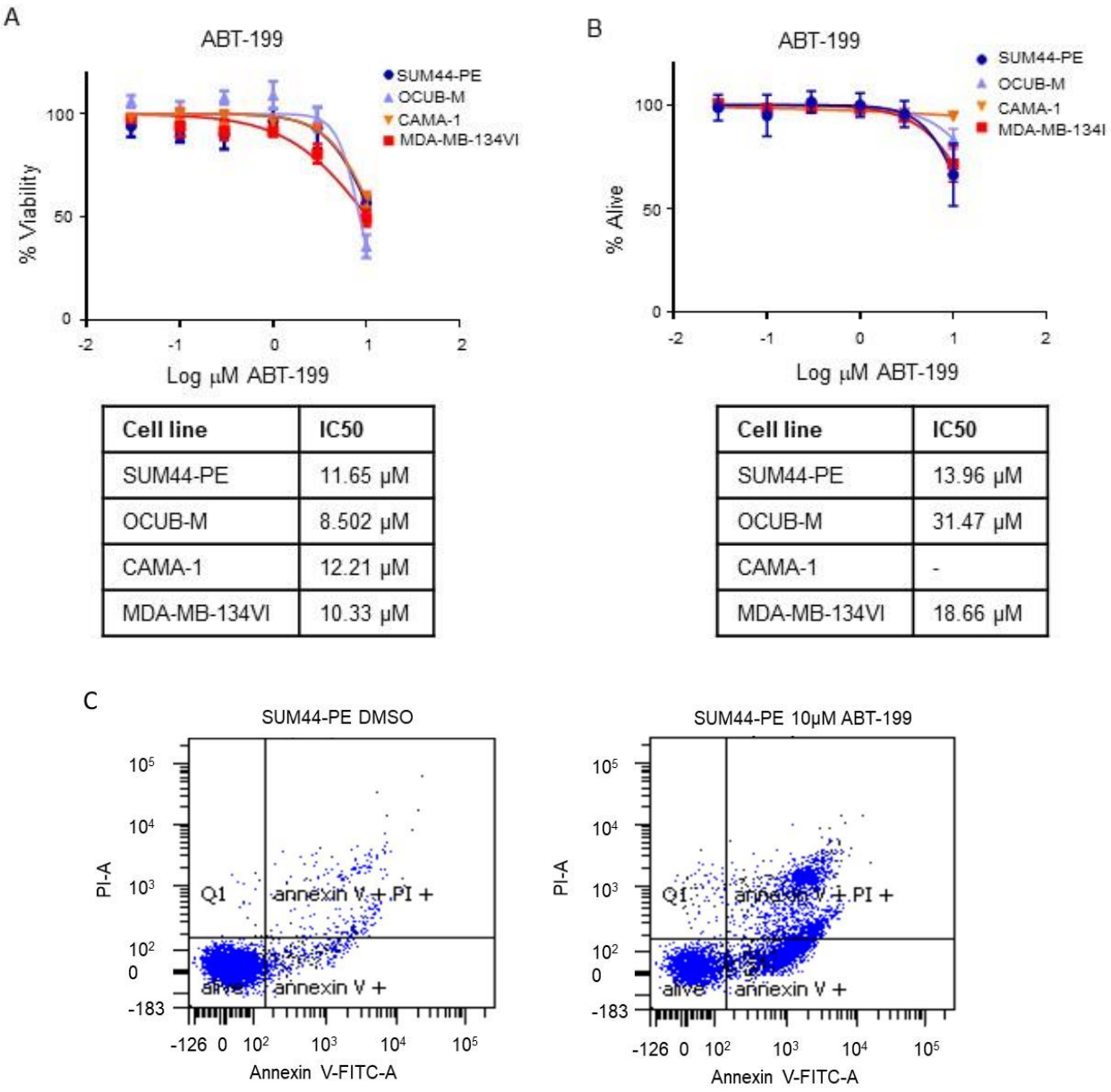

Cell line	IC50
SUM44-PE	11.65 µM
OCUB-M	8.502 µM
CAMA-1	12.21 µM
MDA-MB-134VI	10.33 µM

Cell line	IC50
SUM44-PE	13.96 µM
OCUB-M	31.47 µM
CAMA-1	-
MDA-MB-134VI	18.66 µM

Figure 4.13: ILC cell lines are not sensitive to ABT-199. (A) Cell viability curves after 72 hr of ABT-199 treatment using MTT assay. The IC50 values are listed beside each cell line. Mean of N=3 experiments plotted using nonlinear regression. Error bars indicate +/- SEM. (B) Apoptosis analysis using annexin V-FITC/PI staining and flow cytometry 72 hr following ABT-199 treatment. The IC50 values are listed beside each cell line. Mean of N=3 experiments plotted using nonlinear regression. Error bars show +/- SEM. (C) Representative dot plots from annexin V/PI staining in the SUM44-PE cell line treated with DMSO or 10 µM ABT-199 from the flow cytometer.

Then, the sensitivity of the panel of ILC cell lines to ABT-263 was measured. ABT-263 mediated growth inhibition and apoptosis in the SUM44-PE and MDA-MB-134VI cell lines (Figure 4.14a, b). At higher doses ABT-263 mediates growth inhibition and some apoptosis in the OCUB-M and CAMA-1 cell lines (Figure 4.14a, b). These results suggest that inhibition of BCL-2 alone is not sufficient to induce apoptosis but that inhibition of BCL-2/BCL-XL and BCL-W need to be inhibited.

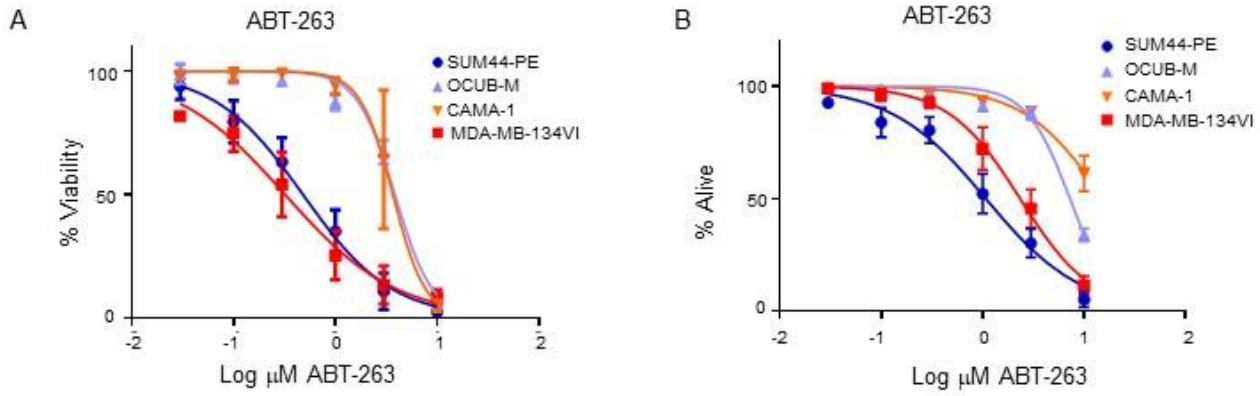

Cell lines	IC50
SUM44-PE	0.483 μM
OCUB-M	3.852 μM
CAMA-1	3.684 μM
MDA-MB-134VI	0.323 μM

Cell lines	IC50
SUM44-PE	1.08 μM
OCUB-M	7.289 μM
CAMA-1	15.68 μM
MDA-MB-134VI	2.352 μM

Figure 4.14: The SUM44-PE and MDA-MB-134VI cell lines are sensitive to ABT-263. (A) Cell viability curves after 72 hr of ABT-263 treatment using MTT assay. The IC50 values are listed beside each cell line. Mean of N=3 experiments plotted using nonlinear regression. Error bars show +/- SEM. (B) Apoptosis analysis using annexin V-FITC/PI staining and flow cytometry 72 hr after ABT-263 treatment. The IC50 values are listed beside each cell line. Mean of N=3 experiments plotted using nonlinear regression. Error bars indicate +/- SEM.

4.3.8 The combination of JQ1 and ABT-199 is not synergistic in ILC cell lines

The panel of ILC cell lines were insensitive to ABT-199 (Figure 4.13a, b), however the cell lines relatively resistant to JQ1-induced apoptosis (MDA-MB-134VI and CAMA-1) have high protein expression of BCL-2 (Figure 4.12a). It was next tested

whether inhibition of BCL-2 enhanced JQ1-induced apoptosis. JQ1 was combined with ABT-199 and cell viability (Figure 4.15a) and apoptosis (Figure 4.15b) was measured following 72 hr treatment. Only minor synergy with a combination index (CI) of < 0.7 was detected in the MDA-MB-134VI and OCUB-M cell lines with the combination of JQ1 and ABT-199 (Figure 4.15a) and importantly apoptosis was not enhanced or induced with the combination of JQ1 and ABT-199 in the sensitive or the relatively resistant cell lines (Figure 4.15b). Enhanced apoptosis was only detected in the MDA-MB-134VI cell line at the highest dose of JQ1 and ABT-199 ($p \leq 0.001$) (Figure 4.15b). These results suggest that inhibition of BCL-2 alone does not enhance JQ1-induced apoptosis, even in the resistant cell lines with high protein expression of BCL-2. BCL-2 is not responsible for JQ1-induced apoptotic resistance in ILC cell lines.

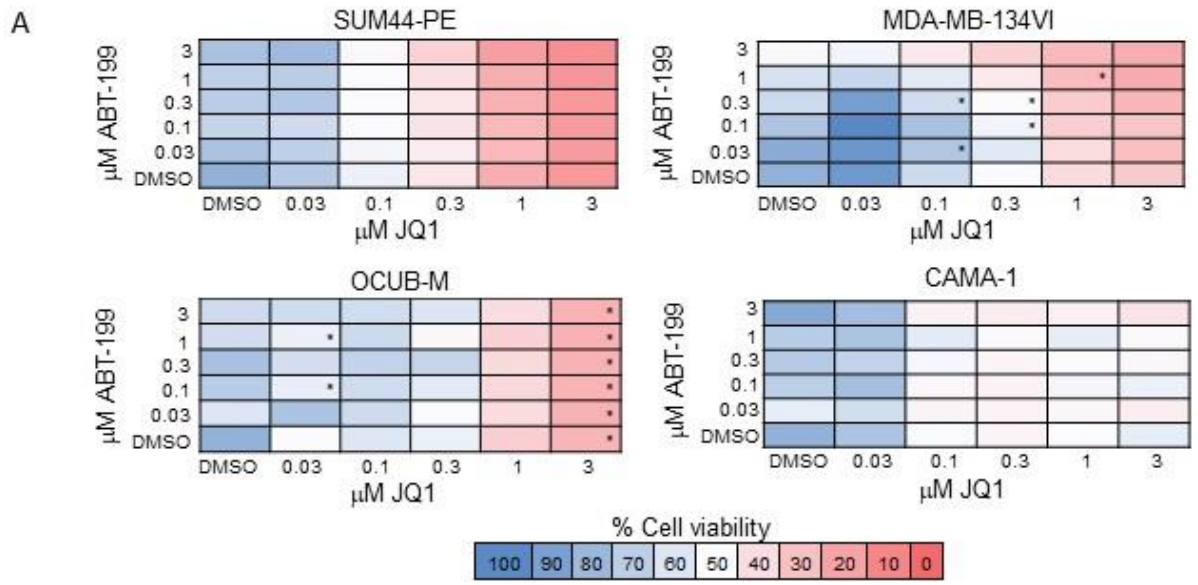

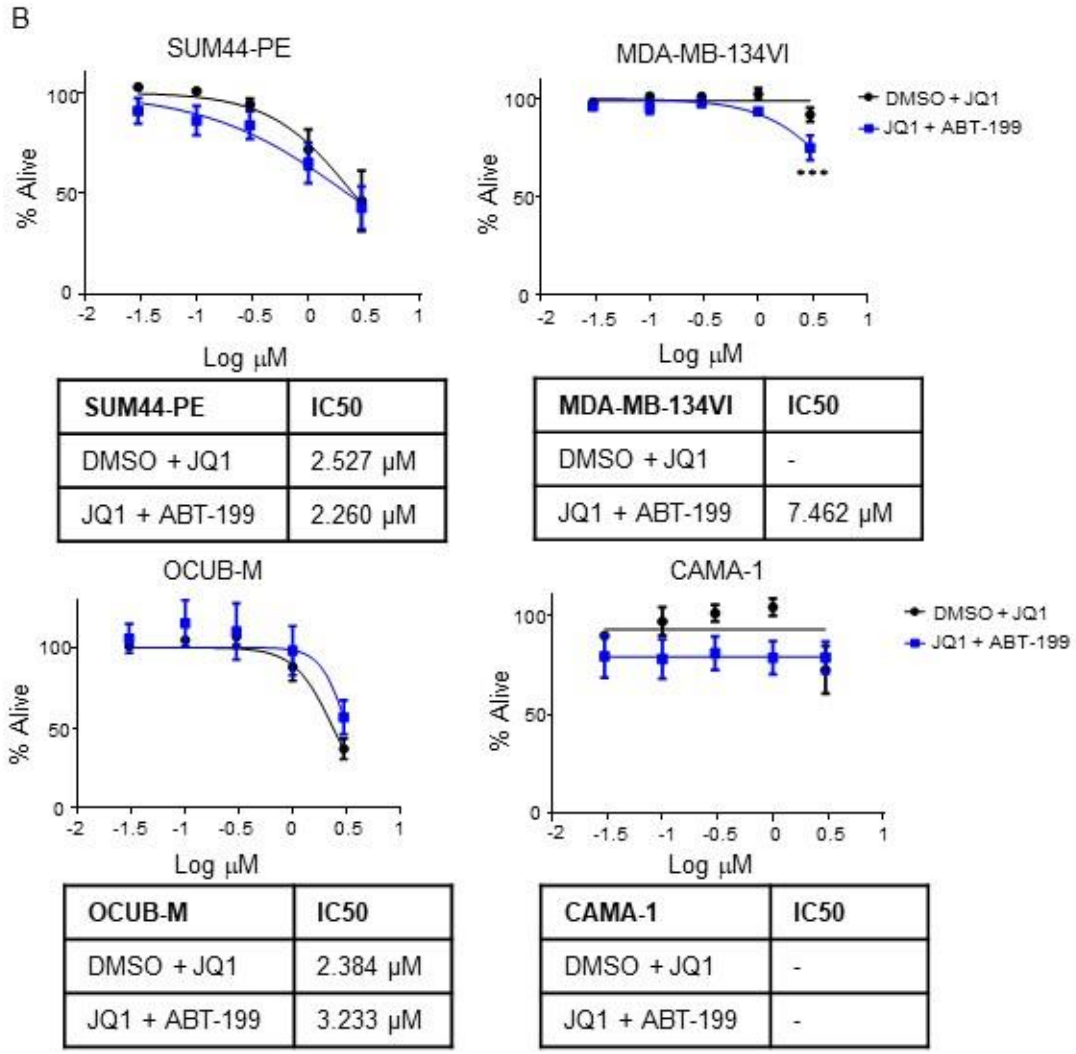

SUM44-PE	IC50
DMSO + JQ1	2.527 μM
JQ1 + ABT-199	2.260 μM

MDA-MB-134VI	IC50
DMSO + JQ1	-
JQ1 + ABT-199	7.462 μM

OCUB-M	IC50
DMSO + JQ1	2.384 μM
JQ1 + ABT-199	3.233 μM

CAMA-1	IC50
DMSO + JQ1	-
JQ1 + ABT-199	-

Figure 4.15: The combination of JQ1 and ABT-199 is not synergistic and does not enhance or induce apoptosis in ILC cell lines. (A) Cell viability heatmap matrix using MTT assay 72 hr after JQ1 and ABT-199 combination treatment. The mean of N=3 experiments was analysed using CompuSyn software to detect synergy. Synergy with a combination index (CI) <0.7 is marked with an asterisk. (B) Apoptosis analysis using annexin V-FITC/PI staining and flow cytometry 72 hr after JQ1 and 1 μM ABT-199 combination treatment. The IC50 values are listed beside each cell line. Mean of N=3 experiments plotted using nonlinear regression. Error bars indicate +/- SEM. Asterisks indicates significance using Two-Way ANOVA p≤ 0.05.

4.3.9 The combination of JQ1 and ABT-263 is synergistic in ILC cell lines

Next it was established whether inhibition of BCL-2/BCL-XL and BCL-W anti-apoptotic proteins using ABT-263 enhanced JQ1-induced apoptosis. JQ1 was combined with ABT-263 and cell viability (Figure 4.16a) and apoptosis (Figure 4.16b) was measured following 72 hr treatment. Synergy was detected with a CI <0.7 in three out of the four ILC cell lines using a cell viability assay (Figure 4.16a). Although synergy was not detected in the CAMA-1 cell line it is evident that the combination of JQ1 and ABT-263 mediated a greater growth inhibitory effect than either drug alone (Figure 4.16a, red). This is because synergy is based on the detection of an IC50 value with JQ1 treatment alone and an IC50 value with ABT-263 treatment alone, and neither drug produced much of a growth inhibiting effect in isolation (Figure 4.16a).

Apoptosis was also measured using annexin V/PI after the JQ1 and ABT-263 drug combination (Figure 4.16b). Interestingly, in the ILC cell lines sensitive to JQ1-induced apoptosis (SUM44-PE and OCUB-M), the combination of JQ1 and ABT-263 seemed to enhance the apoptotic effect of JQ1 treatment alone (Figure 4.16b). Importantly, in the ILC cell lines relatively resistant to JQ1-induced apoptosis (MDA-MB-134VI and CAMA-1), the combination of JQ1 and ABT-263 caused these cell lines to undergo apoptosis that was not occurring with JQ1 treatment alone (Figure 4.16b). These results suggest that either BCL-XL and/or BCL-W may contribute to cell survival in ILC cell lines resistant to JQ1-induced apoptosis and that the combination of JQ1 and ABT-263 may be an effective treatment strategy for overcoming this resistance in these cell lines (Figure 4.16a, b). However, it is important to note that one cannot exclude the possibility that BCL-2 is also required to be co-inhibited. It was hypothesised that BCL-XL is responsible for JQ1-induced apoptotic resistance in ILC cell lines as BCL-XL transcription is maintained or highly expressed following JQ1 treatment as analysed using RNA sequencing and qPCR analysis (Figure 4.11a, b). The combination of JQ1 and ABT-263 may also be an effective treatment strategy for cell lines sensitive to JQ1-induced apoptosis as this drug combination enhanced the apoptotic effect of JQ1 in these cell lines (Figure 4.16a, b).

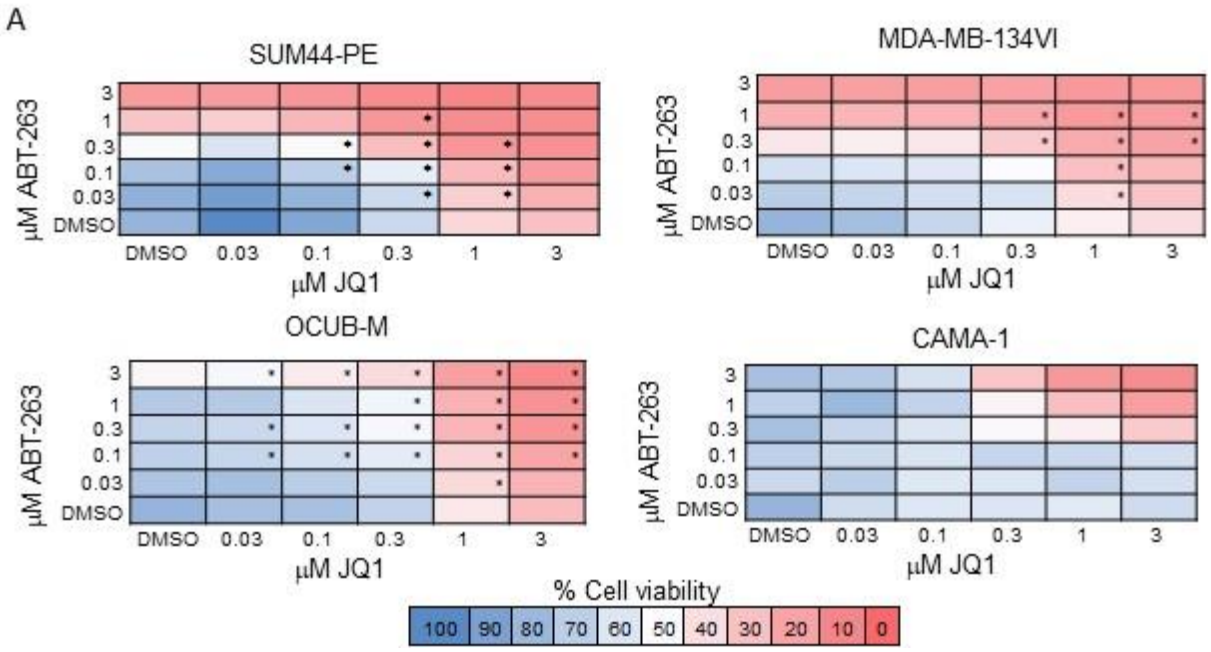

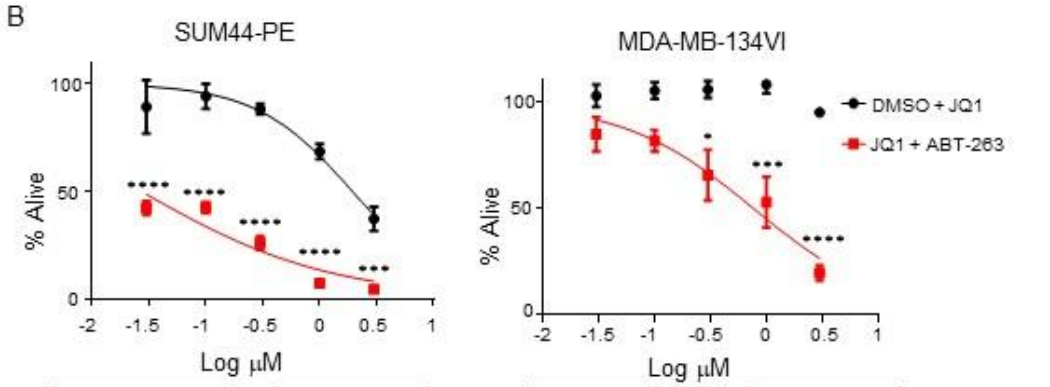

SUM44-PE	IC50
DMSO + JQ1	1.933 µM
JQ1 + ABT-263	0.027 µM

MDA-MB-134VI	IC50
DMSO + JQ1	-
JQ1 + ABT-263	0.771 µM

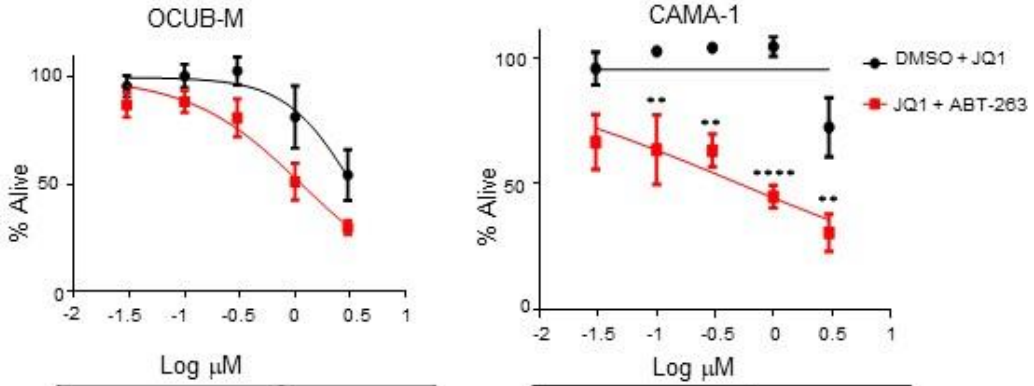

OCUB-M	IC50
DMSO + JQ1	3.293 µM
JQ1 + ABT-263	1.138 µM

CAMA-1	IC50
DMSO + JQ1	-
JQ1 + ABT-263	0.495 µM

Figure 4.16: The combination of JQ1 and ABT-263 is synergistic and enhances or induces apoptosis in ILC cell lines. (A) Cell viability heatmap matrix using MTT assay 72 hr after JQ1 and ABT-263 combination treatment. The mean of N=3 experiments was analysed using CompuSyn software to detect synergy. Synergy with a combination index (CI) <0.7 is marked with an asterisk. (B) Apoptosis analysis using annexin V-FITC/PI staining and flow cytometry 72 hr after JQ1 and 1 μM ABT-263 combination treatment. The IC50 values are listed beside each cell line. Mean of N=3 experiments plotted using nonlinear regression. Error bars indicate +/- SEM. Asterisks indicates significance using Two-Way ANOVA p≤ 0.05.

In order to further dissect the role of BCL-XL in apoptosis resistance, JQ1 was combined with the BCL-XL selective BH3 mimetic WEHI-539, in both a JQ1 apoptotic sensitive cell line (OCUB-M) and in a JQ1 apoptotic resistant cell line (CAMA-1). The combination of JQ1 and WEHI-539 only significantly enhanced apoptosis in the sensitive OCUB-M cell line at the 0.3 μM JQ1 and 1 μM WEHI-539 dose (p≤ 0.05) (Figure 4.17). Interestingly, the combination of JQ1 and WEHI-539 induced the CAMA-1 apoptotic resistant cell line to undergo apoptosis that was highly significant at the 0.3 μM JQ1 and 1 μM WEHI-539 dose (p≤ 0.001), 1 μM JQ1 and 1 μM WEHI-539 dose (p≤ 0.001) and 3 μM JQ1 and 1 μM WEHI-539 dose (p≤ 0.0001) (Figure 4.17). Furthermore, the combination of JQ1 and WEHI-539 (IC50= 0.3634 μM) produced similar results to the combination of JQ1 and ABT-263 (IC50= 0.495 μM) (Figure 4.16b, 4.17) in the CAMA-1 cell line. Surprisingly, the OCUB-M cell line displayed a lower IC50 value with the combination of JQ1 and WEHI-539 (IC50=0.4057 μM) compared to the JQ1 and ABT-263 combination (IC50= 1.138μM) at 72 hr treatment (Figure 4.16b, 4.17). This being said, the combination of JQ1 and WEHI-539 induced apoptosis to a significantly greater degree in the CAMA-1 cell line, than it induced apoptosis in the OCUB-M cell line (Figure 4.17). It may be that both the OCUB-M and CAMA-1 cell lines are reliant on BCL-XL for cell survival, that can be downregulated by JQ1 (Figure 4.12). However, BCL-XL expression may be maintained in the CAMA-1 cell line that requires the combination of JQ1 and ABT-263 or WEHI-539 in order to induce apoptosis, as apoptosis is not occurring in the CAMA-1 cell line but is in the OCUB-M cell line after 96 hr JQ1 treatment (Figure

4.1b). These findings support the hypothesis that BCL-XL may be contributing to JQ1-induced apoptotic resistance in ILC cell lines.

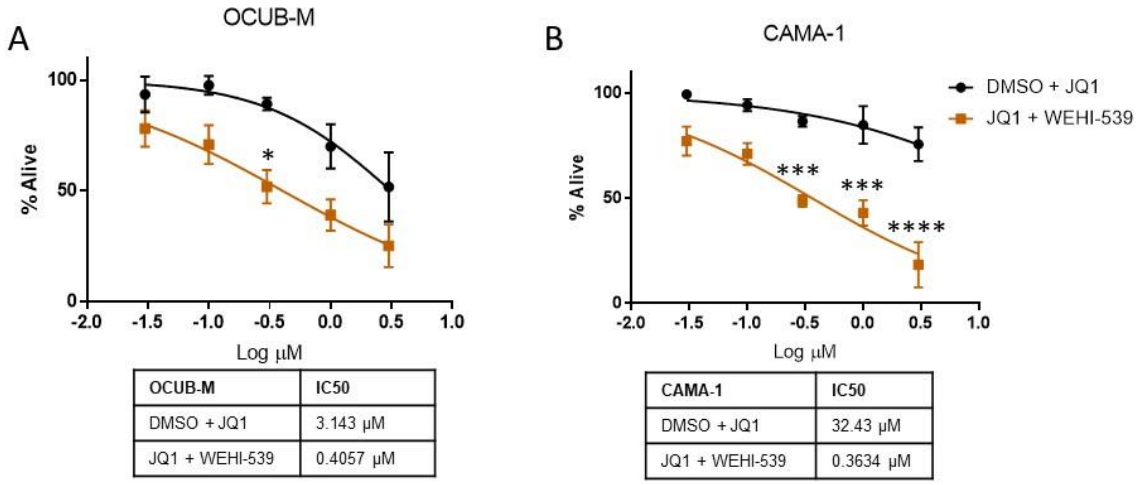

OCUB-M	IC50
DMSO + JQ1	3.143 µM
JQ1 + WEHI-539	0.4057 µM

CAMA-1	IC50
DMSO + JQ1	32.43 µM
JQ1 + WEHI-539	0.3634 µM

Figure 4.17: The combination of JQ1 and WEHI-539 enhances or induces apoptosis in ILC cell lines. Apoptosis analysis in the (A) OCUB-M and (B) CAMA-1 cell lines using annexin V-FITC/PI staining and flow cytometry 72 hr after JQ1 and 1 µM WEHI-539 combination treatment. The IC50 values are listed beside each cell line. Mean of N=3 experiments plotted using nonlinear regression. Error bars indicate +/- SEM. Asterisks indicates significance using Two-Way ANOVA p≤ 0.05.

4.3.10 The combination of JQ1 and 1 µM ABT-263 inhibits the growth and size of 3D spheroids in culture

The combination of JQ1 and ABT-263 was synergistic in ILC cell lines and could enhance apoptosis in ILC cell lines sensitive to JQ1-induced apoptosis or induce apoptosis in ILC cell lines that were relatively more resistant to JQ1-induced apoptosis (Figure 4.16a, b). Next the efficacy of the JQ1 and ABT-263 drug combination was measured using an *in vitro* 3D cell culture assay (345). Importantly, sensitivity to drugs in 3D cell culture has been reported to be better representative of the *in vivo* environment (346). The SUM44-PE (sensitive to JQ1-induced apoptosis) and the MDA-MB-134VI (relatively resistant to JQ1-induced apoptosis) were each seeded in matrigel for 24 hr followed by drug treatment for 72 hr. Following drug treatment, media alone (no drug) was replenished and changed twice weekly and

cells imaged on day 1, day 8 and day 15. The MDA-MB-134VI cell line formed more 3D spheroids compared the SUM44-PE cell line at day 15 (Figure 4.18a, d) and all spheroids remained viable in the controls as illustrated with Calcein AM (green) live stain (347) (Figure 4.18a, d, green). The number and size of 3D spheroids at day 15 were counted. The SUM44-PE cell line has been grown in 3D cell culture previously where the authors describe the cell line forming spherical and/or fused colonies (348), in line with findings from this study (Figure 4.18a). To our knowledge, the MDA-MB-134VI cell line has not been reported grown in 3D cell culture previously.

In the SUM44-PE cell line, JQ1 significantly inhibited both the number ($p \leq 0.05$) and size ($p \leq 0.0001$) of the spheroids formed in 3D cell culture (Figure 4.18b). The combination of JQ1 and ABT-263 inhibited the number of spheroids formed statistically better ($p \leq 0.01$) than JQ1 treatment alone (Figure 4.18b). JQ1 and the combination of JQ1 and ABT-263 inhibited the size of the spheroids in 3D culture to the same extent, that was highly significant ($p \leq 0.0001$) (Figure 4.18b). Similarly, in the MDA-MB-134VI cell line, JQ1 significantly inhibited both the number ($p \leq 0.05$) and size ($p \leq 0.01$) of the spheroids formed in 3D cell culture (Figure 4.18d). Like the SUM44-PE cell line, the combination of JQ1 and ABT-263 inhibited the number of spheroids formed statistically better ($p \leq 0.01$) than JQ1 treatment alone in the MDA-MB-134VI cell line (Figure 4.18d). JQ1 and the combination of JQ1 and ABT-263 inhibited the size of the spheroids formed in 3D culture to the same extent in the MDA-MB-134VI cell line, which was significant ($p \leq 0.01$) (Figure 4.18d). JQ1 and the combination of JQ1 and ABT-263 inhibited the size of the 3D spheroids formed in the SUM44-PE JQ1 apoptotic sensitive cell line to a greater extent ($p \leq 0.0001$) than in the JQ1 apoptotic resistant MDA-MB-134VI cell line ($p \leq 0.01$) (Figure 4.18b, d).

These results indicate that the combination of JQ1 and ABT-263 is more effective than JQ1 treatment alone at inhibiting the number of 3D spheroids grown in 3D culture, as shown for the SUM44-PE sensitive cell line and MDA-MB-134VI cell line that is relatively resistant to JQ1-induced apoptosis (Figure 4.18b, d, left).

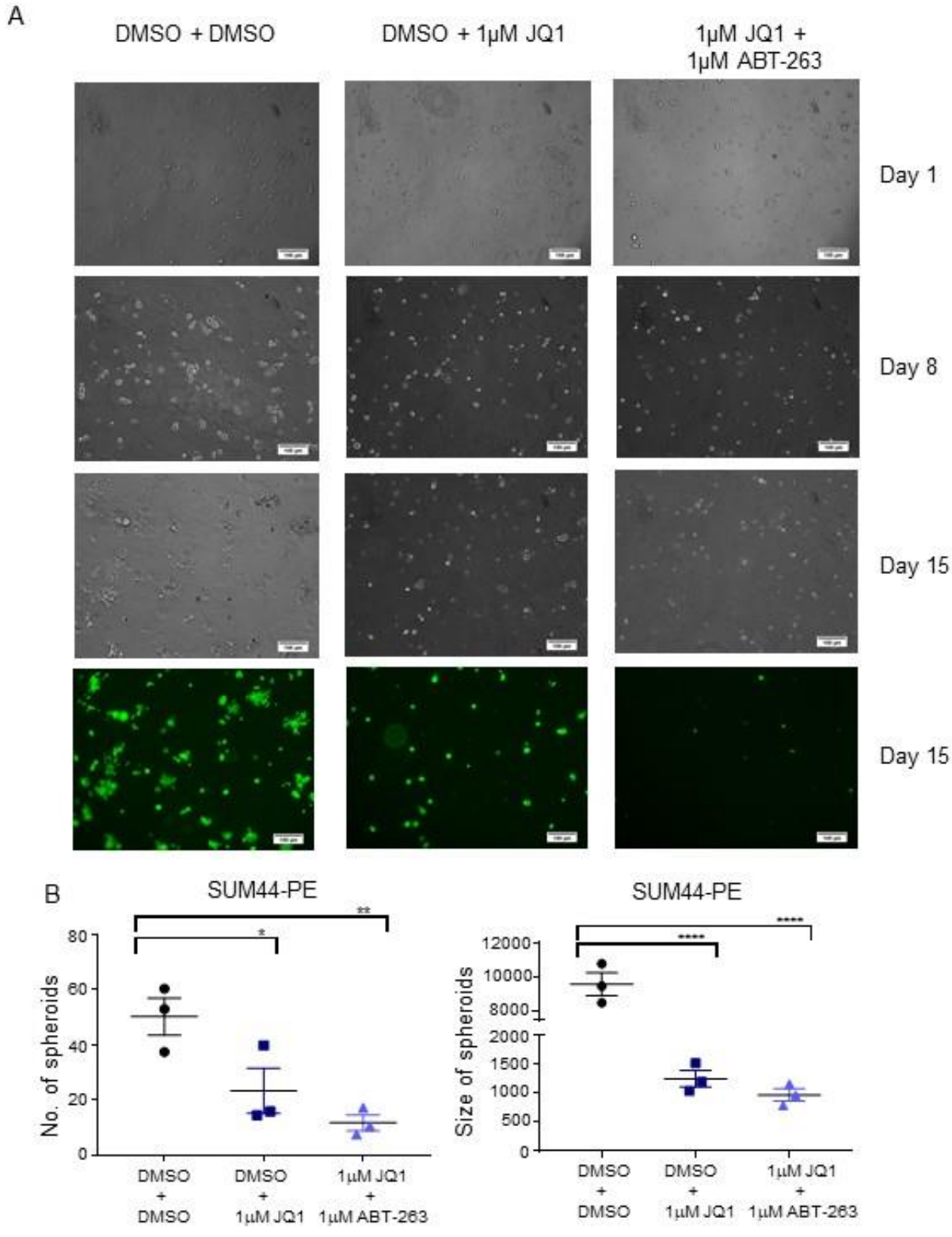
A
DMSO + DMSO
DMSO + 1μM JQ1
1μM JQ1 +
1μM ABT-263
Day 1
Day 8
Day 15
Day 15
B
SUM44-PE
No. of spheroids
80
60
40
20
0
*
**
DMSO
+
DMSO
DMSO
+
1μM JQ1
1μM JQ1
+
1μM ABT-263
SUM44-PE
Size of spheroids
12000
10000
8000
2000
1500
1000
500
0
****
****
DMSO
+
DMSO
DMSO
+
1μM JQ1
1μM JQ1
+
1μM ABT-263

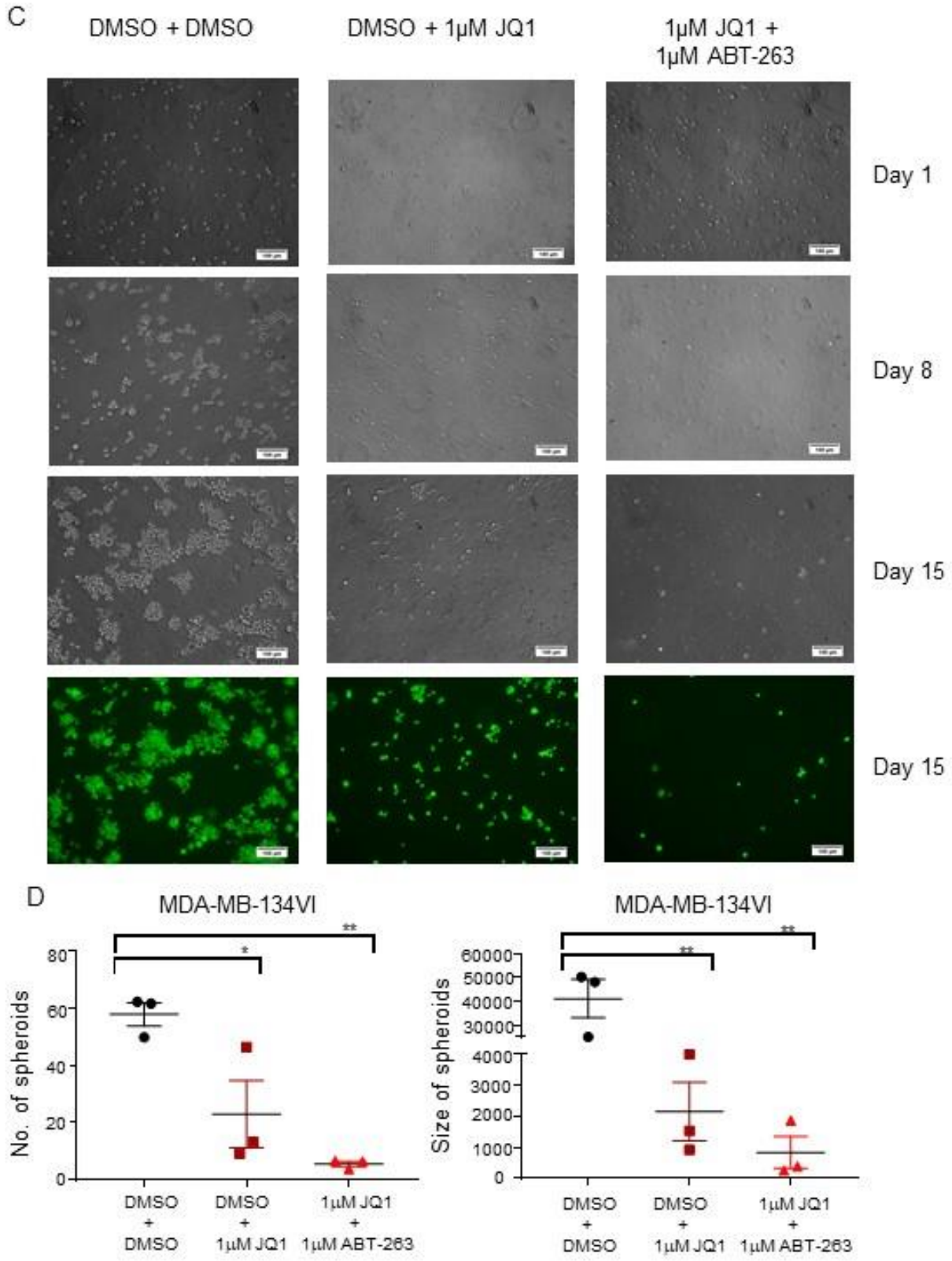

Figure 4.18: The combination of JQ1 and ABT-263 can inhibit both the number and size of 3D spheroids in 3D culture. Representative brightfield images of 1 μM JQ1 and the combination of 1 μM JQ1 and 1 μM ABT-263 treatments for 72 hr in 3D

culture in the (A) SUM44-PE cell line and (C) MDA-MB-134VI cell line on day 1, day 8 and day 15. 10X images were taken and scale bar indicates 100 μm. Cells are viable at day 15 as indicated with calcein AM green fluorescent staining using confocal imaging. The number (manual cell counting) and size in square pixels (ImageJ software) of the 3D spheroids at day 15 were quantified in the (B) SUM44-PE cell line and (D) MDA-MB-134VI cell line. Mean of N=3 experiments. Error bars show +/- SEM and asterisks indicates significance using One-Way ANOVA $p \leq 0.05$.

4.3.11 Optimisation of antibodies in ILC cell lines for flow cytometry analyses of patient tumour sample and PDX

A ILC patient primary sample (T509) and an ILC PDX sample (T638) was available for this study, which were grown *ex vivo* and analysed in single cell suspension by flow cytometry. For the T509 primary sample a CD45-PE antibody was optimised in order to identify any white blood cells (301) and remove them from the analysis. The CD45-PE antibody was optimised in ILC cell lines and a Jurkat leukemic cell line prior to staining the T509 primary sample. ILC cell lines were negative for CD45, whereas the Jurkat leukemic cell line is positive for CD45 (data not shown).

For the T638 ILC PDX sample a EpCAM-APC antibody was optimised, as the PDX was grown in NOD-SCID mice and would be CD45 negative. EpCAM-APC was used as a positive selection marker in order to identify tumour cells in the ILC PDX. The EpCAM antibody was optimised in ILC cell lines and the Jurkat leukemic cell line prior to staining the ILC PDX T638 sample. The SUM44-PE is the representative ILC cell line shown and is positive for EpCAM, which is an epithelial cell marker (302), whereas the Jurkat leukemic cell line is negative for EpCAM (Figure 4.19).

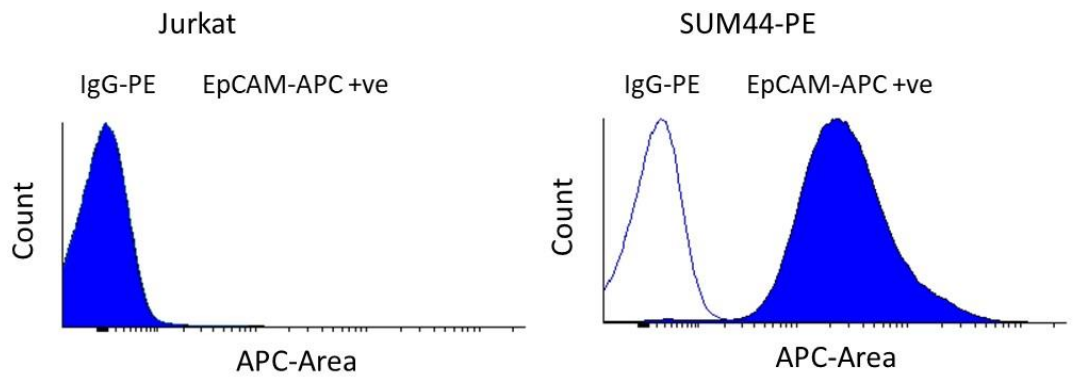

Figure 4.19: Optimisation of EpCAM-APC antibody in the SUM44-PE (ILC) and Jurkat (leukemia) cell line. Representative histograms showing Jurkat or SUM44-PE cells stained with IgG-APC and EpCAM-APC. Histograms were overlapped using the Cyflogic software. The ILC SUM44-PE cell line is positive for EpCAM-APC but not the Jurkat leukemic cell line.

4.3.12 The combination of JQ1 and ABT-263 causes apoptosis in a ILC primary sample *ex vivo*

The previous results showed that the combination of JQ1 and ABT-263 was effective at inhibiting the number and size of 3D spheroids in 3D cell cultures of ILC cell lines (Figure 4.18b, d). Due to a lack of ILC cell lines available, the efficacy of the JQ1 and ABT-263 combination was assessed in a ILC primary sample.

The T509 primary ILC sample was obtained with consent from Beaumont Hospital, Dublin, Ireland in collaboration with Prof. Leonie Young, RCSI, Ireland. The primary sample was treatment naive. The ILC primary patient T509 sample was ER positive, PgR positive and HER2 negative (Figure 4.20). Images were taken of the IHC receptor slides obtained from Beaumont Hospital for patient T509 that were analysed by the in house pathologist (Figure 4.20).

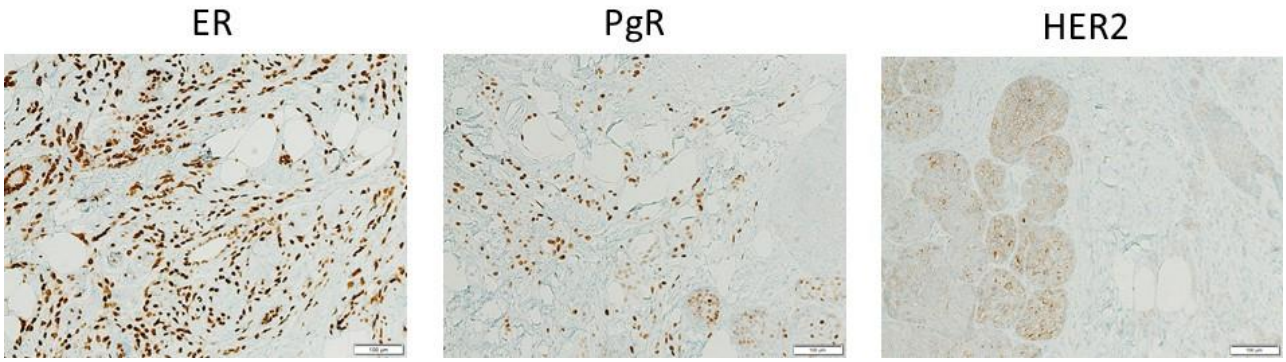

Figure 4.20: IHC analysis of the T509 primary ILC sample. 10X images of receptor status of the T509 primary sample by IHC. The IHC slides were obtained from Beaumont Hospital, Dublin, Ireland. Scale bar indicates 100 μm.

T509 primary tumour pieces were treated with DMSO + DMSO or 1 μM JQ1 + 1 μM ABT-263 for 48 hr *ex vivo* on sponges (Figure 4.21) and then the tumour pieces were put into single cell suspension and stained with CD45-PE/annexin V-FITC. *Ex vivo* models enable the evaluation of drug efficacy in the intact tumour microenvironment of human tumours, improving preclinical testing (303). This is a novel method of analysing the tumours by flow cytometry that have been grown *ex vivo* on dental sponges (303-305), to our knowledge.

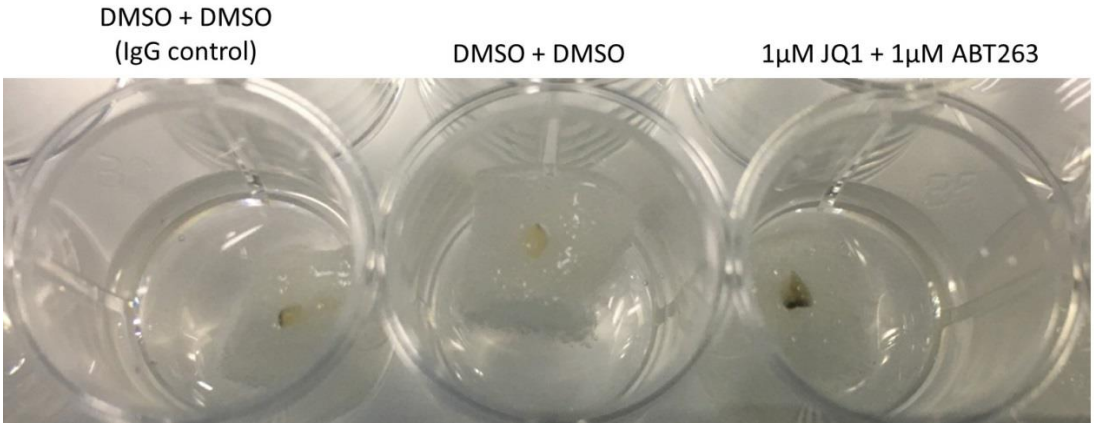

Figure 4.21: The T509 primary ILC patient sample grown *ex vivo* on dental sponges. The T509 primary patient sample was cut into small pieces and placed on dental sponge pre-soaked with HBEC media and drug for 48 hr. Conditions: DMSO + DMSO or 1 μM JQ1 + 1 μM ABT-263.

The single cell suspension of each tumour sample was sorted based on CD45-PE negativity, in order to remove white blood cells from the analysis (Figure 4.22a, left). Surprisingly, there were very few CD45 positive cells in the cell population. Annexin V-FITC positivity was then measured in this CD45-PE negative cell population in order to measure apoptosis (Figure 4.22a, right). There was a 40.3% increase in annexin V positivity with the combination of JQ1 and ABT-263 versus the control (Figure 4.22b). These results indicate that the combination of JQ1 and ABT-263 can induce apoptosis in a primary ILC sample and may be a potential rational drug combination for ILC.

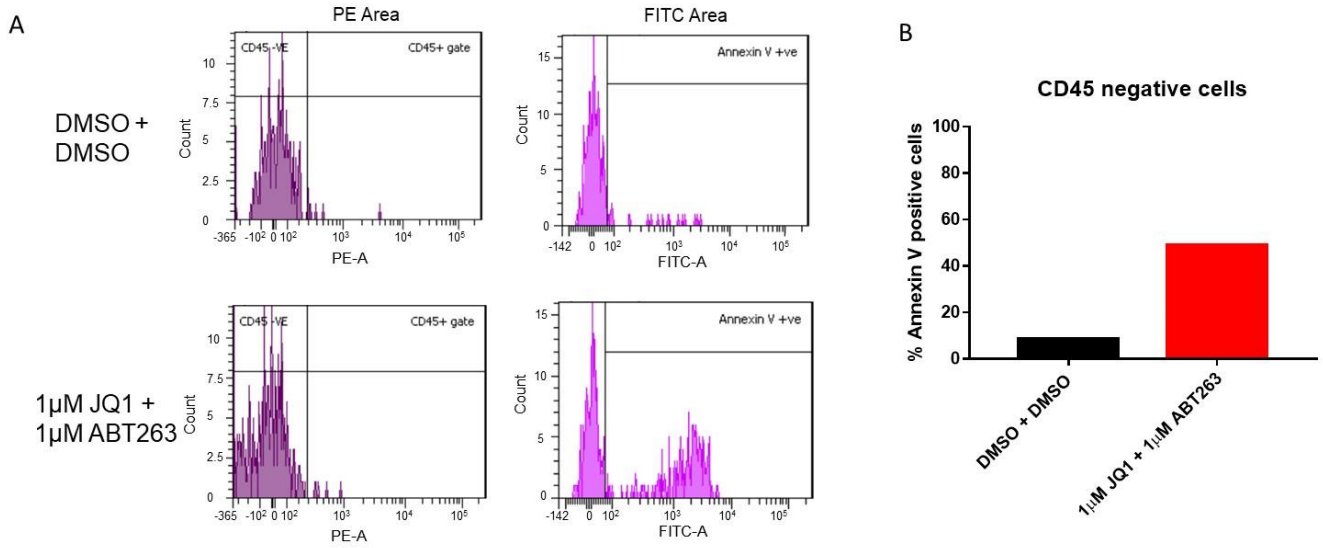

Figure 4.22: The combination of 1 μM JQ1 and 1 μM ABT-263 causes apoptosis in the T509 ILC primary patient sample grown *ex vivo*. (A) Flow cytometry analysis of the T509 primary ILC sample. CD45 negative cells were gated in order to remove white blood cell contaminants from the analysis (left histogram plots, purple). Annexin V positivity was measured in CD45 negative cells (right histograms, pink). (B) Apoptosis analysis of the T509 primary ILC sample in a bar chart by plotting the percentage (%) of annexin V positive cells in the CD45 negative population.

4.3.13 The combination of JQ1 and ABT-263 in the T638 ILC PDX could not be accurately measured *ex vivo* by either flow cytometry or IHC analysis

Additionally, a ILC PDX sample was available for this study that was also obtained in collaboration with Prof. Leonie Young, RCSI, Ireland. This ILC PDX sample, T638, was from a ILC patient whom had been previously treated with chemotherapy, radiotherapy and tamoxifen but had unfortunately relapsed and metastasised to the bone and brain. The T638 ILC PDX was established from brain metastases of this patient by Prof. Leonie Young's laboratory. For this experiment, the T638 sample was again grown *ex vivo* on dental sponge as previously described (303-305) but the PDX sample was treated with drug for 72 hr in order to increase the amount of apoptosis obtained with a longer time point. For the T638 ILC PDX sample, there was enough tumour sample to include DMSO + DMSO, DMSO + 1 µM JQ1 and 1 µM JQ1 + 1 µM ABT-263 treatment groups. After 72 hr, the tumour samples were put into single cell suspension and stained with EpCAM-APC.

The T638 ILC PDX sample was positive for ER as well as PgR but negative for HER2 as assessed by a pathologist in Beaumont Hospital (Figure 4.23a). The PDX was also negative for E-cadherin, which is a characteristic of ILC (Figure 4.23a). Images were taken of the IHC receptor and E-cadherin slides obtained from Beaumont Hospital for patient T638 (Figure 4.23a). After 72 hr drug treatment *ex vivo*, the PDX was put into single cell suspension, stained with EpCAM-APC/annexin V-FITC and analysed by flow cytometry. Tumour cells were selected based on EpCAM-APC positivity (Figure 4.23b, left). Annexin V-FITC positivity was then measured in the EpCAM-APC positive cell population in order to measure apoptosis (Figure 4.23b, right). Unexpectedly, there was a huge amount of death in all treatment samples, including the controls (Figure 4.23c), and no effect of the JQ1 single treatment or the JQ1 and ABT-263 combination treatment was able to be inferred from this experiment.

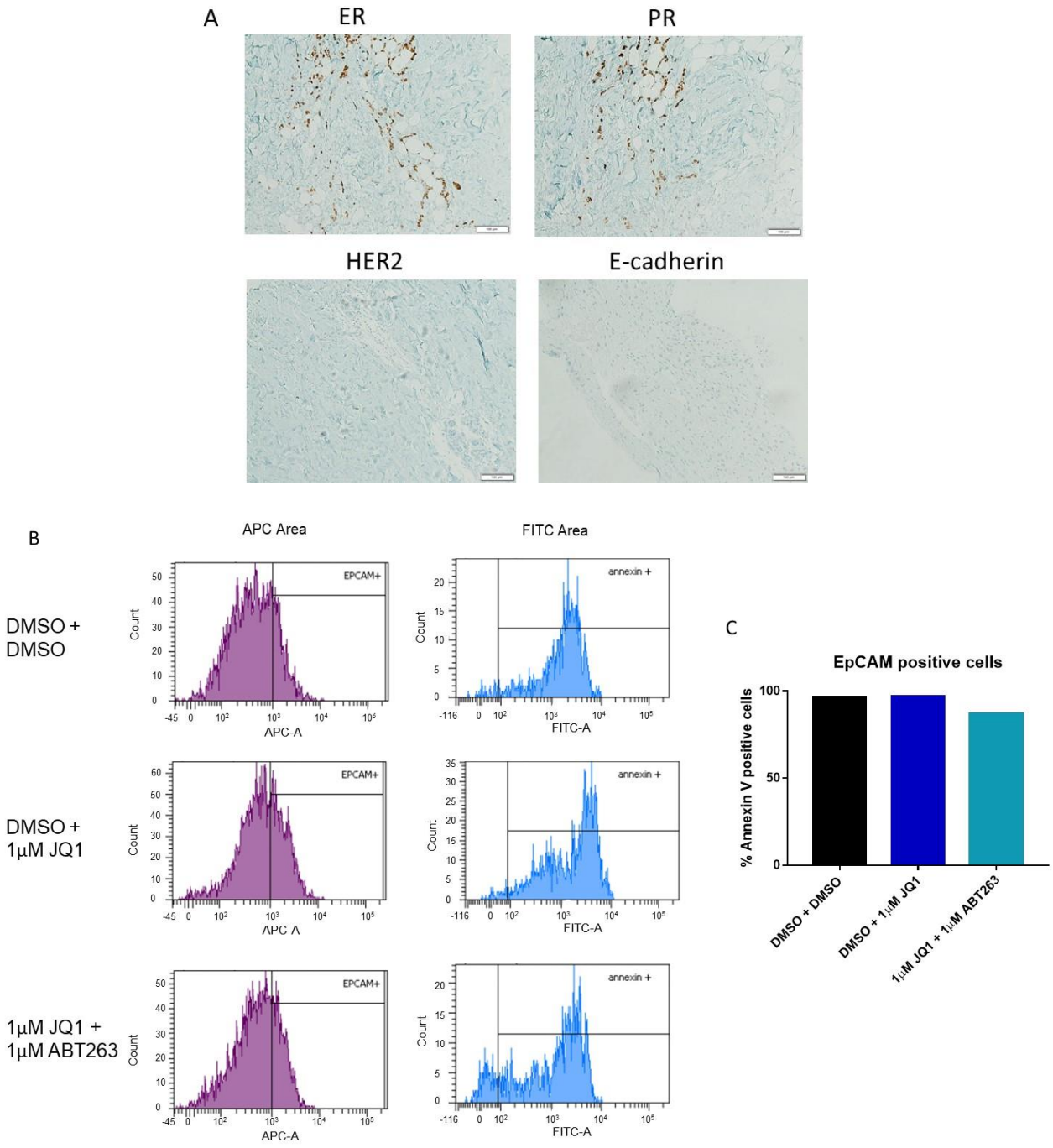

Figure 4.23: The combination of 1 µM JQ1 and 1 µM ABT-263 does not enhance apoptosis in the T638 ILC PDX sample grown *ex vivo*. (A) 10X images of receptor status and E-cadherin negativity of the T638 ILC PDX sample by IHC. The IHC slides were obtained from Beaumont Hospital, Dublin, Ireland. (B) Flow cytometry analysis of T638 ILC PDX sample. EpCAM positive cells were gated in order to include tumour cells in the analysis (left histogram plots, purple). Annexin V positivity was measured in EpCAM positive cells (right histograms, blue). (C)

Apoptosis analysis of the T638 ILC PDX sample in a bar chart by plotting the percentage (%) of annexin V positive cells in the EpCAM positive cell population.

There was one more ILC PDX T638 sample available for analysis. As the flow cytometry did not produce any usable data, this PDX was analysed by IHC. The ILC PDX was again cut into pieces, set up *ex vivo* on the dental sponges and treated with drug for 72 hr. After the 72 hr drug treatment, the tumour pieces were fixed, processed and embedded in wax. Sections were cut from the tumour blocks and mounted on slides for each tumour condition. H & E staining was carried out to confirm presence of tumour cells (Figure 4.24a, top panel). After confirming the presence of tumour cells, the tumour slides were stained for cleaved caspase 3 (Figure 4.24a, middle panel) and also for BCL-XL (Figure 4.24a, bottom panel). The T638 ILC PDX was stained for cleaved caspase 3 in order to detect apoptosis. The T638 ILC PDX was stained for BCL-XL in order to assess whether sensitivity to apoptosis as indicated by cleaved caspase 3 staining could be predicted based on BCL-XL expression. The data to date would suggest that JQ1 treatment alone would be sufficient to induce apoptosis in a tumour with low BCL-XL expression, but in a tumour with high BCL-XL expression the combination of JQ1 and ABT-263 would be required to induce apoptosis (Figure 4.1b; 4.11a, b; 4.12a; 4.16b; 4.17).

Two non-consecutive tumour slides were stained for cleaved caspase 3 and BCL-XL for each treatment condition. A pathologist, Dr. Claudia Aura Gonzalez (University College Dublin, Ireland), who was blinded to the study quantified the IHC slides using the H-score method (349) (Figure 4.24b, c). The results from the IHC data are extremely variable, with the DMSO + 1 µM JQ1 treatment only showing increased caspase 3 cleavage in one out of two replicates and the combination treatment of 1 µM JQ1 and 1 µM ABT-263 displaying similar levels of caspase 3 cleavage compared to control (Figure 4.24b). Likewise, BCL-XL showed the same trend, in that the DMSO + 1 µM JQ1 treatment only showed decreased BCL-XL expression in one out of two replicates and the combination treatment of 1 µM JQ1 and 1 µM ABT-263 displayed similar levels of BCL-XL compared to control (Figure 4.24c). The IHC results are in contrast to the working hypothesis and mirrors the inaccurate data obtained with the flow cytometry for this PDX sample. It was expected that the

combination treatment of JQ1 and ABT-263 would be as effective if not more efficacious compared to the JQ1 treatment alone.

For the ILC PDX T638 experiments the treatment time point was increased from 48 hr (used in the primary T509 patient sample) to 72 hr, which could have negatively impacted the experiment. The DMSO treatment in the control may have become toxic after 72 hr providing inaccurate data. Others in the Prof. Leonie Young laboratory have grown IDC tumours on dental sponges for more than 5 days, however no one has attempted this with ILC tumours previously.

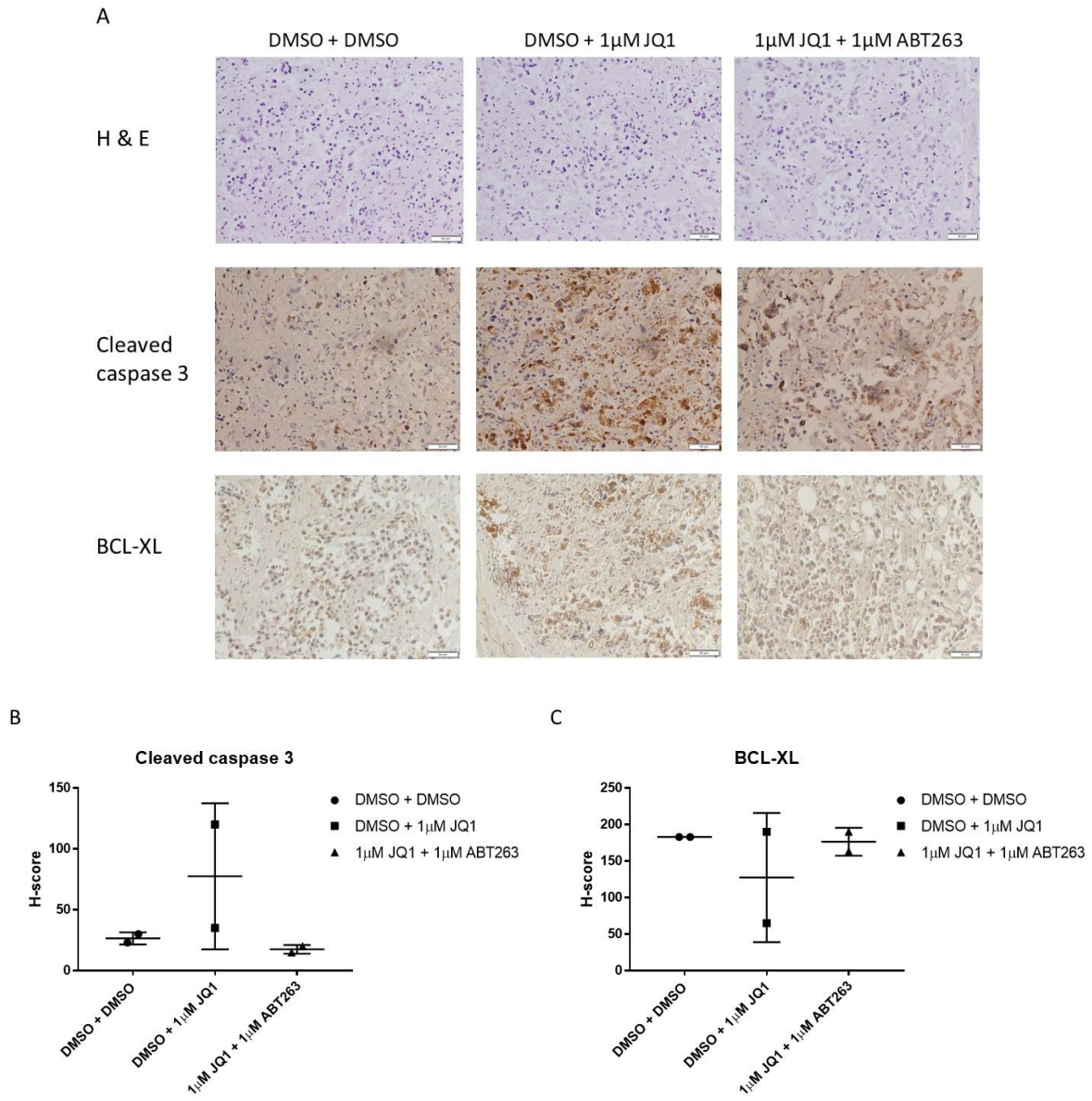

Figure 4.24: IHC analysis of the T638 ILC PDX sample. (A) 10X images of H & E staining of the ILC PDX in the first panel, followed by IHC staining for cleaved caspase 3 and BCL-XL in subsequent panels. (B) H-score quantification of cleaved caspase 3 was done by a pathologist (Dr. Claudia Aura Gonzalez) who was blinded to the study. (C) H-score quantification of BCL-XL was done by a pathologist (Dr. Claudia Aura Gonzalez) who was blinded to the study. H-score= % positive cells with intensity category 1 x 1 + % positive cells with intensity category 2 x 2 + % positive cells with intensity category 3 x 3 (349). Scale bar indicates 100 μm.

4.3.14 ABT-263 in combination with the CDK7 inhibitor THZ1 is synergistic in TNBC

TNBC is a breast cancer subtype that has poor prognosis (350). There is no targeted therapy available to TNBC patients and they mainly rely on cytotoxic chemotherapy (32). TNBC patients with residual disease following chemotherapy display significantly worse survival compared to other breast cancers (32), therefore novel therapeutic options are urgently needed. Others in the laboratory identified that high CDK7 mRNA expression was associated with poor prognosis in TNBC from two breast cancer cohorts, that was subsequently confirmed at the protein level (351). For this study, two available CDK7 inhibitors, BS-181 and THZ1 (217, 223), were tested in two TNBC cell lines, BT549 and MDA-MB-231. THZ1 inhibited the growth of TNBC at a considerably higher potency compared to BS-181 in both cell lines (Figure 4.25a, b). This may be in part due to the covalent nature of CDK7 inhibition by THZ1 (217).

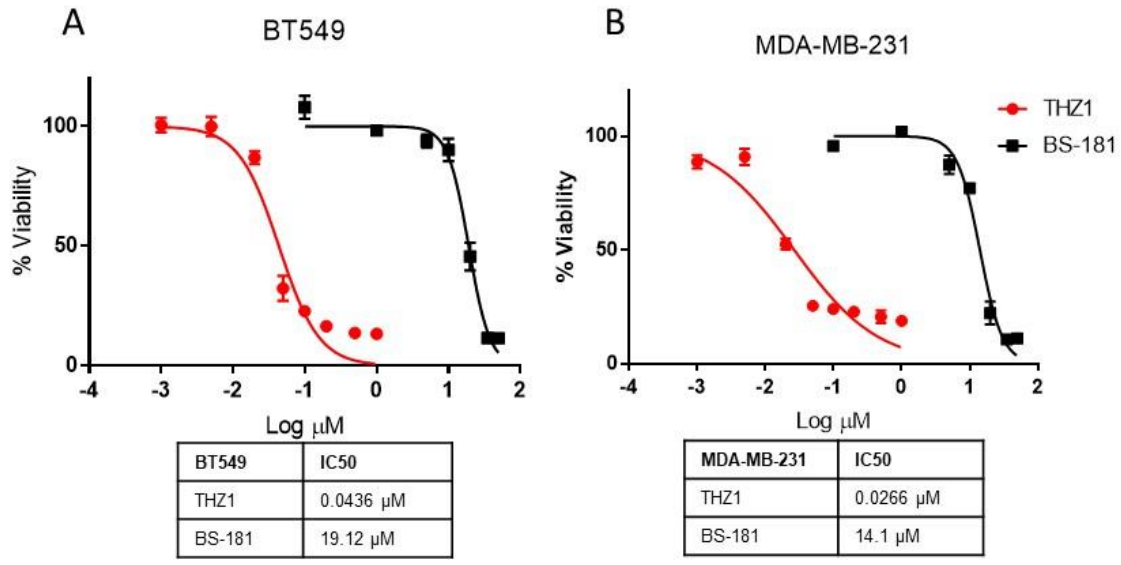

BT549	IC50
THZ1	0.0436 μM
BS-181	19.12 μM

MDA-MB-231	IC50
THZ1	0.0266 μM
BS-181	14.1 μM

Figure 4.25: TNBC cell lines are sensitive to growth inhibition mediated by CDK7 inhibitors. Dose response curves after 72 hr of BS-181 or THZ1 treatment using MTT assay. The IC50 values are listed beside each cell line. Mean of N=3 experiments plotted using nonlinear regression. Error bars show +/- SEM.

Next it was assessed whether BS-181 and THZ1 could induce apoptosis in TNBC cell lines. The BT549 cell line was sensitive to both THZ1- and BS-181-mediated

apoptosis (Figure 4.26a). However, the MDA-MB-231 cell line was relatively insensitive to THZ1-mediated apoptosis and was only sensitive to BS-181 induced apoptosis at very high doses (Figure 4.26b).

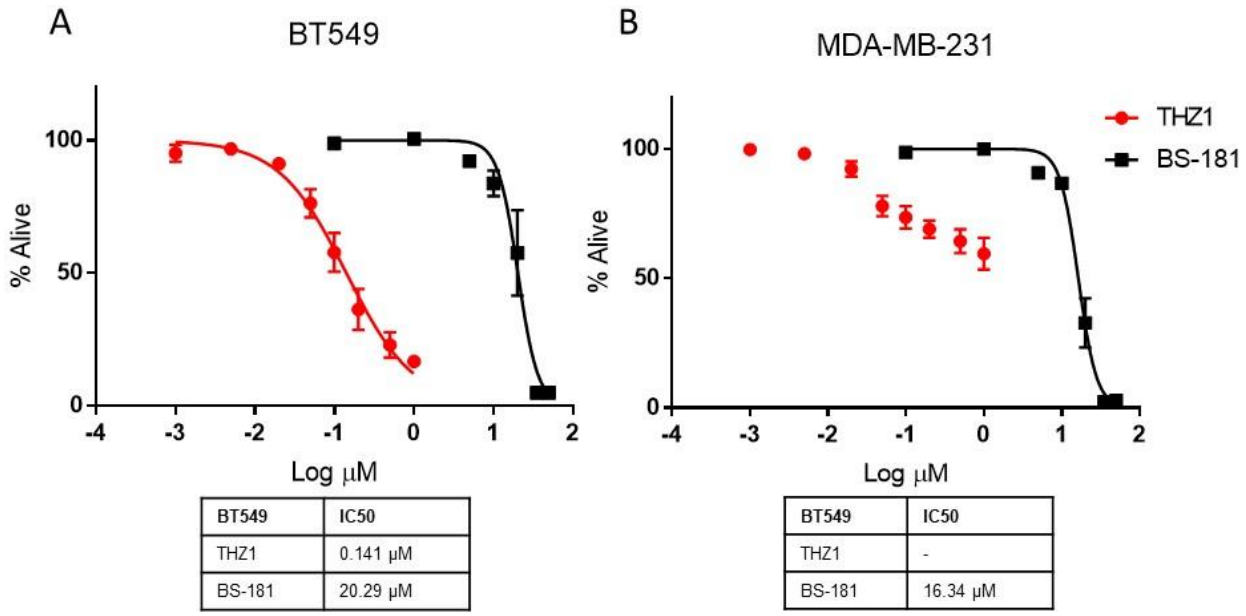

BT549	IC50
THZ1	0.141 μM
BS-181	20.29 μM

BT549	IC50
THZ1	-
BS-181	16.34 μM

Figure 4.26: Some TNBC cell lines are sensitive to CDK7 inhibition induced apoptosis. Apoptosis analysis in the (A) BT549 and (B) MDA-MB-231 cell lines using annexin V-FITC/PI staining and flow cytometry 48 hr following BS-181 or THZ1 treatment. The IC50 values are listed beside each cell line. Mean of N=3 experiments plotted using nonlinear regression. Error bars indicate +/- SEM.

As the MDA-MB-231 cell line is relatively resistant to CDK7 inhibitor-induced apoptosis, dynamic BH3 profiling was performed in order to identify anti-apoptotic dependencies in this cell line (Figure 4.27). Following treatment with THZ1, there was an increased loss of cytochrome *c* following treatment with the BAD and HRK peptide that was statistically significant ($p \leq 0.01$) (Figure 4.27). BH3 peptides have specific binding interactions (Figure 1.9) (263). BAD binds the BCL-2, BCL-XL and BCL-W proteins, whereas HRK binds BCL-XL (263). Increased cytochrome *c* loss following both BAD and HRK peptides indicates dependency on BCL-XL anti-apoptotic protein, as has been shown by others (352).

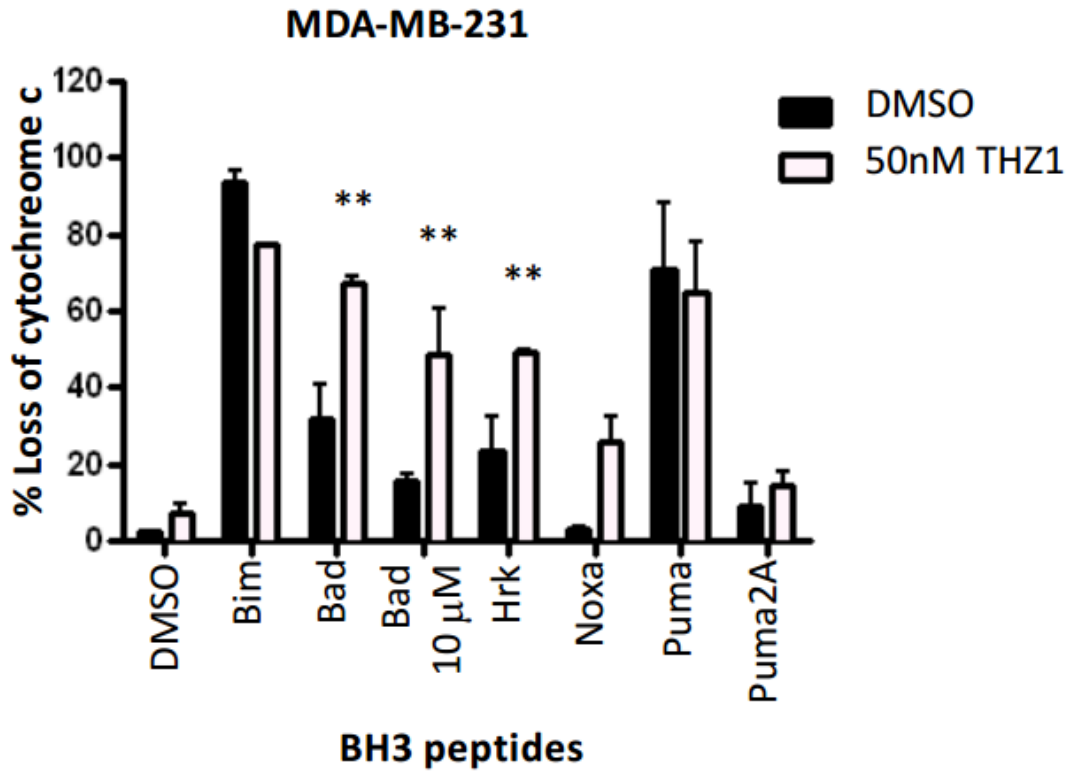

Figure 4.27: The MDA-MB-231 cell line is dependent on the BCL-XL anti-apoptotic protein. % loss of cytochrome *c* released was measured following 16 hr THZ1 treatment in the MDA-MB-231 cell line by dynamic iBH3 profiling using flow cytometry. Cells were treated with 100µM peptide unless stated otherwise. Mean of N=3 experiments. Error bars show +/- SEM. Asterisks indicates significance using t-test p≤ 0.05.

In order to address this prediction, others in the laboratory combined THZ1 with the BH3 mimetics, ABT-199 and ABT-263 (351). The combination of THZ1 and ABT-263 mediated synergistic growth inhibition in both the BT549 and MDA-MB-231 cell lines, whereas the combination of THZ1 and ABT-199 was only synergistic in the BT549 cell line. Furthermore, the combination of THZ1 and ABT-263 was synergistic at inducing apoptosis at low doses in both the BT549 and MDA-MB-231 cell lines. The combination of THZ1 and ABT-199 was synergistic in these cell lines only after treatment with high concentration of drug (351). Following on from this, the combination of THZ1 and BH3 mimetics was further validated in 4 more TNBC cell lines (Figure 4.28a, b). Synergistic growth inhibition was detected in three out of the four TNBC cell lines with the combination of THZ1 and ABT-263 (CI <0.7) (Figure

4.28a). In contrast, only minor synergy was detected at high doses with the combination of THZ1 and ABT-199 in the HCC1937 cell line (Figure 4.28b). The BT20 cell line was relatively resistant to both the THZ1 and ABT-263 combination as well as the THZ1 and ABT-199 combination (Figure 4.28a, b).

These findings suggest that the combination of CDK7 inhibition and BH3 mimetics may be a therapeutic option for TNBC patients.

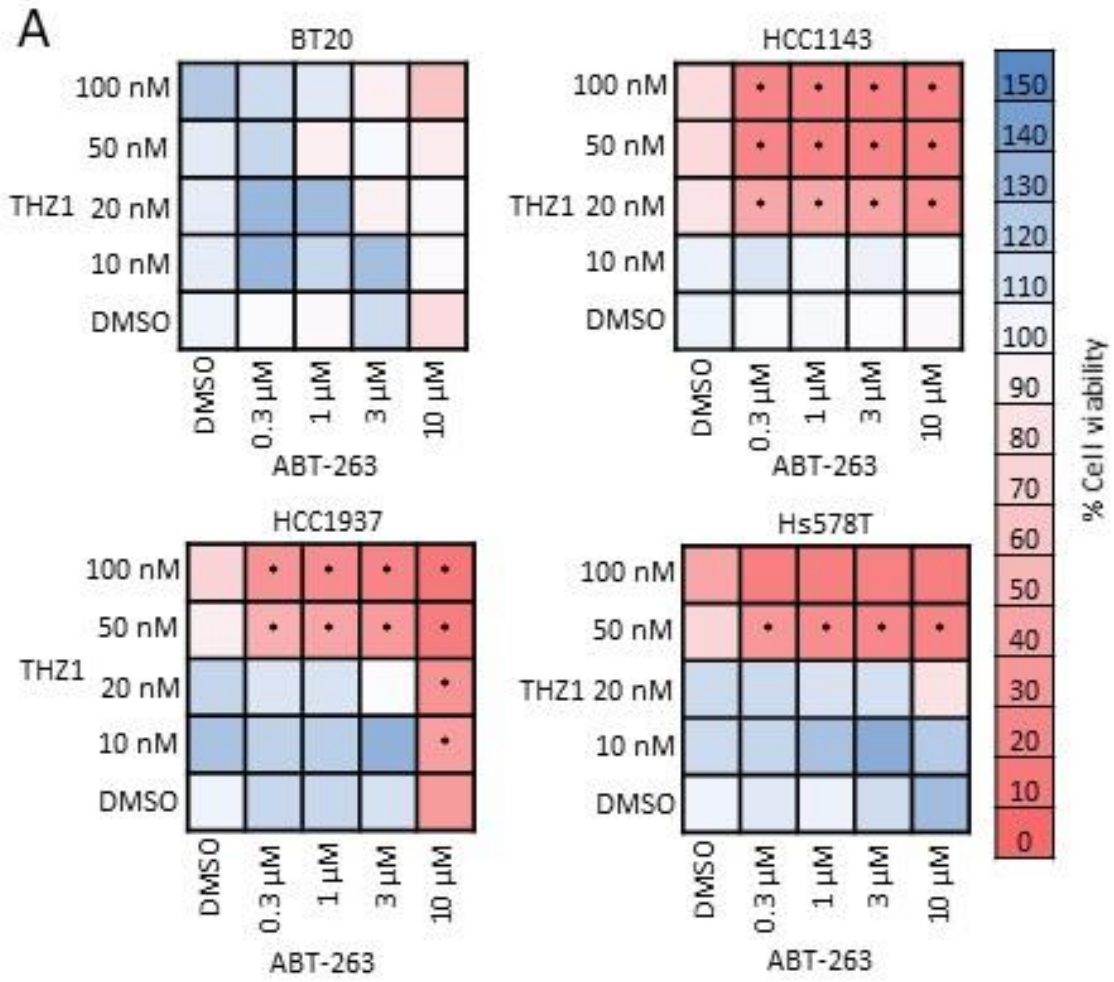

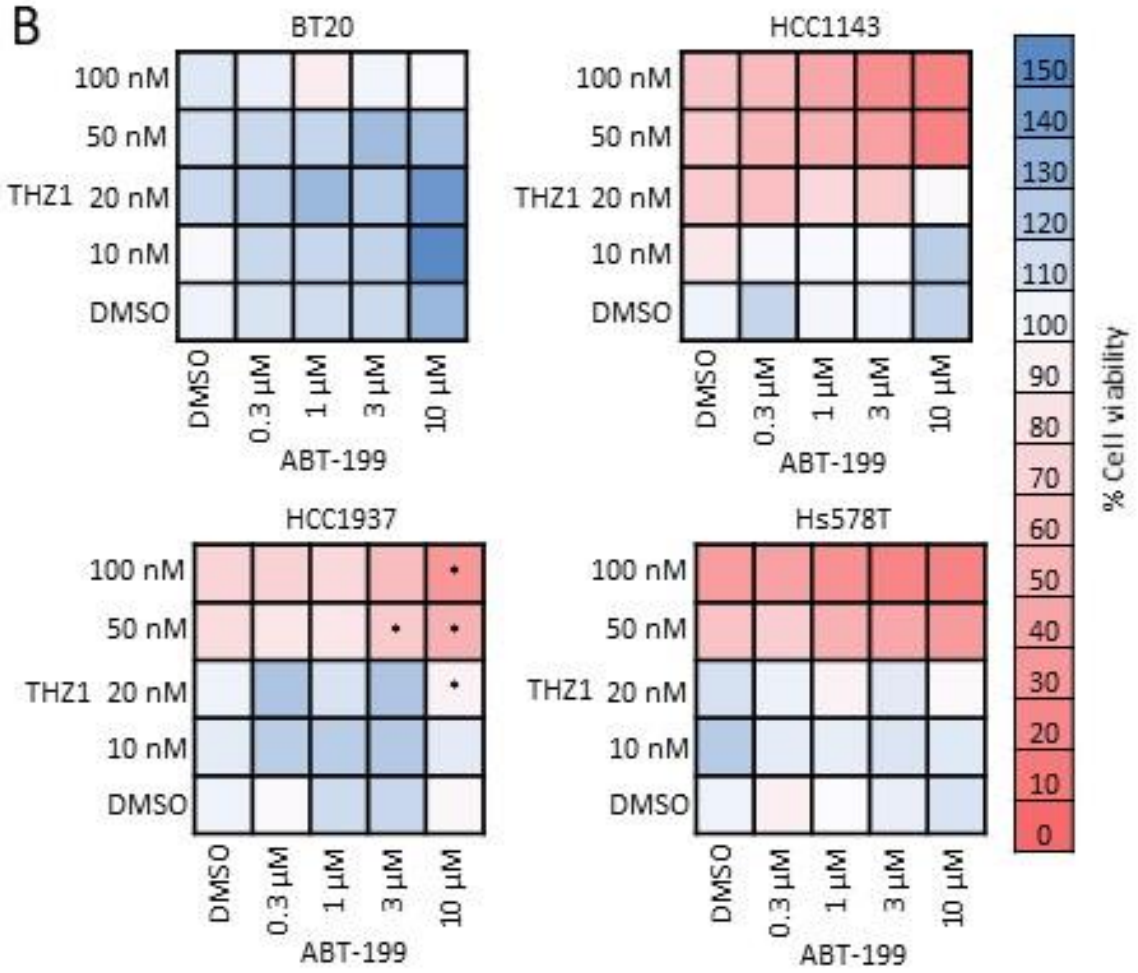

Figure 4.28: The combination of THZ1 and ABT-263 is synergistic in TNBC cell lines. Cell viability heatmap matrix using MTT assay 48 hr after (A) THZ1 and ABT-263 or (B) THZ1 and ABT-199 combination treatment in four TNBC cell lines. The mean of N=3 experiments was analysed using CompuSyn software to detect synergy. Synergy with a combination index (CI) <0.7 is marked with an asterisk.

4.4 Discussion

In this study it was identified that JQ1 induced apoptosis in two out of the panel of four ILC cell lines. The SUM44-PE and OCUB-M cell lines were sensitive to JQ1-induced apoptosis whereas the MDA-MB-134VI and CAMA-1 cell lines were relatively more resistant to JQ1-induced apoptosis (Figure 4.1b). This was confirmed using cell cycle analysis. In the apoptotic sensitive SUM44-PE and OCUB-M cell lines the percentage of cells in the sub G1 phase increased following JQ1 treatment

(Figure 4.1d). In contrast, the CAMA-1 cell line, which is the most resistant to JQ1-induced apoptosis, arrested in the G1 phase of the cell cycle following JQ1 treatment (Figure 4.1d). The MDA-MB-134VI cell line also arrested in G1 at low doses of JQ1, but at higher doses of JQ1, the percentage of cells increased in the sub G1 phase (Figure 4.1d). This is in accordance with the annexin V/PI data in which some MDA-MB-134VI cells undergo apoptosis at higher JQ1 concentrations (Figure 4.1b). Furthermore, BH3 profiling may be able to predict response to cell death caused by JQ1 treatment in ILC (Figure 4.2b), however further cell lines and patient samples are required to test this hypothesis. BH3 profiling has also been shown to predict response to BH3 mimetics and chemotherapy in numerous cancers such as lymphoma, chronic lymphocytic leukaemia (CLL), multiple myeloma, acute myelogenous leukemia, ovarian cancer and T-cell acute lymphoblastic leukemia (270, 352-354). Additionally, basal BH3 profiling suggested that there was dependence on BCL-2 and/or BCL-XL and/or BCL-W anti-apoptotic proteins as indicated by increased mitochondrial depolarisation following treatment with the BAD BH3 peptide (263) (Figure 4.2a).

RNA sequencing was then performed on a sensitive cell line (SUM44-PE) and on a cell line relatively more resistant to JQ1-induced apoptosis (MDA-MB-134VI) in order to identify factors contributing to JQ1-induced apoptotic resistance. The sequencing data was of good quality and reproducibility as evident by both a PCA plot (Figure 4.3) and individual heatmaps for each cell line in which treatment conditions clustered together (4.4a. 4.5a). From the sequencing data, it was evident that JQ1 alters the expression of a huge number of genes in both cell lines (Figure 4.4a, 4.5a), with JQ1 altering the expression of genes in common to both cell lines as well as exclusive regulation of other genes (4.6a). As the MDA-MB-134VI cell line is relatively more resistant to JQ1-induced apoptosis, genes were of interest that were upregulated in the MDA-MB-134VI cell line following JQ1 treatment, but were not upregulated in the sensitive SUM44-PE cell line. Gene ontology analysis using DAVID (299, 300) identified numerous pathways that were distinctly upregulated in the MDA-MB-134VI JQ1 apoptotic resistant cell line, following JQ1 treatment (Figure 4.6b). These were the circadian rhythm pathway, the MAPK signalling pathway, SNARE interactions in vesicular transport, the Wnt signalling pathway, long-term potentiation and insulin resistance (Figure 4.6b). Resistance to BET inhibition in

cancer has been previously reported in the literature. Pancreatic cancer cells resistant to BET inhibition displayed increased expression of some JQ1 target genes and maintained expression and dependency on Myc through GLI2 regulation (355), adaptive kinome reprogramming was attributed to BET inhibitor resistance in ovarian cancer cells (356) and loss of TRIM33 in colorectal cells promotes BET inhibitor resistance by increasing TGF-β signalling and reversing, in part, Myc downregulation (357). In TNBC, JQ1 resistant cells remain reliant on BRD4 (204). In these cells BRD4 is hyperphosphorylated and is indirectly recruited to chromatin via MED1. Furthermore, JQ1 resistant cells gained super-enhancer regions in survival genes including BCL-XL that was attributed to increased BRD4 binding (204). In HER2 positive luminal breast cancer, Myc downregulation did not predict sensitivity to JQ1 and exogenous Myc did not confer BET inhibitor resistance. The authors reported that overexpression of mutant PIK3CA conferred resistance to JQ1 in this model (358).

Wnt signalling has also been reported to play a role in resistance to BET inhibition. In acute myeloid leukemia (AML), BET inhibitor resistance was promoted by inhibition of the PRC2 complex causing epigenetic remodelling of chromatin and re-expression of BET inhibitor targets, such as Myc, that is facilitated by Wnt signalling machinery (334). Rathert et al. identified that a focal Myc enhancer is activated via this mechanism (334). Similarly, another study revealed that BET inhibitor resistance emerges from AML stem cells that display transcriptional rewiring and utilise the Wnt signalling pathway in order to maintain the expression of BET inhibitor target genes such as Myc (333). In this study, the Wnt pathway was significantly upregulated in the MDA-MB-134VI cell line ($p= 0.0142$), which is relatively resistant to JQ1-induced apoptosis, but not in the SUM44-PE cell line that is sensitive to JQ1-induced apoptosis (Figure 4.6b). As the Wnt signalling pathway has been previously associated with the development of BET inhibitor resistance in cancer (333, 334), the role of Wnt signalling in an ILC model of JQ1 apoptotic resistance was assessed.

The Wnt11 ligand was identified as being significantly upregulated in ILC cell lines relatively resistant to JQ1-induced apoptosis, but not in cell lines sensitive to JQ1-induced apoptosis, by both RNA sequencing and qPCR analysis (Figure 4.7a-c). Thus the non-canonical Wnt ligand, Wnt11 (359, 360), that signals via the non-canonical/ β-catenin-independent Wnt pathway, may be a potential factor

contributing to apoptotic resistance in the panel of ILC cell lines. Next the role of Wnt11 in JQ1-induced apoptosis resistance was interrogated using siRNA knockdown. Wnt11 knockdown was confirmed at the mRNA level using 2 individual siRNA's after 72 hr (Figure 4.8b). It was then assessed whether Wnt11 knockdown could increase sensitivity of the apoptotic resistant CAMA-1 cell line to JQ1. Wnt11 was knocked down for 72 hr followed by a further 72 hr treatment with JQ1. No difference was found in the apoptotic response in the CAMA-1 cell following JQ1 treatment and Wnt11 knockdown (Figure 4.8c). This was likely because there was no Wnt11 knockdown at the protein level in either the CAMA-1 or MDA-MB-134VI resistant cell lines using siRNA (Figure 4.9a). Additionally, following JQ1 treatment over time no difference in Wnt11 expression at the protein level was detected in neither JQ1 apoptotic sensitive or relatively resistant ILC cell lines (Figure 4.9b). Wnt4 knockdown was also attempted due to its reported role in endocrine resistance in ILC (340) using siRNA but similar results were obtained (Figure 4.10a, b). Unfortunately, due to time constraints of the project Wnt11 stable knockdown/knockout cell lines were unable to be developed, but it is a focus of future work of the laboratory which will shed light on whether Wnt11 has a role in JQ1 apoptotic resistance in ILC. Previous studies have shown that Wnt11 is associated with migration (336, 337, 339) and the promotion of cell proliferation in various cancer models (337, 339), and it would be important to determine if JQ1 treatment can increase EMT via Wnt11 in ILC cell lines/patients before proceeding to the clinic. Of note, although β-catenin was DE in the RNA sequencing data, β-catenin is not expressed at the protein level in ILC patient samples (361). Therefore, it is likely that if Wnt signalling is indeed promoting apoptotic resistance to JQ1 that it will be via the non-canonical rather than the canonical/ β-catenin-dependent pathway which makes Wnt11 a good potential target to pursue.

JQ1 was shown to induce apoptosis in some ILC cell lines (Figure 4.1b, d), thus the anti-apoptotic proteins BCL-2, BCL-XL and BCL-W and also the pro-apoptotic BIM protein were interrogated in the RNA sequencing data to identify any changes following JQ1 treatment (Figure 4.11a). In the SUM44-PE apoptotic sensitive cell line, following JQ1 treatment, transcription of both the BCL-2 and BCL-XL anti-apoptotic proteins was downregulated (Figure 4.11a, left). However, following JQ1 treatment in the resistant MDA-MB-134VI cell line, BCL-2 transcription was

downregulated but interestingly transcription of the anti-apoptotic BCL-XL was upregulated (Figure 4.11a, right). These findings were then validated using qPCR in the ILC cell lines sensitive to JQ1-induced apoptosis (SUM44-PE and OCUB-M) and in the ILC cell lines relatively more resistant to JQ1-induced apoptosis (MDA-MB-134VI and CAMA-1) (Figure 4.11b). These findings suggest that the anti-apoptotic protein BCL-XL may contribute to JQ1-induced apoptotic resistance as BCL-XL transcription is either maintained (MDA-MB-134VI cell line) or upregulated (CAMA-1 cell line) following JQ1 treatment (Figure 4.11a, b).

Next the BCL-2 anti-apoptotic proteins were investigated following JQ1 at the protein level. Surprisingly, JQ1 does not alter the protein expression of the BCL-2 anti-apoptotic protein in ILC cell lines (Figure 4.12a), even though transcription is downregulated in all ILC cell lines tested at the mRNA level (Figure 4.11b). BCL-2 protein expression was also highly expressed in ILC cell lines relatively resistant to JQ1-induced apoptosis (Figure 4.12a). Therefore, it was hypothesised that BCL-2 may be responsible for JQ1-induced apoptotic resistance in the MDA-MB-134VI and CAMA-1 cell lines. However, ILC cell lines were not sensitive to the BCL-2 selective inhibitor ABT-199 (281) by either growth inhibition or apoptosis (Figure 4.13a, b). Furthermore, the combination of JQ1 and ABT-199 did not enhance or induce apoptosis in ILC cell lines (Figure 4.15b), suggesting that inhibition of BCL-2 protein alone is not sufficient to reverse JQ1-induced apoptotic resistance. JQ1 in combination with ABT-199 has been shown to be effective in other cancers. This drug combination was shown to be effective at inhibiting the growth of an aggressive triple hit B-cell lymphoma cell line (362) and was synergistic in double hit B-cell lymphoma cells (363). Furthermore, JQ1 in combination with ABT-199 was recently shown to be synergistic in T-ALL cell lines, T-ALL resistant patient samples and also in patient-derived xenografts (364). This study suggested that the effectiveness of this drug combination may be due to the downregulation of BCL-2 and induction of BIM by JQ1 that facilitates ABT-199 due to increased BIM: BCL-2 binding ratio (364). Notably, It has been reported that high expression of BCL-2 but low expression of either BAD or BCL-XL can be used as predictive biomarkers for a robust apoptotic response following BET inhibition as assessed in cell lines of ALL origin, solid malignancies and haematological origin (323). This is in contrast to results from this

study where the ILC cell lines relatively resistant to JQ1-induced apoptosis have high expression of BCL-2.

As mentioned previously, it was hypothesised that maintained or high BCL-XL transcription may promote JQ1-induced apoptotic resistance in the MDA-MB-134VI and CAMA-1 cell lines from the RNA sequencing and qPCR validation data (Figure 4.11a, b). Unexpectedly, BCL-XL protein expression was downregulated following JQ1 treatment in these cell lines (Figure 4.12a). However, and importantly, basal expression of BCL-XL is much higher in the MDA-MB-134VI and CAMA-1 JQ1 apoptotic resistant cell lines compared to basal expression of BCL-XL in the SUM44-PE and OCUB-M sensitive cell lines (Figure 4.12a). Transcriptional rewiring may be occurring following JQ1 treatment that enables maintained BCL-XL transcription in ILC cell lines relatively resistant to JQ1-induced apoptosis. Transcriptional re-wiring has been described for the ER via GATA3 previously following JQ1 treatment (207). BET proteins have been shown to associate with BCL-2 and BCL-XL on chromatin and JQ1 alters BCL-2 and BCL-XL gene transcription by displacing BET proteins from these regions on chromatin (197, 203, 365). The SUM44-PE and MDA-MB-134VI cell lines were sensitive ABT-263, which inhibits BCL-2, BCL-XL and BCL-W (275), suggesting that inhibition of BCL-2 alone is not sufficient to induce apoptosis but that BCL-2/BCL-XL and BCL-W need to be inhibited (Figure 4.14a, b). Importantly, the combination of JQ1 and ABT-263 displayed synergistic growth inhibition in three out of four ILC cell lines, enhanced apoptosis in ILC cell lines sensitive to JQ1-induced apoptosis and induced apoptosis in ILC cell lines previously resistant to JQ1-induced apoptosis (Figure 4.16a, b). This finding further suggests that BCL-XL may be responsible for JQ1-induced apoptotic resistance in ILC cell lines. However, co-inhibition of BCL-2 may also be required for the efficacy of the JQ1 and ABT-263 combination treatment as ABT-263 inhibits BCL-2, BCL-XL and BCL-W anti-apoptotic proteins. In order to address this, JQ1 was combined with WEHI-539 a BCL-XL selective inhibitor (290). In the JQ1 apoptosis resistant CAMA-1 cell line, the combination of JQ1 and WEHI-539 significantly induced apoptosis to a similar degree as did the combination of JQ1 and ABT-263 (Figure 4.16b, 4.17). This finding further suggests that BCL-XL may mediate JQ1 apoptotic resistance in ILC cell lines. In accordance with this hypothesis, resistance to apoptosis has been reported to be attributed to BET inhibitor resistance, with BCL-XL playing a front role

(204, 323). TNBC cell lines resistant to JQ1 gained a BCL-XL super-enhancer, corresponding to increased protein expression, which was accredited to increased BRD4 binding in the resistant cell line (204). The combination of JQ1 and ABT-737 displayed synergy in this resistant cell line, further implicating the role of BCL-XL in apoptotic resistance to JQ1 (204). The apoptotic response was also attenuated in melanoma and AML cell lines resistant to the BET inhibitor CPI203 (366) and displayed upregulation of the anti-apoptotic protein BCL-XL (323). Knockdown of BCL-XL in the melanoma or AML BET inhibitor resistant cell lines promoted apoptosis and inhibited growth (323). Furthermore, the combination of CPI203 and ABT-737 in both the melanoma and AML resistant cell lines promoted apoptosis and inhibited proliferation in these cell lines (323). Additionally, androgen receptor signalling positive prostate cancer cell lines that are sensitive to JQ1 showed decreased expression of BCL-XL following JQ1 treatment due to loss of BRD2/3/4 at the BCL-XL promoter (203). However, in androgen receptor signalling negative cell lines that are resistant to JQ1, BCL-XL RNA levels remained unchanged (203). Although the potential role of BCL-XL and the combination of JQ1 and BH3 mimetics targeting BCL-XL have been reported in the literature previously, this is the first study to report the sensitivity of ILC cell lines to JQ1 as well as identify a potential combination therapy to target resistance. This is of importance as ILC patients display poor response to chemotherapy (157) and may not respond as well to endocrine therapy (154-156). Therefore, ILC patients urgently require alternative therapeutic options. Furthermore, very few molecular biology studies have been carried out in ILC and resources are difficult to come by (73).

The JQ1 and ABT-263 combination also inhibited the number of 3D spheroids grown in 3D culture in both a JQ1 apoptotic sensitive cell line and a relatively resistant ILC cell line, which is more effective than JQ1 treatment alone (Figure 4.18b, d, left). JQ1 and the combination of JQ1 and ABT-263 inhibited the size of 3D spheroids to a similar extent in both the cell lines (Figure 4.18b, d, right). Testing sensitivity of the cell lines to the combination of JQ1 and ABT-263 in 3D cell culture is important. This is because 3D cell culture has been shown to be better representative of the *in vivo* environment and many drugs previously sensitive in 2D growth environments can be resistant in 3D growth environments (346). The combination of JQ1 and ABT-263 was also shown to cause apoptosis in an ILC primary sample (T509) grown *ex vivo*

in drug for 48 hr (Figure 4.22a, b). Primary samples grown *ex vivo* are translationally relevant (303, 304). *Ex vivo* models maintain the tissue architecture, histological integrity, hormone responsiveness and cell signalling of the primary tumour (303, 304). These features enable the evaluation of drug efficacy in the intact tumour microenvironment of human tumours, that is not found with cell lines or animal models (303). Unfortunately, the efficacy of the drug combination in the ILC PDX (T638) *ex vivo* following 72 hr JQ1 treatment was unable to be evaluated (Figure 4.23b, c, 4.24). Many other researchers in the Prof. Leonie Young lab have cultured breast tumours *ex vivo* for longer time periods (305), but this study is the first to our knowledge to have grown ILC tumours *ex vivo* in this manner. 72 hr may have been too long for the tumour to have maintained viability *ex vivo* on the sponge. Furthermore, a study found that out of 82 ILC primary tumours, 43.9% of tumours weakly express EpCAM, 10.98% of tumours moderately express EpCAM and 3.66% of tumours highly express EpCAM (302). So, although EpCAM expression was validated in ILC cell lines (Figure 4.19) prior to the flow cytometry analysis of the T638 PDX sample, EpCAM in hindsight may not have been the best selection marker to identify ILC tumour cells and all the tumour cells may not have been detected.

Taken together, results from this study have identified that the anti-apoptotic BCL-XL may be implicated in apoptotic resistance following JQ1 treatment in ILC and supports the notion that the combination of JQ1 and ABT-263 may be an effective treatment strategy for ILC patients. The combination of JQ1 and ABT-263 may also have the added benefit of preventing JQ1 apoptotic resistance either de novo or acquired in ILC treated with JQ1 alone.

Furthermore, a side project carried out during my PhD provided evidence for the therapeutic benefit of CDK7 inhibition in combination with BH3 mimetics for the treatment of TNBC. TNBC occurs in approximately 15% of breast cancers (31). The TNBC subtype of breast cancer is so-called as it lacks expression of ER, PgR and HER2. As TNBC lacks hormonal receptors and HER2 there is currently no available targeted therapy and treatment mainly involves cytotoxic chemotherapy (32). TNBC is associated with poor survival and displays worse outcomes compared to other subtypes of breast cancer (350). The 5-year survival rate for TNBC patients is 76%, compared to a 5-year survival rate of 96% in hormone receptor positive breast

cancer (367). Risk of distant recurrence is also increased in patients with TNBC (368). CDK7 inhibition has been shown to target the Myc oncogene (217, 218). Previous studies have shown that Myc is amplified in TNBC and that Myc expression is a marker of poor prognosis (330, 369). Others in the laboratory identified that high CDK7 expression is associated with poor prognosis in TNBC (351). CDK7 inhibition using both the BS-181 and THZ1 selective inhibitors inhibited the growth of TNBC cell lines (Figure 4.25a, b), but apoptosis was only induced in one of the two TNBC cell lines tested (Figure 4.26a, b). THZ1 was more potent at inhibiting growth and inducing apoptosis in TNBC cell lines, likely attributed to its covalent mechanism of inhibition (217). In order to identify anti-apoptotic dependencies in the MDA-MB-231 cell line that is resistant to CDK7 inhibition induced apoptosis, dynamic BH3 profiling (370) was performed following THZ1 treatment. Increased cytochrome *c* response from the BAD and HRK peptides after THZ1 treatment indicated BCL-XL dependence (Figure 4.27). In support of BCL-XL dependence, combination treatments with THZ1 and ABT-263 displayed synergistic growth inhibition in a panel of TNBC cell lines (Figure 4.28). This study provides rational for the therapeutic potential of CDK7 inhibition in combination with BH3 mimetics for the treatment of TNBC.

Chapter 5: Discussion

5.1 Discussion

This PhD project has provided rational to therapeutically combine transcriptional inhibitors (JQ1 and THZ1) with BH3 mimetics (ABT-263) for the treatment of specific subtypes of breast cancer, namely ILC and TNBC.

ILC represents a difficult-to-treat breast cancer subtype in which research and resources are lacking (73). ILC is distinct from ER positive IDC, however, ILC and IDC ER positive breast cancer are often grouped together in clinical trials (74). Emerging evidence has now shown that although both ILC and IDC breast cancer are strictly classified as 'ER positive', ILC patients may display worse survival on endocrine treatment compared to IDC patients (154-156). ILC is also molecularly distinct from IDC with distinct gene expression and potential alternative regulation of ER (117). Moreover, detection of ILC is more difficult compared to IDC, both manually and by mammography. Manual detection of ILC is difficult due to the single-file nature of the disease as it may not form palpable masses and mammography often produces false negative results (86). Therefore, patients who present to the clinic are often older with larger tumours and lymph node metastases (40, 75). Additionally, surgery is not as successful in ILC compared to IDC as it is difficult to obtain clear margins, again, due to the single-file nature of the disease (119, 120). ILC patients also have a poor response to neoadjuvant chemotherapy due to low mitotic count (80, 157). These findings outline the importance of identifying alternative therapeutic targets for the treatment of ILC breast cancer that is often difficult to detect, chemoresistant, may have worse survival compared to IDC breast cancer on endocrine treatment and surgery is not as successful.

In this study a two-pronged approach was used. Firstly, *in silico* screening of RNA sequencing gene expression data from two separate cohorts was performed comprising a combined total of 160 ILC patients in order to identify a novel therapeutic target for the treatment of ILC breast cancer. Secondly, the identified therapeutic target was targeted with an available inhibitor and the sensitivity of a panel of ILC cell lines and patient samples to this inhibitor was assessed, in which mechanisms of resistance and combination treatment options were identified. This is one of the few studies that has carried out extensive molecular biology analysis in

ILC breast cancer and the only study to our knowledge implicating an epigenetic reader in the survival of ILC.

In this study high expression of the epigenetic reader BRD3 was identified to be associated with poor survival in ILC in two separate cohorts (Figure 3.1, 3.2). Importantly, high expression of BRD3 was not associated with poor survival in breast cancer as a whole (Figure 3.3) indicating that this finding is specific for ILC breast cancer. JQ1 is an inhibitor of the BET family of proteins, which targets BRD3 (195). JQ1 mediated growth inhibition in all ILC cell lines tested (Figure 3.7) and is more effective at inhibiting ILC growth when compared to the endocrine therapies tamoxifen or fulvestrant (Figure 3.6a, b). This is an important finding as more than 90% of ILC primary samples are ER positive (40) and therefore treated with endocrine therapy. Alternative therapeutics to endocrine treatment is required as endocrine treatment is known to fail in one third of women and as many as 40% will relapse on endocrine treatment (151, 152).

The combination of JQ1 and tamoxifen was synergistic in two out of the three ER positive ILC cell lines, including the SUM44-PE cell line in which ER signalling was increased following JQ1 treatment and the MDA-MB-134VI cell line in which ER signalling was abrogated by JQ1 (Figure 3.9a). The combination of JQ1 and fulvestrant was also synergistic in two out of three ER positive ILC cell lines in which ER signalling was abrogated by JQ1 treatment alone, namely the MDA-MB-134VI and CAMA-1 cell lines (Figure 3.9b). Supporting this finding, the combination of JQ1 and fulvestrant has been reported to be synergic at inhibiting tumour growth in an *in vivo* model of IDC tamoxifen-resistant breast cancer (207). Taken together, these findings suggest that JQ1 displays context specific regulation of the ER and ER signalling in ILC cell lines and the combination of JQ1 and endocrine therapy is synergistic in ILC.

Apoptosis was induced in two out of the panel of four ILC cell lines tested (Figure 4.1b, d). The SUM44-PE and OCUB-M cell line was sensitive to JQ1-induced apoptosis, whereas the MDA-MB-134VI and CAMA-1 cell lines were relatively more resistant to JQ1 induced apoptosis (Figure 4.1b, d). In order to identify factors contributing to JQ1 apoptosis resistance in ILC cell lines, RNA sequencing following JQ1 treatment was performed. Gene ontology analysis revealed that the Wnt

pathway was significantly altered in the MDA-MB-134VI JQ1 apoptotic resistant cell line (Figure 4.6b), and Wnt signalling has previously been implicated in BET inhibitor resistance (333, 334). From this analysis, the Wnt11 non-canonical Wnt ligand was identified to be downregulated in cell lines sensitive to JQ1-induced apoptosis and upregulated in cell lines resistant to JQ1-induced apoptosis by both RNA sequencing and qPCR validation (Figure 4.7a-c). Wnt11 has been associated with migration in numerous cancer models, including prostate cancer, colorectal cancer and high grade serious ovarian cancer (336, 337, 339). Although Wnt11 was unable to be knocked down in this study (Figure 4.9a), it would be imperative to determine the precise role of Wnt11 following JQ1 treatment. If Wnt11 is upregulated following JQ1 treatment, does this enhance the metastatic potential of ILC cells? Although upregulation of Wnt11 at the protein level was not detected following JQ1 treatment, longer time points may be required to detect any potential upregulation of Wnt11 (Figure 4.9b).

Altered expression of anti-apoptotic proteins is a recurring them in cancer. For example, BCL-XL is highly expressed in breast cancer and hormone resistant prostate cancer whereas BCL-2 is highly expressed in breast cancer, melanoma, lymphoid malignancies and lung cancer (371). In ILC cell lines sensitive to JQ1-induced apoptosis, the BCL-2 and BCL-XL anti-apoptotic proteins were transcriptionally downregulated by JQ1 following RNA sequencing and qPCR validation (Figure 4.11a, b). However, in ILC cell lines relatively resistant to JQ1-induced apoptosis, BCL-2 transcription was downregulated but BCL-XL transcription was either maintained or enhanced (Figure 4.11a, b). Importantly, BET proteins have been previously shown to associate with BCL-2 and BCL-XL on chromatin and JQ1 alters BCL-2 and BCL-XL gene transcription by displacing BET proteins from these regions on chromatin (197, 203, 365).

The precise role of BCL-2 in ER-positive breast cancer is controversial. BCL-2 expression is marker of good prognosis in ER positive breast cancer (327), but of poor prognosis in TNBC (328). Conversely, increased expression of the anti-apoptotic protein BCL-2 has been associated with resistance to chemotherapy in breast cancer samples (329). BCL-2 is an ER target gene (372). Although ER protein (Figure 3.8a) and ER gene transcription (PgR, TFF1, BCL-2; Figure 3.8b, 4.11b) was downregulated following JQ1 in the MDA-MB-134VI and CAMA-1 cell lines that are

resistant to JQ1-induced apoptosis, BCL-2 protein levels remained high and unchanged in these cell lines (Figure 4.12a). Because ILC cell lines resistant to JQ1-induced apoptosis had high expression of BCL-2, JQ1 was combined with the BCL-2 selective inhibitor ABT-199 (281). This drug combination only mediated minor synergy in ILC cell lines and importantly did not enhance or induce apoptosis in ILC cell lines (Figure 4.15a, b). This drug combination has been recently reported to be synergistic in T-ALL, which displays BCL-2 dependence in the early T-cell progenitor subtype (352, 364). The results from this study suggest that BCL-2 inhibition alone is not sufficient to overcome JQ1-induced apoptotic resistance in ILC cell lines.

It was hypothesised from the RNA sequencing and qPCR validation data that BCL-XL may contribute to JQ1-induced apoptotic resistance in ILC cell lines, as BCL-XL transcription is maintained or upregulated following JQ1 treatment (Figure 4.11a, b). Basal protein expression of BCL-XL is higher in cell lines relatively resistant to JQ1-induced apoptosis (MDA-MB-134VI and CAMA-1 cell lines) compared to JQ1 apoptotic sensitive cell lines (Figure 4.12a). Surprisingly, BCL-XL protein is downregulated in the JQ1 apoptotic sensitive OCUB-M cell line as well as the cell lines relatively resistant to JQ1-induced apoptosis, following JQ1 treatment (Figure 4.12a). However, sustained or upregulated BCL-XL transcription in apoptotic resistant cell lines following JQ1 (Figure 4.11a, b) could suggest that transcriptional rewiring may be occurring to maintain some protein expression of BCL-XL in these cell lines in order to promote cell survival. In order to target BCL-XL, JQ1 was combined with ABT-263, an inhibitor of BCL-2, BCL-XL and BCL-W proteins (275). The combination of JQ1 and ABT-263 was synergistic at inhibiting growth in three out of four ILC cell lines (Figure 4.16a). Interestingly, the combination of JQ1 and ABT-263 enhanced apoptosis in sensitive cell lines and induced apoptosis in ILC cell lines resistant to JQ1-induced apoptosis (Figure 4.16b). Additionally, the combination of JQ1 and the BCL-XL selective inhibitor induced apoptosis in the CAMA-1 JQ1 apoptotic resistant cell line that was similar to the combination of JQ1 and ABT-263 (Figure 4.16b, 4.17). The results from this study propose a hypothesised mechanism of action as follows. In ILC cell lines sensitive to JQ1-induced apoptosis, BCL-XL transcription is downregulated by JQ1 resulting in apoptosis (Figure 5.1). However, in ILC cell lines relatively resistant to JQ1-induced apoptosis, BCL-XL transcription is maintained or enhanced and the combination of JQ1 and ABT-263 is required for

these cell lines to undergo apoptosis (Figure 5.1). Importantly the combination of JQ1 and ABT-263 also enhanced the apoptotic effect of JQ1 treatment alone in ILC apoptotic sensitive cell lines (Figure 5.1).

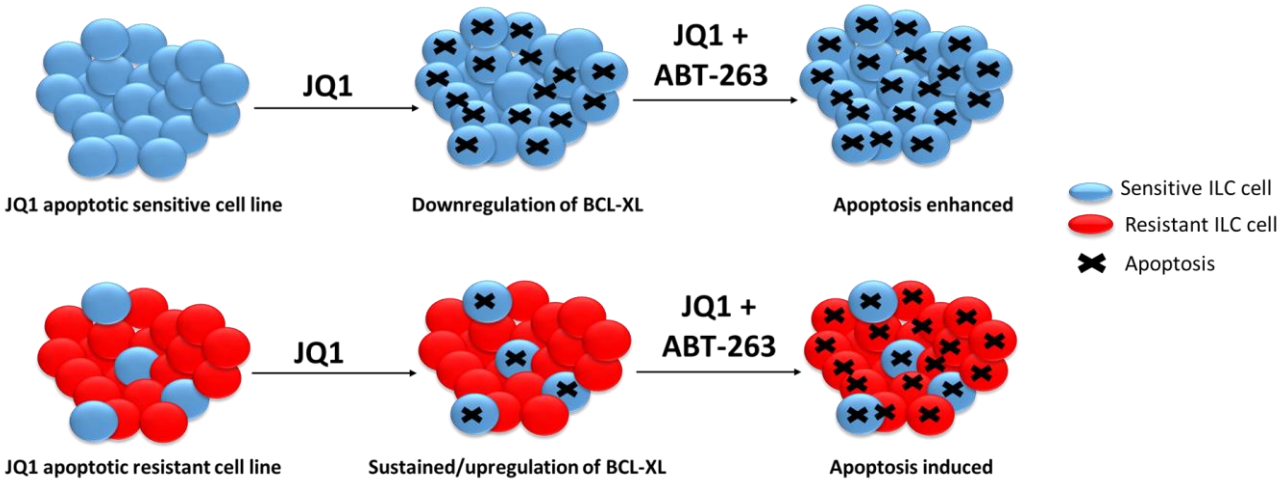

Figure 5.1: Proposed mechanism of JQ1-induced apoptotic resistance in ILC. In ILC cell lines sensitive to JQ1, BCL-XL is efficiently downregulated at the mRNA level following JQ1 treatment and apoptosis occurs. The combination of JQ1 and ABT-263 enhances the apoptotic effect of JQ1 treatment alone in sensitive cell lines. In contrast, in ILC cell lines relatively resistant to JQ1-induced apoptosis, BCL-XL transcription is either maintained or enhanced, promoting resistance to apoptosis. The combination of JQ1 and ABT-263 is required to induce apoptosis in JQ1 apoptotic resistant ILC cell lines.

The hypothesis that BCL-XL may contribute to JQ1-induced apoptotic resistance in ILC cell lines and findings from the JQ1 and ABT-263 combination experiments are supported by the current literature (204, 323). A TNBC cell line resistant to JQ1 gained a BCL-XL super-enhancer that was accredited to increased BRD4 binding in the resistant cell line, and the combination of JQ1 and ABT-737 was synergistic in this model of JQ1 resistance (204). Additionally, melanoma and AML cell lines resistant to the BET inhibitor CPI203 (366) displayed upregulation of BCL-XL (323). Knockdown of BCL-XL or the combination of JQ1 and ABT-737 in these resistant cell

lines promoted apoptosis and inhibited growth (323). Although it is hypothesised that BCL-XL is responsible for JQ1-induced apoptotic resistance, one cannot exclude the possible need for co-inhibition of BCL-2 for efficacy of the JQ1 and ABT-263 combination.

Of translational importance, the combination of JQ1 and ABT-263 was shown to be effective at inhibiting both the number and size of spheroids grown in 3D cell cultures (Figure 4.18b, d) as well as inducing apoptosis in an *ex vivo* culture of a primary ILC sample (4.22a, b). 3D cell culture has been shown to be better representative of the *in vivo* environment and many drugs previously sensitive in 2D cell culture can be resistant in 3D cell culture environments (346), therefore it is important to demonstrate sensitivity to the combination of JQ1 and ABT-263 in both 2D and 3D cell culture. Additionally, e*x vivo* models are translationally important as the combination of JQ1 and ABT-263 can be tested in an environment that maintains the tissue architecture, histological integrity, hormone responsiveness and cell signalling of the primary tumour (303, 304).

In conclusion, these findings suggest that the combination of JQ1 and ABT-263 is an effective treatment strategy for ILC and may be a rational combination treatment to overcome and anticipate JQ1-induced apoptotic resistance in ILC. Despite these conclusions, it is important to note the limitations of the current study. Due to the lack of available resources to study ILC (73), only two ‘true’ ILC cell lines were included in this study that represent the main two cell lines used in ILC publications. This is a low number of ILC cell lines and although the findings of the current study were validated in two other ‘ILC-like’ cell lines, the results should be interpreted with cation and require validation in other available ILC models (93). Additionally, JQ1 has a short half-life *in vivo* (195) and is not suitable for progression to the clinic, despite tolerance *in vivo* (195, 207, 208) and non-toxic effects on normal cells (199, 209). Other BET inhibitors such as OTX015 are in clinical trials, however, toxicities with OTX015 have been observed, including thrombocytopenia (214-216). A major side effect of ABT-263 is thrombocytopenia (276-280) and therefore caution needs to be taken with combining BET inhibition and ABT-263 in the clinic.

Furthermore, a side project carried out during my PhD provided rational for CDK7 inhibition in combination with ABT-263 for the treatment of TNBC. TNBC occurs in

approximately 15% of breast cancers (31). As TNBC lacks hormonal receptors and HER2 there is currently no available targeted therapy and treatment mainly relies on chemotherapy (32). TNBC is a subtype of poor survival that displays worse outcomes compared to other subtypes (350) and the risk of distant recurrence is increased in patients with TNBC (368). Others in laboratory identified that high expression of CDK7 was associated with poor prognosis in TNBC (351). As targeting CDK7 inhibits Myc transcription (217, 218) and the importance of Myc in TNBC (330, 369), the therapeutic potential of targeting CDK7 in TNBC was investigated (351).

CDK7 inhibition using both the BS-181 and THZ1 selective inhibitors inhibited the growth of both TNBC cell lines tested (Figure 4.25a, b). However, apoptosis was only induced in one of the two TNBC cell lines tested, with the MDA-MB-231 cell line relatively resistant to apoptosis (Figure 4.26a, b). THZ1 was remarkably more potent compared to BS-181 (Figure 4.25a, b; 4.26a, b), likely attributed to its covalent mechanism of inhibition (217). Dynamic BH3 profiling (370) following THZ1 treatment identified dependence on the BCL-XL anti-apoptotic in the MDA-MB-231 cell line that was resistant to CDK7 inhibition-induced apoptosis (Figure 4.27). In support of BCL-XL dependence, combination treatments with THZ1 and ABT-263 displayed synergistic growth inhibition in a panel of TNBC cell lines (Figure 4.28a), with only minor synergy detected in one cell line treated with the THZ1 and ABT-199 combination (Figure 4.28b). This study provides rational for the therapeutic potential of CDK7 inhibition in combination with BH3 mimetics for the treatment of TNBC.

5.2 Future perspectives

Although this study provided insight into the molecular biology of ILC following JQ1 treatment, this study also raised important questions that unfortunately were unable to be addressed. Future work on this project will involve determining the precise role of BRD3 in ILC gene regulation and whether it differs from BRD2 and BRD4 gene regulation in ILC. Chromatin immunoprecipitation (CHIP)-sequencing experiments would provide insights into this and also identify BET protein super-enhancers that are disrupted following JQ1 treatment, as has been done by others (203, 204, 210). Additionally, BCL-2 is highly expressed in ILC cell lines relatively resistant to JQ1-induced apoptosis and it would be interesting to assess whether high expression of BCL-2 may be used as a predictive biomarker in order to identify ILC patients who

are resistant to JQ1-induced apoptosis and require the combination of JQ1 and ABT-263 treatment from the onset. High BCL-2 expression and low expression of either BCL-XL or BAD has been reported to act as predictive biomarkers for a favourable apoptotic response following BET inhibition, which is in contrast to findings from this study (323). Furthermore, in order to dissect anti-apoptotic dependencies in JQ1-induced apoptotic resistant cell lines, it would be informative to immunoprecipitate BCL-2 and BCL-XL in order to measure bound pro-apoptotic members.

In order to improve the translational significance of this study it is imperative to evaluate the efficacy of JQ1 and the combination of JQ1 and ABT-263 in *in vivo* ILC PDX models. With these *in vivo* models, tumour volume, weight, metastases as well as adverse reactions can be measured which will inform on the efficacy of the combination of JQ1 and ABT-263 in a whole organism, validate potential predictive biomarkers such as BCL-2, and determine whether progression to the clinic is warranted.

It will also be important to identify the role of Wnt11 in JQ1-induced apoptotic resistance through Wnt11 stable knockdown or knockout ILC cell lines. Wnt11 signalling has been associated with migration and invasion in many cancer types (336-339). Therefore, it would be important to establish whether ILC cell lines relatively resistant to JQ1-induced apoptosis, following JQ1 treatment, display a more metastatic phenotype due to Wnt11 transcriptional upregulation and whether the combination of JQ1 and ABT-263 can abrogate this metastatic phenotype or not.

Moreover, further research is warranted to elucidate mechanisms determining response to the combination of JQ1 and specific endocrine therapies. It is unclear why the combination of JQ1 and tamoxifen is synergistic in one cell line but the combination of JQ1 and fulvestrant is not synergistic in the same cell line and vice versa. The combination of JQ1 and fulvestrant has been reported to display synergistic anti-tumour activity in an IDC breast cancer xenograft that was resistant to tamoxifen (207) and it would be interesting to evaluate the potential of this drug combination and the combination of JQ1 and tamoxifen in the endocrine resistant ILC setting.

6. References

1. SEER Stat Fact Sheets: Female Breast Cancer [Internet]. Washington (DC): National Cancer Institute. Surveillance E, and End Results Program; 2012. [cited 2015 Nov 1]. Available from: http://seer.cancer.gov/statfacts/html/breast.html
2. Ferlay J, Soerjomataram I, Dikshit R, Eser S, Mathers C, Rebelo M, et al. Cancer incidence and mortality worldwide: sources, methods and major patterns in GLOBOCAN 2012. Int J Cancer. 2015;136(5):E359-86.
3. World Health Organisation. http://wwwwhoint/cancer/detection/breastcancer/en/index1html.
4. National Cancer Registry Ireland. http://wwwncriie/.
5. First results on mortality reduction in the UK Trial of Early Detection of Breast Cancer. UK Trial of Early Detection of Breast Cancer Group. Lancet. 1988;2(8608):411-6.
6. Early Breast Cancer Trialists' Collaborative G. Effects of chemotherapy and hormonal therapy for early breast cancer on recurrence and 15-year survival: an overview of the randomised trials. Lancet. 2005;365(9472):1687-717.
7. Chen S, Parmigiani G. Meta-analysis of BRCA1 and BRCA2 penetrance. J Clin Oncol. 2007;25(11):1329-33.
8. Jones ME, Schoemaker MJ, Wright L, McFadden E, Griffin J, Thomas D, et al. Menopausal hormone therapy and breast cancer: what is the true size of the increased risk? Br J Cancer. 2016;115(5):607-15.
9. Nelson HD, Zakher B, Cantor A, Fu R, Griffin J, O'Meara ES, et al. Risk factors for breast cancer for women aged 40 to 49 years: a systematic review and meta-analysis. Ann Intern Med. 2012;156(9):635-48.
10. Johnson KC, Hu J, Mao Y, Canadian Cancer Registries Epidemiology Research G. Passive and active smoking and breast cancer risk in Canada, 1994-97. Cancer Causes Control. 2000;11(3):211-21.
11. Collaborative Group on Hormonal Factors in Breast C. Menarche, menopause, and breast cancer risk: individual participant meta-analysis, including 118 964 women with breast cancer from 117 epidemiological studies. Lancet Oncol. 2012;13(11):1141-51.
12. Neuhouser ML, Aragaki AK, Prentice RL, Manson JE, Chlebowski R, Carty CL, et al. Overweight, Obesity, and Postmenopausal Invasive Breast Cancer Risk: A Secondary Analysis of the Women's Health Initiative Randomized Clinical Trials. JAMA Oncol. 2015;1(5):611-21.
13. Chen WY, Rosner B, Hankinson SE, Colditz GA, Willett WC. Moderate alcohol consumption during adult life, drinking patterns, and breast cancer risk. JAMA. 2011;306(17):1884-90.
14. Yoshida K, Miki Y. Role of BRCA1 and BRCA2 as regulators of DNA repair, transcription, and cell cycle in response to DNA damage. Cancer Sci. 2004;95(11):866-71.
15. Breast Cancer Ireland. https://www.breastcancerireland.com/facts-and-figures/.
16. Sorlie T, Tibshirani R, Parker J, Hastie T, Marron JS, Nobel A, et al. Repeated observation of breast tumor subtypes in independent gene expression data sets. Proc Natl Acad Sci U S A. 2003;100(14):8418-23.
17. Perou CM, Sorlie T, Eisen MB, van de Rijn M, Jeffrey SS, Rees CA, et al. Molecular portraits of human breast tumours. Nature. 2000;406(6797):747-52.
18. Sorlie T, Perou CM, Tibshirani R, Aas T, Geisler S, Johnsen H, et al. Gene expression patterns of breast carcinomas distinguish tumor subclasses with clinical implications. Proc Natl Acad Sci U S A. 2001;98(19):10869-74.
19. Cook KL, Shajahan AN, Clarke R. Autophagy and endocrine resistance in breast cancer. Expert Rev Anticancer Ther. 2011;11(8):1283-94.
20. Bai Z, Gust R. Breast cancer, estrogen receptor and ligands. Arch Pharm (Weinheim). 2009;342(3):133-49.

21. Fisher B, Costantino J, Redmond C, Poisson R, Bowman D, Couture J, et al. A randomized clinical trial evaluating tamoxifen in the treatment of patients with node-negative breast cancer who have estrogen-receptor-positive tumors. N Engl J Med. 1989;320(8):479-84.
22. Breast International Group 1-98 Collaborative G, Thurlimann B, Keshaviah A, Coates AS, Mouridsen H, Mauriac L, et al. A comparison of letrozole and tamoxifen in postmenopausal women with early breast cancer. N Engl J Med. 2005;353(26):2747-57.
23. Early Breast Cancer Trialists' Collaborative G, Davies C, Godwin J, Gray R, Clarke M, Cutter D, et al. Relevance of breast cancer hormone receptors and other factors to the efficacy of adjuvant tamoxifen: patient-level meta-analysis of randomised trials. Lancet. 2011;378(9793):771-84.
24. Samaan NA, Buzdar AU, Aldinger KA, Schultz PN, Yang KP, Romsdahl MM, et al. Estrogen receptor: a prognostic factor in breast cancer. Cancer. 1981;47(3):554-60.
25. Slamon DJ, Godolphin W, Jones LA, Holt JA, Wong SG, Keith DE, et al. Studies of the HER-2/neu proto-oncogene in human breast and ovarian cancer. Science. 1989;244(4905):707-12.
26. Agus DB, Akita RW, Fox WD, Lewis GD, Higgins B, Pisacane PI, et al. Targeting ligand-activated ErbB2 signaling inhibits breast and prostate tumor growth. Cancer Cell. 2002;2(2):127-37.
27. Slamon DJ, Leyland-Jones B, Shak S, Fuchs H, Paton V, Bajamonde A, et al. Use of chemotherapy plus a monoclonal antibody against HER2 for metastatic breast cancer that overexpresses HER2. N Engl J Med. 2001;344(11):783-92.
28. Wood ER, Truesdale AT, McDonald OB, Yuan D, Hassell A, Dickerson SH, et al. A unique structure for epidermal growth factor receptor bound to GW572016 (Lapatinib): relationships among protein conformation, inhibitor off-rate, and receptor activity in tumor cells. Cancer Res. 2004;64(18):6652-9.
29. Rusnak DW, Lackey K, Affleck K, Wood ER, Alligood KJ, Rhodes N, et al. The effects of the novel, reversible epidermal growth factor receptor/ErbB-2 tyrosine kinase inhibitor, GW2016, on the growth of human normal and tumor-derived cell lines in vitro and in vivo. Mol Cancer Ther. 2001;1(2):85-94.
30. Lin NU, Winer EP, Wheatley D, Carey LA, Houston S, Mendelson D, et al. A phase II study of afatinib (BIBW 2992), an irreversible ErbB family blocker, in patients with HER2-positive metastatic breast cancer progressing after trastuzumab. Breast Cancer Res Treat. 2012;133(3):1057-65.
31. Dent R, Trudeau M, Pritchard KI, Hanna WM, Kahn HK, Sawka CA, et al. Triple-negative breast cancer: clinical features and patterns of recurrence. Clin Cancer Res. 2007;13(15 Pt 1):4429-34.
32. Liedtke C, Mazouni C, Hess KR, Andre F, Tordai A, Mejia JA, et al. Response to neoadjuvant therapy and long-term survival in patients with triple-negative breast cancer. J Clin Oncol. 2008;26(8):1275-81.
33. Bertucci F, Finetti P, Cervera N, Esterni B, Hermitte F, Viens P, et al. How basal are triple-negative breast cancers? Int J Cancer. 2008;123(1):236-40.
34. Alluri P, Newman LA. Basal-like and triple-negative breast cancers: searching for positives among many negatives. Surg Oncol Clin N Am. 2014;23(3):567-77.
35. Dai X, Li T, Bai Z, Yang Y, Liu X, Zhan J, et al. Breast cancer intrinsic subtype classification, clinical use and future trends. Am J Cancer Res. 2015;5(10):2929-43.
36. Curtis C, Shah SP, Chin SF, Turashvili G, Rueda OM, Dunning MJ, et al. The genomic and transcriptomic architecture of 2,000 breast tumours reveals novel subgroups. Nature. 2012;486(7403):346-52.
37. Malhotra GK, Zhao X, Band H, Band V. Histological, molecular and functional subtypes of breast cancers. Cancer Biol Ther. 2010;10(10):955-60.
38. Lagios MD, Margolin FR, Westdahl PR, Rose MR. Mammographically detected duct carcinoma in situ. Frequency of local recurrence following tylectomy and prognostic effect of nuclear grade on local recurrence. Cancer. 1989;63(4):618-24.
39. Li CI, Anderson BO, Daling JR, Moe RE. Trends in incidence rates of invasive lobular and ductal breast carcinoma. JAMA. 2003;289(11):1421-4.

40. Arpino G, Bardou VJ, Clark GM, Elledge RM. Infiltrating lobular carcinoma of the breast: tumor characteristics and clinical outcome. Breast Cancer Res. 2004;6(3):R149-56.
41. Denoix PF. Nomenclature des cancers. Bull Inst Nat Hyg (Paris). 1994;1:1-69 and 5-82.
42. Sobin LH, Gospodarowicz, M.K. and Wittekind, Ch. TNM Classification of Malignant Tumours UICC International Union Against Cancer Seventh Edition. 2009.
43. Elston CW, Ellis IO. Pathological prognostic factors in breast cancer. I. The value of histological grade in breast cancer: experience from a large study with long-term follow-up. Histopathology. 1991;19(5):403-10.
44. Galea MH, Blamey RW, Elston CE, Ellis IO. The Nottingham Prognostic Index in primary breast cancer. Breast Cancer Res Treat. 1992;22(3):207-19.
45. Green AR, Soria D, Powe DG, Nolan CC, Aleskandarany M, Szasz MA, et al. Nottingham prognostic index plus (NPI+) predicts risk of distant metastases in primary breast cancer. Breast Cancer Res Treat. 2016;157(1):65-75.
46. Rakha EA, Soria D, Green AR, Lemetre C, Powe DG, Nolan CC, et al. Nottingham Prognostic Index Plus (NPI+): a modern clinical decision making tool in breast cancer. Br J Cancer. 2014;110(7):1688-97.
47. van 't Veer LJ, Dai H, van de Vijver MJ, He YD, Hart AA, Mao M, et al. Gene expression profiling predicts clinical outcome of breast cancer. Nature. 2002;415(6871):530-6.
48. van de Vijver MJ, He YD, van't Veer LJ, Dai H, Hart AA, Voskuil DW, et al. A gene-expression signature as a predictor of survival in breast cancer. N Engl J Med. 2002;347(25):1999-2009.
49. Paik S, Shak S, Tang G, Kim C, Baker J, Cronin M, et al. A multigene assay to predict recurrence of tamoxifen-treated, node-negative breast cancer. N Engl J Med. 2004;351(27):2817-26.
50. Paik S, Tang G, Shak S, Kim C, Baker J, Kim W, et al. Gene expression and benefit of chemotherapy in women with node-negative, estrogen receptor-positive breast cancer. J Clin Oncol. 2006;24(23):3726-34.
51. Sparano JA, Gray RJ, Makower DF, Pritchard KI, Albain KS, Hayes DF, et al. Prospective Validation of a 21-Gene Expression Assay in Breast Cancer. N Engl J Med. 2015;373(21):2005-14.
52. Gluz O, Nitz UA, Christgen M, Kates RE, Shak S, Clemens M, et al. West German Study Group Phase III PlanB Trial: First Prospective Outcome Data for the 21-Gene Recurrence Score Assay and Concordance of Prognostic Markers by Central and Local Pathology Assessment. J Clin Oncol. 2016;34(20):2341-9.
53. Sommer S, Fuqua SA. Estrogen receptor and breast cancer. Semin Cancer Biol. 2001;11(5):339-52.
54. Renoir JM, Marsaud V, Lazennec G. Estrogen receptor signaling as a target for novel breast cancer therapeutics. Biochem Pharmacol. 2013;85(4):449-65.
55. Pratt WB, Toft DO. Steroid receptor interactions with heat shock protein and immunophilin chaperones. Endocr Rev. 1997;18(3):306-60.
56. Le Romancer M, Poulard C, Cohen P, Sentis S, Renoir JM, Corbo L. Cracking the estrogen receptor's posttranslational code in breast tumors. Endocr Rev. 2011;32(5):597-622.
57. Dutertre M, Smith CL. Ligand-independent interactions of p160/steroid receptor coactivators and CREB-binding protein (CBP) with estrogen receptor-alpha: regulation by phosphorylation sites in the A/B region depends on other receptor domains. Mol Endocrinol. 2003;17(7):1296-314.
58. Shah YM, Rowan BG. The Src kinase pathway promotes tamoxifen agonist action in Ishikawa endometrial cells through phosphorylation-dependent stabilization of estrogen receptor (alpha) promoter interaction and elevated steroid receptor coactivator 1 activity. Mol Endocrinol. 2005;19(3):732-48.
59. Sheeler CQ, Singleton DW, Khan SA. Mutation of serines 104, 106, and 118 inhibits dimerization of the human estrogen receptor in yeast. Endocr Res. 2003;29(2):237-55.
60. Bunone G, Briand PA, Miksicek RJ, Picard D. Activation of the unliganded estrogen receptor by EGF involves the MAP kinase pathway and direct phosphorylation. EMBO J. 1996;15(9):2174-83.

61. Ali S, Metzger D, Bornert JM, Chambon P. Modulation of transcriptional activation by ligand-dependent phosphorylation of the human oestrogen receptor A/B region. EMBO J. 1993;12(3):1153-60.
62. Cheng J, Zhang C, Shapiro DJ. A functional serine 118 phosphorylation site in estrogen receptor-alpha is required for down-regulation of gene expression by 17beta-estradiol and 4-hydroxytamoxifen. Endocrinology. 2007;148(10):4634-41.
63. Thomas RS, Sarwar N, Phoenix F, Coombes RC, Ali S. Phosphorylation at serines 104 and 106 by Erk1/2 MAPK is important for estrogen receptor-alpha activity. J Mol Endocrinol. 2008;40(4):173-84.
64. Michalides R, Griekspoor A, Balkenende A, Verwoerd D, Janssen L, Jalink K, et al. Tamoxifen resistance by a conformational arrest of the estrogen receptor alpha after PKA activation in breast cancer. Cancer Cell. 2004;5(6):597-605.
65. Joel PB, Smith J, Sturgill TW, Fisher TL, Blenis J, Lannigan DA. pp90rsk1 regulates estrogen receptor-mediated transcription through phosphorylation of Ser-167. Mol Cell Biol. 1998;18(4):1978-84.
66. Chen D, Pace PE, Coombes RC, Ali S. Phosphorylation of human estrogen receptor alpha by protein kinase A regulates dimerization. Mol Cell Biol. 1999;19(2):1002-15.
67. Tsai HW, Katzenellenbogen JA, Katzenellenbogen BS, Shupnik MA. Protein kinase A activation of estrogen receptor alpha transcription does not require proteasome activity and protects the receptor from ligand-mediated degradation. Endocrinology. 2004;145(6):2730-8.
68. Hanstein B, Eckner R, DiRenzo J, Halachmi S, Liu H, Searcy B, et al. p300 is a component of an estrogen receptor coactivator complex. Proc Natl Acad Sci U S A. 1996;93(21):11540-5.
69. Smith CL, Onate SA, Tsai MJ, O'Malley BW. CREB binding protein acts synergistically with steroid receptor coactivator-1 to enhance steroid receptor-dependent transcription. Proc Natl Acad Sci U S A. 1996;93(17):8884-8.
70. Sterner DE, Berger SL. Acetylation of histones and transcription-related factors. Microbiol Mol Biol Rev. 2000;64(2):435-59.
71. Yang XJ, Ogryzko VV, Nishikawa J, Howard BH, Nakatani Y. A p300/CBP-associated factor that competes with the adenoviral oncoprotein E1A. Nature. 1996;382(6589):319-24.
72. Imhof A, Yang XJ, Ogryzko VV, Nakatani Y, Wolffe AP, Ge H. Acetylation of general transcription factors by histone acetyltransferases. Curr Biol. 1997;7(9):689-92.
73. Sikora MJ, Jankowitz RC, Dabbs DJ, Oesterreich S. Invasive lobular carcinoma of the breast: patient response to systemic endocrine therapy and hormone response in model systems. Steroids. 2013;78(6):568-75.
74. Barroso-Sousa R, Metzger-Filho O. Differences between invasive lobular and invasive ductal carcinoma of the breast: results and therapeutic implications. Ther Adv Med Oncol. 2016;8(4):261-6.
75. Li CI, Uribe DJ, Daling JR. Clinical characteristics of different histologic types of breast cancer. Br J Cancer. 2005;93(9):1046-52.
76. Sastre-Garau X, Jouve M, Asselain B, Vincent-Salomon A, Beuzeboc P, Dorval T, et al. Infiltrating lobular carcinoma of the breast. Clinicopathologic analysis of 975 cases with reference to data on conservative therapy and metastatic patterns. Cancer. 1996;77(1):113-20.
77. Rakha EA, El-Sayed ME, Powe DG, Green AR, Habashy H, Grainge MJ, et al. Invasive lobular carcinoma of the breast: response to hormonal therapy and outcomes. Eur J Cancer. 2008;44(1):73-83.
78. Orvieto E, Maiorano E, Bottiglieri L, Maisonneuve P, Rotmensz N, Galimberti V, et al. Clinicopathologic characteristics of invasive lobular carcinoma of the breast: results of an analysis of 530 cases from a single institution. Cancer. 2008;113(7):1511-20.
79. Iorfida M, Maiorano E, Orvieto E, Maisonneuve P, Bottiglieri L, Rotmensz N, et al. Invasive lobular breast cancer: subtypes and outcome. Breast Cancer Res Treat. 2012;133(2):713-23.
80. McCart Reed AE, Kutasovic JR, Lakhani SR, Simpson PT. Invasive lobular carcinoma of the breast: morphology, biomarkers and 'omics. Breast Cancer Res. 2015;17:12.

81. Zhao H, Langerod A, Ji Y, Nowels KW, Nesland JM, Tibshirani R, et al. Different gene expression patterns in invasive lobular and ductal carcinomas of the breast. Mol Biol Cell. 2004;15(6):2523-36.
82. Ercan C, van Diest PJ, van der Ende B, Hinrichs J, Bult P, Buerger H, et al. p53 mutations in classic and pleomorphic invasive lobular carcinoma of the breast. Cell Oncol (Dordr). 2012;35(2):111-8.
83. Simpson PT, Reis-Filho JS, Lambros MB, Jones C, Steele D, Mackay A, et al. Molecular profiling pleomorphic lobular carcinomas of the breast: evidence for a common molecular genetic pathway with classic lobular carcinomas. J Pathol. 2008;215(3):231-44.
84. Bertucci F, Orsetti B, Negre V, Finetti P, Rouge C, Ahomadegbe JC, et al. Lobular and ductal carcinomas of the breast have distinct genomic and expression profiles. Oncogene. 2008;27(40):5359-72.
85. Christgen M, Steinemann D, Kuhnle E, Langer F, Gluz O, Harbeck N, et al. Lobular breast cancer: Clinical, molecular and morphological characteristics. Pathol Res Pract. 2016;212(7):583-97.
86. Krecke KN, Gisvold JJ. Invasive lobular carcinoma of the breast: mammographic findings and extent of disease at diagnosis in 184 patients. AJR Am J Roentgenol. 1993;161(5):957-60.
87. Weinstein SP, Orel SG, Heller R, Reynolds C, Czerniecki B, Solin LJ, et al. MR imaging of the breast in patients with invasive lobular carcinoma. AJR Am J Roentgenol. 2001;176(2):399-406.
88. Pritt B, Ashikaga T, Oppenheimer RG, Weaver DL. Influence of breast cancer histology on the relationship between ultrasound and pathology tumor size measurements. Mod Pathol. 2004;17(8):905-10.
89. Selinko VL, Middleton LP, Dempsey PJ. Role of sonography in diagnosing and staging invasive lobular carcinoma. J Clin Ultrasound. 2004;32(7):323-32.
90. Qureshi HS, Linden MD, Divine G, Raju UB. E-cadherin status in breast cancer correlates with histologic type but does not correlate with established prognostic parameters. Am J Clin Pathol. 2006;125(3):377-85.
91. Yu HA, Kim EY, Seo M-J, Chung E, Cho M-J, Oh H-J, et al. Stomach and Colon Metastasis from Breast Cancer. Ewha Med J. 2014;37(2):98-104.
92. Vermeulen JF, van de Ven RA, Ercan C, van der Groep P, van der Wall E, Bult P, et al. Nuclear Kaiso expression is associated with high grade and triple-negative invasive breast cancer. PLoS One. 2012;7(5):e37864.
93. Christgen M, Derksen P. Lobular breast cancer: molecular basis, mouse and cellular models. Breast Cancer Res. 2015;17:16.
94. van Roy F, Berx G. The cell-cell adhesion molecule E-cadherin. Cell Mol Life Sci. 2008;65(23):3756-88.
95. Strumane K, Berx G, Van Roy F. Cadherins in cancer. Handb Exp Pharmacol. 2004(165):69-103.
96. Cleton-Jansen AM, Callen DF, Seshadri R, Goldup S, McCallum B, Crawford J, et al. Loss of heterozygosity mapping at chromosome arm 16q in 712 breast tumors reveals factors that influence delineation of candidate regions. Cancer Res. 2001;61(3):1171-7.
97. Berx G, Cleton-Jansen AM, Strumane K, de Leeuw WJ, Nollet F, van Roy F, et al. E-cadherin is inactivated in a majority of invasive human lobular breast cancers by truncation mutations throughout its extracellular domain. Oncogene. 1996;13(9):1919-25.
98. Machado JC, Oliveira C, Carvalho R, Soares P, Berx G, Caldas C, et al. E-cadherin gene (CDH1) promoter methylation as the second hit in sporadic diffuse gastric carcinoma. Oncogene. 2001;20(12):1525-8.
99. Saito T, Oda Y, Sugimachi K, Kawaguchi K, Tamiya S, Tanaka K, et al. E-cadherin gene mutations frequently occur in synovial sarcoma as a determinant of histological features. Am J Pathol. 2001;159(6):2117-24.

100. Becker KF, Atkinson MJ, Reich U, Huang HH, Nekarda H, Siewert JR, et al. Exon skipping in the E-cadherin gene transcript in metastatic human gastric carcinomas. Hum Mol Genet. 1993;2(6):803-4.
101. Berx G, Becker KF, Hofler H, van Roy F. Mutations of the human E-cadherin (CDH1) gene. Hum Mutat. 1998;12(4):226-37.
102. Berx G, Cleton-Jansen AM, Nollet F, de Leeuw WJ, van de Vijver M, Cornelisse C, et al. E-cadherin is a tumour/invasion suppressor gene mutated in human lobular breast cancers. EMBO J. 1995;14(24):6107-15.
103. Droufakou S, Deshmane V, Roylance R, Hanby A, Tomlinson I, Hart IR. Multiple ways of silencing E-cadherin gene expression in lobular carcinoma of the breast. Int J Cancer. 2001;92(3):404-8.
104. Petridis C, Shinomiya I, Kohut K, Gorman P, Caneppele M, Shah V, et al. Germline CDH1 mutations in bilateral lobular carcinoma in situ. Br J Cancer. 2014;110(4):1053-7.
105. Moll R, Mitze M, Frixen UH, Birchmeier W. Differential loss of E-cadherin expression in infiltrating ductal and lobular breast carcinomas. Am J Pathol. 1993;143(6):1731-42.
106. Vos CB, Cleton-Jansen AM, Berx G, de Leeuw WJ, ter Haar NT, van Roy F, et al. E-cadherin inactivation in lobular carcinoma in situ of the breast: an early event in tumorigenesis. Br J Cancer. 1997;76(9):1131-3.
107. Riethmacher D, Brinkmann V, Birchmeier C. A targeted mutation in the mouse E-cadherin gene results in defective preimplantation development. Proc Natl Acad Sci U S A. 1995;92(3):855-9.
108. Boussadia O, Kutsch S, Hierholzer A, Delmas V, Kemler R. E-cadherin is a survival factor for the lactating mouse mammary gland. Mech Dev. 2002;115(1-2):53-62.
109. Derksen PW, Liu X, Saridin F, van der Gulden H, Zevenhoven J, Evers B, et al. Somatic inactivation of E-cadherin and p53 in mice leads to metastatic lobular mammary carcinoma through induction of anoikis resistance and angiogenesis. Cancer Cell. 2006;10(5):437-49.
110. Derksen PW, Braumuller TM, van der Burg E, Hornsveld M, Mesman E, Wesseling J, et al. Mammary-specific inactivation of E-cadherin and p53 impairs functional gland development and leads to pleomorphic invasive lobular carcinoma in mice. Dis Model Mech. 2011;4(3):347-58.
111. Dabbs DJ, Bhargava R, Chivukula M. Lobular versus ductal breast neoplasms: the diagnostic utility of p120 catenin. Am J Surg Pathol. 2007;31(3):427-37.
112. Sarrio D, Perez-Mies B, Hardisson D, Moreno-Bueno G, Suarez A, Cano A, et al. Cytoplasmic localization of p120ctn and E-cadherin loss characterize lobular breast carcinoma from preinvasive to metastatic lesions. Oncogene. 2004;23(19):3272-83.
113. Schackmann RC, van Amersfoort M, Haarhuis JH, Vlug EJ, Halim VA, Roodhart JM, et al. Cytosolic p120-catenin regulates growth of metastatic lobular carcinoma through Rock1-mediated anoikis resistance. J Clin Invest. 2011;121(8):3176-88.
114. Vivanco I, Sawyers CL. The phosphatidylinositol 3-Kinase AKT pathway in human cancer. Nat Rev Cancer. 2002;2(7):489-501.
115. Samuels Y, Wang Z, Bardelli A, Silliman N, Ptak J, Szabo S, et al. High frequency of mutations of the PIK3CA gene in human cancers. Science. 2004;304(5670):554.
116. Christgen M, Noskowicz M, Schipper E, Christgen H, Heil C, Krech T, et al. Oncogenic PIK3CA mutations in lobular breast cancer progression. Genes Chromosomes Cancer. 2013;52(1):69-80.
117. Ciriello G, Gatza ML, Beck AH, Wilkerson MD, Rhie SK, Pastore A, et al. Comprehensive Molecular Portraits of Invasive Lobular Breast Cancer. Cell. 2015;163(2):506-19.
118. Michaut M, Chin SF, Majewski I, Severson TM, Bismeijer T, de Koning L, et al. Integration of genomic, transcriptomic and proteomic data identifies two biologically distinct subtypes of invasive lobular breast cancer. Sci Rep. 2016;6:18517.
119. Yeatman TJ, Cantor AB, Smith TJ, Smith SK, Reintgen DS, Miller MS, et al. Tumor biology of infiltrating lobular carcinoma. Implications for management. Ann Surg. 1995;222(4):549-59; discussion 59-61.

120. Moore MM, Borossa G, Imbrie JZ, Fechner RE, Harvey JA, Slingluff CL, Jr., et al. Association of infiltrating lobular carcinoma with positive surgical margins after breast-conservation therapy. Ann Surg. 2000;231(6):877-82.
121. Helvie MA, Paramagul C, Oberman HA, Adler DD. Invasive lobular carcinoma. Imaging features and clinical detection. Invest Radiol. 1993;28(3):202-7.
122. Dixon JM, Anderson TJ, Page DL, Lee D, Duffy SW, Stewart HJ. Infiltrating lobular carcinoma of the breast: an evaluation of the incidence and consequence of bilateral disease. Br J Surg. 1983;70(9):513-6.
123. Lesser ML, Rosen PP, Kinne DW. Multicentricity and bilaterality in invasive breast carcinoma. Surgery. 1982;91(2):234-40.
124. du Toit RS, Locker AP, Ellis IO, Elston CW, Nicholson RI, Robertson JF, et al. An evaluation of differences in prognosis, recurrence patterns and receptor status between invasive lobular and other invasive carcinomas of the breast. Eur J Surg Oncol. 1991;17(3):251-7.
125. Hussien M, Lioe TF, Finnegan J, Spence RA. Surgical treatment for invasive lobular carcinoma of the breast. Breast. 2003;12(1):23-35.
126. Holland PA, Shah A, Howell A, Baildam AD, Bundred NJ. Lobular Carcinoma of the Breast Can Be Managed by Breast-Conserving Therapy. Brit J Surg. 1995;82(10):1364-6.
127. Warneke J, Berger R, Johnson C, Stea D, Villar H. Lumpectomy and radiation treatment for invasive lobular carcinoma of the breast. Am J Surg. 1996;172(5):496-500.
128. Chung MA, Cole B, Wanebo HJ, Bland KI, Chang HR. Optimal surgical treatment of invasive lobular carcinoma of the breast. Ann Surg Oncol. 1997;4(7):545-50.
129. Singletary SE, Patel-Parekh L, Bland KI. Treatment trends in early-stage invasive lobular carcinoma: a report from the National Cancer Data Base. Ann Surg. 2005;242(2):281-9.
130. Brown AM, Jeltsch JM, Roberts M, Chambon P. Activation of pS2 gene transcription is a primary response to estrogen in the human breast cancer cell line MCF-7. Proc Natl Acad Sci U S A. 1984;81(20):6344-8.
131. Yu WC, Leung BS, Gao YL. Effects of 17 beta-estradiol on progesterone receptors and the uptake of thymidine in human breast cancer cell line CAMA-1. Cancer Res. 1981;41(12 Pt 1):5004-9.
132. Daniel AR, Hagan CR, Lange CA. Progesterone receptor action: defining a role in breast cancer. Expert Rev Endocrinol Metab. 2011;6(3):359-69.
133. Amiry N, Kong X, Muniraj N, Kannan N, Grandison PM, Lin J, et al. Trefoil factor-1 (TFF1) enhances oncogenicity of mammary carcinoma cells. Endocrinology. 2009;150(10):4473-83.
134. Buache E, Etique N, Alpy F, Stoll I, Muckensturm M, Reina-San-Martin B, et al. Deficiency in trefoil factor 1 (TFF1) increases tumorigenicity of human breast cancer cells and mammary tumor development in TFF1-knockout mice. Oncogene. 2011;30(29):3261-73.
135. Prest SJ, May FE, Westley BR. The estrogen-regulated protein, TFF1, stimulates migration of human breast cancer cells. FASEB J. 2002;16(6):592-4.
136. . !!! INVALID CITATION !!! (76, 77).
137. Dutertre M, Smith CL. Molecular mechanisms of selective estrogen receptor modulator (SERM) action. J Pharmacol Exp Ther. 2000;295(2):431-7.
138. Shiau AK, Barstad D, Loria PM, Cheng L, Kushner PJ, Agard DA, et al. The structural basis of estrogen receptor/coactivator recognition and the antagonism of this interaction by tamoxifen. Cell. 1998;95(7):927-37.
139. Brzozowski AM, Pike AC, Dauter Z, Hubbard RE, Bonn T, Engstrom O, et al. Molecular basis of agonism and antagonism in the oestrogen receptor. Nature. 1997;389(6652):753-8.
140. Shang Y, Brown M. Molecular determinants for the tissue specificity of SERMs. Science. 2002;295(5564):2465-8.
141. Harper MJ, Walpole AL. A new derivative of triphenylethylene: effect on implantation and mode of action in rats. J Reprod Fertil. 1967;13(1):101-19.
142. Jordan VC. Tamoxifen (ICI46,474) as a targeted therapy to treat and prevent breast cancer. Br J Pharmacol. 2006;147 Suppl 1:S269-76.

143. Vogel VG. The NSABP Study of Tamoxifen and Raloxifene (STAR) trial. Expert Rev Anticancer Ther. 2009;9(1):51-60.
144. McDonnell DP, Wardell SE, Norris JD. Oral Selective Estrogen Receptor Downregulators (SERDs), a Breakthrough Endocrine Therapy for Breast Cancer. J Med Chem. 2015;58(12):4883-7.
145. Osborne CK, Wakeling A, Nicholson RI. Fulvestrant: an oestrogen receptor antagonist with a novel mechanism of action. Br J Cancer. 2004;90 Suppl 1:S2-6.
146. Wakeling AE, Dukes M, Bowler J. A potent specific pure antiestrogen with clinical potential. Cancer Res. 1991;51(15):3867-73.
147. Bross PF, Cohen MH, Williams GA, Pazdur R. FDA drug approval summaries: fulvestrant. Oncologist. 2002;7(6):477-80.
148. Robertson JFR, Bondarenko IM, Trishkina E, Dvorkin M, Panasci L, Manikhas A, et al. Fulvestrant 500 mg versus anastrozole 1 mg for hormone receptor-positive advanced breast cancer (FALCON): an international, randomised, double-blind, phase 3 trial. Lancet. 2016;388(10063):2997-3005.
149. Smith IE, Dowsett M. Aromatase inhibitors in breast cancer. N Engl J Med. 2003;348(24):2431-42.
150. Johnston SR. Endocrinology and hormone therapy in breast cancer: selective oestrogen receptor modulators and downregulators for breast cancer - have they lost their way? Breast Cancer Res. 2005;7(3):119-30.
151. Ring A, Dowsett M. Mechanisms of tamoxifen resistance. Endocr Relat Cancer. 2004;11(4):643-58.
152. Clarke R, Skaar TC, Bouker KB, Davis N, Lee YR, Welch JN, et al. Molecular and pharmacological aspects of antiestrogen resistance. J Steroid Biochem Mol Biol. 2001;76(1-5):71-84.
153. van de Water W, Fontein DB, van Nes JG, Bartlett JM, Hille ET, Putter H, et al. Influence of semi-quantitative oestrogen receptor expression on adjuvant endocrine therapy efficacy in ductal and lobular breast cancer - a TEAM study analysis. Eur J Cancer. 2013;49(2):297-304.
154. Pestalozzi BC, Zahrieh D, Mallon E, Gusterson BA, Price KN, Gelber RD, et al. Distinct clinical and prognostic features of infiltrating lobular carcinoma of the breast: combined results of 15 International Breast Cancer Study Group clinical trials. J Clin Oncol. 2008;26(18):3006-14.
155. Adachi Y, Ishiguro J, Kotani H, Hisada T, Ichikawa M, Gondo N, et al. Comparison of clinical outcomes between luminal invasive ductal carcinoma and luminal invasive lobular carcinoma. Bmc Cancer. 2016;16.
156. Metzger Filho O, Giobbie-Hurder A, Mallon E, Gusterson B, Viale G, Winer EP, et al. Relative Effectiveness of Letrozole Compared With Tamoxifen for Patients With Lobular Carcinoma in the BIG 1-98 Trial. J Clin Oncol. 2015;33(25):2772-9.
157. Mathieu MC, Rouzier R, Llombart-Cussac A, Sideris L, Koscielny S, Travagli JP, et al. The poor responsiveness of infiltrating lobular breast carcinomas to neoadjuvant chemotherapy can be explained by their biological profile. Eur J Cancer. 2004;40(3):342-51.
158. Tubiana-Hulin M, Stevens D, Lasry S, Guinebretiere JM, Bouita L, Cohen-Solal C, et al. Response to neoadjuvant chemotherapy in lobular and ductal breast carcinomas: a retrospective study on 860 patients from one institution. Ann Oncol. 2006;17(8):1228-33.
159. Sharma S, Kelly TK, Jones PA. Epigenetics in cancer. Carcinogenesis. 2010;31(1):27-36.
160. Berger SL, Kouzarides T, Shiekhattar R, Shilatifard A. An operational definition of epigenetics. Genes Dev. 2009;23(7):781-3.
161. Baylin SB, Jones PA. A decade of exploring the cancer epigenome - biological and translational implications. Nat Rev Cancer. 2011;11(10):726-34.
162. Luger K, Mader AW, Richmond RK, Sargent DF, Richmond TJ. Crystal structure of the nucleosome core particle at 2.8 A resolution. Nature. 1997;389(6648):251-60.
163. Strahl BD, Allis CD. The language of covalent histone modifications. Nature. 2000;403(6765):41-5.

164. Simo-Riudalbas L, Esteller M. Targeting the histone orthography of cancer: drugs for writers, erasers and readers. Br J Pharmacol. 2015;172(11):2716-32.
165. Jenuwein T, Allis CD. Translating the histone code. Science. 2001;293(5532):1074-80.
166. You JS, Jones PA. Cancer genetics and epigenetics: two sides of the same coin? Cancer Cell. 2012;22(1):9-20.
167. Dworkin AM, Huang TH, Toland AE. Epigenetic alterations in the breast: Implications for breast cancer detection, prognosis and treatment. Semin Cancer Biol. 2009;19(3):165-71.
168. Yang XJ, Seto E. HATs and HDACs: from structure, function and regulation to novel strategies for therapy and prevention. Oncogene. 2007;26(37):5310-8.
169. Zhang W, Prakash C, Sum C, Gong Y, Li Y, Kwok JJ, et al. Bromodomain-containing protein 4 (BRD4) regulates RNA polymerase II serine 2 phosphorylation in human CD4+ T cells. J Biol Chem. 2012;287(51):43137-55.
170. Yang Z, Yik JH, Chen R, He N, Jang MK, Ozato K, et al. Recruitment of P-TEFb for stimulation of transcriptional elongation by the bromodomain protein Brd4. Mol Cell. 2005;19(4):535-45.
171. Jang MK, Mochizuki K, Zhou M, Jeong HS, Brady JN, Ozato K. The bromodomain protein Brd4 is a positive regulatory component of P-TEFb and stimulates RNA polymerase II-dependent transcription. Mol Cell. 2005;19(4):523-34.
172. Knoechel B, Roderick JE, Williamson KE, Zhu J, Lohr JG, Cotton MJ, et al. An epigenetic mechanism of resistance to targeted therapy in T cell acute lymphoblastic leukemia. Nat Genet. 2014;46(4):364-70.
173. Sharma SV, Lee DY, Li B, Quinlan MP, Takahashi F, Maheswaran S, et al. A chromatin-mediated reversible drug-tolerant state in cancer cell subpopulations. Cell. 2010;141(1):69-80.
174. Ramirez M, Rajaram S, Steininger RJ, Osipchuk D, Roth MA, Morinishi LS, et al. Diverse drug-resistance mechanisms can emerge from drug-tolerant cancer persister cells. Nat Commun. 2016;7:10690.
175. Taniguchi Y. The Bromodomain and Extra-Terminal Domain (BET) Family: Functional Anatomy of BET Paralogous Proteins. Int J Mol Sci. 2016;17(11).
176. Pivot-Pajot C, Caron C, Govin J, Vion A, Rousseaux S, Khochbin S. Acetylation-dependent chromatin reorganization by BRDT, a testis-specific bromodomain-containing protein. Mol Cell Biol. 2003;23(15):5354-65.
177. Haynes SR, Dollard C, Winston F, Beck S, Trowsdale J, Dawid IB. The bromodomain: a conserved sequence found in human, Drosophila and yeast proteins. Nucleic Acids Res. 1992;20(10):2603.
178. Padmanabhan B, Mathur S, Manjula R, Tripathi S. Bromodomain and extra-terminal (BET) family proteins: New therapeutic targets in major diseases. J Biosci. 2016;41(2):295-311.
179. Hebbes TR, Thorne AW, Crane-Robinson C. A direct link between core histone acetylation and transcriptionally active chromatin. EMBO J. 1988;7(5):1395-402.
180. Denis GV, McComb ME, Faller DV, Sinha A, Romesser PB, Costello CE. Identification of transcription complexes that contain the double bromodomain protein Brd2 and chromatin remodeling machines. J Proteome Res. 2006;5(3):502-11.
181. Crowley TE, Kaine EM, Yoshida M, Nandi A, Wolgemuth DJ. Reproductive cycle regulation of nuclear import, euchromatic localization, and association with components of Pol II mediator of a mammalian double-bromodomain protein. Mol Endocrinol. 2002;16(8):1727-37.
182. Sinha A, Faller DV, Denis GV. Bromodomain analysis of Brd2-dependent transcriptional activation of cyclin A. Biochem J. 2005;387(Pt 1):257-69.
183. Jiang YW, Veschambre P, Erdjument-Bromage H, Tempst P, Conaway JW, Conaway RC, et al. Mammalian mediator of transcriptional regulation and its possible role as an end-point of signal transduction pathways. Proc Natl Acad Sci U S A. 1998;95(15):8538-43.
184. Zhou Q, Li T, Price DH. RNA polymerase II elongation control. Annu Rev Biochem. 2012;81:119-43.

185. Devaiah BN, Lewis BA, Cherman N, Hewitt MC, Albrecht BK, Robey PG, et al. BRD4 is an atypical kinase that phosphorylates serine2 of the RNA polymerase II carboxy-terminal domain. Proc Natl Acad Sci U S A. 2012;109(18):6927-32.
186. Dey A, Nishiyama A, Karpova T, McNally J, Ozato K. Brd4 marks select genes on mitotic chromatin and directs postmitotic transcription. Mol Biol Cell. 2009;20(23):4899-909.
187. Gamsjaeger R, Webb SR, Lamonica JM, Billin A, Blobel GA, Mackay JP. Structural basis and specificity of acetylated transcription factor GATA1 recognition by BET family bromodomain protein Brd3. Mol Cell Biol. 2011;31(13):2632-40.
188. Denis GV, Vaziri C, Guo N, Faller DV. RING3 kinase transactivates promoters of cell cycle regulatory genes through E2F. Cell Growth Differ. 2000;11(8):417-24.
189. Guo N, Faller DV, Denis GV. Activation-induced nuclear translocation of RING3. J Cell Sci. 2000;113 (Pt 17):3085-91.
190. LeRoy G, Rickards B, Flint SJ. The double bromodomain proteins Brd2 and Brd3 couple histone acetylation to transcription. Mol Cell. 2008;30(1):51-60.
191. Belkina AC, Denis GV. BET domain co-regulators in obesity, inflammation and cancer. Nat Rev Cancer. 2012;12(7):465-77.
192. McLure KG, Gesner EM, Tsujikawa L, Kharenko OA, Attwell S, Campeau E, et al. RVX-208, an inducer of ApoA-I in humans, is a BET bromodomain antagonist. PLoS One. 2013;8(12):e83190.
193. French CA, Ramirez CL, Kolmakova J, Hickman TT, Cameron MJ, Thyne ME, et al. BRD-NUT oncoproteins: a family of closely related nuclear proteins that block epithelial differentiation and maintain the growth of carcinoma cells. Oncogene. 2008;27(15):2237-42.
194. Greenwald RJ, Tumang JR, Sinha A, Currier N, Cardiff RD, Rothstein TL, et al. E mu-BRD2 transgenic mice develop B-cell lymphoma and leukemia. Blood. 2004;103(4):1475-84.
195. Filippakopoulos P, Qi J, Picaud S, Shen Y, Smith WB, Fedorov O, et al. Selective inhibition of BET bromodomains. Nature. 2010;468(7327):1067-73.
196. Coude mM, Berrou J, Bertrand S, Riveiro E, Herait P, Baruchel A, et al. Preclinical Study Of The Bromodomain Inhibitor OTX015 In Acute Myeloid (AML) and Lymphoid (ALL) Leukemias. Blood. 2013;122(21):4218-.
197. Dawson MA, Prinjha RK, Dittmann A, Giotopoulos G, Bantscheff M, Chan WI, et al. Inhibition of BET recruitment to chromatin as an effective treatment for MLL-fusion leukaemia. Nature. 2011;478(7370):529-33.
198. Mirguet O, Gosmini R, Toum J, Clement CA, Barnathan M, Brusq JM, et al. Discovery of epigenetic regulator I-BET762: lead optimization to afford a clinical candidate inhibitor of the BET bromodomains. J Med Chem. 2013;56(19):7501-15.
199. Delmore JE, Issa GC, Lemieux ME, Rahl PB, Shi J, Jacobs HM, et al. BET bromodomain inhibition as a therapeutic strategy to target c-Myc. Cell. 2011;146(6):904-17.
200. Chaidos A, Caputo V, Gouvedenou K, Liu B, Marigo I, Chaudhry MS, et al. Potent antimyeloma activity of the novel bromodomain inhibitors I-BET151 and I-BET762. Blood. 2014;123(5):697-705.
201. Puissant A, Frumm SM, Alexe G, Bassil CF, Qi J, Chanthery YH, et al. Targeting MYCN in neuroblastoma by BET bromodomain inhibition. Cancer Discov. 2013;3(3):308-23.
202. Wyce A, Ganji G, Smitheman KN, Chung CW, Korenchuk S, Bai Y, et al. BET inhibition silences expression of MYCN and BCL2 and induces cytotoxicity in neuroblastoma tumor models. PLoS One. 2013;8(8):e72967.
203. Asangani IA, Dommeti VL, Wang X, Malik R, Cieslik M, Yang R, et al. Therapeutic targeting of BET bromodomain proteins in castration-resistant prostate cancer. Nature. 2014;510(7504):278-82.
204. Shu S, Lin CY, He HH, Witwicki RM, Tabassum DP, Roberts JM, et al. Response and resistance to BET bromodomain inhibitors in triple-negative breast cancer. Nature. 2016;529(7586):413-7.
205. Shi J, Wang Y, Zeng L, Wu Y, Deng J, Zhang Q, et al. Disrupting the interaction of BRD4 with diacetylated Twist suppresses tumorigenesis in basal-like breast cancer. Cancer Cell. 2014;25(2):210-25.

206. Stuhlmiller TJ, Miller SM, Zawistowski JS, Nakamura K, Beltran AS, Duncan JS, et al. Inhibition of Lapatinib-Induced Kinome Reprogramming in ERBB2-Positive Breast Cancer by Targeting BET Family Bromodomains. Cell Rep. 2015;11(3):390-404.
207. Feng Q, Zhang Z, Shea MJ, Creighton CJ, Coarfa C, Hilsenbeck SG, et al. An epigenomic approach to therapy for tamoxifen-resistant breast cancer. Cell Res. 2014;24(7):809-19.
208. Mertz JA, Conery AR, Bryant BM, Sandy P, Balasubramanian S, Mele DA, et al. Targeting MYC dependence in cancer by inhibiting BET bromodomains. Proc Natl Acad Sci U S A. 2011;108(40):16669-74.
209. Bhadury J, Nilsson LM, Muralidharan SV, Green LC, Li Z, Gesner EM, et al. BET and HDAC inhibitors induce similar genes and biological effects and synergize to kill in Myc-induced murine lymphoma. Proc Natl Acad Sci U S A. 2014;111(26):E2721-30.
210. Loven J, Hoke HA, Lin CY, Lau A, Orlando DA, Vakoc CR, et al. Selective inhibition of tumor oncogenes by disruption of super-enhancers. Cell. 2013;153(2):320-34.
211. Hnisz D, Abraham BJ, Lee TI, Lau A, Saint-Andre V, Sigova AA, et al. Super-enhancers in the control of cell identity and disease. Cell. 2013;155(4):934-47.
212. Ott CJ, Kopp N, Bird L, Paranal RM, Qi J, Bowman T, et al. BET bromodomain inhibition targets both c-Myc and IL7R in high-risk acute lymphoblastic leukemia. Blood. 2012;120(14):2843-52.
213. Shu S, Polyak K. BET Bromodomain Proteins as Cancer Therapeutic Targets. Cold Spring Harb Symp Quant Biol. 2016;81:123-9.
214. Stathis A, Zucca E, Bekradda M, Gomez-Roca C, Delord JP, de La Motte Rouge T, et al. Clinical Response of Carcinomas Harboring the BRD4-NUT Oncoprotein to the Targeted Bromodomain Inhibitor OTX015/MK-8628. Cancer Discov. 2016;6(5):492-500.
215. Berthon C, Raffoux E, Thomas X, Vey N, Gomez-Roca C, Yee K, et al. Bromodomain inhibitor OTX015 in patients with acute leukaemia: a dose-escalation, phase 1 study. Lancet Haematol. 2016;3(4):e186-95.
216. Amorim S, Stathis A, Gleeson M, Iyengar S, Magarotto V, Leleu X, et al. Bromodomain inhibitor OTX015 in patients with lymphoma or multiple myeloma: a dose-escalation, open-label, pharmacokinetic, phase 1 study. Lancet Haematol. 2016;3(4):e196-204.
217. Kwiatkowski N, Zhang T, Rahl PB, Abraham BJ, Reddy J, Ficarro SB, et al. Targeting transcription regulation in cancer with a covalent CDK7 inhibitor. Nature. 2014;511(7511):616-20.
218. Christensen CL, Kwiatkowski N, Abraham BJ, Carretero J, Al-Shahrour F, Zhang T, et al. Targeting transcriptional addictions in small cell lung cancer with a covalent CDK7 inhibitor. Cancer Cell. 2014;26(6):909-22.
219. Nigg EA. Cyclin-dependent kinase 7: at the cross-roads of transcription, DNA repair and cell cycle control? Current Opinion in Cell Biology. 1996;8(3):312-7.
220. Larochelle S, Pandur J, Fisher RP, Salz HK, Suter B. Cdk7 is essential for mitosis and for in vivo Cdk-activating kinase activity. Genes & Development. 1998;12(3):370-81.
221. Neganova I, Lako M. G1 to S phase cell cycle transition in somatic and embryonic stem cells. J Anat. 2008;213(1):30-44.
222. Larochelle S, Merrick KA, Terret ME, Wohlbold L, Barboza NM, Zhang C, et al. Requirements for Cdk7 in the assembly of Cdk1/cyclin B and activation of Cdk2 revealed by chemical genetics in human cells. Mol Cell. 2007;25(6):839-50.
223. Ali S, Heathcote DA, Kroll SH, Jogalekar AS, Scheiper B, Patel H, et al. The development of a selective cyclin-dependent kinase inhibitor that shows antitumor activity. Cancer Res. 2009;69(15):6208-15.
224. Chipumuro E, Marco E, Christensen CL, Kwiatkowski N, Zhang T, Hatheway CM, et al. CDK7 inhibition suppresses super-enhancer-linked oncogenic transcription in MYCN-driven cancer. Cell. 2014;159(5):1126-39.
225. Elmore S. Apoptosis: a review of programmed cell death. Toxicol Pathol. 2007;35(4):495-516.

226. Ashkenazi A. Targeting the extrinsic apoptotic pathway in cancer: lessons learned and future directions. J Clin Invest. 2015;125(2):487-9.
227. Baker SJ, Reddy EP. Modulation of life and death by the TNF receptor superfamily. Oncogene. 1998;17(25):3261-70.
228. Fulda S, Debatin KM. Extrinsic versus intrinsic apoptosis pathways in anticancer chemotherapy. Oncogene. 2006;25(34):4798-811.
229. Kischkel FC, Hellbardt S, Behrmann I, Germer M, Pawlita M, Krammer PH, et al. Cytotoxicity-dependent APO-1 (Fas/CD95)-associated proteins form a death-inducing signaling complex (DISC) with the receptor. EMBO J. 1995;14(22):5579-88.
230. Eberstadt M, Huang B, Chen Z, Meadows RP, Ng SC, Zheng L, et al. NMR structure and mutagenesis of the FADD (Mort1) death-effector domain. Nature. 1998;392(6679):941-5.
231. Peter ME, Krammer PH. The CD95(APO-1/Fas) DISC and beyond. Cell Death Differ. 2003;10(1):26-35.
232. Hughes MA, Powley IR, Jukes-Jones R, Horn S, Feoktistova M, Fairall L, et al. Co-operative and Hierarchical Binding of c-FLIP and Caspase-8: A Unified Model Defines How c-FLIP Isoforms Differentially Control Cell Fate. Mol Cell. 2016;61(6):834-49.
233. Stennicke HR, Jurgensmeier JM, Shin H, Deveraux Q, Wolf BB, Yang X, et al. Pro-caspase-3 is a major physiologic target of caspase-8. J Biol Chem. 1998;273(42):27084-90.
234. Billen LP, Shamas-Din A, Andrews DW. Bid: a Bax-like BH3 protein. Oncogene. 2008;27 Suppl 1:S93-104.
235. Wu H. Cell Death: Mechanism and Disease. 2014:pg 47-8.
236. Bruce LJ, Anstee DJ. Unconventional cell death in erythroid cells. Blood. 2016;127(1):12-4.
237. Lopez J, Tait SW. Mitochondrial apoptosis: killing cancer using the enemy within. Br J Cancer. 2015;112(6):957-62.
238. Petros AM, Olejniczak ET, Fesik SW. Structural biology of the Bcl-2 family of proteins. Biochim Biophys Acta. 2004;1644(2-3):83-94.
239. Lomonosova E, Chinnadurai G. BH3-only proteins in apoptosis and beyond: an overview. Oncogene. 2008;27 Suppl 1:S2-19.
240. Del Gaizo Moore V, Letai A. BH3 profiling--measuring integrated function of the mitochondrial apoptotic pathway to predict cell fate decisions. Cancer Lett. 2013;332(2):202-5.
241. Chipuk JE, Moldoveanu T, Llambi F, Parsons MJ, Green DR. The BCL-2 family reunion. Mol Cell. 2010;37(3):299-310.
242. Tsujimoto Y, Cossman J, Jaffe E, Croce CM. Involvement of the bcl-2 gene in human follicular lymphoma. Science. 1985;228(4706):1440-3.
243. Sarosiek KA, Ni Chonghaile T, Letai A. Mitochondria: gatekeepers of response to chemotherapy. Trends Cell Biol. 2013;23(12):612-9.
244. Czabotar PE, Lessene G, Strasser A, Adams JM. Control of apoptosis by the BCL-2 protein family: implications for physiology and therapy. Nat Rev Mol Cell Biol. 2014;15(1):49-63.
245. Shamas-Din A, Brahmbhatt H, Leber B, Andrews DW. BH3-only proteins: Orchestrators of apoptosis. Biochim Biophys Acta. 2011;1813(4):508-20.
246. Letai A, Bassik MC, Walensky LD, Sorcinelli MD, Weiler S, Korsmeyer SJ. Distinct BH3 domains either sensitize or activate mitochondrial apoptosis, serving as prototype cancer therapeutics. Cancer Cell. 2002;2(3):183-92.
247. Sarosiek KA, Chi X, Bachman JA, Sims JJ, Montero J, Patel L, et al. BID preferentially activates BAK while BIM preferentially activates BAX, affecting chemotherapy response. Mol Cell. 2013;51(6):751-65.
248. Kim H, Tu HC, Ren D, Takeuchi O, Jeffers JR, Zambetti GP, et al. Stepwise activation of BAX and BAK by tBID, BIM, and PUMA initiates mitochondrial apoptosis. Mol Cell. 2009;36(3):487-99.
249. Llambi F, Wang YM, Victor B, Yang M, Schneider DM, Gingras S, et al. BOK Is a Non-canonical BCL-2 Family Effector of Apoptosis Regulated by ER-Associated Degradation. Cell. 2016;165(2):421-33.

250. Garrido C, Galluzzi L, Brunet M, Puig PE, Didelot C, Kroemer G. Mechanisms of cytochrome c release from mitochondria. Cell Death Differ. 2006;13(9):1423-33.
251. Schafer ZT, Kornbluth S. The apoptosome: physiological, developmental, and pathological modes of regulation. Dev Cell. 2006;10(5):549-61.
252. Pop C, Timmer J, Sperandio S, Salvesen GS. The apoptosome activates caspase-9 by dimerization. Mol Cell. 2006;22(2):269-75.
253. Li Y, Zhou M, Hu Q, Bai XC, Huang W, Scheres SH, et al. Mechanistic insights into caspase-9 activation by the structure of the apoptosome holoenzyme. Proc Natl Acad Sci U S A. 2017;114(7):1542-7.
254. Earnshaw WC, Martins LM, Kaufmann SH. Mammalian caspases: structure, activation, substrates, and functions during apoptosis. Annu Rev Biochem. 1999;68:383-424.
255. Li P, Nijhawan D, Budihardjo I, Srinivasula SM, Ahmad M, Alnemri ES, et al. Cytochrome c and dATP-dependent formation of Apaf-1/caspase-9 complex initiates an apoptotic protease cascade. Cell. 1997;91(4):479-89.
256. Shi Y. Mechanisms of caspase activation and inhibition during apoptosis. Mol Cell. 2002;9(3):459-70.
257. Segawa K, Kurata S, Yanagihashi Y, Brummelkamp TR, Matsuda F, Nagata S. Caspase-mediated cleavage of phospholipid flippase for apoptotic phosphatidylserine exposure. Science. 2014;344(6188):1164-8.
258. Nagata S, Suzuki J, Segawa K, Fujii T. Exposure of phosphatidylserine on the cell surface. Cell Death Differ. 2016;23(6):952-61.
259. Nagata S. Apoptotic DNA fragmentation. Exp Cell Res. 2000;256(1):12-8.
260. Tait SW, Green DR. Mitochondria and cell death: outer membrane permeabilization and beyond. Nat Rev Mol Cell Biol. 2010;11(9):621-32.
261. Cande C, Cohen I, Daugas E, Ravagnan L, Larochette N, Zamzami N, et al. Apoptosis-inducing factor (AIF): a novel caspase-independent death effector released from mitochondria. Biochimie. 2002;84(2-3):215-22.
262. Ryan J, Letai A. BH3 profiling in whole cells by fluorimeter or FACS. Methods. 2013;61(2):156-64.
263. Certo M, Del Gaizo Moore V, Nishino M, Wei G, Korsmeyer S, Armstrong SA, et al. Mitochondria primed by death signals determine cellular addiction to antiapoptotic BCL-2 family members. Cancer Cell. 2006;9(5):351-65.
264. Cojohari O, Burrer CM, Peppenelli MA, Abulwerdi FA, Nikolovska-Coleska Z, Chan GC. BH3 Profiling Reveals Selectivity by Herpesviruses for Specific Bcl-2 Proteins To Mediate Survival of Latently Infected Cells. J Virol. 2015;89(10):5739-46.
265. Ryan J, Montero J, Rocco J, Letai A. iBH3: simple, fixable BH3 profiling to determine apoptotic priming in primary tissue by flow cytometry. Biol Chem. 2016;397(7):671-8.
266. Davids MS, Letai A. ABT-199: A New Hope for Selective BCL-2 Inhibition. Cancer cell. 2013;23(2):139-41.
267. Zinzalla G, Thurston DE. Targeting protein-protein interactions for therapeutic intervention: a challenge for the future. Future Med Chem. 2009;1(1):65-93.
268. Oltersdorf T, Elmore SW, Shoemaker AR, Armstrong RC, Augeri DJ, Belli BA, et al. An inhibitor of Bcl-2 family proteins induces regression of solid tumours. Nature. 2005;435(7042):677-81.
269. Chauhan D, Velankar M, Brahmandam M, Hideshima T, Podar K, Richardson P, et al. A novel Bcl-2/Bcl-X(L)/Bcl-w inhibitor ABT-737 as therapy in multiple myeloma. Oncogene. 2007;26(16):2374-80.
270. Del Gaizo Moore V, Brown JR, Certo M, Love TM, Novina CD, Letai A. Chronic lymphocytic leukemia requires BCL2 to sequester prodeath BIM, explaining sensitivity to BCL2 antagonist ABT-737. J Clin Invest. 2007;117(1):112-21.
271. Baev DV, Krawczyk J, M OD, Szegezdi E. The BH3-mimetic ABT-737 effectively kills acute myeloid leukemia initiating cells. Leuk Res Rep. 2014;3(2):79-82.

272. Konopleva M, Contractor R, Tsao T, Samudio I, Ruvolo PP, Kitada S, et al. Mechanisms of apoptosis sensitivity and resistance to the BH3 mimetic ABT-737 in acute myeloid leukemia. Cancer Cell. 2006;10(5):375-88.
273. van Delft MF, Wei AH, Mason KD, Vandenberg CJ, Chen L, Czabotar PE, et al. The BH3 mimetic ABT-737 targets selective Bcl-2 proteins and efficiently induces apoptosis via Bak/Bax if Mcl-1 is neutralized. Cancer Cell. 2006;10(5):389-99.
274. Wan Y, Dai N, Tang Z, Fang H. Small-molecule Mcl-1 inhibitors: Emerging anti-tumor agents. Eur J Med Chem. 2018;146:471-82.
275. Tse C, Shoemaker AR, Adickes J, Anderson MG, Chen J, Jin S, et al. ABT-263: a potent and orally bioavailable Bcl-2 family inhibitor. Cancer Res. 2008;68(9):3421-8.
276. Roberts AW, Seymour JF, Brown JR, Wierda WG, Kipps TJ, Khaw SL, et al. Substantial susceptibility of chronic lymphocytic leukemia to BCL2 inhibition: results of a phase I study of navitoclax in patients with relapsed or refractory disease. J Clin Oncol. 2012;30(5):488-96.
277. Brachet P.E. F, Leary A., Medioni J., Follana P., Lesoin A., Frenel J-S., Abadie Lacourtoisie S., Floquet A., Gladieff L., You B., Gavoille C., Kalbacher E., Briand M., Just P-A., Blanc-Fournier C., Leconte A., Lequesne J., Poulain L., and Joly Lobbedez F. 973P

A GINECO phase II study of Navitoclax (ABT 263) in women with platinum resistant/refractory recurrent ovarian cancer (ROC). Annals of Oncology. 2017;28(5).
278. Rudin CM, Hann CL, Garon EB, Ribeiro de Oliveira M, Bonomi PD, Camidge DR, et al. Phase II study of single-agent navitoclax (ABT-263) and biomarker correlates in patients with relapsed small cell lung cancer. Clin Cancer Res. 2012;18(11):3163-9.
279. Wilson WH, O'Connor OA, Czuczman MS, LaCasce AS, Gerecitano JF, Leonard JP, et al. Navitoclax, a targeted high-affinity inhibitor of BCL-2, in lymphoid malignancies: a phase 1 dose-escalation study of safety, pharmacokinetics, pharmacodynamics, and antitumour activity. Lancet Oncol. 2010;11(12):1149-59.
280. Kaefer A, Yang J, Noertersheuser P, Mensing S, Humerickhouse R, Awni W, et al. Mechanism-based pharmacokinetic/pharmacodynamic meta-analysis of navitoclax (ABT-263) induced thrombocytopenia. Cancer Chemother Pharmacol. 2014;74(3):593-602.
281. Souers AJ, Leverson JD, Boghaert ER, Ackler SL, Catron ND, Chen J, et al. ABT-199, a potent and selective BCL-2 inhibitor, achieves antitumor activity while sparing platelets. Nat Med. 2013;19(2):202-8.
282. Roberts AW, Davids MS, Pagel JM, Kahl BS, Puvvada SD, Gerecitano JF, et al. Targeting BCL2 with Venetoclax in Relapsed Chronic Lymphocytic Leukemia. N Engl J Med. 2016;374(4):311-22.
283. Stilgenbauer S, Eichhorst B, Schetelig J, Coutre S, Seymour JF, Munir T, et al. Venetoclax in relapsed or refractory chronic lymphocytic leukaemia with 17p deletion: a multicentre, open-label, phase 2 study. Lancet Oncol. 2016;17(6):768-78.
284. Green DR. A BH3 Mimetic for Killing Cancer Cells. Cell. 2016;165(7):1560.
285. Deeks ED. Venetoclax: First Global Approval. Drugs. 2016;76(9):979-87.
286. Croce CM, Reed JC. Finally, An Apoptosis-Targeting Therapeutic for Cancer. Cancer Res. 2016;76(20):5914-20.
287. Beroukhim R, Mermel CH, Porter D, Wei G, Raychaudhuri S, Donovan J, et al. The landscape of somatic copy-number alteration across human cancers. Nature. 2010;463(7283):899-905.
288. Vogler M. Targeting BCL2-Proteins for the Treatment of Solid Tumours. Adv Med. 2014;2014:943648.
289. Amundson SA, Myers TG, Scudiero D, Kitada S, Reed JC, Fornace AJ, Jr. An informatics approach identifying markers of chemosensitivity in human cancer cell lines. Cancer Res. 2000;60(21):6101-10.
290. Lessene G, Czabotar PE, Sleebs BE, Zobel K, Lowes KN, Adams JM, et al. Structure-guided design of a selective BCL-X(L) inhibitor. Nat Chem Biol. 2013;9(6):390-7.

291. Zolnowska B, Slawinski J, Belka M, Baczek T, Kawiak A, Chojnacki J, et al. Synthesis, Molecular Structure, Metabolic Stability and QSAR Studies of a Novel Series of Anticancer N-Acylbenzenesulfonamides. Molecules. 2015;20(10):19101-29.
292. Tarrant Fp-. Bioinformatic Analysis of Invasive Lobular Carcinoma. PhD Thesis University College Dublin. 2015.
293. Dobin A, Davis CA, Schlesinger F, Drenkow J, Zaleski C, Jha S, et al. STAR: ultrafast universal RNA-seq aligner. Bioinformatics. 2013;29(1):15-21.
294. Liao Y, Smyth GK, Shi W. featureCounts: an efficient general purpose program for assigning sequence reads to genomic features. Bioinformatics. 2014;30(7):923-30.
295. Love MI, Huber W, Anders S. Moderated estimation of fold change and dispersion for RNA-seq data with DESeq2. Genome biology. 2014;15(12):550.
296. Team RDC. R: A Language and Environment for Statistical Computing. . R Foundation for Statistical Computing, Vienna, Austria (http://wwwR-projectorg/). 2012.
297. McCarthy DJ, Chen Y, Smyth GK. Differential expression analysis of multifactor RNA-Seq experiments with respect to biological variation. Nucleic Acids Res. 2012;40(10):4288-97.
298. Tyanova S, Temu T, Sinitcyn P, Carlson A, Hein MY, Geiger T, et al. The Perseus computational platform for comprehensive analysis of (prote)omics data. Nature methods. 2016;13(9):731-40.
299. Huang da W, Sherman BT, Lempicki RA. Systematic and integrative analysis of large gene lists using DAVID bioinformatics resources. Nature protocols. 2009;4(1):44-57.
300. Huang da W, Sherman BT, Lempicki RA. Bioinformatics enrichment tools: paths toward the comprehensive functional analysis of large gene lists. Nucleic Acids Res. 2009;37(1):1-13.
301. Faucher JL, Lacronique-Gazaille C, Frebet E, Trimoreau F, Donnard M, Bordessoule D, et al. "6 markers/5 colors" extended white blood cell differential by flow cytometry. Cytometry A. 2007;71(11):934-44.
302. Spizzo G, Fong D, Wurm M, Ensinger C, Obrist P, Hofer C, et al. EpCAM expression in primary tumour tissues and metastases: an immunohistochemical analysis. J Clin Pathol. 2011;64(5):415-20.
303. Centenera MM, Gillis JL, Hanson AR, Jindal S, Taylor RA, Risbridger GP, et al. Evidence for efficacy of new Hsp90 inhibitors revealed by ex vivo culture of human prostate tumors. Clin Cancer Res. 2012;18(13):3562-70.
304. Dean JL, McClendon AK, Hickey TE, Butler LM, Tilley WD, Witkiewicz AK, et al. Therapeutic response to CDK4/6 inhibition in breast cancer defined by ex vivo analyses of human tumors. Cell Cycle. 2012;11(14):2756-61.
305. Charmsaz S, Hughes É, Bane FT, Tibbitts P, McIlroy M, Byrne C, et al. S100β as a serum marker in endocrine resistant breast cancer. BMC Medicine. 2017;15:79.
306. Lamonica JM, Deng W, Kadauke S, Campbell AE, Gamsjaeger R, Wang H, et al. Bromodomain protein Brd3 associates with acetylated GATA1 to promote its chromatin occupancy at erythroid target genes. Proc Natl Acad Sci U S A. 2011;108(22):E159-68.
307. Madden SF, Clarke C, Gaule P, Aherne ST, O'Donovan N, Clynes M, et al. BreastMark: an integrated approach to mining publicly available transcriptomic datasets relating to breast cancer outcome. Breast Cancer Res. 2013;15(4):R52.
308. Kenny PA, Lee GY, Myers CA, Neve RM, Semeiks JR, Spellman PT, et al. The morphologies of breast cancer cell lines in three-dimensional assays correlate with their profiles of gene expression. Mol Oncol. 2007;1(1):84-96.
309. Sawada T, Chung YS, Nakata B, Kubo T, Kondo Y, Sogabe T, et al. [Establishment and characterization of a human breast cancer cell line, OCUB-1]. Hum Cell. 1994;7(3):138-44.
310. Lombaerts M, van Wezel T, Philippo K, Dierssen JW, Zimmerman RM, Oosting J, et al. E-cadherin transcriptional downregulation by promoter methylation but not mutation is related to epithelial-to-mesenchymal transition in breast cancer cell lines. Br J Cancer. 2006;94(5):661-71.

311. Friedland JC, Smith DL, Sang J, Acquaviva J, He S, Zhang C, et al. Targeted inhibition of Hsp90 by ganetespib is effective across a broad spectrum of breast cancer subtypes. Invest New Drugs. 2014;32(1):14-24.
312. Hollestelle A, Elstrodt F, Timmermans M, Sieuwerts AM, Klijn JG, Foekens JA, et al. Four human breast cancer cell lines with biallelic inactivating alpha-catenin gene mutations. Breast Cancer Res Treat. 2010;122(1):125-33.
313. van Horssen R, Hollestelle A, Rens JA, Eggermont AM, Schutte M, Ten Hagen TL. E-cadherin promotor methylation and mutation are inversely related to motility capacity of breast cancer cells. Breast Cancer Res Treat. 2012;136(2):365-77.
314. CAMA-1: Human Breast Cancer Cell Line (ATCC HT-21). https://www.mskcc.org/research-advantage/support/technology/tangible-material/human-breast-cell-line-cama-1 Memorial Sloan Kettering Cancer Center. 2018.
315. Reinbolt RE, Mangini N, Hill JL, Levine LB, Dempsey JL, Singaravelu J, et al. Endocrine therapy in breast cancer: the neoadjuvant, adjuvant, and metastatic approach. Semin Oncol Nurs. 2015;31(2):146-55.
316. Sikora MJ, Cooper KL, Bahreini A, Luthra S, Wang G, Chandran UR, et al. Invasive lobular carcinoma cell lines are characterized by unique estrogen-mediated gene expression patterns and altered tamoxifen response. Cancer Res. 2014;74(5):1463-74.
317. Liu Z, Merkurjev D, Yang F, Li W, Oh S, Friedman MJ, et al. Enhancer activation requires trans-recruitment of a mega transcription factor complex. Cell. 2014;159(2):358-73.
318. Liao DJ, Dickson RB. c-Myc in breast cancer. Endocr Relat Cancer. 2000;7(3):143-64.
319. Naidu R, Wahab NA, Yadav M, Kutty MK. Protein expression and molecular analysis of c-myc gene in primary breast carcinomas using immunohistochemistry and differential polymerase chain reaction. Int J Mol Med. 2002;9(2):189-96.
320. Janocko LE, Brown KA, Smith CA, Gu LP, Pollice AA, Singh SG, et al. Distinctive patterns of Her-2/neu, c-myc, and cyclin D1 gene amplification by fluorescence in situ hybridization in primary human breast cancers. Cytometry. 2001;46(3):136-49.
321. Green AR, Aleskandarany MA, Agarwal D, Elsheikh S, Nolan CC, Diez-Rodriguez M, et al. MYC functions are specific in biological subtypes of breast cancer and confers resistance to endocrine therapy in luminal tumours. Br J Cancer. 2016;114(8):917-28.
322. Nagarajan S, Hossan T, Alawi M, Najafova Z, Indenbirken D, Bedi U, et al. Bromodomain protein BRD4 is required for estrogen receptor-dependent enhancer activation and gene transcription. Cell Rep. 2014;8(2):460-9.
323. Conery AR, Centore RC, Spillane KL, Follmer NE, Bommi-Reddy A, Hatton C, et al. Preclinical Anticancer Efficacy of BET Bromodomain Inhibitors Is Determined by the Apoptotic Response. Cancer Res. 2016;76(6):1313-9.
324. Dong L, Wang W, Wang F, Stoner M, Reed JC, Harigai M, et al. Mechanisms of transcriptional activation of bcl-2 gene expression by 17beta-estradiol in breast cancer cells. J Biol Chem. 1999;274(45):32099-107.
325. Teixeira C, Reed JC, Pratt MA. Estrogen promotes chemotherapeutic drug resistance by a mechanism involving Bcl-2 proto-oncogene expression in human breast cancer cells. Cancer Res. 1995;55(17):3902-7.
326. Dawson SJ, Makretsov N, Blows FM, Driver KE, Provenzano E, Le Quesne J, et al. BCL2 in breast cancer: a favourable prognostic marker across molecular subtypes and independent of adjuvant therapy received. Br J Cancer. 2010;103(5):668-75.
327. Joensuu H, Pylkkanen L, Toikkanen S. Bcl-2 protein expression and long-term survival in breast cancer. Am J Pathol. 1994;145(5):1191-8.
328. Honma N, Horii R, Ito Y, Saji S, Younes M, Iwase T, et al. Differences in clinical importance of Bcl-2 in breast cancer according to hormone receptors status or adjuvant endocrine therapy. Bmc Cancer. 2015;15:698.

329. Ellis PA, Smith IE, Detre S, Burton SA, Salter J, A'Hern R, et al. Reduced apoptosis and proliferation and increased Bcl-2 in residual breast cancer following preoperative chemotherapy. Breast Cancer Res Treat. 1998;48(2):107-16.
330. Balko JM, Giltnane JM, Wang K, Schwarz LJ, Young CD, Cook RS, et al. Molecular profiling of the residual disease of triple-negative breast cancers after neoadjuvant chemotherapy identifies actionable therapeutic targets. Cancer Discov. 2014;4(2):232-45.
331. Crawford A, Nahta R. Targeting Bcl-2 in Herceptin-Resistant Breast Cancer Cell Lines. Curr Pharmacogenomics Person Med. 2011;9(3):184-90.
332. Cittelly DM, Das PM, Salvo VA, Fonseca JP, Burow ME, Jones FE. Oncogenic HER2{Delta}16 suppresses miR-15a/16 and deregulates BCL-2 to promote endocrine resistance of breast tumors. Carcinogenesis. 2010;31(12):2049-57.
333. Fong CY, Gilan O, Lam EY, Rubin AF, Ftouni S, Tyler D, et al. BET inhibitor resistance emerges from leukaemia stem cells. Nature. 2015;525(7570):538-42.
334. Rathert P, Roth M, Neumann T, Muerdter F, Roe JS, Muhar M, et al. Transcriptional plasticity promotes primary and acquired resistance to BET inhibition. Nature. 2015;525(7570):543-7.
335. Grumolato L, Liu G, Mong P, Mudbhary R, Biswas R, Arroyave R, et al. Canonical and noncanonical Wnts use a common mechanism to activate completely unrelated coreceptors. Genes Dev. 2010;24(22):2517-30.
336. Uysal-Onganer P, Kawano Y, Caro M, Walker MM, Diez S, Darrington RS, et al. Wnt-11 promotes neuroendocrine-like differentiation, survival and migration of prostate cancer cells. Mol Cancer. 2010;9:55.
337. Nishioka M, Ueno K, Hazama S, Okada T, Sakai K, Suehiro Y, et al. Possible involvement of Wnt11 in colorectal cancer progression. Mol Carcinog. 2013;52(3):207-17.
338. Ouko L, Ziegler TR, Gu LH, Eisenberg LM, Yang VW. Wnt11 signaling promotes proliferation, transformation, and migration of IEC6 intestinal epithelial cells. J Biol Chem. 2004;279(25):26707-15.
339. Jannesari-Ladani F, Hossein G, Izadi-Mood N. Differential Wnt11 expression related to Wnt5a in high- and low-grade serous ovarian cancer: implications for migration, adhesion and survival. Asian Pac J Cancer Prev. 2014;15(3):1489-95.
340. Sikora MJ, Jacobsen BM, Levine K, Chen J, Davidson NE, Lee AV, et al. WNT4 mediates estrogen receptor signaling and endocrine resistance in invasive lobular carcinoma cell lines. Breast Cancer Res. 2016;18(1):92.
341. Soldani C, Scovassi AI. Poly(ADP-ribose) polymerase-1 cleavage during apoptosis: an update. Apoptosis. 2002;7(4):321-8.
342. Cadigan KM, Waterman ML. TCF/LEFs and Wnt signaling in the nucleus. Cold Spring Harb Perspect Biol. 2012;4(11).
343. Yochum GS, Sherrick CM, Macpartlin M, Goodman RH. A beta-catenin/TCF-coordinated chromatin loop at MYC integrates 5' and 3' Wnt responsive enhancers. Proc Natl Acad Sci U S A. 2010;107(1):145-50.
344. Gallagher SJ, Mijatov B, Gunatilake D, Tiffen JC, Gowrishankar K, Jin L, et al. The epigenetic regulator I-BET151 induces BIM-dependent apoptosis and cell cycle arrest of human melanoma cells. J Invest Dermatol. 2014;134(11):2795-805.
345. Breslin S, O'Driscoll L. Three-dimensional cell culture: the missing link in drug discovery. Drug Discov Today. 2013;18(5-6):240-9.
346. Edmondson R, Broglie JJ, Adcock AF, Yang L. Three-dimensional cell culture systems and their applications in drug discovery and cell-based biosensors. Assay Drug Dev Technol. 2014;12(4):207-18.
347. Bratosin D, Mitrofan L, Palii C, Estaquier J, Montreuil J. Novel fluorescence assay using calcein-AM for the determination of human erythrocyte viability and aging. Cytometry A. 2005;66(1):78-84.

348. Zajchowski DA, Bartholdi MF, Gong Y, Webster L, Liu HL, Munishkin A, et al. Identification of gene expression profiles that predict the aggressive behavior of breast cancer cells. Cancer Res. 2001;61(13):5168-78.
349. Detre S, Saclani Jotti G, Dowsett M. A "quickscore" method for immunohistochemical semiquantitation: validation for oestrogen receptor in breast carcinomas. J Clin Pathol. 1995;48(9):876-8.
350. Pal SK, Childs BH, Pegram M. Triple negative breast cancer: unmet medical needs. Breast Cancer Res Treat. 2011;125(3):627-36.
351. Li B, Ni Chonghaile T, Fan Y, Madden SF, Klinger R, O'Connor AE, et al. Therapeutic Rationale to Target Highly Expressed CDK7 Conferring Poor Outcomes in Triple-Negative Breast Cancer. Cancer Res. 2017;77(14):3834-45.
352. Chonghaile TN, Roderick JE, Glenfield C, Ryan J, Sallan SE, Silverman LB, et al. Maturation stage of T-cell acute lymphoblastic leukemia determines BCL-2 versus BCL-XL dependence and sensitivity to ABT-199. Cancer Discov. 2014;4(9):1074-87.
353. Deng J, Carlson N, Takeyama K, Dal Cin P, Shipp M, Letai A. BH3 profiling identifies three distinct classes of apoptotic blocks to predict response to ABT-737 and conventional chemotherapeutic agents. Cancer Cell. 2007;12(2):171-85.
354. Ni Chonghaile T, Sarosiek KA, Vo TT, Ryan JA, Tammareddi A, Moore Vdel G, et al. Pretreatment mitochondrial priming correlates with clinical response to cytotoxic chemotherapy. Science. 2011;334(6059):1129-33.
355. Kumar K, Raza SS, Knab LM, Chow CR, Kwok B, Bentrem DJ, et al. GLI2-dependent c-MYC upregulation mediates resistance of pancreatic cancer cells to the BET bromodomain inhibitor JQ1. Sci Rep. 2015;5:9489.
356. Kurimchak AM, Shelton C, Duncan KE, Johnson KJ, Brown J, O'Brien S, et al. Resistance to BET Bromodomain Inhibitors Is Mediated by Kinome Reprogramming in Ovarian Cancer. Cell Rep. 2016;16(5):1273-86.
357. Shi X, Mihaylova VT, Kuruvilla L, Chen F, Viviano S, Baldassarre M, et al. Loss of TRIM33 causes resistance to BET bromodomain inhibitors through MYC- and TGF-beta-dependent mechanisms. Proc Natl Acad Sci U S A. 2016;113(31):E4558-66.
358. Marcotte R, Sayad A, Brown KR, Sanchez-Garcia F, Reimand J, Haider M, et al. Functional Genomic Landscape of Human Breast Cancer Drivers, Vulnerabilities, and Resistance. Cell. 2016;164(1-2):293-309.
359. Komiya Y, Habas R. Wnt signal transduction pathways. Organogenesis. 2008;4(2):68-75.
360. Flaherty MP, Dawn B. Noncanonical Wnt11 signaling and cardiomyogenic differentiation. Trends Cardiovasc Med. 2008;18(7):260-8.
361. De Leeuw WJ, Berx G, Vos CB, Peterse JL, Van de Vijver MJ, Litvinov S, et al. Simultaneous loss of E-cadherin and catenins in invasive lobular breast cancer and lobular carcinoma in situ. J Pathol. 1997;183(4):404-11.
362. Cinar M, Rosenfelt F, Rokhsar S, Lopategui J, Pillai R, Cervania M, et al. Concurrent inhibition of MYC and BCL2 is a potentially effective treatment strategy for double hit and triple hit B-cell lymphomas. Leuk Res. 2015;39(7):730-8.
363. Johnson-Farley N, Veliz J, Bhagavathi S, Bertino JR. ABT-199, a BH3 mimetic that specifically targets Bcl-2, enhances the antitumor activity of chemotherapy, bortezomib and JQ1 in "double hit" lymphoma cells. Leuk Lymphoma. 2015;56(7):2146-52.
364. Peirs S, Frismantas V, Matthijssens F, Van Loocke W, Pieters T, Vandamme N, et al. Targeting BET proteins improves the therapeutic efficacy of BCL-2 inhibition in T-cell acute lymphoblastic leukemia. Leukemia. 2017;31(10):2037-47.
365. Cheng Z, Gong Y, Ma Y, Lu K, Lu X, Pierce LA, et al. Inhibition of BET bromodomain targets genetically diverse glioblastoma. Clin Cancer Res. 2013;19(7):1748-59.

366. Wong C, Laddha SV, Tang L, Vosburgh E, Levine AJ, Normant E, et al. The bromodomain and extra-terminal inhibitor CPI203 enhances the antiproliferative effects of rapamycin on human neuroendocrine tumors. Cell Death Dis. 2014;5:e1450.
367. Parise CA, Bauer KR, Brown MM, Caggiano V. Breast cancer subtypes as defined by the estrogen receptor (ER), progesterone receptor (PR), and the human epidermal growth factor receptor 2 (HER2) among women with invasive breast cancer in California, 1999-2004. Breast J. 2009;15(6):593-602.
368. Dent R, Hanna WM, Trudeau M, Rawlinson E, Sun P, Narod SA. Pattern of metastatic spread in triple-negative breast cancer. Breast Cancer Res Treat. 2009;115(2):423-8.
369. Horiuchi D, Kusdra L, Huskey NE, Chandriani S, Lenburg ME, Gonzalez-Angulo AM, et al. MYC pathway activation in triple-negative breast cancer is synthetic lethal with CDK inhibition. J Exp Med. 2012;209(4):679-96.
370. Montero J, Sarosiek KA, DeAngelo JD, Maertens O, Ryan J, Ercan D, et al. Drug-induced death signaling strategy rapidly predicts cancer response to chemotherapy. Cell. 2015;160(5):977-89.
371. Dai H, Meng X, Kaufmann S. BCL2 Family, Mitochondrial Apoptosis, and Beyond. Cancer Translational Medicine. 2016;2(1):7-20.
372. Perillo B, Sasso A, Abbondanza C, Palumbo G. 17beta-estradiol inhibits apoptosis in MCF-7 cells, inducing bcl-2 expression via two estrogen-responsive elements present in the coding sequence. Mol Cell Biol. 2000;20(8):2890-901.

Appendix 1: Published papers

Expert Review of Molecular Diagnostics

ISSN: 1473-7159 (Print) 1744-8352 (Online) Journal homepage: http://www.tandfonline.com/loi/iero20

Diagnostic and Therapeutic Implications of Histone Epigenetic Modulators in Breast Cancer

Louise Walsh, William M. Gallagher, Darran P. O'Connor & Tríona Ní Chonghaile

Taylor Fr
Taylor & Francis Group

REVIEW

Diagnostic and Therapeutic Implications of Histone Epigenetic Modulators in Breast Cancer

Louise Walsh[a,b], William M. Gallagher[c,d], Darran P. O'Connor[a] and Tríona Ní Chonghaile[b]

[a]Department of Molecular and Cellular Therapeutics, Royal College of Surgeons in Ireland, Dublin 2, Ireland; [b]Department of Physiology and Medical Physics, Royal College of Surgeons in Ireland, Dublin 2, Ireland; [c]Cancer Biology and Therapeutics Laboratory, UCD School of Biomolecular and Biomedical Science, UCD Conway Institute, University College Dublin, Dublin 4, Ireland; [d]OncoMark Limited, NovaUCD, Belfield Innovation Park, Belfield, Dublin 4, Ireland

ABSTRACT

Breast cancer is the most common cancer in women and great advancements have been made for individualised patient treatment. Through understanding the underlying altered biology in the different subtypes of breast cancer, targeted therapeutics have been developed. Unfortunately, resistance to targeted therapy, intrinsic or acquired, is a recurring theme in cancer treatment. Epigenetic-mediated resistance to targeted therapy has been identified across different types of cancer. In addition, tumorigenesis has also been linked to altered expression of epigenetic modifiers. Due to the reversible nature of epigenetic modifications, epigenetic proteins are appealing as therapeutic targets in both the primary and relapsed/resistant setting. In this review, we will discuss the current state of targetable

6]

and of a more favorable clinical outcome [7]. The HER2 oncogene is a member of the epidermal growth factor receptor family and is amplified in 25% of breast cancers [8]. HER2 overexpressing breast cancers are dependent on HER2 signaling. Inhibition of HER2 with either monoclonal antibodies (e.g. trastuzamab, pertuzamab) [9,10] or with small molecule kinase inhibitors (e.g. lapatinib, afatinib) is an effective treatment strategy [11–13]. Lastly, TNBC occurs in approximately 15% of breast cancers [14]. The TNBC subtype of breast cancer is so-called as it lacks expression of ER, progesterone receptor (PR) and HER2. To date, a form of targeted therapy has not been identified for TNBC and it is routinely treated with cytotoxic chemotherapy [15]. Basal-like breast cancer also does not express ER, PR and HER2 and overlaps in approximately 77% of cases with TNBC [16,17]. However, basal-like breast cancer additionally expresses basal markers [18] and therefore should be considered a distinct breast cancer subtype.

Unfortunately, resistance to targeted therapy in breast cancer treatment is a major problem in the clinic [19–21]. In ER-positive breast cancer, 40% of patients will develop resistance to tamoxifen treatment [22]. While in metastatic HER2-positive breast cancer, only 35% of patients respond to first line trastuzumab therapy [23]. Similarly, TNBC is initially sensitive to chemotherapy; however, many patients relapse on treatment and have an overall worse survival compared to other breast cancer subtypes [15]. Resistance to treatment can be intrinsic or it can be acquired due to the selection of pre-existing genetic clones capable of resisting the treatment [19,21]. Recently, there is also evidence for epigenetic-mediated resistance to therapy in cancer [24–26]. In order to improve the overall survival of breast cancer patients, we need more effective treatment strategies for resistant disease across the distinct breast cancer subtypes.

Epigenetics

Epigenetics can be defined as heritable changes in gene expression without alterations in DNA sequence [27]. The regulation of the epigenome is crucial for normal growth and development, while alterations to the epigenome are associated with aberrant gene expression and diseases

CONTACT Tríona Ní Chonghaile tnichonghaile@rcsi.ie Physiology and Medical Physics, Royal College of Surgeons in Ireland, 123 St. Stephen's Green, Dublin 02, Ireland; Darran P. O'Connor darranoconnor@rcsi.ie Department of Molecular and Cellular Therapeutics, Royal College of Surgeons in Ireland, 123 St. Stephen's Green, Dublin 02, Ireland

including cancer [28]. Chromatin is comprised of the repeating basic units known as nucleosomes, which consist of DNA coiled around core histone proteins H2A, H2B, H3 and H4 along with non-histone proteins [29]. Dynamic changes in the chromatin are brought about through a series of post-translational modifications. To date, more than sixteen various histone modifications have been identified including acetylation and methylation and they usually occur at the unstructured amino terminal tail of the histone [30]. Epigenetic modifiers can be assembled into three main groups: (i) epigenetic writers are enzymes that catalyse the addition of specific chemical covalent modifications to a histone tail, (ii) epigenetic readers recognize and bind specific histone modifications and subsequently recruit other proteins to the chromatin, and finally, (iii) epigenetic erasers remove specific covalent histone modifications from the histone tails [31]. In simplistic terms, chromatin structure is altered by either enabling access of transcriptional machinery to the underlying DNA through an 'open' chromatin state known as euchromatin, or, by preventing access to the underlying DNA through a 'closed' heterochromatin [32]. In addition to genetic mutations, epigenetic alterations also contribute to tumorigenesis with many examples in breast cancer [33,34]. In this review, we will discuss some of the epigenetic events at histones that have diagnostic potential or that can be therapeutically targeted in breast cancer. For reviews on DNA modifications including methylation in relation to breast cancer, the reader is referred to the following excellent publications [35–37].

Histone acetylation in breast cancer

Histone acetyltransferases

Two enzyme families regulate histone acetylation; histone acetyltransferases (HATs) 'write' the acetylation mark while histone deacetylases (HDACs) 'erase' the acetylation mark (Figure 1). The balance of HATs and HDACs can interchange rapidly and are required for appropriate gene transcription [38,39]. Histone acetylation by HATs plays a role in the regulation of DNA repair, nucleosome assembly, replication and transcription [40–42]. Histone acetylation neutralizes the positive charge on the ε-amino group of lysine residues reducing the electrostatic interaction with negatively charged phosphates of DNA, enabling access by transcriptional machinery [43] and by docking proteins which can regulate transcription either directly or indirectly [44]. The majority of identified HATs also function as transcriptional co-activators [45,46]. There are two main subtypes of HATs based on cellular localization, type A and type B. Type A HATs are mainly nuclear and are classified into cyclic-AMP-response-element-binding protein (CBP)/p300, GNAT and MYST families, which acetylate nucleosomal histones. Type B HATs are cytoplasmic and add the acetylation modification to free histones [47]. Histone acetylation results in an open chromatin structure and is most commonly known as a mark of active gene transcription. The role of HATs in tumorigenesis is complicated in that HATs can function either as oncogenes or can act as tumor suppressors depending on the cellular context [48]. CBP/p300 HATs are transcriptional coactivators, which modulate transcriptional regulators, recruit the transcriptional machinery to gene promoters and have been shown to regulate proliferation and apoptosis [49]. Inactivation of p300 through a truncating mutation, suggesting a tumor suppressor role, has previously been identified in breast cancer [50]. Conversely, overexpression of p300 has also been identified supporting the argument of p300 as an oncogene and is associated with poor prognosis [51]. What is not clear is whether in certain breast cancer subtypes there are truncating p300 mutations, while in another subtypes, high expression may lead to poor prognosis. The human males-absent on the first (hMOF) is another HAT which has been implicated in the regulation of DNA repair [52,53] and is required for pro-apoptotic target of methylation-mediated silencing (TMSI) gene activity [54]. Mutation or downregulation of hMOF has also been identified in breast cancer [55]. Numerous examples also exist in leukemia of altered HAT expression or activity, with evidence of inactivating mutations in CBP [56] and also of CBP fusing with mixed lineage leukemia proteins (MLL) [57]. In terms of targeting HATs, then both HAT inhibitors and HAT activators could be therapeutically useful depending on the cellular context. To date, a limited number of HAT inhibitors (HATi) have been developed including curcumin and anacardic acid [58–60] both of which inhibit CBP/p300 HATs, although there is concern over HATi specificity and cell permeability [48,58]. Curcumin has been shown to resensitize chemoresistant breast cancer cells to chemotherapy by inhibiting the NF-kB pathway [61]. Recently, a new CBP/p300 inhibitor that specifically inhibits bromodomains has been developed, I-CBP112, which induced differentiation without cytotoxicity of leukemia cells [62]. N-(4-chloro-3-trifluoromethylphenyl)-2-ethoxy-6-pentadecyl-benzimidine (CTBP) is an anacardic acid derivative and is the first characterized HAT activator [59]. CTBP specifically activates p300; however, there are problems with permeability of this compound [63]. HAT activators to date have not been tested in breast cancer but may also be potential

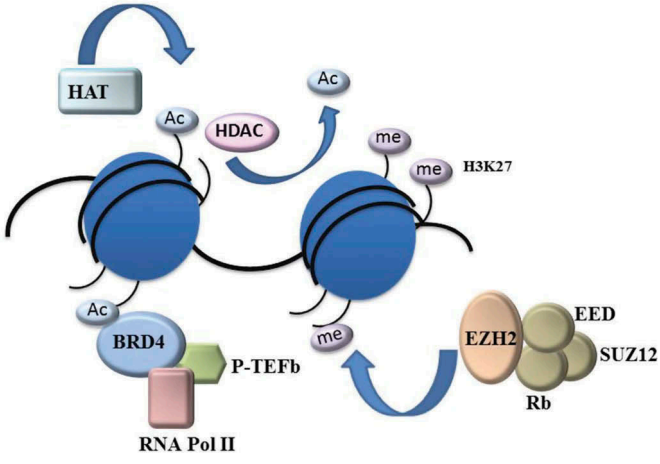

Figure 1. Epigenetic Regulation of Histones. HATs write the acetylation mark on the ε-amino group of histone lysine residues [38]. BRD4 reads this acetylation mark, recruits P-EFb to promoters with RNA-Pol II [64–66]. EZH2 is the enzymatic subunit of the PRC2 complex (EED, SUZ12, RB Asp46/48), which catalyses H3K27 trimethylation [67]. HDACs erase the acetylation mark made by HATs [38]. AC = acetylation; me = methylation.

methylated on lysine or arginine residues and they can be monomethylated, dimethylated or trimethylated [150]. The enhancer of zeste homolog 2 (EZH2) is a member of the polycomb repressive complex of proteins 2 (PRC2) and a methyltransferase [67]. EZH2 catalyzes the trimethylation of histone H3 at lysine 27 (H3K27me3), this serves as an epigenetic mark to recruit PRC1 and repress transcription [67]. PRC2 is composed of the core components EZH2 (or its homolog EZH1), embryonic ectoderm development (EED), suppressor of zeste-12 (SUZ12) and Rb Asp46/48, which are essential for PRC2 enzymatic activity (Figure 1) [67,151]. EZH2 is important in determining cell fate [152–155], embryonic development [155] and cellular memory [156]. Overexpression of PRC2 components has been associated with numerous cancers including B-cell lymphomas [157–159], prostate cancer [160] and lung cancer [161]. EZH2 has been suggested to act as a precancerous molecular marker in normal breast tissue [162]. EZH2 expression is enhanced in breast cancer tumor initiating cells and causes downregulation of DNA-damage repair enzymes [163]. Similarly, EZH2 expression is increased in metastases and invasive carcinoma and the increased expression is associated with poor clinical response [164,165]. Indeed, ectopic overexpression of EZH2 in a normal breast cell line mediated cell invasion and anchorage-independent growth both in vitro and in vivo, which was dependent on an induced HDAC activity [166]. EZH2 mediates cell invasion by suppressing Raf-1 kinase inhibitor protein [167] and/or E-cadherin in breast cancer cell lines and this is reversed by the HDACi SAHA [168]. Indeed other histone methyltransferases repress E-cadherin expression including disruptor of telomeric silencing-1-like (DOT1L) and G9a [169,170]. Interestingly, although commonly known as a transcriptional repressor, it has been reported that EZH2 directly interacts with ER alpha and β-catenin leading to transactivation of gene expression (Figure 2), which was independent of its methyltransferase activity [99,171]. EZH2 expression is also induced in vitro and in vivo by estradiol, which promotes ERs and ER coregulators to bind the EZH2 promoter (Figure 2) [172]. Thereby, there is potential for EZH2 to act in a positive feedback loop with estradiol causing increased expression of EZH2 to amplify ER-regulated genes.

From the aforementioned studies there is clear rationale for targeting EZH2 in breast cancer. A previous study used siRNA technology to target EZH2; this caused a G_2/M delay, reduced cell proliferation and upregulated BRCA1 in ER-negative breast cancer cell lines [100]. The first two published EZH2 inhibitors are GSK126 and EPZ005687, which are highly selective for EZH2 over other human methyltransferases [173,174]. Both GSK126 and EPZ005687 show efficacy in B cell lymphoma, however EPZ005687 was not suitable for in vivo studies. Since then, a series of other EZH2 inhibitors have been developed with UNC1999 being the first orally bioavailable inhibitor with improved pharmacokinetic properties [175]. Interestingly, HDACi may be able to function as a surrogate to EZH2 inhibitors, as is suggested by some studies [166,168]. There are currently no clinical trials for EZH2 inhibitors in the breast cancer arena; the only current on-going trials are for B-cell lymphoma [112].

Expert commentary

There has been huge interest in epigenetic modulators for the treatment of cancers over the past decade. This is because of the concept that epigenetic abnormalities play an important role in determining both the course of tumor development and in the process of tumor cell addiction to abnormal signaling pathways [176,177]. To date, a series of HDACi have been approved by the FDA including SAHA and romidepsin for T-cell cutaneous lymphoma and pabinostat (farydak) for the treatment of multiple myeloma patients in the relapsed/refractory setting [109–111]. Numerous on-going clinical trials are assessing the efficacy of HDACi in combination with other treatments, in the different subtypes of breast cancer. It will be interesting to see if the more selective HDACi are as effective clinically as the pan-HDACi and whether there is efficacy in the upfront setting. With the development of specific and selective inhibitors to the BET proteins [128,130,131], methyltransferases [173–175] and HATs [62], there is a new arsenal of epigenetic therapeutics to be assessed for preclinical and clinical efficacy in breast cancer. However, it is likely that the therapeutic benefit from targeting the epigenetic proteins described in this review will come from combinations with current therapy or from combinations with each other. Given the evidence for epigenetic rewiring to overcome targeted therapeutics [98,103,104,136], the use of epigenetic inhibitors in the relapsed/resistant setting of targeted agents in breast cancer needs to be evaluated in the clinic.

Five-year view

Over the next few years we will have a better understanding as to why certain cancers are sensitive to epigenetic modulators. Transcriptionally driven tumors appear to be specifically sensitive to epigenetic modifiers, likely because of the role of epigenetic proteins at super-enhancer regions of highly transcribed genes [137]. What needs to be elucidated is whether the epigenetic modifiers HDACs, BETs or HATs play overlapping roles at the super-enhancer regions in cancer and whether redundancy in the function of the proteins provides opportunities for resistance. This can be achieved by identifying biomarkers of response or transcriptional signatures predictive of response. Resistance to epigenetic modulators is also inevitable in the clinic [178], as is with all targeted therapeutics. Resistant mechanisms must be identified and resistant biomarkers established in order to inform rationale combinations with conventional treatments or with other epigenetic modifiers. The importance of this is exemplified by the recent publication which identified mechanisms of BETi resistance in TNBC and informed effective treatment combinations [147]. While we still have a lot of pieces to fit into the epigenetic puzzle, especially around solid tumors, it is an exciting time for research in this area and results from on-going clinical trials will likely guide the use of epigenetic modulators in the clinic.

Financial disclosure and competing interests disclosure

W Gallagher is a co-founder, shareholder, and part-time employee of OncoMark Limited. This work was supported by the Irish Cancer Society Collaborative Cancer Research Centre BREAST-PREDICT [grant CCRC13GAL] (www.breastpredict.com) and the European Union Framework Programme (FP7/2007-2013) under the RATHER project (Rational Therapy for Breast Cancer) [grant agreement no. 258967] (www.ratherproject.com). The authors have no other relevant affiliations or financial involvement with any organization or entity with a financial interest in or financial conflict with the subject matter or materials discussed in the manuscript apart from those disclosed.

Key issues

- Epigenetic changes play an important role in tumorigenesis.
- Epigenetic alterations are involved in resistance to targeted therapeutics.
- Many inhibitors of epigenetic histone modulators have been developed.
- Inhibitors of epigenetic modulators appear to preferentially inhibit highly transcribed genes.
- Combination treatments with inhibitors of epigenetic modulators and targeted therapy may reverse acquired resistance.
- Overlapping and distinct functions of inhibitors of epigenetic modulators need to be established.
- Biomarkers of response to epigenetic modifiers need to be determined.
- Mechanisms of resistance to epigenetic therapeutics need to be resolved.

References

Papers of special note have been highlighted as:
• of interest
•• of considerable interest

1. SEER Stat Fact Sheets: Female Breast Cancer [Internet]. Washington (DC): National Cancer Institute. Surveillance, Epidemiology, and End Results Program; 2012. [cited 2015 Nov 1]. Available from: http://seer.cancer.gov/statfacts/html/breast.html
2. Ferlay J, Soerjomataram I, Dikshit R, et al. Cancer incidence and mortality worldwide: sources, methods and major patterns in GLOBOCAN 2012. Int J Cancer. 2015;136(5):E359–E386.
3. Estimated incidence, mortality & prevalence [Internet]. Lyon: Health Organization. International Agency for Research on Cancer World; 2012. [cited 2015 Nov 1]. Available from: http://eu-cancer.iarc.fr/EUCAN/CancerOne.aspx?Cancer=46&Gender=2#block-mapc-f
4. Fisher B, Costantino J, Redmond C, et al. A randomized clinical trial evaluating tamoxifen in the treatment of patients with node-negative breast cancer who have estrogen-receptor–positive tumors. N Engl J Med. 1989;320(8):479–484.
5. Thurlimann B, Keshaviah A, Coates AS, et al. A comparison of letrozole and tamoxifen in postmenopausal women with early breast cancer. N Engl J Med. 2005;353(26):2747–2757.
6. Early Breast Cancer Trialists' Collaborative Group (EBCTCG). Relevance of breast cancer hormone receptors and other factors to the efficacy of adjuvant tamoxifen: patient-level meta-analysis of randomised trials. Lancet. 2001;378(9793):771–784.
7. Samaan NA, Buzdar AU, Aldinger KA, et al. Estrogen receptor: A prognostic factor in breast cancer. Cancer. 1981;47(3):554–560.
8. Slamon DJ, Godolphin W, Jones LA, et al. Studies of the HER-2/neu proto-oncogene in human breast and ovarian cancer. Science. 1989;244(4905):707–712.
9. Agus DB, Akita RW, Fox WD, et al. Targeting ligand-activated ErbB2 signaling inhibits breast and prostate tumor growth. Cancer Cell. 2002;2(2):127–137.
10. Slamon DJ, Leyland-Jones B, Shak S, et al. Use of chemotherapy plus a monoclonal antibody against HER2 for metastatic breast cancer that overexpresses HER2. N Engl J Med. 2001;344(11):783–792.
11. Wood ER, Truesdale AT, McDonald OB, et al. A unique structure for epidermal growth factor receptor bound to GW572016 (Lapatinib): relationships among protein conformation, inhibitor off-rate, and receptor activity in tumor cells. Cancer Res. 2004;64(18):6652–6659.
12. Rusnak DW, Lackey K, Affleck K, et al. The effects of the novel, reversible epidermal growth factor receptor/ErbB-2 tyrosine kinase inhibitor, GW2016, on the growth of human normal and tumor-derived cell lines in vitro and in vivo. Mol Cancer Ther. 2001;1(2):85–94.
13. Lin NU, Winer EP, Wheatley D, et al. A phase II study of afatanib (BIBW 2992), an irreversible ErbB family blocker, in patients with HER2-positive metastatic breast cancer progressing after trastuzamab. Breast Cancer Res Treat. 2012;133(3):1057–1065.
14. Dent R, Trudeau M, Pritchard KI, et al. Triple-negative breast cancer: clinical features and patterns of recurrence. Clin Cancer Res. 2007;13(15):4429–4434.
15. Liedtke C, Mazouni C, Hess KR, et al. Response to neoadjuvant therapy and long-term survival in patients with triple-negative breast cancer. J Clin Oncol. 2008;26(8):1275–1281.
16. Bertucci F, Finetti P, Cervera N, et al. How basal are triple-negative breast cancers? Int J Cancer. 2008;123(1):236–240.
17. Perou CM, Sorlie T, Eisen MB, et al. Molecular portraits of human breast tumours. Nature. 2000;406(6797):747–752.
18. Alluri P, Newman LA. Basal-Like and triple-negative breast cancers: searching for positives among many negatives. Surg Oncol Clin N Am. 2014;23(3):567–577.
19. Rexer BN, Arteaga CL. Intrinsic and acquired resistance to HER2-targeted therapies in HER2 gene-amplified breast cancer: mechanisms and clinical implications. Crit Rev Oncog. 2012;17(1):1–16.
20. Robinson DR, Wu YM, Vats P, et al. Activating ESR1 mutations in hormone-resistant metastatic breast cancer. Nat Genet. 2013;45(12):1446–1451.
21. Osborne CK, Schiff R. Mechanisms of endocrine resistance in breast cancer. Annu Rev Med. 2011;62:233–247.
22. Ring A, Dowsett M. Mechanisms of tamoxifen resistance. Endocr Relat Cancer. 2004;11(4):643–658.
23. Vogel CL, Cobleigh MA, Tripathy D, et al. Efficacy and safety of trastuzumab as a single agent in first-line treatment of HER2-overexpressing metastatic breast cancer. J Clin Oncol. 2002;20(3):719–726.
24. Easwaran H, Tsai H-C, Baylin SB. Cancer epigenetics: tumor heterogeneity, plasticity of stem-like states, and drug resistance. Mol Cell. 2014;54(5):716–727.
25. Vijayaraghavalu S, Dermawan JK, Cheriyath V, et al. Highly synergistic effect of sequential treatment with epigenetic and anticancer drugs to overcome drug resistance in breast cancer cells is mediated via activation of p21 gene expression leading to G2/M cycle arrest. Mol Pharm. 2013;10(1):337–352.
26. Candelaria M, Gallardo-Rincón D, Arce C, et al. A phase II study of epigenetic therapy with hydralazine and magnesium valproate to overcome chemotherapy resistance in refractory solid tumors. Ann Oncol. 2007;18(9):1529–1538.
27. Berger SL, Kouzarides T, Shiekhattar R, et al. An operational definition of epigenetics. Genes Dev. 2009;23(7):781–783.
28. Baylin SB, Jones PA. A decade of exploring the cancer epigenome - biological and translational implications. Nat Rev Cancer. 2011;11(10):726–734.

114. Stearns V, Jacobs LK, Fackler M, et al. Biomarker modulation following short-term vorinostat in women with newly diagnosed primary breast cancer. Clin Cancer Res. 2013;19(14):4008–4016.
115. Connolly R, Zhao F, Miller K, et al. [OT2-01-04] E2112: randomized phase III trial of endocrine therapy plus entinostat/placebo in patients with hormone receptor-positive advanced breast cancer. A trial of the ECOG-ACRIN cancer research group. SABCS. 2015.
116. Leroy G, Rickards B, Flint SJ. The double bromodomain proteins Brd2 and Brd3 couple histone acetylation to transcription. Mol Cell. 2008;30(1):51–60.
117. Pivot-Pajot C, Caron C, Govin J, et al. Acetylation-dependent chromatin reorganization by BRDT, a testis-specific bromodomain-containing protein. Mol Cell Biol. 2003;23(15):5354–5365.
118. Shang EY, Salazar G, Crowley TE, et al. Identification of unique, differentiation stage-specific patterns of expression of the bromodomain-containing genes Brd2, Br3, Brd4, and Brdt in the mouse testis. Gene Expr Patterns. 2004;4(5):513–519.
119. Haynes SR, Dollard C, Winston F, et al. The bromodomain: a conserved sequence found in human, drosophila and yeast proteins. Nucleic Acids Res. 1992;20(10):2603–2603.
120. Hebbes TR, Thorne AW, Cranerobinson C. A direct link between core histone acetylation and transcriptionally active chromatin. Embo J. 1988;7(5):1395–1402.
121. Denis GV, McComb ME, Faller DV, et al. Identification of transcription complexes that contain the double bromodomain protein Brd2 and chromatin remodeling machines. J Proteome Res. 2006;5(3):502–511.
122. Crowley TE, Kaine EM, Yoshida M, et al. Reproductive cycle regulation of nuclear import, euchromatic localization, and assoication with components of Pol II mediator of a mammalian double-bromodomain protein. Mol Endocrinol. 2002;16(8):1727–1737.
123. Sinha A, Faller DV, Denis GV. Bromodomain analysis of Brd2-dependent transcriptional activation of cyclin A1. Biochem J. 2005;387(1):257–269.
124. Zhou Q, Li TD, Price DH. RNA polymerase II elongation control. Annu Rev Biochem. 2012;81:119–143.
125. Devaiah BN, Lewis BA, Cherman N, et al. BRD4 is an atypical kinase that phosphorylates serine2 of the RNA polymerase II carboxy-terminal domain. Proc Natl Acad Sci U S A. 2012;109(18):6927–6932.
126. French CA, Ramirez CL, Kolmakova J, et al. BRD-NUT oncoproteins: a family of closely related nuclear proteins that block epithelial differentiation and maintain the growth of carcinoma cells. Oncogene. 2007;27(15):2237–2242.
127. Greenwald RJ, Tumang JR, Sinha A, et al. E mu-BRD2 transgenic mice develop B-cell lymphoma and leukemia. Blood. 2004;103(4):1475–1484.
128. Filippakopoulos P, Qi J, Picaud S, et al. Selective inhibition of BET bromodomains. Nature. 2010;468(7327):1067–1073.
•• **Development of JQ1 as a BET protein inhibitor**.
129. Berrou J, Bertrand S, Riveiro E, et al. Preclinical study of the bromodomain inhibitor OTX015 in acute myeloid (AML) and lymphoid (ALL) leukemias. Blood. 2013;122(21):4218–4218.
130. Dawson MA, Prinjha RK, Dittmann A, et al. Inhibition of BET recruitment to chromatin as an effective treatment for MLL-fusion leukaemia. Nature. 2011;478(7370):529–533.
131. Mirguet O, Gosmini R, Toum J, et al. Discovery of epigenetic regulator I-BET762: lead optimization to afford a clinical candidate inhibitor of the BET bromodomains. J Med Chem. 2013;56(19):7501–7515.
132. Delmore JE, Issa GC, Lemieux ME, et al. BET bromodomain inhibition as a therapeutic strategy to target c-Myc. Cell. 2011;146(6):904–917.
133. Chaidos A, Caputo V, Gouvedenou K, et al. Potent antimyeloma activity of the novel bromodomain inhibitors I-BET151 and I-BET762. Blood. 2014;123(5):697–705.
134. Puissant A, Frumm SM, Alexe G, et al. Targeting MYCN in neuroblastoma by BET bromodomain inhibition. Cancer Discov. 2013;3(3):308–323.
135. Wyce A, Ganji G, Smitheman KN, et al. BET inhibition silences expression of MYCN and BCL2 and induces cytotoxicity in neuroblastoma tumor models. PLoS One. 2013;8(8):e72967.
136. Stuhlmiller TJ, Miller SM, Zawistowski JS, et al. Inhibition of lapatinib-induced kinome reprogramming in ERBB2-positive breast cancer by targeting BET family bromodomains. Cell Rep. 2015;11(3):390–404.
•• **This paper shows the kinome remodeling which occurs following treatment with the kinase inhibitor lapatanib and that BET inhibitors can inhibit this reprograming**.
137. Loven J, Hoke HA, Lin CY, et al. Selective inhibition of tumor oncogenes by disruption of super-enhancers. Cell. 2013;153(2):320–334.
138. Hnisz D, Abraham BJ, Lee TI, et al. Super-enhancers in the control of cell identity and disease. Cell. 2013;155(4):934–947.
139. Mertz JA, Conery AR, Bryant BM, et al. Targeting MYC dependence in cancer by inhibiting BET bromodomains. Proc Natl Acad Sci U S A. 2011;108(40):16669–16674.
140. Ott CJ, Kopp N, Bird L, et al. BET bromodomain inhibition targets both c-Myc and IL7R in high-risk acute lymphoblastic leukemia. Blood. 2012;120(14):2843–2852.
141. Nagarajan S, Hossan T, Alawi M, et al. Bromodomain protein BRD4 is required for estrogen receptor-dependent enhancer activation and gene transcription. Cell Rep. 2014;8(2):459–468.
142. Rakha EA, Reis-Filho JS, Ellis IO. Basal-like breast cancer: a critical review. J Clin Oncol. 2008;26(15):2568–2581.
143. Brady-West DC, McGrowder DA. Triple negative breast cancer: therapeutic and prognostic implications. Asian Pac J Cancer Prev. 2011;12(8):2139–2143.
144. Horiuchi D, Kusdra L, Huskey NE, et al. MYC pathway activation in triple-negative breast cancer is synthetic lethal with CDK inhibition. J Exp Med. 2012;209(4):679–696.
145. Balko JM, Giltnane JM, Wang K, et al. Molecular profiling of the residual disease of triple-negative breast cancers after neoadjuvant chemotherapy identifies actionable therapeutic targets. Cancer Discov. 2014;4(2):232–245.
146. Borbely G, Haldosen LA, Dahlman-Wright K, et al. Induction of USP17 by combining BET and HDAC inhibitors in breast cancer cells. Oncotarget. 2015;6(32):33623–33635.
147. Shu S, Lin CY, He HH, et al. Response and resistance to BET bromodomain inhibitors in triple-negative breast cancer. Nature. 2016;529:413–417.
148. Shi J, Wang Y, Zeng L, et al. Disrupting the interaction of BRD4 with diacetylated Twist suppresses tumorigenesis in basal-like breast cancer. Cancer Cell. 2014;25(2):210–225.
149. A dose-finding study of OTX105/MK-8628, a small molecule inhibitor of the Bromodomain and Extra-Terminal (BET) proteins, in adults with selected advanced solid tumors (MK-8628-003). ClinicalTrials.gov: A service of the U.S National Institutes of Health. 2014 [cited 2015 Nov 15]. Available from: https://clinicaltrials.gov/ct2/show/NCT02259114?term=BROMODOMAIN+INHIBITORS%26rank=6
150. Spannhoff A, Hauser AT, Heinke R, et al. The emerging therapeutic potential of histone methyltransferase and demethylase inhibitors. ChemMedChem. 2009;4(10):1568–1582.
151. Xu B, Konze KD, Jin J, et al. Targeting EZH2 and PRC2 dependence as novel anti-cancer therapy. Exp Hematol. 2015;43(8):698–712.
152. Caganova M, Carrisi C, Varano G, et al. Germinal center dysregulation by histone methyltransferase EZH2 promotes lymphomagenesis. J Clin Invest. 2013;123(12):5009–5022.
153. Béguelin W, Popovic R, Teater M, et al. EZH2 is required for germinal center formation and somatic EZH2 mutations promote lymphoid transformation. Cancer Cell. 2013;23(5):677–692.

154. Mochizuki-Kashio M, Mishima Y, Miyagi S, et al. Dependency on the polycomb gene Ezh2 distinguishes fetal from adult hematopoietic stem cells. Blood. 2011;118(25):6553–6561.
155. Bracken AP, Dietrich N, Pasini D, et al. Genome-wide mapping of polycomb target genes unravels their roles in cell fate transitions. Genes Dev. 2006;20(9):1123–1136.
156. Laible G, Wolf A, Dorn R, et al. Mammalian homologues of the polycomb-group gene enhancer of zeste mediate gene silencing in drosophila heterochromatin and at S. cerevisiae telomeres. Embo J. 1997;16(11):3219–3232.
157. Morin RD, Mendez-Lago M, Mungall AJ, et al. Frequent mutation of histone-modifying genes in non-Hodgkin lymphoma. Nature. 2011;476(7360):298–303.
158. Morin RD, Johnson NA, Severson TM, et al. Somatic mutations altering EZH2 (Tyr641) in follicular and diffuse large B-cell lymphomas of germinal-center origin. Nat Genet. 2010;42(2):181–185.
159. Okosun J, Bodor C, Wang J, et al. Integrated genomic analysis identifies recurrent mutations and evolution patterns driving the initiation and progression of follicular lymphoma. Nat Genet. 2014;46(2):176–181.
160. Varambally S, Dhanasekaran SM, Zhou M, et al. The polycomb group protein EZH2 is involved in progression of prostate cancer. Nature. 2002;419(6907):624–629.
161. Watanabe H, Soejima K, Yasuda H, et al. Deregulation of histone lysine methyltransferases contributes to oncogenic transformation of human bronchoepithelial cells. Cancer Cell Int. 2008;8:15–26.
162. Ding L, Erdmann C, Chinnaiyan AM, et al. Identification of EZH2 as a molecular marker for a precancerous state in morphologically normal breast tissues. Cancer Res. 2006;66(8):4095–4099.
163. Chang CJ, Yang JY, Xia WY, et al. EZH2 promotes expansion of breast tumor initiating cells through activation of RAF1-beta-catenin signaling. Cancer Cell. 2011;19(1):86–100.
164. Raaphorst FM, Meijer CJ, Fieret E, et al. Poorly differentiated breast carcinoma is associated with increased expression of the human polycomb group EZH2 gene. Neoplasia. 2003;5(6):481–488.
165. Bracken AP, Pasini D, Capra M, et al. EZH2 is downstream of the pRB-E2F pathway, essential for proliferation and amplified in cancer. Embo J. 2003;22(20):5323–5335.
166. Kleer CG, Cao Q, Varambally S, et al. EZH2 is a marker of aggressive breast cancer and promotes neoplastic transformation of breast epithelial cells. Proc Natl Acad Sci U S A. 2003;100(20):11606–11611.
• **The first study showing the potential prognostic significance of EZH2 expression**.
167. Ren G, Baritaki S, Marathe H, et al. Polycomb protein EZH2 regulates tumor invasion via the transcriptional repression of the metastasis suppressor RKIP in breast and prostate cancer. Cancer Res. 2012;72(12):3091–3104.
168. Cao Q, Yu J, Dhanasekaran SM, et al. Repression of E-cadherin by the polycomb group protein EZH2 in cancer. Oncogene. 2008;27(58):7274–7284.
169. Dong C, Wu Y, Yao J, et al. G9a interacts with snail and is critical for snail-mediated E-cadherin repression in human breast cancer. J Clin Invest. 2012;122(4):1469–1486.
170. Cho MH, Park JH, Choi HJ, et al. DOT1L cooperates with the c-Myc-p300 complex to epigenetically derepress CDH1 transcription factors in breast cancer progression. Nat Commun. 2015;6:7821–7834.
171. Li X, Gonzalez ME, Toy K, et al. Targeted overexpression of EZH2 in the mammary gland disrupts ductal morphogenesis and causes epithelial hyperplasia. Am J Pathol. 2009;175(3):1246–1254.
172. Bhan A, Hussain I, Ansari KI, et al. Histone methyltransferase EZH2 is transcriptionally induced by estradiol as well as estrogenic endocrine disruptors bisphenol-A and diethylstilbestrol. J Mol Biol. 2014;426(20):3426–3441.
173. McCabe MT, Ott HM, Ganji G, et al. EZH2 inhibition as a therapeutic strategy for lymphoma with EZH2-activating mutations. Nature. 2012;492(7427):108–112.
• **The development of an EZH2 inhibitor as a potential therapeutic**.
174. Knutson SK, Wigle TJ, Warholic NM, et al. A selective inhibitor of EZH2 blocks H3K27 methylation and kills mutant lymphoma cells. Nat Chem Biol. 2012;8(11):890–896.
175. Konze KD, Ma A, Li FL, et al. An orally bioavailable chemical probe of the lysine methyltransferases EZH2 and EZH1. ACS Chem Biol. 2013;8(6):1324–1334.
176. Sharma S, Kelly TK, Jones PA. Epigenetics in cancer. Carcinogenesis. 2010;31(1):27–36.
177. Baylin SB, Ohm JE. Epigenetic gene silencing in cancer – a mechanism for early oncogenic pathway addiction? Nat Rev Cancer. 2006;6(2):107–116.
178. Fong CY, Gilan O, Lam EY, et al. BET inhibitor resistance emerges from leukaemia stem cells. Nature. 2015;525(7570):538–542.

Published OnlineFirst April 28, 2017; DOI: 10.1158/0008-5472.CAN-16-2546

Therapeutics, Targets, and Chemical Biology

Cancer Research

Therapeutic Rationale to Target Highly Expressed CDK7 Conferring Poor Outcomes in Triple-Negative Breast Cancer

Bo Li[1], Triona Ni Chonghaile[2], Yue Fan[1], Stephen F. Madden[3], Rut Klinger[1], Aisling E. O'Connor[1], Louise Walsh[4], Gillian O'Hurley[5], Girish Mallya Udupi[5], Jesuchristopher Joseph[5], Finbarr Tarrant[1], Emer Conroy[1], Alexander Gaber[6], Suet-Feung Chin[7], Helen A. Bardwell[7], Elena Provenzano[8], John Crown[9], Thierry Dubois[10], Sabine Linn[11], Karin Jirstrom[6], Carlos Caldas[7], Darran P. O'Connor[4], and William M. Gallagher[1,5]

Abstract

Triple-negative breast cancer (TNBC) patients commonly exhibit poor prognosis and high relapse after treatment, but there remains a lack of biomarkers and effective targeted therapies for this disease. Here, we report evidence highlighting the cell-cycle–related kinase CDK7 as a driver and candidate therapeutic target in TNBC. Using publicly available transcriptomic data from a collated set of TNBC patients (n ¼ 383) and the METABRIC TNBC dataset (n ¼ 217), we found CDK7 mRNA levels to be correlated with patient prognosis. High CDK7 protein expression was associated with poor prognosis within the RATHER TNBC cohort (n ¼ 109) and the METABRIC TNBC cohort (n ¼ 203). The highly specific CDK7 kinase inhibitors, BS-181 and THZ1, each downregulated CDK7-mediated phosphorylation of RNA polymerase II, indicative of transcriptional inhibition, with THZ1 exhibiting 500-fold greater potency than BS-181. Mechanistic investigations revealed that the survival of MDA-MB-231 TNBC cells relied heavily on the BCL-2/BCL-XL signaling axes in cells. Accordingly, we found that combining the BCL-2/BCL-XL inhibitors ABT-263/ABT199 with the CDK7 inhibitor THZ1 synergized in producing growth inhibition and apoptosis of human TNBC cells. Collectively, our results highlight elevated CDK7 expression as a candidate biomarker of poor prognosis in TNBC, and they offer a preclinical proof of concept for combining CDK7 and BCL-2/BCL-XL inhibitors as a mechanism-based therapeutic strategy to improve TNBC treatment. Cancer Res; 77(14); 3834–45. ©2017 AACR.

Introduction

Triple-negative breast cancer (TNBC), which is denoted by negative expression of estrogen receptor (ER), progesterone receptor (PR), and HER2, is a heterogeneous subgroup that exhibits substantial genotypic and phenotypic diversity (1, 2). Currently, no established targeted therapeutics or biomarkers of outcome/response have been clinically approved in the context of TNBC. TNBC patients commonly exhibit poor prognosis and high relapse rates at early stages after conventional neoadjuvant chemotherapy treatment (3, 4). The aggressive nature of TNBC is also reflected by an increased likelihood of distant recurrence and death within 5 years following primary intervention (3) and a shorter survival once diagnosed with metastatic disease (5). Interestingly, patients with a pathologic complete response following primary systemic chemotherapy have an excellent 3-year overall survival. In contrast, in patients with residual disease, those with TNBC displayed shorter overall survival (4). This clearly demonstrates that the poorer outcomes observed in TNBC may be largely due to the fraction of patients with chemoresistant disease, which represent over 50% of cases (6). This observation underscores the need to identify the patients that are unlikely to benefit from existing chemotherapeutics using prognostic markers and to develop alternative therapeutic options.

CDK7 belongs to the cyclin-dependent kinase family, a major class of kinases involved in cell-cycle regulation. It binds to cyclin

[1]UCD School of Biomolecular and Biomedical Science, UCD Conway Institute, University College Dublin, Dublin, Ireland. [2]Department of Physiology & Medical Physics, Royal College of Surgeons in Ireland, Dublin, Ireland. [3]Population Health Sciences Division, Royal College of Surgeons in Ireland, Dublin, Ireland. [4]Department of Molecular & Cellular Therapeutics, Royal College of Surgeons in Ireland, Dublin, Ireland. [5]OncoMark Ltd, Belfield Innovation Park, Dublin, Ireland. [6]Lund University, Lund, Sweden. [7]Cancer Research UK Cambridge Institute, University of Cambridge, Li Ka Shing Centre, Cambridge, United Kingdom. [8]Cambridge Experimental Cancer Medicine Centre (ECMR) and NIHR Cambridge Biomedical Research Centre, Cambridge University Hospitals NHS Foundation Trust, Cambridge, United Kingdom. [9]Department of Medical Oncology, St. Vincent's University Hospital, Dublin, Ireland. [10]Institut Curie, PSL Research University, Department of Translational Research, Breast Cancer Biology Group, Paris, France. [11]The Netherlands Cancer Institute, Amsterdam, the Netherlands.

Note: Supplementary data for this article are available at Cancer Research Online (http://cancerres.aacrjournals.org/).

B. Li and T. Ni Chonghaile contributed equally to this article.

D.P. O'Connor and W.M. Gallagher share senior authorship of this article.

Corresponding Author: William Gallagher, UCD School of Bimolecular and Biomedical Science, UCD Conway Institute, University College Dublin, Belfield, Dublin D4, Ireland. Phone: 353-1716-6743; E-mail: william.gallagher@ucd.ie

doi: 10.1158/0008-5472.CAN-16-2546

Published OnlineFirst April 28, 2017; DOI: 10.1158/0008-5472.CAN-16-2546

H and MAT1 forming a trimeric cyclin-activating kinase (CAK) that executes its function by phosphorylating other CDKs involved in cell-cycle control (7). Each complex controls specific transitions between two subsequent phases in the cell cycle. CDK7 is required for both activation and complex formation of CDK1/cyclin-B during the G_2–M transition and for activation of CDK2/cyclin-E during the G_1–S transition (8). In addition, CDK7 regulates polymerase II–mediated RNA transcription through the binding of CAK to the TFIIH basal transcription factor complex, which phosphorylates the C-terminal domain of the largest subunit of RNA polymerase II (RNAPII) (9, 10). Previously, it was shown that CAK also phosphorylates and enhances activities of transcriptional regulators (11, 12). Therefore, CDK7 affects both cell-cycle progression and transcriptional activity. Recent studies highlighted the role of CDK7 as a transcriptional regulator, a key mechanism that many aggressive cancers rely on, which provided a promising therapeutic target in these hard-to-treat diseases, particularly in TNBC and other cancers that follow MYC-driven oncogenic transcription addiction (13–16).

Numerous attempts have been made to identify key oncogenic pathways altered at the molecular level in TNBC. Previously, a high frequency of mutations in the TP53 tumor suppressor gene, along with amplification of the transcription factor–encoding MYC and the anti-apoptotic MCL-1 genes, were found in residual neoadjuvant chemotherapy–treated TNBC (17). MYC, a pleiotropic transcription factor that dimerizes with MAX to bind to enhancer box (E-box) sequences in the promoters of active genes, plays a key role in a myriad of tumor types (18). Aberrant expression of MYC family members commonly leads to deregulated transcription and metabolism, resulting in uncontrolled tumor growth and proliferation, and elevated expression of these oncogenes is often linked to poor prognosis (19, 20).

MCL-1 is a member of the antiapoptotic BCL-2 family that governs mitochondrial apoptosis through protein–protein interaction. Given MCL-1 its short half-life, MCL-1 is significantly affected by transcriptional inhibition and is one of the most commonly amplified genes in cancer (21). To date, the small-molecule inhibitors of MCL-1 that have been developed (22) do not have nanomolar affinity of binding equivalent to the BH3 mimetics ABT-263 (binds to BCL-2, BCL-XL and BCL-W; refs. 23–25) and ABT-199 (binds to BCL-2; refs. 26, 27). Inhibition of the antiapoptotic proteins is capable of killing cells that are dependent on those antiapoptotic proteins for survival. BH3 profiling is a useful tool for assessing antiapoptotic dependency. BH3 peptides generated from the functional BH3 domain of particular proapoptotic proteins are added to permeabilized cells and loss of mitochondrial potential or cytochrome c is measured as a functional readout of antiapoptotic dependency (28, 29).

Here, we proposed to use an unbiased in silico analysis of transcriptomic data to identify kinases whose expression was associated with clinical outcomes in TNBC and validate the findings at the protein level using IHC on tissue microarrays (TMA). From this analysis, expression of CDK7, a cyclin-dependent kinase, was found to be closely associated with poor prognosis at both mRNA and protein levels. Moreover, we evaluated the response in vitro to CDK7 inhibition using both short hairpin RNAs (shRNA) and two specific CDK7 inhibitors in TNBC. Inhibition of CDK7 caused inhibition of proliferation, phosphorylation of RNAPII, an indication of transcriptional inhibition, along with induction of apoptosis. MCL-1 and MYC were downregulated in a dose- and time-dependent manner following CDK7 inhibition. Using BH3 profiling, we identified an increased dependency on BCL-2/BCL-XL following CDK7 inhibition and discovered the synergistic combination of the BH3 mimetic ABT-263 with the CDK7 inhibitor THZ1.

Materials and Methods

Study populations

Public TNBC transcriptomic dataset (Cohort I). An in silico method was adopted to explore a publicly available TNBC dataset (30) in which a method for assigning TNBC status to transcriptomic data from human breast cancer tissues was employed. A TNBC microarray dataset (n ¼ 383) was reanalyzed to identify genes associated with survival, with a particular focus on kinases. TNBC patient samples were defined on the basis of negative mRNA expression of ER, PR, and HER2 genes. The TNBC microarray dataset was split into training (n ¼ 297) and test (n ¼ 86) datasets. The training dataset was used for the discovery study. Univariate Cox regression with proportional hazards models was employed to investigate kinase genes that were significantly associated with patient survival in the training dataset. Candidate survival-associated kinases were then validated in the remaining test dataset. This entire TNBC microarray dataset was derived from patients with a median age of 50 years (range, 28–88 years) at the time of diagnosis, and a median follow-up of 51 months (range, 0–10 years). Patients exhibited tumor grade 1 and grade 2 (n ¼ 104) or grade 3 (n ¼ 234). Information on tumor grade was missing for 45 patients. Patients were either treated with adjuvant chemotherapy (n ¼ 259), or not treated with chemotherapy (n ¼ 87). Information on chemotherapy treatment was missing for 37 patients.

Public breast cancer transcriptomic dataset (Cohort II). The online tool, BreastMark, was used to identify association between CDK7 mRNA expression and clinical outcomes in a breast cancer cohort with all subtypes. Information on the BreastMark system was previously described (31). In this study, CDK7 mRNA expression data were analyzed from 2,656 breast cancer patients of mixed subtypes censored at 10 years.

METABRIC breast cancer transcriptomic (Cohort III) and TMA (Cohort V) datasets. The METABRIC study protocol and molecular profiling of the entire cohort were previously described (32). The entire METABRIC transcriptomic dataset consists of 1,992 breast cancer patients. In this study, 1,277 breast cancer patients censored at 10 years were analyzed (Cohort III). TNBC samples were defined by negative mRNA expression of ER, PR and HER2 genes (n ¼ 217). TNBC patients from this sub-cohort had a median age of 56 years (range, 28–96 years) at the time of diagnosis. The median follow-up was 44 months (range, 0–119 months). Patients were either not treated with any type of therapy (n ¼ 33), or treated with chemotherapy, hormonal therapy, radiotherapy, or a combination of these therapies (n ¼ 184). Patients exhibited tumor grade 1 (n ¼ 4), grade 2 (n ¼ 24), or grade 3 (n ¼ 189). A total number of 1,992 breast cancer patients, containing mRNA expression data pertaining to CDK7 and MYC, was analyzed for comparison between each subtype of breast cancer in the METABRIC transcriptomic dataset.

The METABRIC TMA cohort (Cohort V) contains 1,286 breast cancer tissues with 218 TNBC cases. In this study, 203 TNBC patient samples censored at 15 years were analyzed. TNBC patients had a median age of 56 years (range, 27–96 years) at

Published OnlineFirst April 28, 2017; DOI: 10.1158/0008-5472.CAN-16-2546

the time of diagnosis. The median follow-up was 62 months (range, 0–176 months). Patients were not treated with any therapy (n ¼ 29) or treated with either chemotherapy, hormonal therapy, radiotherapy only, or with combined therapies (n ¼ 174). Patients exhibited tumor grade 1 (n ¼ 2), grade 2 (n ¼ 27), and grade 3 (n ¼ 171). Information on tumor grade was missing for 3 patients.

RATHER TMA cohort (Cohort IV). The RATHER TNBC TMA cohort contains tissues from 138 TNBC patients. In this study, 109 TNBC patient samples censored at 15 years were analyzed. These patients were diagnosed between 1986 and 2010 with a median age of 54 years (range, 26–87 years) at the time of diagnosis. The median follow-up was 61 months (range, 1–173 months). Patients were treated with adjuvant chemotherapy (n ¼ 47) or not treated with adjuvant chemotherapy (n ¼ 62). Patients were treated with radiotherapy (n ¼ 29) or not treated with radiotherapy (n ¼ 80). Patients exhibited tumor grade 2 (n ¼ 12) or grade 3 (n ¼ 96). Information on tumor grade was missing for 1 patient.

Consecutive breast cancer TMA cohort (Cohort VI). The consecutive TMA cohort consists of 512 consecutive breast cancer patients diagnosed at the Department of Pathology, Malmo University Hospital, Sweden, during 1988–1992 (33). In this study, a total number of 346 breast cancer patients were censored at 15 years with a median age of 67 years (range, 28–96 years). The median follow-up was 82 months (range, 0–180 months). Patients were not treated with chemotherapy (n ¼ 247) or treated with chemotherapy (n ¼ 20). Information on chemotherapy was missing for 79 patients.

TCGA breast cancer transcriptomic dataset (Cohort VII). In this study, the The Cancer Genome Atlas (TCGA) breast cancer transcriptomic dataset consisting of 422 breast cancer patients with mixed subtypes was analyzed for CDK7 and MYC mRNA expression in each individual subtype of breast cancer.

Cell culture

All TNBC cell lines were originally purchased from the ATCC in May 2008 and were regularly authenticated by short tandem repeat profiling. The most recent reauthentication was completed in January 2017. BT20 cells were maintained in EMEM medium. BT549, HCC1143, and HCC1937 cells were maintained in RPMI1640 medium. Hs578T and MDA-MB-231 cells were maintained in DMEM medium. All cell culture media were supplemented with 10% FBS, 1% L-glutamine, and 1% penicillin/streptomycin and cells were incubated at 37°C with 5% CO_2. Mycoplasma testing was performed on a monthly basis.

shRNA-mediated knockdown of CDK7

Commercially available (Sigma Aldrich) pLKO vector-based constructs expressing shRNAs targeting CDK7 (CCGGGCTGTAGAAGTGAGTTTGTAACTCGAGTTACAAACTCACTTCTACAGCTTTTT, and CCGGCATTTAAGAGTTTCCCTGGAACTCGAGTTCCAGGGAAACTCTTAAATGTTTTT) or a pLKO.1-puro nonmammalian shRNA control plasmid DNA (CCGGCAACAAGATGAAGAGCACCAACTCGAGTTGGTGCTCTTCATCTTGTTGTTTTT; Sigma Aldrich) were transfected into HEK293 cells using the Genejuice method. Live viruses were collected, filtered, and used to transfect BT549 and MDA-MB-231 cells for 24 hours. Cells were selected using 3 mg/mL puromycin for 5 days.

Colony formation assay

BT549 and MDA-MB-231 transfectants (expressing either non-targeting control shRNA or CDK7 shRNAs) were seeded at 500 cells/well of 6-well plates in 2-mL growth media for 15 days, with media being replaced by fresh growth media every 5 days until colonies were visible. Colonies were stained with crystal violet solution and counted manually.

Wound healing assay

BT549 and MDA-MB-231 transfectants (expressing either non-targeting control shRNA or CDK7 shRNAs) were seeded at 3 × 10^5 cells per well of 12-well plates in 1-mL growth medium overnight. Growth media were replaced by serum-free media and incubated for 8 hours before scratches were made. Initial pictures were taken immediately after scratches were made and medium was replaced by fresh serum-free media (0 hour time point). Additional pictures were taken at 24 and 48 hours after medium replacement. Analysis was carried out using the T-Scratch software (ETH Zurich) that analyzed the area occupied by cells in the images. Results were graphed as percentage wound closure over time.

Proliferation: MTT cell viability assay

Cell viability was measured using an MTT (3-(4,5-dimethylthiazol-2-yl)-2,5-diphenyltetrazolium bromide) colorimetric assay. BT549 and MDA-MB-231 cells were seeded in sextuplicate at a density of 2,000 cells/well in 96-well plates and were incubated at 37°C in growth media overnight. Cells were treated with various doses of BS-181 and THZ1 for 72 hours. Cells were then incubated with MTT reagent (5 mg/mL) for 3 hours, after which they were solubilized in dimethyl sulfoxide (DMSO). Absorbance was measured using a Wallac 1420 multi-label plate reader at 570 nm. For the combination treatments, cells were seeded at a density of 2,000 cells/well (BT549 and MDA-MB-231), 3,000 cells/well (BT20), and 5,000 cells/well (HCC1937, HCC1143 and Hs578T) in 96-well plates and were incubated at 37°C overnight. Cells were treated for 48 hours simultaneously with THZ1 and ABT-263/ABT-199 at various doses and synergy was measured using the CompuSyn software. Results were normalized to a DMSO-only control and dose–response curves were created using GraphPad Prism.

Immunoblotting

The following antibodies were purchased from Cell Signaling Technology: anti-CDK7 (2916), anti-CDK1 (9116), anti-p-CDK1 (9111), anti-p-RNAPII Ser-2 (8798), anti-p-RNAPII Ser-5 (8807), anti-p-RNAPII Ser-7 (13780), anti-c-MYC (5605), anti-MCL-1 (5453), anti-BCL-2 (2870), and anti-BCL-XL (2764). Antibodies against RNAPII (sc-17798), vinculin (sc-5573), and a-tubulin (sc-5286) were purchased from Santa Cruz Biotechnology. The anti-b-actin (A5316) antibody was obtained from Sigma-Aldrich.

Cell-cycle analysis by flow cytometry

BT549 and MDA-MB-231 cells were collected at 1 × 10^6 per cell line, washed with PBS and resuspended in PBS (1 mL) per cell line. Prechilled 70% ethanol (2.5 mL) was added to each cell

Published OnlineFirst April 28, 2017; DOI: 10.1158/0008-5472.CAN-16-2546

suspension dropwise while vortexing. Cells were immediately stored at 4°C overnight. Cells were washed with PBS and resuspended in PBS (500 mL) and RNaseA (1 mL of 2.5 mg/mL) was added to each sample and incubated at 37°C for 30 minutes. Propidium iodide (50 mL of 0.5 mg/mL; Sigma P4170) was added to each sample. The BD Accuri C6 plus (BD Biosciences) flow cytometer was subsequently utilized for the cell-cycle analysis.

Immunohistochemistry

Sample slides were deparaffinized and rehydrated using a Leica Autostainer XL. Samples were treated with 1× citrate buffer pH 6.0 at 95°C in the PT module (LabVision, Thermo Fisher Scientific), incubated with 3% H_2O_2, blocked using UV-Block reagent and treated with the anti-CDK7 antibody. Samples were then treated with primary antibody enhancer (PAE), horseradish peroxidase–labeled polymer, DAB, and counterstained with hematoxylin.

Digital slide scanning and automated image analysis

The Aperio ScanScope XT slide scanner (Aperio Technologies) was used for digital scanning at ×20 magnification. ImageScope analysis software was used for viewing and analyzing digital images. Spectrum was used to generate individual tissue spot images for automated analysis. The Nuclear Algorithm (Aperio Technologies) was used to analyze percentage of positive nuclei against total nuclei. Positive intensity was also measured on cell pellet control slides using the Color Deconvolution Algorithm (Aperio Technologies).

Cell death assay: Annexin V/propidium iodide staining

Apoptosis was measured using an Annexin V/propidium iodide assay. Cells were seeded at a density of 3×10^4 (BT549) and 4×10^4 cells/well (MDA-MB-231) in 24-well plates and were incubated at 37°C in growth media overnight. Cells were then treated with various doses of BS-181 and THZ1 for 48 hours or in combination with ABT-263 or ABT-199 for 24 hours. Cells were washed with PBS and resuspended in Annexin binding buffer (10 mmol/L HEPES pH 7.4, 140 mmol/L NaCl, and 2.5 mmol/L CaCl). Cells were then stained with 0.5 mg/mL Annexin V-FITC and 0.5 mg/mL propidium iodide for 15 minutes before analyzing on the BD Accuri 6 plus (BD Biosciences). Results were normalized to a DMSO-only control and dose–response curves were created using GraphPad Prism.

BH3 profiling

The sequence of the BH3-only peptides and method of synthesis used were described previously (34). BH3 profiling was performed by flow cytometry. Briefly, BH3 peptides at 70 mmol/L were incubated with cells that were being gently permeabilized with 0.005% digitonin. Following 60-minute incubation, cells were fixed with 8% formaldehyde for 15 minutes prior to neutralization and staining with cytochrome c at 4°C overnight. The loss of cytochrome was measured on a CyAn ADP Analyzer (Beckman Coulter) using the FITC channel. The percentage of peptide-induced mitochondrial depolarization was calculated by normalization to the solvent-only control DMSO (0%).

Study design, implementation, and statistical analysis

Due consideration of REMARK guidelines was given in respect to study design, implementation, and analysis (35). Kaplan–Meier survival analysis was performed using the SPSS statistical analysis software (IBM). The Cox proportional hazard model was used for multivariate analysis to illustrate the relationships between gene/protein expression and breast cancer–specific survival (BCSS), recurrence-free survival (RFS), distant recurrence-free survival (DRFS), and overall survival (OS). Hazard ratios (HR) and 95% confidence intervals (95% CI) were evaluated for each clinicopathologic variable. A two-tailed test with P value < 0.05 was considered to be significant. The CompuSyn method was used to assess synergy of combination drug treatment (36). A combination index value of under 1 was considered to be significant.

Results

High *CDK7* mRNA expression is associated with poor clinical outcomes of patients with TNBC

To identify kinases that are associated with clinical outcomes in TNBC, we reanalyzed publicly available transcriptomic data from a combined cohort of 579 TNBC patients, of which 383 had associated clinical outcome data (Cohort I, public TNBC; ref. 30). From this analysis, CDK7 mRNA expression was linked to poor prognosis in a TNBC context. Kaplan–Meier survival analysis in Cohort I (n ¼ 383) demonstrated that, when a median CDK7 mRNA expression cut-off point was used for stratification, high CDK7 mRNA expression was strongly correlated with reduced RFS (P < 0.001; HR ¼ 2.152; CI ¼ 1.576–2.939; Supplementary Fig. S1A). Further survival analysis was carried out using BreastMark, an online integrated resource to allow evaluation of genes that are associated with survival outcomes in breast cancer and its molecular subtypes, in an unstratified cohort of 2,656 breast cancer patients (Cohort II, BreastMark; ref. 31), which demonstrated no significant association between CDK7 mRNA expression and RFS (Supplementary Fig. S1B), suggesting that CDK7 is not a prognostic factor in breast cancer as a whole, but rather specifically predicts outcomes in TNBC.

To further validate our findings, we examined CDK7 mRNA expression in an independent cohort of the METABRIC (Molecular Taxonomy of Breast Cancer International Consortium; Cohort III), which was composed of a discovery set of 997 primary tumors and a validation set of 995 tumors with long-term clinical outcomes (32). Within Cohort III, when a median cut-off point of CDK7 mRNA expression was used, high CDK7 mRNA expression was again significantly associated with poor BCSS specifically in the TNBC cohort (P ¼ 0.023; HR ¼ 1.598; CI ¼ 1.061–2.406; Supplementary Fig. S1C). We observed no evidence of association between CDK7 mRNA expression and clinical outcomes when the entire cohort was examined (P ¼ 0.195; HR ¼ 0.885; CI ¼ 0.735–1.065; Supplementary Fig. S1D), again indicating that CDK7 mRNA expression appeared to specifically predict survival outcomes in a TNBC context.

High CDK7 protein expression is associated with poor clinical outcomes in a TNBC context

In silico analysis of transcriptomic data suggested that CDK7 mRNA level may differentiate TNBC patients with good versus poor outcomes. Here, we attempted to validate these results at the protein level in an independent cohort of patient samples. TNBC tissues obtained from the RATHER consortium (Rational Therapy for Breast Cancer, www.ratherproject.com; Cohort IV, n ¼ 109) were immunohistochemically assessed using an optimized anti-CDK7 antibody (Supplementary Fig. S2). Automated image analysis was used to score percentage of tumor nuclei positive for CDK7 protein expression (over total number of tumor cells)

Published OnlineFirst April 28, 2017; DOI: 10.1158/0008-5472.CAN-16-2546

across all samples and was subsequently assessed for associations with clinicopathologic variables. A median cut-off point was chosen in respect of positivity percentage of CDK7, with representative tissue cores illustrating high and low CDK7 protein expression shown in Fig. 1A. Across the RATHER TNBC TMA cohort, a high percentage of CDK7-positive tumor cells was significantly associated with reduced BCSS (P ¼ 0.012; HR ¼ 2.516; CI ¼ 1.189–5.324; Fig. 1B), RFS (P ¼ 0.019; HR ¼ 2.208; CI ¼ 1.123–4.344; Supplementary Fig. S3A) and DRFS (P ¼ 0.013; HR ¼ 2.506; CI ¼ 1.185–5.299; Supplementary Fig. S3C). Multivariate Cox regression analysis demonstrated that CDK7 protein expression and tumor size were independent prognostic factors for reduced BCSS in TNBC (Table 1; for CDK7, P ¼ 0.006; HR ¼ 3.045; CI ¼ 1.383–6.701).

Given that we previously observed no correlations between CDK7 mRNA expression and outcomes in a noncategorized breast cancer cohort, we subsequently analyzed CDK7 protein expression in tumor tissues from a representative cohort of 346 breast cancer patients comprised of all major subtypes, namely the Consecutive array (Cohort VI; ref. 33), which included 33 TNBC cases. Again, no correlations between CDK7 protein expression and BCSS (P ¼ 0.313; HR ¼ 0.794; CI ¼ 0.507□1.245; Fig. 1C), RFS (P ¼ 0.364; HR ¼ 0.852; CI ¼ 0.601□1.206; Supplementary Fig. S3B), or DRFS (P ¼ 0.662; HR ¼ 0.916; CI ¼ 0.617□1.359; Supplementary Fig. S3D) were found within this cohort, further reinforcing a particular association of CDK7 expression with poor clinical outcomes in patients with TNBC.

To further validate the prognostic value of CDK7 at the protein level in TNBC, we carried out TMA analysis in the METABRIC cohort, which was composed of 203 TNBC tissues plus additional 948 breast cancer tissues from other subtypes. When a median cut-off point was used to stratify low and high expression of CDK7 protein, Kaplan–Meier survival analysis demonstrated a strong negative correlation between CDK7 protein expression and BCSS (P ¼ 0.007; HR ¼ 1.921; CI ¼ 1.185–3.113; Fig. 1D), as well as OS (P ¼ 0.042; HR ¼ 1.489; CI ¼ 1.011–2.193; Supplementary Fig.

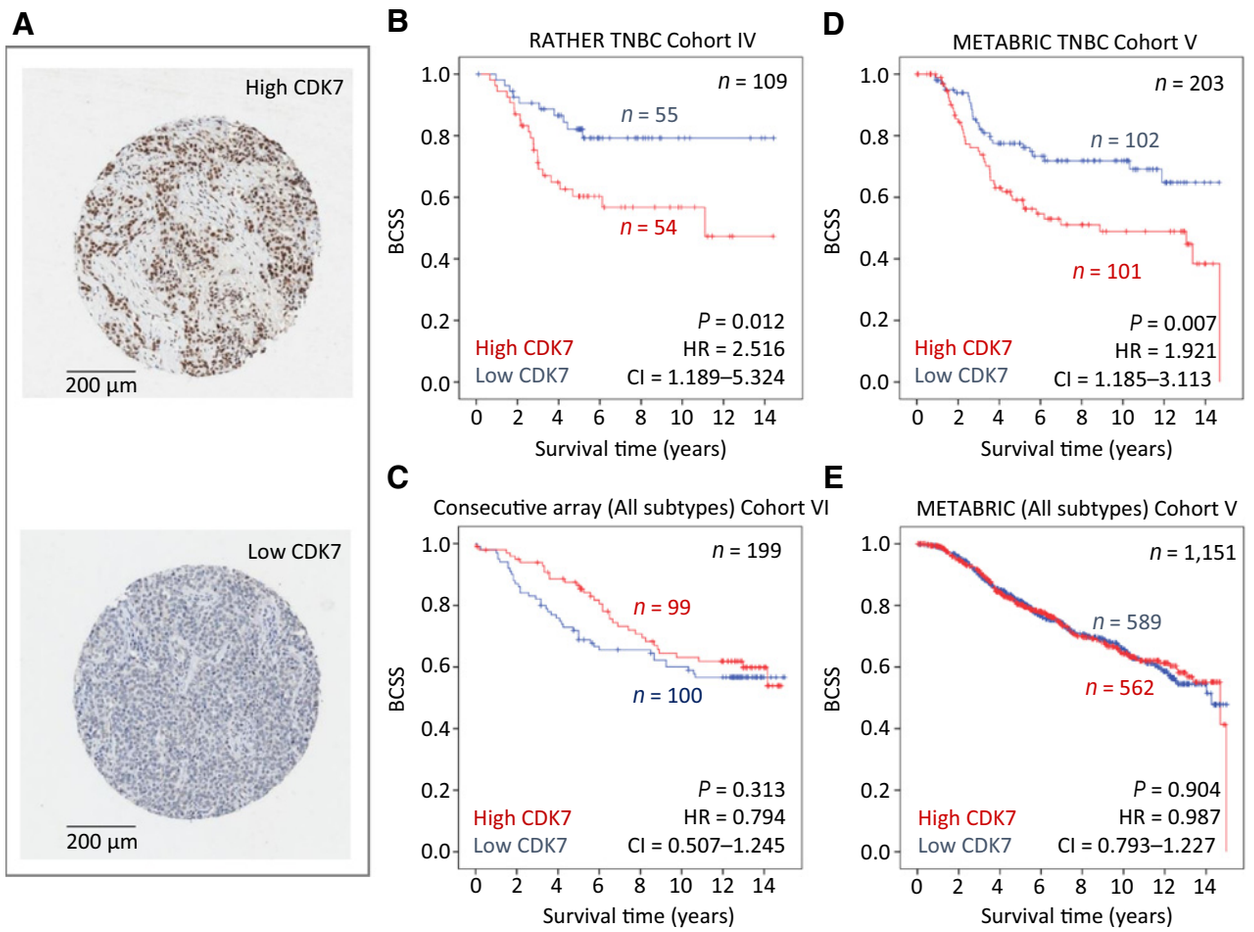

Figure 1.

High CDK7 protein expression is associated with poor prognosis in TNBC tissues. A, Representative scanned images of tumor cores with low or high CDK7 protein expression, as determined by IHC. B, Kaplan–Meier survival curves showing the relationship between CDK7 protein expression and BCSS in the RATHER TNBC TMA cohort censored at 15 years (n ¼ 109). C, Kaplan–Meier survival curves showing the relationship between CDK7 protein expression and BCSS in the Consecutive breast cancer TMA cohort censored at 15 years (n ¼ 199). D, Kaplan–Meier survival curves showing the relationship between CDK7 protein expression and BCSS in the METABRIC TNBC TMA cohort censored at 15 years (n ¼ 203). E, Kaplan–Meier survival curves showing the relationship between CDK7 protein expression and BCSS in the METABRIC breast cancer TMA cohort censored at 15 years (n ¼ 1,151).

Published OnlineFirst April 28, 2017; DOI: 10.1158/0008-5472.CAN-16-2546

Table 1. Multivariate Cox regression analysis of BCSS in the RATHER TNBC dataset

	BCSS	
Clinicopathologic variables	*P*	HR (95% CI)
CDK7 protein	0.006	
Low		1
High		3.045 (1.383–6.701)
Age (continuous)	0.427	1.010 (0.985–1.036)
Tumor size (continuous)	0.002	1.397 (1.128–1.730)
Tumor grade	0.802	
Grade 2		1
Grade 3		0.880 (0.323–2.396)
Nodal status	0.675	
No		1
Yes		1.189 (0.530–2.667)
Chemotherapy	0.912	
No		1
Yes		1.044 (0.487–2.237)

S3E), within the TNBC subset of the cohort. Multivariate Cox regression analysis confirmed that CDK7 protein expression and nodal status were independent prognostic factors of reduced BCSS in the TNBC subset (Table 2; for CDK7, P ¼ 0.003; HR ¼ 2.136; CI ¼ 1.294–3.526). Similarly, using a median cut-off point, we observed no correlations between CDK7 protein expression and either BCSS (P ¼ 0.904; HR ¼ 0.987; CI ¼ 0.793–1.227; Fig. 1E) or OS (P ¼ 0.168; HR ¼ 1.122; CI ¼ 0.952–1.322; Supplementary Fig. S3F) across the entire set of METABRIC breast cancer samples. Therefore, we have validated both at the mRNA and at the protein levels that high CDK7 expression is associated with poor prognosis specifically in TNBC.

To further understand the underlying basis of CDK7's association with poor prognosis in TNBC, we compared *CDK7* mRNA expression levels between different subtypes of breast cancer and found that *CDK7* mRNA expression was lower in TNBC compared with luminal A and luminal B subtypes in the METABRIC transcriptomic dataset (n ¼ 1,992; P < 0.0001; Supplementary Fig. S4A) and the TCGA transcriptomic dataset (n ¼ 422; P < 0.0001; Supplementary Fig. S4B). Previous studies have shown a critical role for CDK7 in mediating superenhancer–linked oncogenic transcription in *MYC*-driven cancer (14) and elevated MYC signaling has been associated with poor prognosis in TNBC (37). Accordingly, we found that *MYC* mRNA expression was higher in TNBC compared with other subtypes of breast cancer in the METABRIC transcriptomic dataset (P < 0.0001; Supplementary Fig. S4C), and the TCGA transcriptomic dataset (P < 0.0001; Supplementary Fig. S4D).

Table 2. Multivariate Cox regression analysis of BCSS in the METABRIC TNBC dataset

	BCSS	
Clinicopathologic variables	*P*	HR (95% CI)
CDK7 protein	0.003	
Low		1
High		2.136 (1.294–3.526)
Age (continuous)	0.254	0.988 (0.967–1.009)
Tumor size (continuous)	0.183	1.008 (0.996–1.020)
Tumor grade	0.131	
Grade 1þ2		1
Grade 3		1.957 (0.819–4.676)
Nodal status	0.018	
No		1
Yes		2.446 (1.169–5.117)
Chemotherapy	0.449	
No		1
Yes		0.744 (0.346–1.600)

Knockdown of CDK7 leads to reduced cell proliferation, migration, and increased response to doxorubicin

To investigate the functional impact of CDK7 on TNBC cells, we performed shRNA-mediated knockdown of CDK7 in BT549 and MDA-MB-231 cells. Following efficient knockdown of CDK7 at both mRNA and protein levels detected via RT-PCR and immunoblotting, respectively (Fig. 2A), both BT549 and MDA-MB-231 cell lines with ablated CDK7 demonstrated significantly reduced number of colonies compared with their respective nontargeting controls (Fig. 2B). Cell proliferation was also significantly reduced upon CDK7 knockdown compared with the respective nontargeting controls in both cell lines (Fig. 2C). Moreover, cell migration rate was found dramatically decreased at 24 and 48 hours in cells with CDK7 knockdown (Fig. 2D). Finally, knockdown of CDK7 led to increased TNBC cell sensitivity to doxorubicin following 72 hours of treatment, and only marginally increased responses to carboplatin and no altered response to docetaxel were observed (Fig. 2E), which may be due to a role of CDK7 in the regulation of chemotherapeutic agent–induced DNA damage (38, 39).

Targeting CDK7 with specific inhibitors affects proliferation, apoptosis, and transcription

Recently, a highly specific covalent CDK7 inhibitor THZ1 was developed (13). Here, we compared the efficacy of THZ1 versus a previously discovered noncovalent CDK7 inhibitor BS-181 in the TNBC cell lines BT549 and MDA-MB-231. Cell growth curves demonstrated that both inhibitors reduced cell proliferation in the two cell lines tested (Fig. 3A). Interestingly, the newly developed THZ1 demonstrated an approximately 500-fold higher potency than BS-181 (Fig. 3A). We next assessed whether inhibition of CDK7 caused apoptotic cell death by measuring Annexin V and propidium iodide positivity. Both CDK7 inhibitors induced apoptosis in the BT549 and MDA-MB-231 cell lines (Fig. 3B). Similar to the cell growth curves, THZ1 displayed higher potency in terms of apoptosis induction in comparison with BS-181. Inhibition of CDK7 with THZ1 caused a modest cell-cycle phase redistribution in the MDA-MB-231 cell line, with an approximate increase of 10% of cells in the G_2–M phase (Fig. 3C); a similar trend was observed for BT549 cells but this was not statistically significant. CDK1 is the only essential CDK required for completion of cell mitosis, which is stringently regulated by CDK7 (40). Treatment with THZ1 and BS-181 caused a reduction in phospho-CDK1 in a dose-dependent manner in BT549 and MDA-MB-231 cells (Fig. 3D). In addition, CDK7 plays a key role in RNA transcription regulation by phosphorylating RNAPII (10). Treatment with THZ1 and BS-181 also caused a dose-dependent reduction of phosphorylation of RNAPII at the serine 2, the serine 5 and the serine 7 sites in BT549 and MDA-MB-231 cells (Fig. 3E), suggestive of RNA transcription inhibition through CDK7 inactivation.

The above data demonstrate that CDK7 inhibitors BS-181 and THZ1 trigger antitumor effects by inducing transcription inhibition and apoptosis in a dose-dependent manner.

Combination treatment of THZ1 with ABT-263 shows synergistic effects causing reduced TNBC cell survival

Given the negative effect on RNAPII phosphorylation with CDK7 inhibitor treatment, we assessed the expression of two

Published OnlineFirst April 28, 2017; DOI: 10.1158/0008-5472.CAN-16-2546

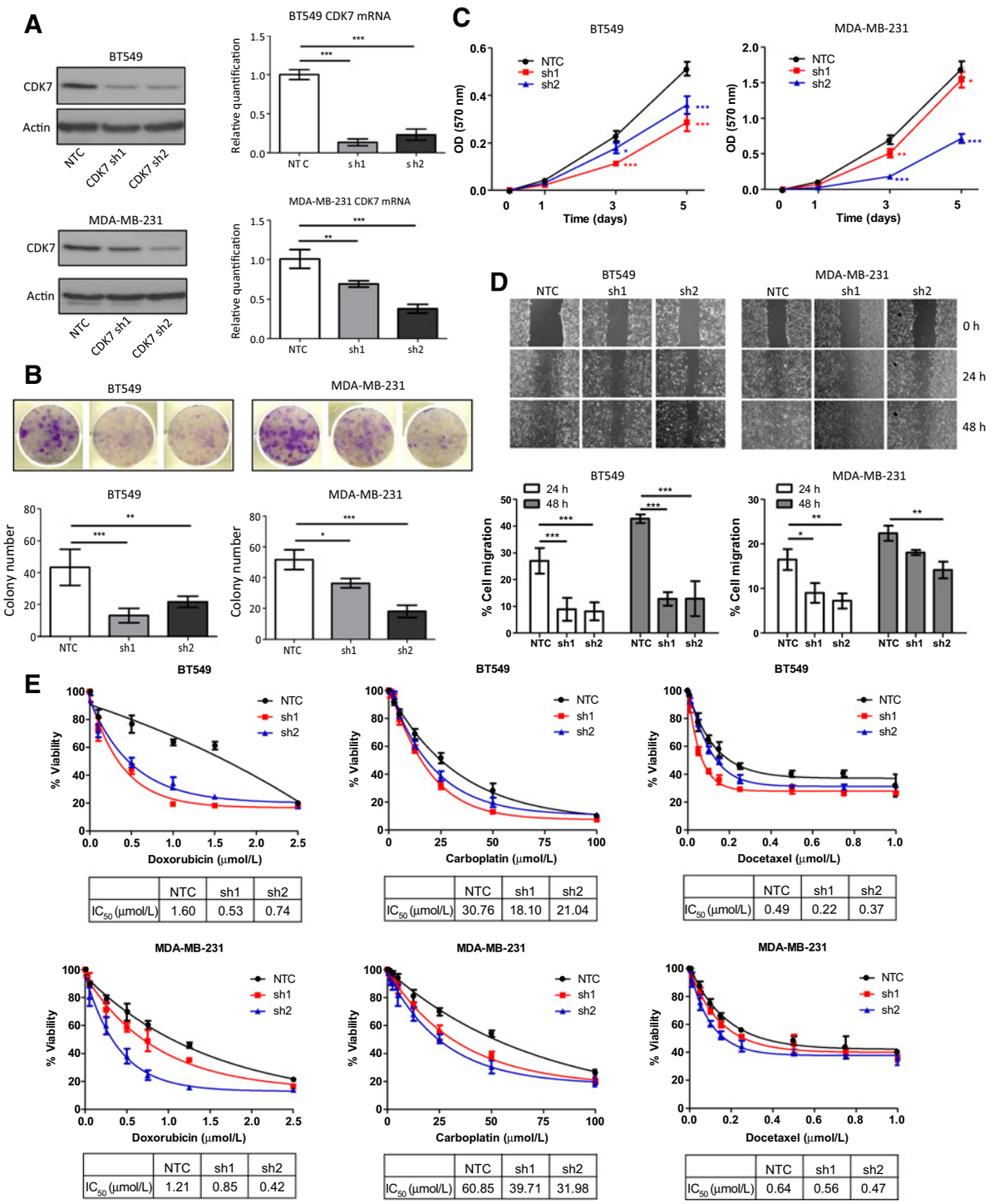

Figure 2.

Knockdown of CDK7 diminishes cell viability, proliferation, migration, and increases cell response to doxorubicin. A, Immunoblotting and qRT-PCR analysis of *CDK7* mRNA expression post-shRNA knockdown of CDK7 in BT549 and MDA-MB-231 cells (n ¼ 3). A nontargeting shRNA and two independent hairpins targeting CDK7 (shRNA1 and shRNA2) are represented by NTC, sh1, and sh2. Data are presented as mean □ SD (□□, $P < 0.01$; □□□, $P < 0.001$). B, Colony formation assay following CDK7 knockdown in BT549 and MDA-MB-231 cells (n ¼ 3). Colony numbers are presented as mean □ SD (□, $P < 0.05$; □□, $P < 0.01$; □□□, $P < 0.001$). C, MTT cell viability assay following CDK7 knockdown in BT549 and MDA-MB-231 cells (n ¼ 3). Proliferation is presented as mean absorbance □ SD (□□, $P < 0.01$; □□□, $P < 0.001$). D, Cell migration analysis following CDK7 knockdown (n ¼ 3). Migration is presented as mean closure distance □ SD (□, $P < 0.05$; □□, $P < 0.01$; □□□, $P < 0.001$). E, MTT cell viability assay following CDK7 knockdown and treatment with chemotherapeutic agents for 72 hours in BT549 and MDA-MB-231 cells (n ¼ 3). IC_{50} values of NTC, shRNA1, and shRNA2 knockdown cells are presented in the mini-tables.

Published OnlineFirst April 28, 2017; DOI: 10.1158/0008-5472.CAN-16-2546

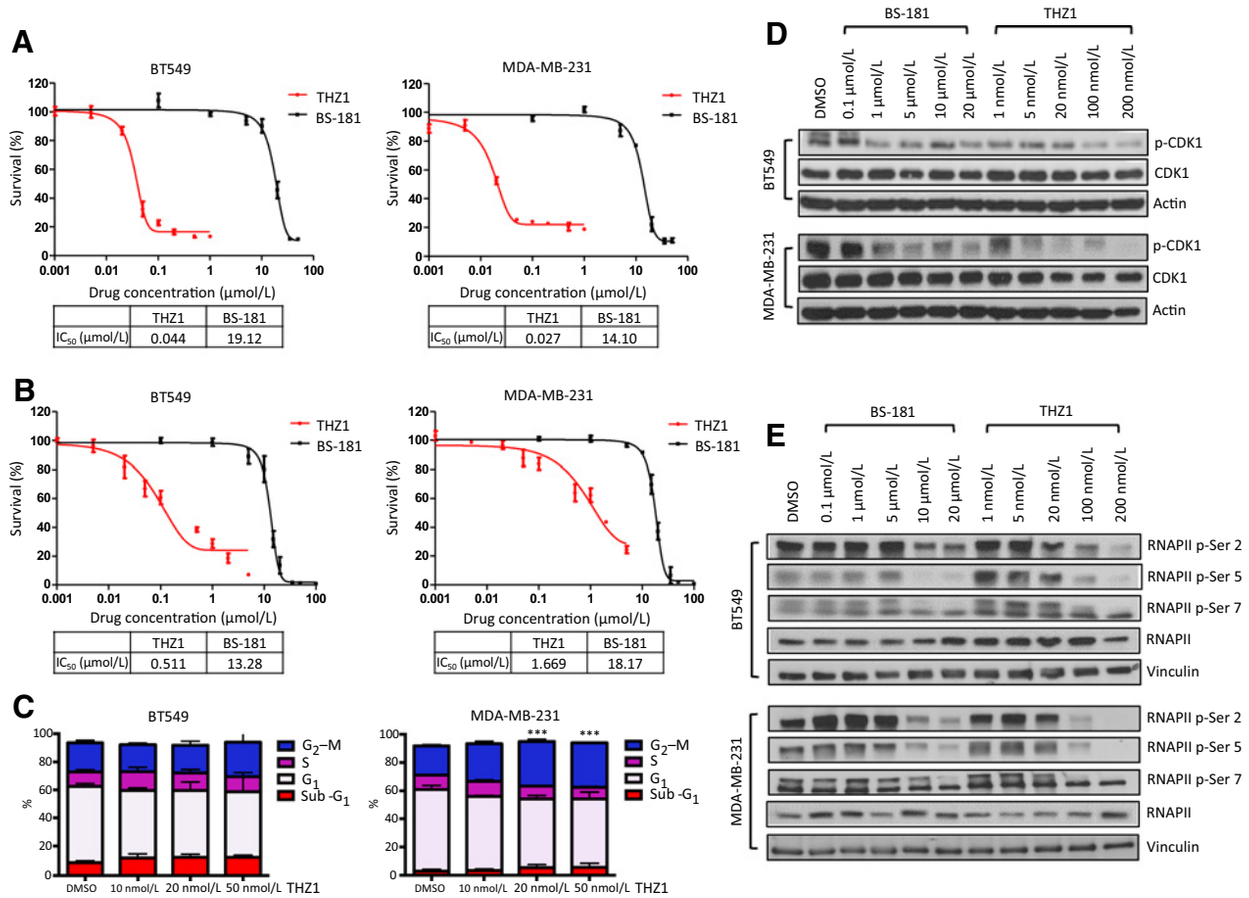

Figure 3.

CDK7 inhibition suppresses cell proliferation and survival via inhibition of RNA transcription. A, Cell survival curves showing IC_{50} values of BS-181 and THZ1 in BT549 and MDA-MB-231 cells following 72 hours of treatment. B, Apoptosis analysis via Annexin V/propidium iodide staining of BT549 and MDA-MB-231 cells at various concentrations of BS-181 and THZ1 following 48 hours of treatment. C, Quantification of percentage of BT549 and MDA-MB-231 cells in different cell-cycle phases following treatment with various doses of THZ1 for 16 hours (n ¼ 3; □□□, $P < 0.001$). D, Immunoblotting of proteins involved in the signaling pathway relating to cell cycle following 4 hours of treatment with various concentrations of BS-181 and THZ1 in BT549 and MDA-MB-231 cells. E, Immunoblotting of proteins involved in transcriptional regulation following 4 hours of treatment with various concentrations of BS-181 and THZ1 in BT549 and MDA-MB-231 cells.

proteins with short half-lives, namely the transcription factor c-MYC and the antiapoptotic protein MCL-1. There was a time-dependent reduction in the expression of both c-MYC and MCL-1 following treatment with either BS-181 or THZ1 (Fig. 4A). We assessed the expression of two other antiapoptotic proteins, BCL-2 and BCL-XL, finding that their levels did not alter greatly following exposure to either CDK7 inhibitor (Fig. 4B). Using dynamic BH3 profiling, we aimed to measure the effect of CDK7 inhibition on mitochondrial priming and anti-apoptotic dependency (28, 41). Following treatment for 16 hours with THZ1, BH3 profiling was performed on the MDA-MB-231 cell line. The BH3 peptides BAD and HRK caused a greater loss of cytochrome c following treatment with THZ1 (Fig. 4C). The BAD peptide binds to the antiapoptotic proteins BCL-2, BCL-XL and BCL-W, while the HRK peptide only binds to BCL-XL. Following treatment with THZ1, there is a reduction in the expression of MCL-1 (Fig. 4A); therefore, the increased response to the HRK and BAD peptides suggest that pro-death proteins that were bound by MCL-1 now bind to BCL-2/BCL-XL following THZ1 treatment. To test this hypothesis, we combined THZ1 treatment with the BH3 mimetic ABT-263 (which inhibits BCL-2, BCL-XL and BCL-W) in both BT549 (Fig. 4D, I) and MDA-MB-231 (Fig. 4D, II) cell lines. As is evident from the heatmap representation of the MTT assay, the combination treatment caused a synergistic inhibition of proliferation. The combination of THZ1 and ABT-199 caused synergy mainly in the BT549 cell line (Fig. 4D, III), while synergy could not be determined in the MDA-MB-231 cell line as an IC_{50} value for ABT-199 could not be calculated by the MTT assay (Fig. 4D, IV). The combination treatment of THZ1 and ABT-263/ABT-199 was tested in 4 additional TNBC cell lines. MTT assays demonstrated synergistic effects in the HCC1143, HCC1937, and Hs578T cell lines with THZ1 and ABT-263 treatment (Supplementary Fig. S5A). However, the combination treatment of THZ1 and ABT-199 only showed synergy in HCC1937 cells (Supplementary Fig. S5B). No synergy was detected in the BT20

Published OnlineFirst April 28, 2017; DOI: 10.1158/0008-5472.CAN-16-2546

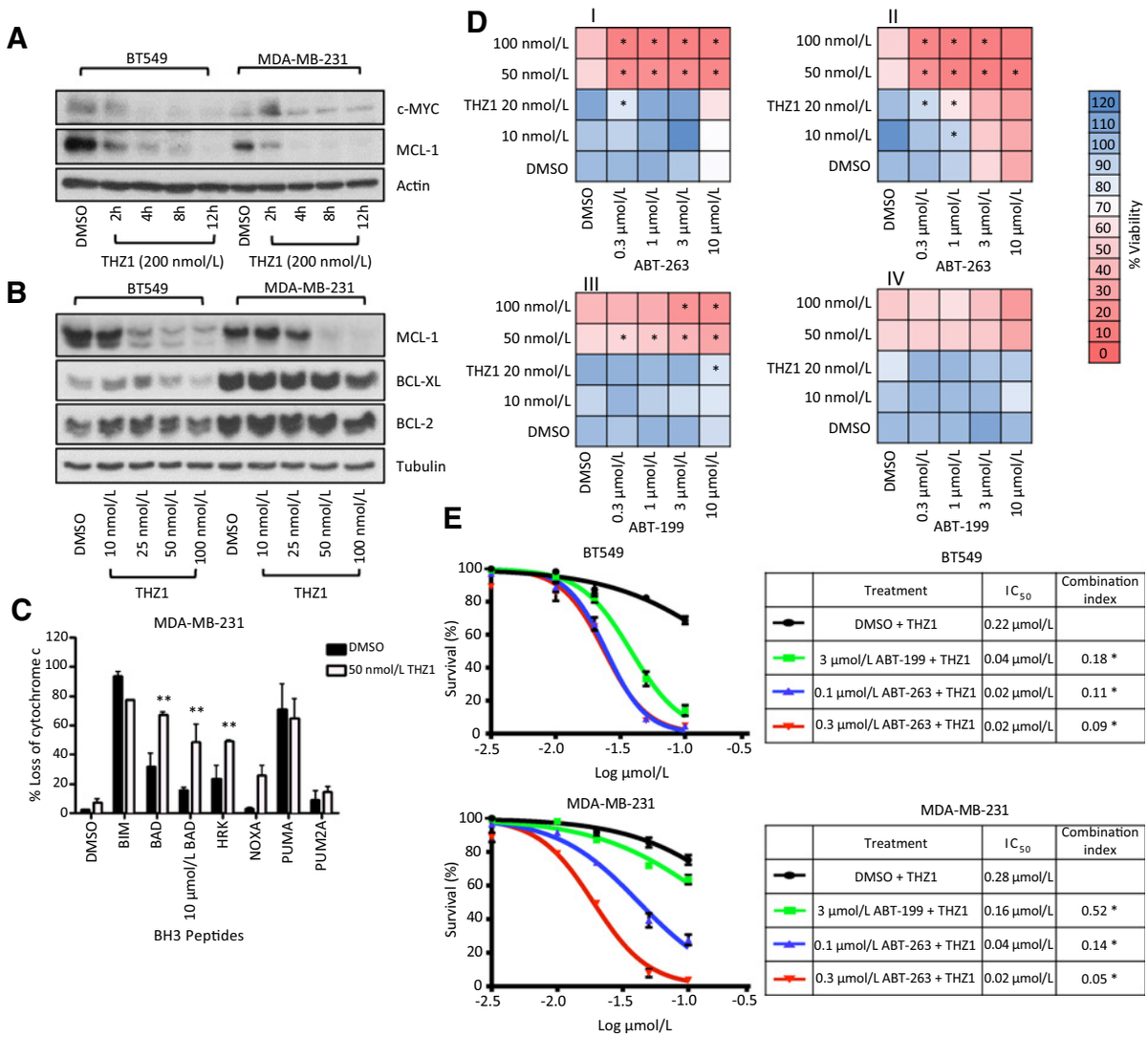

Figure 4.

Identifying rational combination treatments for TNBC. A, Immunoblotting of c-MYC and MCL-1 expression following 200 nmol/L THZ1 treatment at increasing time points in BT549 and MDA-MB-231 cells. B, Immunoblotting of BCL-2 family protein expression following 24 hours of BS-181 and THZ1 treatment at various concentrations in BT549 and MDA-MB-231 cells. C, BH3 profile of MDA-MB-231 cells following treatment with either 50 nmol/L THZ1 or DMSO for 16 hours (**, $P < 0.01$). D, MTT viability assay following treatment for 48 hours with escalating concentrations of THZ1 and ABT-263 in BT549 (I) and MDA-MB-231 (II) cells, or treatment with escalating concentrations of ABT-199 and THZ1 in BT549 (III) or MDA-MB-231 (IV) cells. Synergy was calculated using CompuSyn and a combination index value of under 0.7 is marked with an asterisk (*). E, Apoptosis analysis via Annexin V/propidium iodide staining on BT549 and MDA-MB-231 cells at various THZ1 concentrations in combination with either DMSO, 0.1 mmol/L ABT-263, 0.3 mmol/L ABT-263, or 3 mmol/L ABT-199 and the combination index was calculated.

cells, suggesting an intrinsically resistant cell line to THZ1 and ABT-263/ABT-199 treatment.

To validate that the combination treatment caused apoptosis and not solely inhibition of proliferation, we assessed the combination using Annexin V and propidium iodide staining. As was evident from the combination index, synergy occurred following combined treatment with THZ1 and ABT-263 at low doses and with ABT-199 at a higher dose in both cell lines (Fig. 4E). Potentially, this suggests that combining the BH3 mimetic ABT-263 may be an effective treatment strategy for TNBC.

Discussion

Limited success has so far been achieved in respect of biomarker identification and validation in TNBC, which may be attributable to disease heterogeneity at the molecular level in this particular subtype. Human proteome studies revealed that more than 50% of human proteins undergo phosphorylation supported by kinases (42), whereas abnormal activation of protein phosphorylation is commonly a cause or consequence of oncogenesis. Kinases have become one of the most intensively pursued classes

Published OnlineFirst April 28, 2017; DOI: 10.1158/0008-5472.CAN-16-2546

of drug targets in cancer. To date, 28 small-molecule kinase inhibitors have been approved by the FDA (43), which has invigorated the search for new kinase inhibitors as anticancer drugs. As such, we focused on discovery of novel kinase biomarkers and tailored therapeutic strategies in TNBC taking advantage of molecular profiling data and preclinical models.

CDK7 has been reported to be a potential therapeutic target in MYC-driven and transcription-dependent cancers (13–16). However, little is known about the value of CDK7 as a prognostic or predictive marker. A recent study revealed that the CAK complex was highly expressed in breast cancer and CDK7 expression was inversely associated with poor prognosis in ER-positive breast cancer, which may be attributable to its role in directly interacting with ERa (44). Our data provided evidence of a negative association between CDK7 expression and survival outcomes specifically in TNBC, together with a potential role in terms of modulating response to chemotherapeutic agents.

Previous reports have linked high expression of p53 (45, 46) and elevated MYC signaling (37) with prognosis in TNBC. However, we found that MYC or TP53 mRNA expression was not significantly correlated with RFS in Cohort I (Public TNBC; Supplementary Fig. S6A and S6B). MYC expression showed no association with BCSS in this cohort (Supplementary Fig. S6C), while TP53 expression was only marginally associated with good BCSS in Cohort III (METABRIC TNBC; Supplementary Fig. S6D). Surprisingly, analysis of CDK7 mRNA expression in subgroups of breast cancer showed lower overall CDK7 mRNA expression in the TNBC group compared with the luminal A and luminal B subtypes in Cohort III (METABRIC breast cancer of all subtypes; Supplementary Fig. S4A) and Cohort VII (TCGA; Supplementary Fig. S4B), indicating that CDK7 may be involved in more activities in luminal A and luminal B subtypes compared with TNBC and CDK7's preferential correlation with poor prognosis in TNBC may be due to its roles in the regulation of transcription and cell cycle. Indeed, CDK7 has previously been shown to mediate ligand-dependent activation of ERa via phosphorylation of serine 118 (11), and the expression of CAK (CDK7, cyclin H, and MAT1) has recently been found to be positively associated with ER expression (44), which correlates with our observation of higher CDK7 mRNA levels in the luminal A and luminal B subtypes compared with the HER2 and TNBC subtypes (Supplementary Fig. S4A and S4B). Further analysis revealed that MYC mRNA expression was higher in TNBC compared with other subtypes (Supplementary Fig. S4C and S4D). Together with the finding that CDK7 inhibition led to reduced MYC expression (Fig. 4A), it is postulated that MYC-dependent TNBC largely relies on the activity of CDK7 during tumor progression.

These findings not only highlight the value of CDK7 as a prognostic marker, but also directly point to therapeutic interventions, such as direct inhibition of CDK7 that could benefit TNBC patients. The dual role of CDK7 in transcriptional regulation and cell-cycle control may offer additional benefits for CDK7-targeted therapy in TNBC. Transcription factors have traditionally been considered "undruggable" targets due to difficulties in directly modulating DNA/protein binding (47). In addition, directly targeting the global transcription machinery may cause intolerable toxicity due to an essential dependency of nontransformed tissue on transcription. Recent studies have challenged the predicament and found that the epigenetic modifier JQ1, a BET bromodomain inhibitor, preferentially inhibits the transcription of genes with superenhancer regions (48). Moreover, TNBC was preferentially sensitive to JQ1 treatment when a broad panel of breast cancer cell lines was assessed (49).

Several studies have been involved in the design and validation of CDK7 inhibitors. BS-181, a highly selective small-molecule CDK7 inhibitor, was found to effectively inhibit the growth of an MCF-7 xenograft (50). Recently, Kwiatkowski and colleagues developed a highly potent covalent CDK7 inhibitor, THZ1, which has been extensively evaluated in various types of cancers and achieved astonishing antiproliferative effects (13–15). A common feature of these tumors is that they appear to be transcriptionally driven. THZ1 preferentially inhibited the proliferation of MYCN-driven neuroblastoma and the sensitivity correlated with downregulation of superenhancer-associated genes (14). Similar results were found in small-cell lung cancer with a preferential inhibition of superenhancer-associated genes including MYC, MYCN, and OTX2 (15). A recent publication by Wang and colleagues also indicated a preferential sensitivity of TNBC over other breast cancer subtypes to CDK7 inhibition, using a newly developed CDK7 inhibitor THZ2 with improved pharmacokinetic properties (16).

We directly compared, for the first time, the sensitivity of TNBC cell lines to both BS-181 and THZ1 and found that the covalent inhibitor THZ1 was over 500-fold more effective at inhibiting proliferation. Functional assessment of TNBC cells demonstrated that CDK7 downregulation impaired cell viability and proliferation (Fig. 2B and C), indicating that CDK7 plays a key role in the signaling cascades that are responsible for TNBC progression.

At present, chemotherapy is the main systemic treatment option for TNBC patients. Our data suggest a potential role for CDK7 in modulating the sensitivity of TNBC cells to the chemotherapeutic agent doxorubicin (Fig. 2E). This may provide additional therapeutic strategies for the fraction of TNBC patients with poor inherent response to doxorubicin, as well as those displaying residual disease following good initial response to the treatment. We also observed a moderate level of increased sensitivity following CDK7 knockdown with carboplatin treatment, but not with docetaxel treatment (Fig. 2E), suggesting that the apparent protective effect mediated by CDK7 may be limited to genotoxic agents. Previous studies demonstrated that CDK7 played a positive role in DNA damage–induced p53 activation (38, 39). Further investigation of combination treatment with CDK7 inhibitors and chemotherapeutic agents in a broader panel of breast cancer cell lines and in vivo is warranted to determine the effectiveness of such combination treatment and potential selectivity/utility in a TNBC context.

Profiling of the residual TNBC tumors following neoadjuvant therapy showed evidence of increased amplification of both MCL-1 and MYC genes (17). Both CDK7 inhibitors, BS-181 and THZ1, inhibited phosphorylation of RNAPII in a dose-dependent manner (Fig. 3E) and caused a reduction in the levels of two short half-life proteins, c-MYC and MCL-1 (Fig. 4A), which point toward the assessment of CDK7 treatment in the refractory setting. Interestingly, the most commonly amplified genes in solid tumors include MCL-1 and MYC, as assessed by somatic copy number alterations in 3,181 different cancer specimens (21). Importantly, MCL-1 has been identified as a crucial survival factor in TNBC and MCL-1 knockdown sensitizes TNBC cell response to BCL-XL inhibition (51).

Using BH3 profiling following treatment with THZ1, we found that the cells became more dependent on the

Published OnlineFirst April 28, 2017; DOI: 10.1158/0008-5472.CAN-16-2546

antiapoptotic proteins, BCL-2 and BCL-XL, as indicated by the increased response to the BAD and HRK BH3 peptides (Fig. 4C). This is likely due to the reduced expression of MCL-1 (Fig. 4B) causing a shift of prodeath proteins to BCL-2/BCL-XL. The BIM and PUMA BH3 peptides did not cause any statistical differences in cytochrome c release following THZ1 treatment, indicating that the total expression of prodeath proteins was not altered in response to THZ1. However, a complete dose response of the BIM and PUMA peptides would be required to confirm this. We, therefore, tested the rational combination of THZ1 with the BCL-2/BCL-XL/BCL-W BH3 mimetic ABT-263 or the combination of THZ1 with the BCL-2–specific inhibitor ABT-199.

We found synergy in five out of six triple-negative cell lines treated with ABT-263 and THZ1, demonstrating that the combination shows robust synergy across multiple TNBC cell lines. A recent study showed that the combination of THZ1 and the BH3 mimetic obatoclax was an effective combination treatment for T-cell lymphoma and in vivo treatment with the combination did not show any evidence of enhanced toxicity (52). ABT-199 was recently approved by the FDA for the treatment of chronic lymphocytic leukemia with a chromosomal abnormality of 17p deletion. However, we did not detect robust synergy with the BCL-2 specific inhibitor ABT-199 in combination with THZ1, as only two of the six TNBC cell lines tested showed synergy. This suggests that inhibition of both BCL-XL and BCL-2 is necessary in TNBC to robustly detect synergy with THZ1. Taken together, these observations showed evidence of a promising treatment option for TNBC by targeting CDK7 in combination with BH3 mimetics.

In summary, our data demonstrate that CDK7 is associated with poor prognosis in TNBC. Phenotypic changes after kinase depletion indicate that CDK7 is involved in mediating cell proliferation, migration, and doxorubicin-induced DNA damage. Inhibition of transcription using highly specific CDK7 inhibitors has proven here to be promising in targeting TNBC. Furthermore, combined inhibition of CDK7 and BCL-2/BCL-XL using THZ1 and ABT-263 shows synergistic responses, leading to substantial apoptosis. Considering the lack of established targeted therapeutics against TNBC, we propose that CDK7 will be a powerful poor prognostic marker and attractive therapeutic target for TNBC.

Disclosure of Potential Conflicts of Interest

D. O'Connor is a consultant/advisory board member for Pfizer Inc. W.M. Gallagher is a Chief Scientific Officer at OncoMark Limited, reports receiving a commercial research grant from Carrick Therapeutics, and is a consultant/advisory board member for Carrick Therapeutics. No potential conflicts of interest were disclosed by the other authors.

Authors' Contributions

Conception and design: B. Li, T. Ni Chonghaile, C. Caldas, D. O'Connor, W.M. Gallagher

Development of methodology: B. Li, T. Ni Chonghaile, R. Klinger, D. O'Connor

Acquisition of data (provided animals, acquired and managed patients, provided facilities, etc.): T. Ni Chonghaile, L. Walsh, E. Conroy, A. Gaber, S.-F. Chin, E. Provenzano, S.C. Linn, K. Jirstrom, C. Caldas

Analysis and interpretation of data (e.g., statistical analysis, biostatistics, computational analysis): B. Li, T. Ni Chonghaile, Y. Fan, S. Madden, R. Klinger, L. Walsh, G. O'Hurley, G. Mallya Udupi, J. Joseph, F. Tarrant, T. Dubois, D. O'Connor, W.M. Gallagher

Writing, review, and/or revision of the manuscript: B. Li, T. Ni Chonghaile, Y. Fan, R. Klinger, A.E. O'Connor, J. Crown, T. Dubois, S.C. Linn, K. Jirstrom, C. Caldas, D. O'Connor, W.M. Gallagher

Administrative, technical, or material support (i.e., reporting or organizing data, constructing databases): L. Walsh, G. O'Hurley, E. Conroy, A. Gaber, T. Dubois

Study supervision: T. Ni Chonghaile, R. Klinger, A.E. O'Connor, D. O'Connor, W.M. Gallagher

Other (technical histology services): H.A. Bardwell

Acknowledgments

We thank all members of the RATHER consortium, in particular Prof. Rene Bernards from the Netherlands Cancer Institute (Amsterdam, the Netherlands), who provided constructive suggestions for this study. We also thank Dr. Nathanael Gray from the Dana-Farber Cancer Institute (Boston, MA) for the kind gift of the THZ1 inhibitor.

Grant Support

This study was supported by RATHER (Rational Therapy for Breast Cancer), a Collaborative Project funded under the European Union 7th Framework Programme (grant agreement no. 258967), the Irish Cancer Society Collaborative Cancer Research Centre BREAST-PREDICT (CCRC13GAL), and the Science Foundation Ireland Investigator Programme OPTi-PREDICT (grant code 15/IA/3104).

The costs of publication of this article were defrayed in part by the payment of page charges. This article must therefore be hereby marked advertisement in accordance with 18 U.S.C. Section 1734 solely to indicate this fact.

Received September 26, 2016; revised March 30, 2017; accepted April 21, 2017; published OnlineFirst April 28, 2017.

References

1. Turner N, Lambros MB, Horlings HM, Pearson A, Sharpe R, Natrajan R, et al. Integrative molecular profiling of triple negative breast cancers identifies amplicon drivers and potential therapeutic targets. Oncogene 2010;29:2013–23.
2. Andre F, Job B, Dessen P, Tordai A, Michiels S, Liedtke C, et al. Molecular characterization of breast cancer with high-resolution oligonucleotide comparative genomic hybridization array. Clin Cancer Res 2009;15:441–51.
3. Dent R, Trudeau M, Pritchard KI, Hanna WM, Kahn HK, Sawka CA, et al. Triple-negative breast cancer: clinical features and patterns of recurrence. Clin Cancer Res 2007;13(15 Pt 1):4429–34.
4. Liedtke C, Mazouni C, Hess KR, Andre F, Tordai A, Mejia JA, et al. Response to neoadjuvant therapy and long-term survival in patients with triple-negative breast cancer. J Clin Oncol 2008;26:1275–81.
5. Harris LN, Broadwater G, Lin NU, Miron A, Schnitt SJ, Cowan D, et al. Molecular subtypes of breast cancer in relation to paclitaxel response and outcomes in women with metastatic disease: results from CALGB 9342. Breast Cancer Res 2006;8:R66.
6. Guarneri V, Broglio K, Kau SW, Cristofanilli M, Buzdar AU, Valero V, et al. Prognostic value of pathologic complete response after primary chemotherapy in relation to hormone receptor status and other factors. J Clin Oncol 2006;24:1037–44.
7. Yankulov KY, Bentley DL. Regulation of CDK7 substrate specificity by MAT1 and TFIIH. EMBO J 1997;16:1638–46.
8. Larochelle S, Pandur J, Fisher RP, Salz HK, Suter B. Cdk7 is essential for mitosis and for in vivo Cdk-activating kinase activity. Genes Dev 1998;12:370–81.
9. Serizawa H, Makela TP, Conaway JW, Conaway RC, Weinberg RA, Young RA. Association of Cdk-activating kinase subunits with transcription factor TFIIH. Nature 1995;374:280–2.
10. Feaver WJ, Svejstrup JQ, Henry NL, Kornberg RD. Relationship of CDK-activating kinase and RNA polymerase II CTD kinase TFIIH/TFIIK. Cell 1994;79:1103–9.
11. Chen D, Riedl T, Washbrook E, Pace PE, Coombes RC, Egly JM, et al. Activation of estrogen receptor alpha by S118 phosphorylation involves a

Published OnlineFirst April 28, 2017; DOI: 10.1158/0008-5472.CAN-16-2546

ligand-dependent interaction with TFIIH and participation of CDK7. Mol Cell 2000;6:127–37.
12. Rochette-Egly C, Adam S, Rossignol M, Egly JM, Chambon P. Stimulation of RAR alpha activation function AF-1 through binding to the general transcription factor TFIIH and phosphorylation by CDK7. Cell 1997; 90:97–107.
13. Kwiatkowski N, Zhang T, Rahl PB, Abraham BJ, Reddy J, Ficarro SB, et al. Targeting transcription regulation in cancer with a covalent CDK7 inhibitor. Nature 2014;511:616–20.
14. Chipumuro E, Marco E, Christensen CL, Kwiatkowski N, Zhang T, Hatheway CM, et al. CDK7 inhibition suppresses super-enhancer-linked oncogenic transcription in MYCN-driven cancer. Cell 2014;159:1126–39.
15. Christensen CL, Kwiatkowski N, Abraham BJ, Carretero J, Al-Shahrour F, Zhang T, et al. Targeting transcriptional addictions in small cell lung cancer with a covalent CDK7 inhibitor. Cancer Cell 2014;26:909–22.
16. Wang Y, Zhang T, Kwiatkowski N, Abraham BJ, Lee TI, Xie S, et al. CDK7-dependent transcriptional addiction in triple-negative breast cancer. Cell 2015;163:174–86.
17. Balko JM, Giltnane JM, Wang K, Schwarz LJ, Young CD, Cook RS, et al. Molecular profiling of the residual disease of triple-negative breast cancers after neoadjuvant chemotherapy identifies actionable therapeutic targets. Cancer Discov 2014;4:232–45.
18. Davis LJ, Halazonetis TD. Both the helix-loop-helix and the leucine zipper motifs of c-Myc contribute to its dimerization specificity with Max. Oncogene 1993;8:125–32.
19. Schwab M, Ellison J, Busch M, Rosenau W, Varmus HE, Bishop JM. Enhanced expression of the human gene N-myc consequent to amplification of DNA may contribute to malignant progression of neuroblastoma. Proc Natl Acad Sci U S A 1984;81:4940–4.
20. Brodeur GM, Seeger RC, Schwab M, Varmus HE, Bishop JM. Amplification of N-myc in untreated human neuroblastomas correlates with advanced disease stage. Science 1984;224:1121–4.
21. Beroukhim R, Mermel CH, Porter D, Wei G, Raychaudhuri S, Donovan J, et al. The landscape of somatic copy-number alteration across human cancers. Nature 2010;463:899–905.
22. Leverson JD, Zhang H, Chen J, Tahir SK, Phillips DC, Xue J, et al. Potent and selective small-molecule MCL-1 inhibitors demonstrate on-target cancer cell killing activity as single agents and in combination with ABT-263 (navitoclax). Cell Death Dis 2015;6:e1590.
23. Wilson WH, O'Connor OA, Czuczman MS, LaCasce AS, Gerecitano JF, Leonard JP, et al. Navitoclax, a targeted high-affinity inhibitor of BCL-2, in lymphoid malignancies: a phase 1 dose-escalation study of safety, pharmacokinetics, pharmacodynamics, and antitumour activity. Lancet Oncol 2010;11:1149–59.
24. Roberts AW, Seymour JF, Brown JR, Wierda WG, Kipps TJ, Khaw SL, et al. Substantial susceptibility of chronic lymphocytic leukemia to BCL2 inhibition: results of a phase I study of navitoclax in patients with relapsed or refractory disease. J Clin Oncol 2012;30:488–96.
25. Gandhi L, Camidge DR, Ribeiro de Oliveira M, Bonomi P, Gandara D, Khaira D, et al. Phase I study of navitoclax (ABT-263), a novel Bcl-2 family inhibitor, in patients with small-cell lung cancer and other solid tumors. J Clin Oncol 2011;29:909–16.
26. Souers AJ, Leverson JD, Boghaert ER, Ackler SL, Catron ND, Chen J, et al. ABT-199, a potent and selective BCL-2 inhibitor, achieves antitumor activity while sparing platelets. Nat Med 2013;19:202–8.
27. Cervantes-Gomez F, Lamothe B, Woyach JA, Wierda WG, Keating MJ, Balakrishnan K, et al. Pharmacological and protein profiling suggests venetoclax (ABT-199) as optimal partner with ibrutinib in chronic lymphocytic leukemia. Clin Cancer Res 2015;21:3705–15.
28. Chonghaile TN, Roderick JE, Glenfield C, Ryan J, Sallan SE, Silverman LB, et al. Maturation stage of T-cell acute lymphoblastic leukemia determines BCL-2 versus BCL-XL dependence and sensitivity to ABT-199. Cancer Discov 2014;4:1074–87.
29. Touzeau C, Ryan J, Guerriero J, Moreau P, Chonghaile TN, Le Gouill S, et al. BH3 profiling identifies heterogeneous dependency on Bcl-2 family members in multiple myeloma and predicts sensitivity to BH3 mimetics. Leukemia 2016;30:761–4.
30. Rody A, Karn T, Liedtke C, Pusztai L, Ruckhaeberle E, Hanker L, et al. A clinically relevant gene signature in triple negative and basal-like breast cancer. Breast Cancer Res 2011;13:R97.
31. Madden SF, Clarke C, Gaule P, Aherne ST, O'Donovan N, Clynes M, et al. BreastMark: an integrated approach to mining publicly available transcriptomic datasets relating to breast cancer outcome. Breast Cancer Res 2013; 15:R52.
32. Curtis C, Shah SP, Chin SF, Turashvili G, Rueda OM, Dunning MJ, et al. The genomic and transcriptomic architecture of 2,000 breast tumours reveals novel subgroups. Nature 2012;486:346–52.
33. O'Brien SL, Fagan A, Fox EJ, Millikan RC, Culhane AC, Brennan DJ, et al. CENP-F expression is associated with poor prognosis and chromosomal instability in patients with primary breast cancer. Int J Cancer 2007; 120:1434–43.
34. Ryan J, Letai A. BH3 profiling in whole cells by fluorimeter or FACS. Methods 2013;61:156–64.
35. McShane LM, Altman DG, Sauerbrei W, Taube SE, Gion M, Clark GM, et al. REporting recommendations for tumor MARKer prognostic studies (REMARK). Nat Clin Pract Urol 2005;2:416–22.
36. Chou TC. Drug combination studies and their synergy quantification using the Chou-Talalay method. Cancer Res 2010;70:440–6.
37. Horiuchi D, Kusdra L, Huskey NE, Chandriani S, Lenburg ME, Gonzalez-Angulo AM, et al. MYC pathway activation in triple-negative breast cancer is synthetic lethal with CDK inhibition. J Exp Med 2012;209:679–96.
38. Ko LJ, Shieh SY, Chen X, Jayaraman L, Tamai K, Taya Y, et al. p53 is phosphorylated by CDK7-cyclin H in a p36MAT1-dependent manner. Mol Cell Biol 1997;17:7220–9.
39. Lu H, Fisher RP, Bailey P, Levine AJ. The CDK7-cycH-p36 complex of transcription factor IIH phosphorylates p53, enhancing its sequence-specific DNA binding activity invitro. Mol Cell Biol 1997;17:5923–34.
40. Brown NR, Korolchuk S, Martin MP, Stanley WA, Moukhametzianov R, Noble ME, et al. CDK1 structures reveal conserved and unique features of the essential cell cycle CDK. Nat Commun 2015;6:6769.
41. Ni Chonghaile T, Sarosiek KA, Vo TT, Ryan JA, Tammareddi A, Moore Vdel G, et al. Pretreatment mitochondrial priming correlates with clinical response to cytotoxic chemotherapy. Science 2011;334:1129–33.
42. Wilhelm M, Schlegl J, Hahne H, Moghaddas Gholami A, Lieberenz M, Savitski MM, et al. Mass-spectrometry-based draft of the human proteome. Nature 2014;509:582–7.
43. Wu P, Nielsen TE, Clausen MH. Small-molecule kinase inhibitors: an analysis of FDA-approved drugs. Drug Discov Today 2016;21:5–10.
44. Patel H, Abduljabbar R, Lai CF, Periyasamy M, Harrod A, Gemma C, et al. Expression of CDK7, cyclin H, and MAT1 is elevated in breast cancer and is prognostic in estrogen receptor-positive breast cancer. Clin Cancer Res 2016;22:5929–38.
45. Yamashita H, Nishio M, Toyama T, Sugiura H, Zhang Z, Kobayashi S, et al. Coexistence of HER2 over-expression and p53 protein accumulation is a strong prognostic molecular marker in breast cancer. Breast Cancer Res 2004;6:R24–30.
46. Miller LD, Smeds J, George J, Vega VB, Vergara L, Ploner A, et al. An expression signature for p53 status in human breast cancer predicts mutation status, transcriptional effects, and patient survival. Proc Natl Acad Sci U S A 2005;102:13550–5.
47. Nhili R, Peixoto P, Depauw S, Flajollet S, Dezitter X, Munde MM, et al. Targeting the DNA-binding activity of the human ERG transcription factor using new heterocyclic dithiophene diamidines. Nucleic Acids Res 2013;41:125–38.
48. Loven J, Hoke HA, Lin CY, Lau A, Orlando DA, Vakoc CR, et al. Selective inhibition of tumor oncogenes by disruption of super-enhancers. Cell 2013;153:320–34.
49. Shu S, Lin CY, He HH, Witwicki RM, Tabassum DP, Roberts JM, et al. Response and resistance to BET bromodomain inhibitors in triple-negative breast cancer. Nature 2016;529:413–7.
50. Ali S, Heathcote DA, Kroll SH, Jogalekar AS, Scheiper B, Patel H, et al. The development of a selective cyclin-dependent kinase inhibitor that shows antitumor activity. Cancer Res 2009;69:6208–15.
51. Goodwin CM, Rossanese OW, Olejniczak ET, Fesik SW. Myeloid cell leukemia-1 is an important apoptotic survival factor in triple-negative breast cancer. Cell Death Differ 2015;22:2098–106.
52. Cayrol F, Praditsuktavorn P, Fernando TM, Kwiatkowski N, Marullo R, Calvo-Vidal MN, et al. THZ1 targeting CDK7 suppresses STAT transcriptional activity and sensitizes T-cell lymphomas to BCL2 inhibitors. Nat Commun 2017;8:14290.

Cancer Research
The Journal of Cancer Research (1916–1930) | The American Journal of Cancer (1931–1940)

AACR American Association for Cancer Research

Therapeutic Rationale to Target Highly Expressed CDK7 Conferring Poor Outcomes in Triple-Negative Breast Cancer

Bo Li, Triona Ni Chonghaile, Yue Fan, et al.

Cancer Res 2017;77:3834-3845. Published OnlineFirst April 28, 2017.